

Copyright

by

Ye Yuan

2018

**The Dissertation Committee for Ye Yuan Certifies that this is the approved version
of the following dissertation:**

Mass Transfer Rate in Semi-Aqueous Amines for CO₂ Capture

Committee:

Gary T. Rochelle, Supervisor

Isaac C. Sanchez

Gyeong S. Hwang

Ross E. Dugas

Mass Transfer Rate in Semi-Aqueous Amines for CO₂ Capture

by

Ye Yuan

Dissertation

Presented to the Faculty of the Graduate School of

The University of Texas at Austin

in Partial Fulfillment

of the Requirements

for the Degree of

Doctor of Philosophy

The University of Texas at Austin

August 2018

Dedication

To my family

Acknowledgements

The past five years at the University of Texas at Austin have been the most challenging and rewarding period of my professional and personal life.

First and foremost, I'd like to thank Dr. Rochelle, for his guidance and mentorship during the past five years. His role in my personal and professional development is far greater than the title of advisor would convey. Dr. Rochelle's enthusiasm about research and his scientific curiosity has been an inspiration for me to find joy and value in my own work. He has constantly challenged me to think about problems in new and different ways. The time, passion, and energy he invests in his students is the model of what it means to be an educator. Joining his research group was one of the best decisions I have made. Also, his dedication to his family and community taught me the importance of work-life balance. It's my honor to have him as the witness of my wedding.

I would like to thank Prof. Gyeong Hwang, Prof. Issac Sanchez, and Dr. Ross Dugas for offering their time and professional expertise as members of my dissertation committee.

The faculty and staff at the McKetta Department of Chemical Engineering at The University of Texas at Austin offered invaluable support for this work and my learning. Thank you, Maeve for editing all of the progress reports and helping me improve my writing skill. Those feedbacks are especially valuable for international students.

I have been fortunate to interact with many of Dr. Rochelle's group members over the years, and I also learned a lot from previous student's research outcomes. I want to

acknowledge a few who I have worked closely with over the fast years. First, I'd like to thank Dr. Le Li for mentorship during my first year. I want to thank Dr. Yang Du who carefully guided me through the experiments. I also appreciate Dr. Brent Sherman who taught me Aspen simulation modeling step by step during his most stressful time of finishing his dissertation. I'd also like to thank the many other research group members I collaborated with: Kent Fischer, Yu-Jeng Lin, Yue Zhang, Chao Wang, Di Song, Omkar Namjoshi, Paul Nielsen, Junyuan Ding, Matt Beaudry, Matt Walters, and Nathan Fine. I was lucky to share my time at UT with such an exceptional group of people.

Our work at UT would not be possible without the contributions and support of our sponsors in the Texas Carbon Management Program. It is truly an invaluable experience to interact with so many academic, industrial, and public sector experts/leaders as a student.

Most importantly I would like to thank Mom and Dad, who encouraged and supported me to study abroad. Pursuing B.S. and Ph.D. at top universities in the U.S. could be much tougher without your love and encouragement. You were always there supporting every decision I made. Thank you for giving me everything you have, and I hope we have made them proud. Last but not least, I would like to thank my wife, Sophie S. Yi, for her love and company during the last five years. We have been fortunate to meet each other and pursue Ph.D. together here at UT Austin. Our journey to marriage, much like the experience of this Ph.D. work, has been very memorable and rewarding. The pursuing of Ph.D. would not be so pleasant without her company and encouragement along the way.

Mass Transfer Rate in Semi-Aqueous Amines for CO₂ Capture

Ye Yuan, Ph.D.

The University of Texas at Austin, 2018

Supervisor: Gary T. Rochelle

Amine scrubbing is the most promising solution to address CO₂ emission from power plants. Solvent development can significantly reduce the capital and energy cost of the process. This work rigorously studies the CO₂ mass transfer and solubility at flue gas treating process condition for aqueous and semi-aqueous amines.

A second-generation aqueous amine solvent: 2methylpiperazine (2MPZ) blended with piperazine (PZ) that has been developed with good overall performance. The effect of viscosity on absorption rate and heat exchanger has been identified. Optimal concentration for 2MPZ/PZ is found to be 5 m (5 mole/kg water). Thermodynamic and kinetic model has been developed for 2MPZ/PZ in Aspen Plus to allow economic assessments, and process modeling.

Semi-aqueous MEA/PZ composes of physical solvent, water, and amine has been characterized. Ultra-fast absorption rate at lean loading has been achieved. The effect of viscosity, diffusivity, CO₂ activity (physical solubility), and amine activity on mass transfer rate (k_g') has been studied. k_g' increases because of reduced operating CO₂ loading (higher MEA concentration at the same $P_{CO_2}^*$), greater CO₂ physical solubility, and greater MEA activity. The increase in k_g' becomes less significant at higher loading due to low diffusivity by high viscosity.

The mass transfer model of CO₂ diffusion and reaction with semi-aqueous MEA was built in MATLAB[®]. Sensitive analysis shows the relationship between rate and solvent physical/thermal properties. The pseudo first order approximation is not applicable to semi-aqueous MEA because of surface depletion of MEA.

The energy use of CO₂ capture by amine scrubbing can be estimated by adding minimum work and lost work. Semi-aqueous amines reduces the lost work in the condenser due to less water evaporation in the stripper, which. However; second generation amine processes use advanced stripper configurations can accomplish the same effect with little additional capital cost.

Besides viscosity, thermal conductivity and heat capacity also effect the heat exchanger cost. Comprehensive normalized capacity has been developed. An advanced solvent with high normalized capacity can reduce the CAPEX/OPEX of the heat exchanger no matter the solvent is water lean or not.

$$\Delta C_{norm} = \Delta C_{solv} \left(\frac{\mu}{\mu_{5mPZ}} \right)^{-0.175} \left(\frac{k}{k_{5mPZ}} \right)^{0.325} \left(\frac{C_p}{C_{p,5mPZ}} \right)^{-0.825}$$

Table of Contents

List of Tables	xiv
List of Figures	xvii
Chapter 1: Introduction and Background.....	1
1.1 Global warming and CO ₂ emission.....	1
1.2 Amine scrubbing technology for CO ₂ capture.....	1
1.3 Solvent selection criteria.....	3
1.4 Solvent development, Aqueous amine.....	6
1.5 Solvent development, Semi-aqueous amine	7
1.6 Research objectives.....	8
Chapter 2: Optimal Concentration of Aqueous 2MPZ and 2MPZ/PZ for CO ₂ Capture	10
2.1 Introduction.....	10
2.2 Materials	11
2.3 CO ₂ Solubility.....	13
2.4 CO ₂ Absorption rate.....	17
2.5 Effect of viscosity	22
2.6 Conclusion	25
Chapter 3: Rigorous Thermodynamic and Kinetic Modeling of 2MPZ and 2MPZ/PZ in Aspen Plus®	26
3.1 Introduction.....	26
3.2 Modeling method.....	27
3.2.1 Thermodynamic Modeling.....	27
3.2.2 Kinetic Modeling	29
3.3 Results.....	32
3.3.1 Viscosity	32
3.3.2 Thermodynamic Modeling Results.....	33
3.3.3 Kinetic Modeling	42
3.3.4 Effect of viscosity	44

3.4 Conclusions.....	48
3.5 Acknowledgements.....	49
Chapter 4: CO ₂ Absorption Rate in Semi-Aqueous MEA.....	51
4.1 Introduction.....	51
4.2 Method.....	53
4.2.1 Materials	53
4.2.2 Viscosity	54
4.2.3 CO ₂ solubility and absorption rate by the wetted wall column (WWC).....	54
4.2.4 CO ₂ physical solubility by N ₂ O analogy	57
4.2.5 Volatility/activity measurement using FTIR	59
4.2.6 Pseudo-first-order (PFO) assumption	60
4.3 Results and discussion	61
4.3.1. Absorption rate.....	61
4.3.2. MEA activity.....	65
4.3.3. Viscosity and physical solubility	66
4.3.4. Net effect of amine activity, viscosity, and physical solubility on kg' based on PFO	67
4.3.5 Rate enhancement by 2-(2-Ethoxyethoxy) ethanol (CARBITOL™)	69
4.3.6 Rate behavior in DGA®-Water-NMP	70
4.3.7 Comparison of key properties to 5 m PZ.....	71
4.3.8 Considerations of volatility.....	74
4.4 Conclusions.....	74
Chapter 5: CO ₂ Absorption rate in semi-aqueous PZ.....	77
5.1 introduction	77
5.2 method.....	78
5.2.1 Materials	78
5.2.2 CO ₂ loading by TIC	79
5.2.3 Viscosity	79

5.2.4 CO ₂ solubility and absorption rate by the wetted wall column (WWC).....	79
5.3 Results and discussion	79
5.3.1 PZ in NMP/water and PZ in TEG/water.....	79
5.3.2 CO ₂ solubility and absorption rate of PZ in SUF/water	81
5.3.3 CO ₂ solubility and absorption rate of 5 m PZ in IMI/water	86
5.3.1 Viscosity of 5 m PZ in SUF/water and PZ in IMI/water	90
5.3.1 Comparisons of semi-aqueous PZ solvents	93
5.4 Conclusions.....	95
Chapter 6: Mass Transfer Modeling in Semi-aqueous Amines	96
6.1 Introduction.....	96
6.2 Mass transfer theory.....	97
6.2.1 Mass transfer coefficients	97
6.2.2 Mass Transfer Without Reaction (Physical Absorption).....	98
6.2.2.1 Film Theory	99
6.2.2.2 Penetration theory	101
6.2.2.3 Eddy Diffusivity Theory	102
6.2.3 Mass transfer with chemical reaction	103
6.2.3.1 Instantaneous Reactions.....	103
6.2.3.2 Finite-Rate Reaction	105
6.2.4 CO ₂ mass transfer in MEA-NMP-water	107
6.2.5 Parameter Regression.....	111
6.3 Results.....	112
6.3.1 Mass transfer modeling results	112
6.3.2 Sensitivity analysis.....	114
6.4 Conclusions.....	120
Chapter 7: Energy use estimation by lost work analysis	122
7.1 Introduction.....	122
7.2 Methods.....	124
7.2.1 Minimum work of amine scrubbing	124

7.2.2	Lost work	125
7.2.3	Lost work estimation.....	126
7.2.3.1	Lost work in the absorber	126
7.2.3.2	Lost work in reboiler.....	128
7.2.3.3	Lost work in the compressor.....	129
7.2.3.4	Lost work in the main heat exchanger	129
7.2.3.5	Optimal ΔT_{LM} for main heat exchanger	131
7.3	Results.....	133
7.3.1	Method validation using 5 m aqueous PZ AFS	134
7.3.2	lost work and energy use comparison.....	136
7.3.3	Lost work analysis in the 1CO2BOL/2C16 case.	139
7.4	Normalized capacity of semi-aqueous amines.....	142
7.5	Discussion on energy use.....	144
7.6	Conclusions.....	145
Chapter 8:	Conclusions and Recommendations	147
8.1	Conclusions summary	147
8.1.1	Aqueous piperazine blend.....	147
8.1.2	Semi-aqueous MEA and PZ.....	147
8.1.2.1	Semi-aqueous MEA	147
8.1.2.2	Semi-aqueous PZ	149
8.1.3	Lost work comparison.....	149
8.2	Recommendations for future work	150
8.2.1	Aqueous piperazine blend.....	150
8.2.2	Semi-aqueous MEA and PZ.....	150
8.2.3	Energy use.....	151
Appendix A:	Experimental Methods	152
A.1	Wetted Wall Column	152
A.1.1	Design	152
A.1.2	Operating Procedure	154
A.1.3	Data Analysis.....	156

A.1.4 Gas Film Mass Transfer Coefficient.....	158
A.2 Analytical methods	159
A.2.1 Total Inorganic Carbon Analysis (TIC).....	160
A.2.2 Acid Amine Titration.....	160
A.2.3 Viscosity Measurements	160
Appendix B: Detailed WWC data	161
References.....	190

List of Tables

Table 2.1: Amines tested in this work	11
Table 2.2: Chemical species in 2 m 2MPZ	12
Table 2.3: Chemical species in 4 m 2MPZ	12
Table 2.4: Chemical species in 6 m 2MPZ	12
Table 2.5: Chemical species in 2.5 m/2.5 m 2MPZ/PZ	12
Table 2.6: Chemical species in 3 m HEP	12
Table 2.7: Chemical species in 5 m HEP	12
Table 2.8: Chemical species in 7.7 m HEP	13
Table 2.9: Capacity and $k_{g',avg}$ of 2MPZ and PZ at 40 °C	24
Table 3.1: Molecule and electrolyte components for e-NRTL parameters	28
Table 3.2: Thermodynamic data for the 2MPZ system	29
Table 3.3: Reaction set for 2MPZ/PZ	31
Table 3.4: Viscosity parameters for Equation 3.3	33
Table 3.5: VLE parameters for 2MPZ with their standard deviation.	34
Table 3.6: Additional parameters regressed for data of CO ₂ solubility in 2MPZ/ PZ	39
Table 3.7: Regressed parameters for 2MPZ species	42
Table 3.8: Reaction parameters for reactions.	42
Table 4.1: Materials used for solvent preparation	54
Table 4.2: CO ₂ absorption at lean and rich conditions in 7 m semi-aqueous MEA at 40 °C	63
Table 4.3: Viscosity and γ_{CO2} of 0.37 and 0.45 loaded 7 m semi-aqueous MEA	67

Table 4.4: Relative viscosity, H_{CO_2} , activity, and k_g' of 7 m semi-aqueous MEA at 0.37 mol CO_2 /mol MEA.	68
Table 4.5: Relative viscosity, H_{CO_2} , activity, and k_g' of 7 m semi-aqueous MEA with 0.45 mol CO_2 /mol MEA	69
Table 4.6: μ_{mid} , $k_g'_{avg}$, ΔC_{sol} , and $\Delta C\mu$ of 7 m semi-aqueous MEA and 5 m PZ (aq) (Dugas, 2009).	73
Table 5.1: Materials used for solvent preparation	78
Table 5.2: Chemical species in 5 m PZ in 1TEG/2water.....	78
Table 5.3: Chemical species in 5 m PZ in 1physical solvent/3water.....	79
Table 5.4: Chemical species in 5 m PZ in 1physical solvent/1water.....	79
Table 5.5: Viscosity (cP) in 5 m PZ in 1SUF/1water	91
Table 5.6: Viscosity (cP) in 5 m PZ in 1SUF/3water	91
Table 5.7: Viscosity (cp) in 5 m PZ in 1IMI/1water.....	91
Table 5.8: Cyclic capacity and $k_g'_{avg}$ of 5 m PZ	94
Table 6.1: Summary of k_l dependence on diffusion coefficient by various physical mass transfer models.....	103
Table 6.2: Concentration and activity coefficient in aqueous MEA (Plaza, 2011).....	110
Table 7.1: Summary of empirical correlations of heat transfer for PHE (Lin, 2016).....	133
Table 7.2: Summary of modeling methods used by Lin (2016).	134
Table 7.3: Summary of process specifications for 5 m PZ/AFS.....	134
Table 7.4: Summary of lost work analysis.....	137
Table 7.6: Summary of process specifications for 1CO2BOL/2C16. (Zheng et al., 2016)	140
Table 7.7: lost work in 1CO2BOL/2C16 based on design in Table 7.6.	140

Table 7.8 Normalized capacity of some representative solvents. NMP=N-Methyl-2-pyrrolidone, CARB=2-(2-Ethoxyethoxy)ethanol, SUF=sulfolane. 144

List of Figures

Figure 1.1: Process flow diagram of an amine scrubbing process for CO ₂ recovery from coal-fired power plant flue gas.....	2
Figure 2.1: CO ₂ equilibrium pressure in 4 m 2MPZ in black and 8 m 2MPZ (Chen, 2011) in red	14
Figure 2.2: CO ₂ equilibrium pressure in 2.5/2.5 m 2MPZ/PZ in black and 4/4 m 2MPZ/PZ (Chen, 2011) in red	15
Figure 2.3: CO ₂ equilibrium pressure at 40 °C in 2, 4, 6 m 2MPZ and 8 m 2MPZ (Chen, 2011)	16
Figure 2.4: CO ₂ equilibrium pressure at 40 °C in 3 m, 5 m, and 7.7 m HEP	17
Figure 2.5: k _g ' measured by the wetted wall column in 4 m 2MPZ and 8 m 2MPZ in dash (Chen, 2011)	18
Figure 2.6: k _g ' measured by the wetted wall column in 2.5/2.5 m 2MPZ/PZ and 4/4 m 2MPZ/PZ in dash (Chen, 2011).....	19
Figure 2.7: k _g ' measured by the wetted wall column in 2 m, 4 m, 6 m, and 8 m 2MPZ at 40 °C	20
Figure 2.8: k _g ' measured by the wetted wall column in 3, 5, and 7.7 m HEP at 40 °C	21
Figure 2.9: k _g ' in 4 m 2MPZ, 8 m 2MPZ, 5 m PZ, 8 m PZ, 2.5 m/2.5 m 2MPZ/PZ, and 4 m/4 m 2MPZ/PZ (Dugas, 2009; Chen, 2011).	22
Figure 2.10: k _g ', viscosity, capacity, and normalized capacity of 2MPZ	24
Figure 3.1: 4 m and 8 m 2MPZ viscosity. Solid Points: 8 m data; sold line: 8 m fitted; open points: 4 m data; dash line: 4 m fitted.	32

Figure 3.2: CO ₂ solubility in 4 m 2MPZ. Lines: model prediction; Points: experimental results from WWC.	34
Figure 3.3: CO ₂ solubility in 8 m 2MPZ. Lines: model prediction; Points: experimental data (Chen, 2013; Xu, 2011).	35
Figure 3.4: CO ₂ distribution in loaded 8 m 2MPZ at 40 °C; Points: experimental data (Chen, 2013), lines: model prediction.	36
Figure 3.5: Predicted speciation of 8 m 2MPZ at 40 °C.	37
Figure 3.6: Predicted speciation of 4 m 2MPZ at 40 °C.	38
Figure 3.7: CO ₂ solubility for 4 m 2MPZ/4 m PZ. Lines: model; Points: experimental data (Chen, 2013; Xu, 2011).	39
Figure 3.8: CO ₂ solubility for 2.5 m 2MPZ/2.5 m PZ. Lines: model; Points: experimental data.	40
Figure 3.9: Speciation prediction for 4/4 m 2MPZ/PZ at 40 °C.	41
Figure 3.10: Speciation prediction for 2.5/2.5 m 2MPZ/PZ at 40 °C.	41
Figure 3.11: Flux Predictions ratioed to experimental data. Black for 8 m, red for 4 m 2MPZ.	43
Figure 3.12: Flux Predictions ratioed to experimental data. Black for 4/4 m, red for 2.5/2.5 m 2MPZ/PZ.	44
Figure 3.13: Predicted kg',avg (left y-axis), ΔC , ΔC_u (right y-axis) in 2MPZ, operation condition 50-5000 Pa at 40°C.	46
Figure 3.14: Predicted kg',avg (left y-axis), ΔC , ΔC_u (right y-axis) in PZ, operation condition 50-5000Pa at 40°C.	46
Figure 3.15: Predicted kg',avg (left y-axis), ΔC , ΔC_u (right y-axis) in 2MPZ/PZ, operation condition 50-5000Pa at 40°C.	47

Figure 3.16: Comparing 2MPZ, PZ, 2MPZ/PZ k_g' and normalized capacity at 2, 4, 5, 6, and 8 m.....	48
Figure 4.1: Diagram of the WWC	55
Figure 4.2: Plot of flux of CO ₂ vs. driving force for 0.38 loaded 7 m MEA in 1 NMP/3 water in the WWC.....	56
Figure 4.3: Diagram of the total pressure apparatus.....	57
Figure 4.4: FTIR system for volatility measurement. Figure adapted from Nguyen (2013).....	59
Figure 4.5: CO ₂ solubility of 7 m MEA in NMP/water at 40 °C by WWC.....	62
Figure 4.6: k_g' of 7 m MEA in NMP/H ₂ O at 40 °C by WWC.....	64
Figure 4.7: k_g' of 7 m MEA in NMP (Carbitol)/water and 5 m PZ (aq) (Dugas, 2009) at 40 °C.....	65
Figure 4.8: P_{MEA} above 7 m semi-aqueous MEA at 40 °C by the FTIR.....	66
Figure 4.9: CO ₂ solubility of MEA or DGA [®] in NMP/water at 40 °C by WWC..	70
Figure 4.10: k_g' of MEA or DGA [®] in NMP/H ₂ O at 40 °C by WWC.....	71
Figure 5.1: k_g' of 5 m PZ in 1TEG/2water and 1NMP/3water at 40 °C by WWC	81
Figure 5.2: CO ₂ solubility in 5 m PZ in 1 SUF/3 water.....	82
Figure 5.3: CO ₂ solubility in 5 m PZ in 1 SUF/1 water.....	83
Figure 5.4: k_g' of 5 m PZ in 1 SUF/3 water at 20–60 °C in WWC.....	84
Figure 5.5: k_g' of 5 m PZ in 1 SUF/3 water at 20–60 °C in WWC.....	85
Figure 5.6: k_g' of 5 m PZ in 1 SUF/1 water at 20–60 °C in WWC.....	86
Figure 5.7: CO ₂ solubility in 5 m PZ in 1 IMI/3 water.....	87
Figure 5.8: CO ₂ solubility in 5 m PZ in 1 IMI/1 wat.....	88
Figure 5.9: k_g' of 5 m PZ in 1 IMI/3 water at 20–60 °C in WWC.....	88
Figure 5.10: k_g' of 5 m PZ in 1 IMI/1 water at 20–60 °C in WWC.....	89

Figure 5.11: k_g' of 5 m semi-aqueous PZ at 40 °C in WWC	90
Figure 5.12: Viscosity of 5 m PZ in 1IMI/1water at 20–60 °C in WWC	92
Figure 5.13: Viscosity of 5 m PZ in 1SUF/1water at 20–60 °C in WWC	92
Figure 5.14: Viscosity of 5 m PZ in 1SUF/3water at 20–60 °C in WWC	93
Figure 6.1: Steady state concentration profile of CO ₂ absorption without chemical reaction in the liquid phase, using film theory (not drawn to scale).(Chen, 2011)	100
Figure 6.2: Mass transfer of CO ₂ into bulk liquid with fast chemical reaction. (Cullinane 2005)	106
Figure 6.3: Concentration profiles (not to scale). The entire liquid film (liquid and reaction film) is discretized for numerical integration.....	108
Figure 6.4: Fit of the mass transfer model, red points are 0.37 loading, blue points are 0.45 loading.....	113
Figure 6.5: Sensitivity of k_g' to k_3 and CO ₂ activity coefficient at lean/rich loading. The sensitivity to γ_{CO_2} is negative, absolute value is plotted.	115
Figure 6.6: Sensitivity of k_g' to D_{CO_2} and D_{AM}	116
Figure 6.7: MEA concentration profile near the interface for 7 m MEA (aq). Lean loading: 0.37 mol CO ₂ /mol MEA.	117
Figure 6.8: MEA concentration profile near the interface for 7 m MEA in 1water/19NMP. Lean loading: 0.37 mol CO ₂ /mol MEA.	118
Figure 6.9: MEA concentration profile near the interface for 7 m MEA (aq). Rich loading: 0.45 mol CO ₂ /mol MEA.....	119
Figure 6.10: MEA concentration profile near the interface for 7 m MEA in 1water/19NMP. Rich loading: 0.45 mol CO ₂ /mol MEA.....	120
Figure 7.1: Partial pressure driving force and lost work in an isothermal absorber,	128

Figure 7.2: Optimization of cross exchanger LMTD (Lin, 2016)	130
Figure 7.3: Process diagram of 5 m PZ using the advanced flash stripper.	135
Figure 7.4: Process diagram of CO2BOL/C16. (Mathias et al., 2013).....	137
Figure A.1: Detailed view of the WWC.....	153
Figure A.2: Flow diagram of the entire WWC setup.	155
Figure A.3: Plot of flux of CO ₂ vs. driving force obtained from a set of measurements for 4 m 2-methylpiperazine at 40 °C.....	158

Chapter 1: Introduction and Background

1.1 GLOBAL WARMING AND CO₂ EMISSION

Anthropogenic greenhouse gas emissions are changing climates worldwide (IPCC, 2014). Greenhouse gas, especially carbon dioxide, is believed to be the major cause of global warming. Atmospheric CO₂ has increased from 280 ppm in 1850 to 400 ppm in 2016 (Dlugokencky, 2016) due to anthropogenic activities, primarily the combustion of fossil fuels. Mitigation of greenhouse gas emissions can substantially reduce the risks of climate change in the second half of the 21st century (IPCC, 2014). In 2014, electricity generation accounted for 30% of U.S. greenhouse gas emissions and 31% of world emissions from burning fuels (EPA 2016). Thus, fossil fuel-fired power plants provide a great opportunity to reduce CO₂ emission from point sources. In 2015, the U.S. Environmental Protection Agency (EPA) proposed a new carbon emission standard for the new and existing coal-fired power plant, aiming to reduce carbon emissions by 32% from 2005 levels by 2030 (EPA, 2015). Under this regulation, carbon capture and storage may become necessary on the coal-fired power plants.

CO₂ capture and storage (CCS) is considered as a promising option to reduce CO₂ emission since it allows continuous use of fossil fuel sources while emitting no or very little CO₂ to the atmosphere.

1.2 AMINE SCRUBBING TECHNOLOGY FOR CO₂ CAPTURE

Amine scrubbing was first patented in 1930 for the removal of acid gases (CO₂ and H₂S) from natural gas streams (Bottoms, 1930). It is the most mature technology for post-combustion carbon capture that can be deployed industrially in a relatively quick time scale (Rochelle, 2009). A typical amine scrubbing process for CO₂ capture is shown in Figure 1.1.

Desulfurized flue gas from coal combustion with 12% CO₂ enters the absorber from the bottom and counter-currently contacts with lean amine solvent entered from the top. 90% of CO₂ in the gas stream is picked up by the amine and the treated gas exits the top of the absorber. The rich solution goes through the heat exchanger and flows into the stripper, where it is further heated by a reboiler and CO₂ is released. The released CO₂ is then collected from the top of the stripper and compressed for utilization or sequestration, while the regenerated lean solvent is recycled back to the absorber for the next cycle.

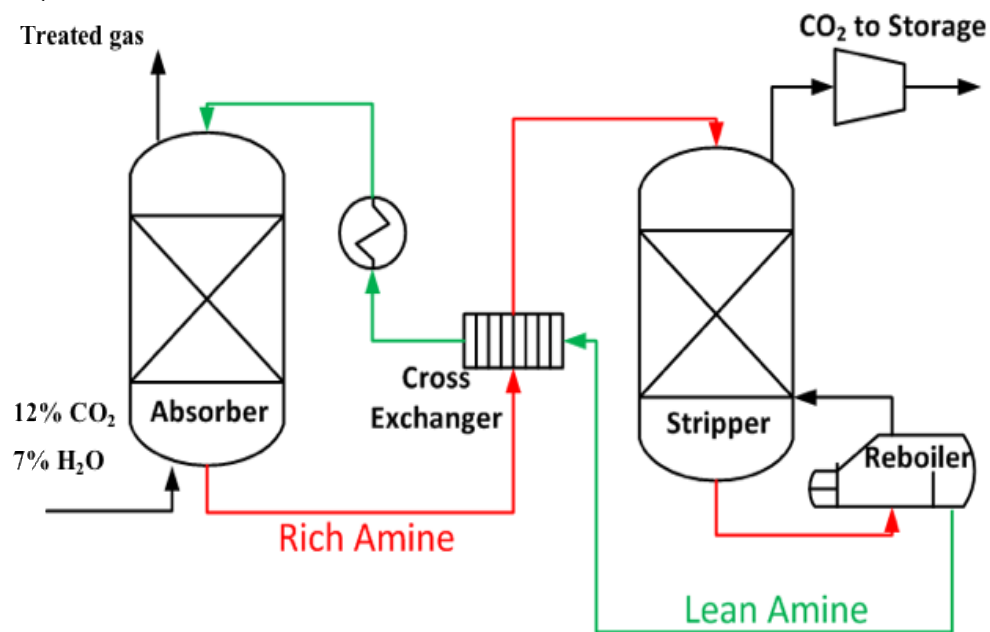


Figure 1.1: Process flow diagram of an amine scrubbing process for CO₂ recovery from coal-fired power plant flue gas.

As a post-combustion capture technology, amine scrubbing offers the opportunity to retrofit existing power plants. However, the overall cost of capture CO₂ including the capital cost of the equipment (CAPEX) and operating energy cost (OPEX) is still too high. Current estimation suggests a capture cost of at least 35 \$/ton CO₂, which is

equivalent to a 3-4 cents/kWh increase in electricity price to remove 90% CO₂ from 12% flue gas (Frailie, 2014). Since equipment capital cost and operating energy cost roughly equally share the total cost, current research efforts focus on 1) finding solvents with competitive chemical and physical properties to reduce equipment sizes; 2) optimizing process design to improve energy efficiency. Rigorous process optimization has improved the overall energy efficiency to 53%, so the margin for further energy reduction is small due to the thermodynamic limit (Lin, 2016). Also, as coal shifts from a base load electricity fuel source to a peak load electricity source, the capacity factor of coal fire power plants decreases, which means CAPEX will become more important than OPEX.

The two most expensive units of the capture plant are the absorber and the main cross exchanger. The absorber consists of about 30% of CAPEX, which is proportional to the required packing height. A greater mass transfer coefficient reduces the packing area at a given partial pressure driving force.

The main cross heat exchanger exchanges heat between the hot lean solvent and cold rich solvent. The heat duty is large, typically 3-5 times of the reboiler duty (Lin, 2016). Solvent properties including cyclic capacity, viscosity, thermal conductivity, and heat capacity determine the optimum size of the heat exchanger, as well as the sensible heat lost with the temperature driving force.

1.3 SOLVENT SELECTION CRITERIA

This work develops solvents that could potentially reduce amine scrubbing CAPEX and OPEX. The solvents fall into two major categories: aqueous piperazine (PZ) blends with other amines and semi-aqueous amines that consist of physical solvent,

water, and amines. Generally, the potential useful solvent should have all the following properties:

1. High CO₂ cyclic capacity

CO₂ cyclic capacity represents the amount of CO₂ removed per unit mass of solvent per cycle. With higher capacity, less solvent is required to circulate in the system to remove the same amount of CO₂. The capacity value directly relates to the sensible heat requirement for stripping, pump work, and the size and cost of the cross-exchanger (L. Li et al., 2013).

2. High mass transfer rate

The mass transfer rate/absorption rate (k_g') determines CO₂ removal in the absorber. With the same driving force, large k_g' reduces the amount of packing required for the same amount of CO₂ removal, which leads to smaller absorber size and lower capital cost. On the other hand, with a fixed amount of packing and CO₂ removal, larger k_g' allows a smaller driving force to be used and thus less energy use.

3. Low viscosity

The effect of viscosity is partially embedded in absorption rate. High viscosity will limit absorption rate due to low diffusivity of species in the solvent. In addition to that, a high viscosity also significantly reduces the heat exchanger performance and increases pumping cost.

4. Low amine volatility

High amine volatility can result in loss in the flue gas giving greater solvent make-up cost and potential environmental impacts. The amine emission in the treated gas must be handled as it can react in the atmosphere to form toxic compounds. Due to environmental hazards and regulations, larger water

wash units are required to capture fugitive amines prior to venting, which translates to higher capital and operating costs (Nguyen et al., 2010).

5. Resistance to thermal degradation

At high temperature, amines can degrade by different mechanisms, resulting in solvent makeup cost and potential EHS issues. The energy performance of the process generally improves with higher stripper operating temperature (Oyenekan and Rochelle, 2007), so good thermal stability at high temperature is preferred.

6. Resistance to oxidation

Oxidation is the degradation of the amine with the presence of oxygen in the flue gas. Oxidation causes the major amine loss in CO₂ capture process for coal-fired flue gas (Nielsen et al., 2013; Strazisar et al., 2003). Also, some oxidative degradation products are corrosive and toxic (Shao and Stangeland, 2009).

7. Low solvent cost

A large amount of solvent is required for large-scale CO₂ capture. For a 300 MW coal-fired power plant, solvent cost generally accounts for 5% of the total capital cost if the solvent is \$3/kg.

8. Good solid solubility in the liquid phase

Solid precipitation should be avoided in the process to maximize process reliability. As temperature and CO₂ concentration vary in the solution, precipitation could appear in some solvents.

The first two criteria: high CO₂ mass transfer rate (k_g') for small absorber and large CO₂ carrying capacity for low heat exchanger are mostly studied in solvent development. Viscosity also played a major role on both absorption rate and heat

exchanger performance. Dugas (2009) shows that 5 m PZ could have k_g ' 30% higher than 8 m PZ mostly due to lower viscosity. Pilot plant results show 5 m PZ use less energy than 8 m PZ (Chen, 2017). Normalized capacity that includes viscosity into cyclic capacity has been developed by Li(2013), which considers the viscosity effect on heat transfer coefficient.

1.4 SOLVENT DEVELOPMENT, AQUEOUS AMINE

Aqueous monoethanolamine (MEA) with a concentration of 15–40 wt % (patent by Bottoms, 1930) has been previously used in similar applications such as CO₂ removal from natural gas and hydrogen, which is the first generation benchmark solvent for flue gas CO₂ capture (Rochelle, 2009). Although amine scrubbing using MEA is a mature technology and has been used in the gas treating industry, the low CO₂ partial pressure (12 kPa) in flue gas leads to high capital and operating costs of the amine scrubbing unit. Current estimates suggest a 40–70% increase in the cost of electricity to remove 90% CO₂ from a coal-fired power plant (Rubin et al., 2007), which discourages the application of flue gas CO₂ capture.

Piperazine (PZ) has been proposed as the new benchmark for CO₂ capture, due to its superior properties (Rochelle et al., 2011). It has been extensively investigated in the Rochelle group (Dugas, 2009; Freeman et al., 2010; Closmann, 2011; Xu, 2011; Chen, 2011; Frailie 2014; Li, 2015; Du, 2016). 8 m aqueous PZ (40 wt%) has double the CO₂ absorption rate and capacity, remarkable resistance to oxidation and thermal degradation, and lower amine volatility than 30 wt % MEA. However, the low water solubility of PZ and its zwitterionic carbamate may cause precipitation under certain conditions in a process, limiting its industrial application (Freeman et al., 2010; Ma et al., 2012).

5 m aqueous PZ (30 wt%) could remediate the solid precipitation issue by lowering PZ concentration. Mass transfer rate in 5 m PZ is about 20% higher than that of 8 m PZ (Dugas, 2009). Also, the viscosity is reduced from 12 cP for 8 m to 4 cP for 5 m PZ, which improves the heat exchanger performance. Recently a pilot plant campaign at the University of Texas at Austin Pickle Research center demonstrated a 2.1–2.5 GJ/tonne CO₂ energy use of 5 m PZ with the advanced flash stripper (Chen et al., 2017). Solid precipitation is avoided in 5 m PZ in normal operation; however, when the CO₂ loading in the solvent is accidentally reduced to less than 0.2 mol CO₂/mol alkalinity, PZ starts to precipitate.

Efforts have been made to blend another useful amine with a smaller amount of PZ to mitigate the precipitation while maintaining the desired solvent properties of concentrated PZ (Chen and Rochelle, 2011; L. Li et al., 2013; Du, 2016). Among many PZ-based amine blends, PZ/N-methyl-diethanolamine (MDEA) (Chen et al., 2011), PZ/2-amino-2-methyl-1-propanol (AMP) (L. Li et al., 2013), and PZ/4-hydroxy-1-methylpiperidine (HMPD) (Du, 2016) have been identified as preferred compositions. However, PZ/MDEA was found to be significantly less thermally stable than PZ alone (Closmann, 2011). AMP was found to have high volatility (Nguyen et al., 2010), which is prohibitive for flue gas CO₂ capture. HMPD is 10-20 times the price of PZ, which prohibits large-scale application.

1.5 SOLVENT DEVELOPMENT, SEMI-AQUEOUS AMINE

Physical absorption is another CO₂ capture approach to absorb CO₂ under high pressure > 2MPa (Ban et al., 2014). Some widely used physical solvents are dimethyl ethers (Selexol[®]), methanol (Rectisol[®]), N-methyl-2-pyrrolidone (NMP), and 2-(2-ethoxyethoxy) ethanol (CARBITOL[™]), which all have good CO₂ physical solubility

(IEAGHG, 2008). Water-lean amines or semi-aqueous amines, consisting of amine, water, and physical solvent, are potentially attractive as they combine the advantages of chemical absorption and physical absorption. MEA in methanol-water (Usubharatana and Tontiwachwuthikul, 2009), MEA in glycerol-water (Shamiro et al., 2016), amines in N-functionalized imidazoles (Bara, 2013), N-methyldiethanolamine (MDEA) in methanol-water (Tamajon et al., 2016), and N-ethylmonoethanolamine (EMEA) in N,N-diethylethanolamine (DEEA) with/without water (Chen et al., 2015) are some recently studied semi-aqueous solvents. The CO₂ binding organic liquid (CO₂BOL) is another novel water lean solvent that takes high physical solubility of the solvent (Mathias et al., 2013; Zheng et al., 2016). Also, a commercial hybrid solvent developed by Shell containing MDEA, PZ, Sulfolane (as physical solvent), and water has been characterized by pilot plant testing (Nikolic et al., 2009). Heldebrant (2017) reviewed water-lean solvent and demonstrated that replacing water could increase k_g' , but most organic solvents except CO₂BOL are much more volatile than MEA and cannot be used in current amine scrubbing designs due to their high volatility.

1.6 RESEARCH OBJECTIVES

The first main objective of this work is to find a useful amine that reduces CO₂ capture CAPEX and OPEX. One approach is to blend a useful amine with less concentrated PZ to maintain the desired properties of concentrated PZ for CO₂ capture but alleviates the precipitation issue. Thermodynamic and kinetic properties of 2-methylpiperazine (2MPZ) blended with PZ were studied. A process model in Aspen Plus has been developed for simulation and optimization.

The effect of viscosity on both absorption rate and heat exchanger performance has been studied. An optimal concentration for 2MPZ/PZ has been found for high absorption rate and high normalized capacity.

Another category of solvent studied is the semi-aqueous amine composed of physical solvents, water, and amines that could potentially increase the absorption rate. Semi-aqueous MEA and PZ are characterized. Absorption rate and normalized capacity are explored.

The secondary objective is to estimate and compare the energy use of semi-aqueous amines with aqueous amines.

Another objective of this work is to understand the mass transfer behavior of CO₂ into the solvents. Scientifically, mass transfer modeling using penetration theory has been done to investigate the dependency of the CO₂ mass transfer rate on chemical and physical properties of amine solvents.

Chapter 2: Optimal Concentration of Aqueous 2MPZ and 2MPZ/PZ for CO₂ Capture¹

2.1 INTRODUCTION

Piperazine (PZ) has high absorption rate, good stability, low viscosity, and high capacity, while a narrow solid solubility window limits its application (Chen, 2011). Aqueous 2-methylpiperazine (2MPZ) and 2MPZ/PZ blend are attractive as they preserve most of the benefits of PZ and overcome its solubility issue. Chen (2011) studied 8 m 2-methylpiperazine (2MPZ) and 4 m/4 m 2MPZ/PZ. The solid solubility of 8 m 2MPZ and 4 m/4 m 2MPZ/PZ blend were good; however, the CO₂ absorption rate, k_g' was reduced to around 70% and 80% of that of 8 m PZ respectively. Dugas (2009) reported that the k_g' of 5 m PZ was approximately 30% higher than that of 8 m PZ. He believed that this increase was from lower viscosity in the more dilute solvent system.

This chapter presents amine screening results on two promising piperazine derivatives: 2methylpiperazine (2MPZ) and 1-(2-Hydroxyethyl)piperazine (HEP). The effect of concentration on CO₂ absorption rate and solvent regeneration cost were studied. As concentration goes up, free amine concentration increases, which should increase k_g' ; However, viscosity also increases, which depresses k_g' due to lower diffusivity of CO₂, amine, and amine products. High viscosity also decreases the heat transfer coefficient, resulting in larger heat exchanger area and greater capital cost. CO₂ solubility and absorption rate of 2,4,6,8 m 2MPZ, 2.5/2.5 m 2MPZ/PZ, and 3, 5, 7.7 m HEP were screened in the wetted wall column.

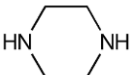
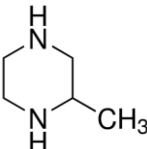
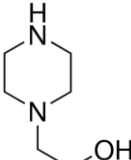
¹This Chapter is based on joint work with Brent Sherman, who contributed greatly to the modeling. Parts of this chapter have been published in the Energy Procedia: Yuan, Y., Sharman, B., Rochelle, G.T., (2016). Effects of viscosity on CO₂ absorption in aqueous piperazine/2methylpiperazine. Energy Procedia, Volume 114,2103-2120

Optimal concentration was found to be 4-6 m for 2MPZ and 2MPZ/PZ. The data allow thermodynamic and kinetics modeling of 2MPZ and 2MPZ/PZ in Chapter 3, and more rigorous optimization is presented in Chapter 3.

2.2 MATERIALS

The solvent was prepared by mixing chemicals gravimetrically. Initial chemical species are 2-methylpiperazine (98%, Sigma-Aldrich), piperazine (99%, Sigma-Aldrich), 1-(2-Hydroxyethyl)piperazine (99%, Sigma-Aldrich), and DDI water (100%, Millipore). To achieve each loading condition, CO₂ was added to the solvent by bubbling gaseous CO₂ (99.99%, Matheson Tri-Gas) into the solvent. The CO₂ absorption rate and CO₂ solubility were measured using the wetted wall column. The method is identical to that used by Chen (2011). Details about experiment method are in Appendix A.

Table 2.1: Amines tested in this work

Name	Chemical structure	Amine Conc. (m)
Piperazine(PZ)		5, 8
2methylpiperazine (2MPZ)		2, 4, 6, 8
PZ/2MPZ		2.5/2.5
1-(2-Hydroxyethyl)piperazine HEP		3, 5, 7.7

Composition of the solvents before adding CO₂ are listed in Tables below.
 Molality (m), mole of amine per kg of water was used through the whole work.

Table 2.2: Chemical species in 2 m 2MPZ

	Molecular weight (g/mol)	Mass (g)	wt %
2MPZ	100.2	260.4	16.70%
Water	18.02	1300	83.30%

Table 2.3: Chemical species in 4 m 2MPZ

	Molecular weight (g/mol)	Mass (g)	Wt %
(2MPZ)	100.16	600.96	28.60%
Water	18.02	1500	71.40%

Table 2.4: Chemical species in 6 m 2MPZ

	Molecular weight (g/mol)	Mass (g)	wt %
2MPZ	100.2	601.0	37.50%
Water	18.02	1000	62.50%

Table 2.5: Chemical species in 2.5 m/2.5 m 2MPZ/PZ

	Molecular weight (g/mol)	Mass (g)	Wt %
PZ	86.14	323.0	14.70%
2MPZ	100.2	375.6	17.10%
Water	18.02	1500	69.20%

Table 2.6: Chemical species in 3 m HEP

	Molecular weight (g/mol)	Mass (g)	wt %
HEP	130.19	429.6	28.10%
Water	18.02	1100	71.90%

Table 2.7: Chemical species in 5 m HEP

	Molecular weight (g/mol)	Mass (g)	wt %
HEP	130.19	651.0	39.40%
Water	18.02	1000	60.60%

Table 2.8: Chemical species in 7.7 m HEP

	Molecular weight (g/mol)	Mass (g)	wt %
HEP	130.19	751	50.0%
Water	18.02	750	50.0%

2.3 CO₂ SOLUBILITY

CO₂ solubility of 4 m 2MPZ and 2.5/2.5 m 2MPZ/PZ were measured at variable CO₂ loading across the lean and rich operating range at 20, 40, 60, 80 and 100 °C. 2 m and 6 m 2MPZ were only screened at 40 °C. The experimental data are attached in Appendix B. The CO₂ equilibrium pressure (P*) is plotted against loading in Figures below, which is normally referred as VLE curve or CO₂ solubility. P*_{CO2} increases as loading and temperature increase.

The VLE curve is used to determine lean and rich loading. For coal-fired power plant flue gas CO₂ capture, typical rich loading corresponds to 5 kPa P*_{CO2} and lean loading is 0.05-0.5 kPa. The VLE curves in different concentrations of 2MPZ or 2MPZ/PZ are slightly different. Smaller slope means greater loading difference between rich and lean loading. 2MPZ has higher cyclic capacity than PZ because 2MPZ is a hindered amine, which can absorb CO₂ by forming HCO₃⁻. The slope of the VLE curve of 4 m 2MPZ is smaller than that of 8 m 2MPZ. This is probably because more HCO₃⁻ will form in 4 m 2MPZ than in 8 m 2MPZ. Details about the speciation are in Chapter 3.

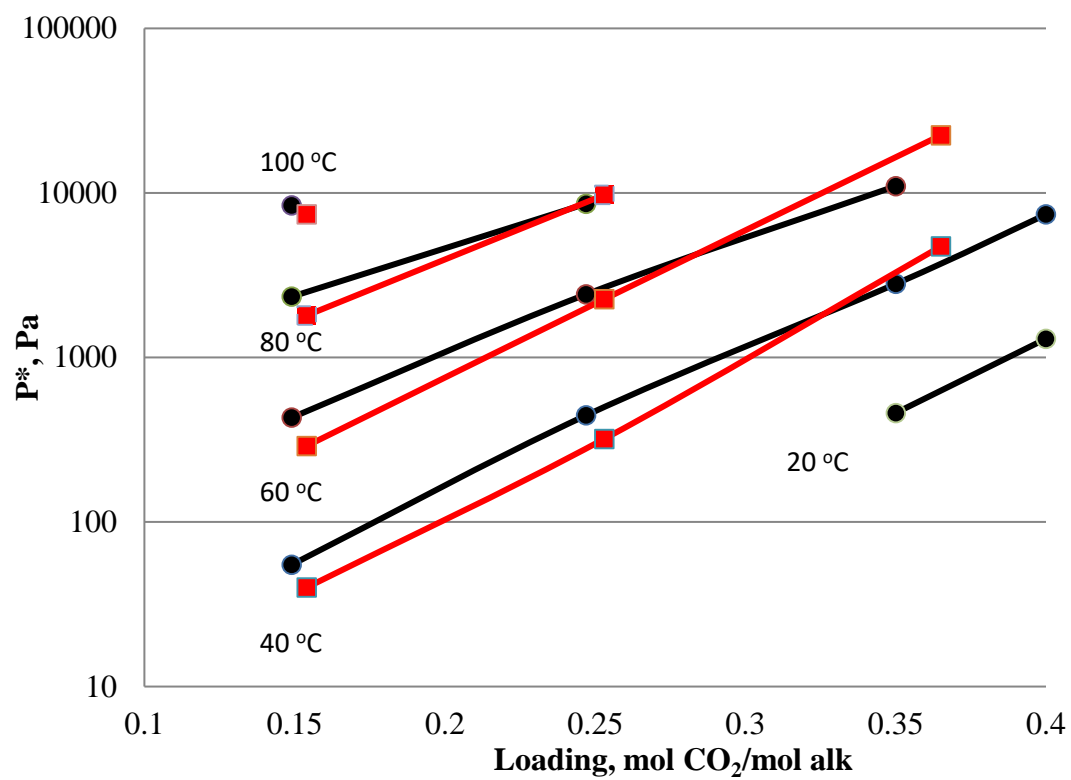


Figure 2.1: CO₂ equilibrium pressure in 4 m 2MPZ in black and 8 m 2MPZ (Chen, 2011) in red

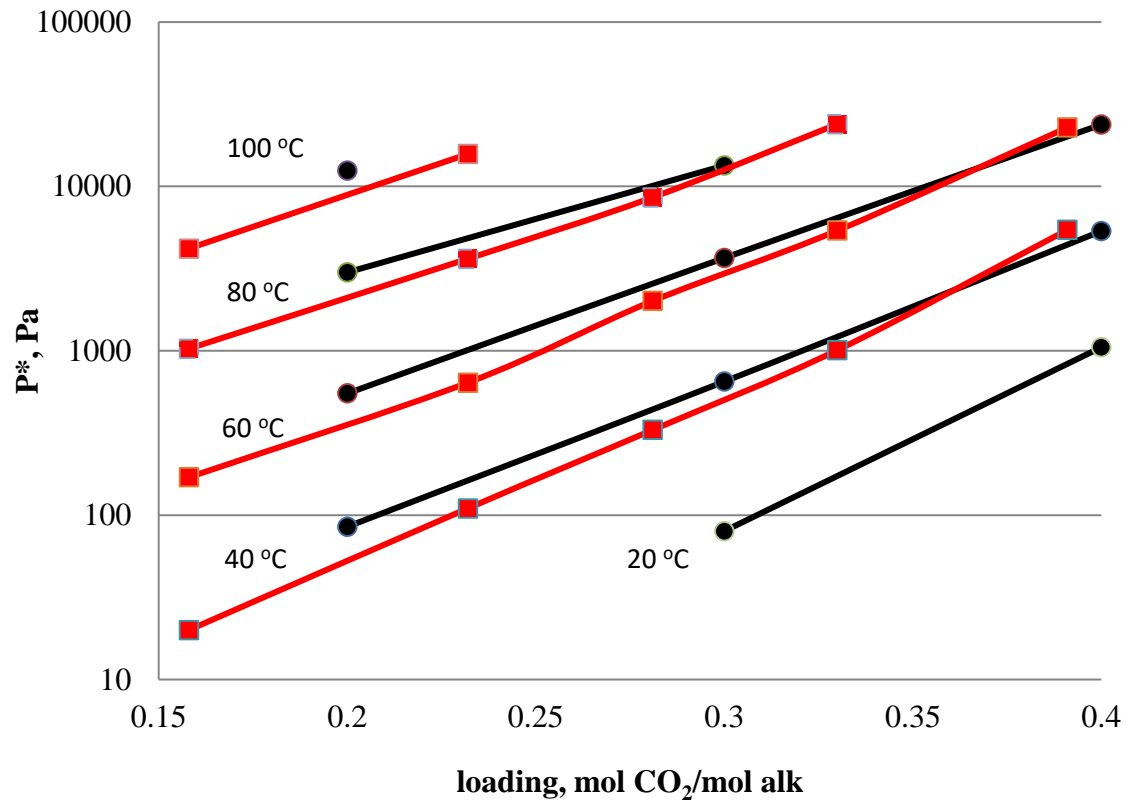


Figure 2.2: CO₂ equilibrium pressure in 2.5/2.5 m 2MPZ/PZ in black and 4/4 m 2MPZ/PZ (Chen, 2011) in red

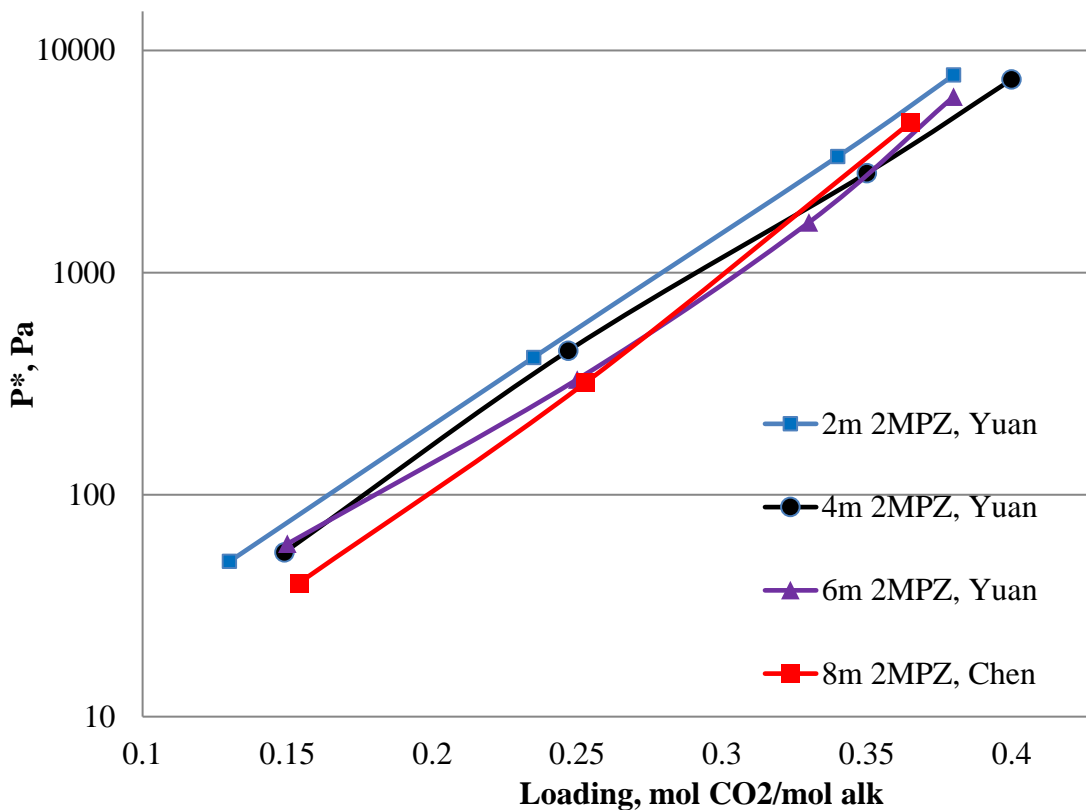


Figure 2.3: CO₂ equilibrium pressure at 40 °C in 2, 4, 6 m 2MPZ and 8 m 2MPZ (Chen, 2011)

Unlike 2MPZ, CO₂ solubility in different concentrations of HEP is the same. This is because 2MPZ is a hindered amine, but HEP is not. No or little HCO₃⁻ forms in CO₂-HEP-water. The calculated CO₂ cyclic capacities are 0.35, 0.46, and 0.6 mol CO₂/kg solvent for 3 m, 5 m, and 7.7 m, respectively. The capacity is much lower than PZ and 2MPZ with similar wt %, probably because the pK_a of the tertiary nitrogen in HEP is not high enough, and cannot act as a base. Also, the molecular weight of HEP is high, which reduces capacity of mole CO₂ per kg solvent.

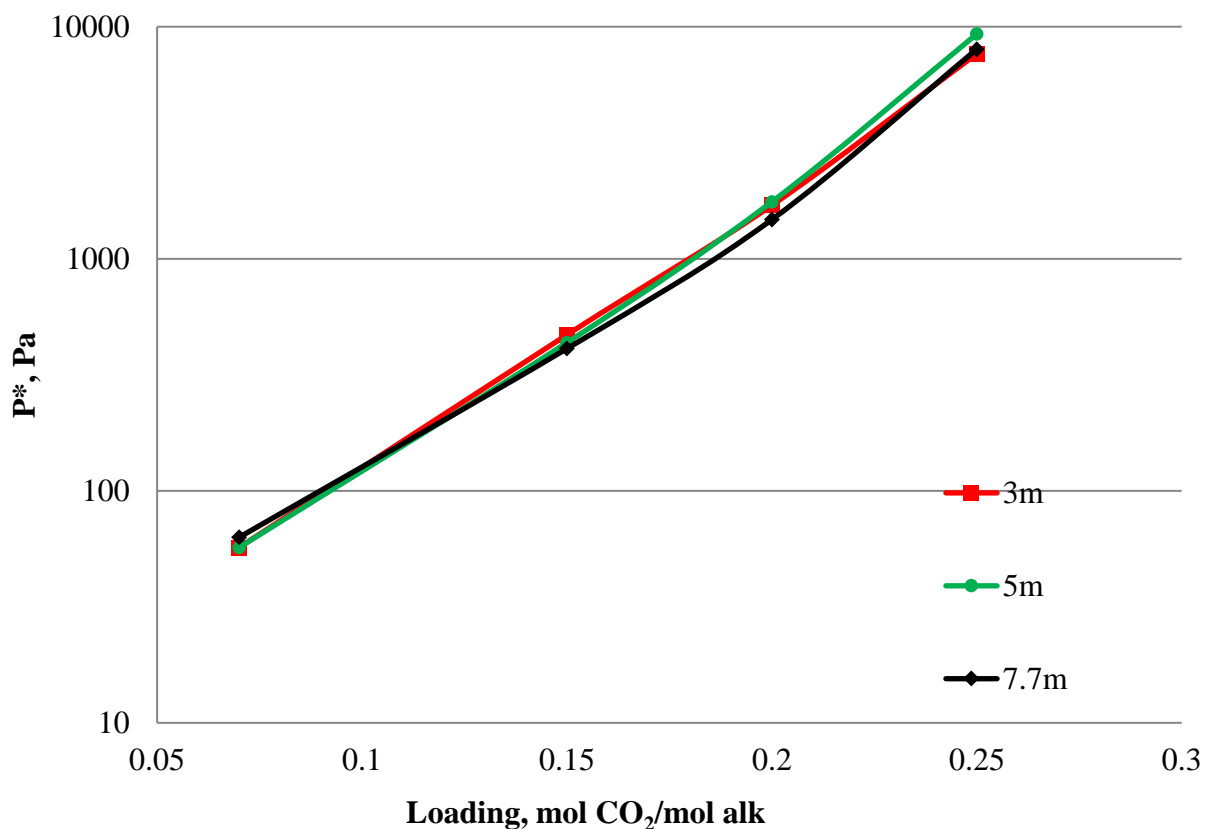


Figure 2.4: CO₂ equilibrium pressure at 40 °C in 3 m, 5 m, and 7.7 m HEP

2.4 CO₂ ABSORPTION RATE

CO₂ absorption rate, also called the liquid-film mass coefficient (k_g') of 4 m 2MPZ and 2.5/2.5 m 2MPZ/PZ at 20, 40, 60, and 80 °C are plotted in Figures 2.5 and 2.6. Compared to 8 m 2MPZ, 4 m 2MPZ shows higher k_g' when P^* is greater than 500 Pa. This should result from lower viscosity of 4 m 2MPZ. Also, less decrease in k_g' is observed in 4 m 2MPZ as temperature increases. Similar results are found in 2MPZ/PZ blend: k_g' is higher in 2.5/2.5 m than in 4/4 m. To compare k_g' of 2MPZ to other solvents on the same basis, k_g' is plotted against $P^*_{CO_2}$ at 40 °C instead of CO₂ loading.

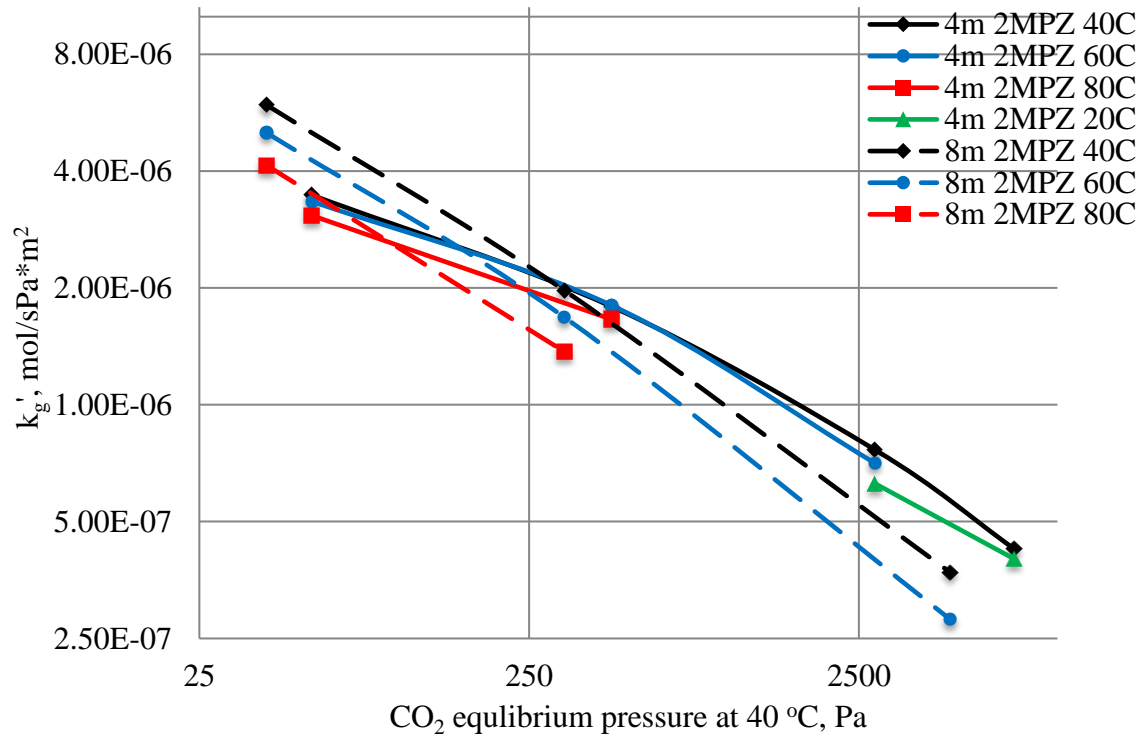


Figure 2.5: k_g' measured by the wetted wall column in 4 m 2MPZ and 8 m 2MPZ in dash (Chen, 2011)

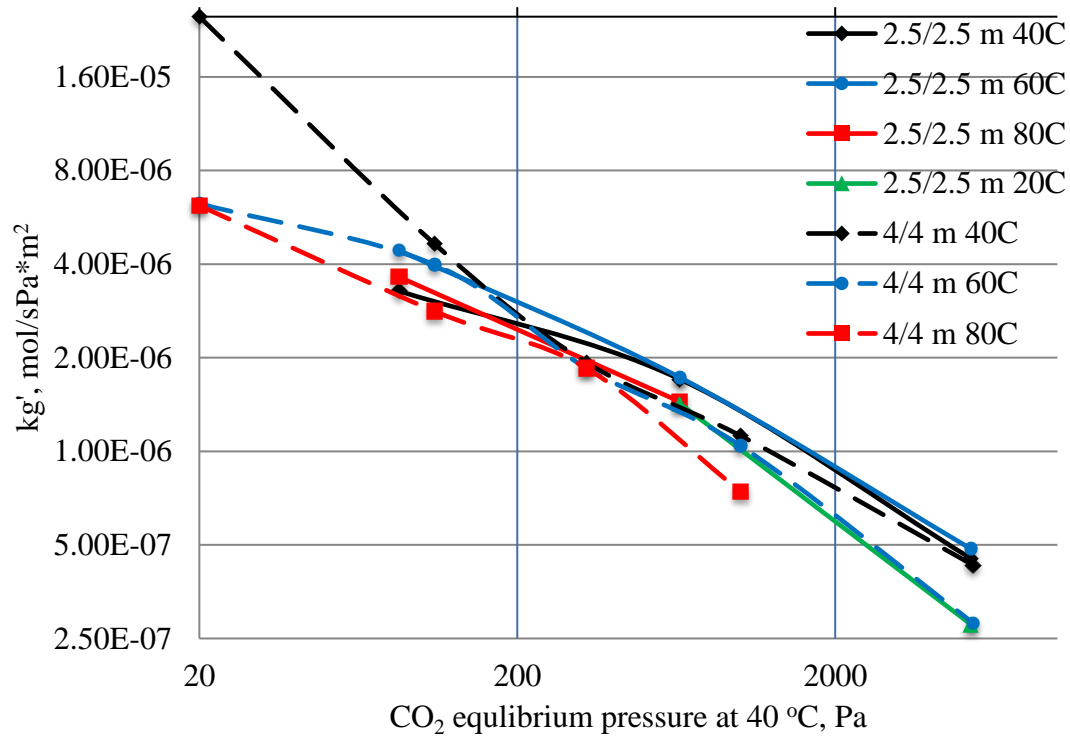


Figure 2.6: k_g' measured by the wetted wall column in 2.5/2.5 m 2MPZ/PZ and 4/4 m 2MPZ/PZ in dash (Chen, 2011)

k_g' of 2, 4, 6, 8 m 2MPZ at 40 °C is compared in Figure 2.7. In the operating range of P^* from 0.5 kPa to 5 kPa, 4 m 2MPZ shows the highest k_g' , followed by 6 m and 2 m 2MPZ, with 8 m 2MPZ the lowest. Equation 2.1 is the pseudo-first-order rate expression of k_g' . Assuming the chemical reaction rate (k_3) and physical solubility H_{CO_2} do not vary much as concentration changes, 2MPZ at high concentration seems to have greater k_g' due to higher free amine concentration; However, diffusivity is lower because of the higher viscosity in more concentrated solution. This implies an optimal concentration for k_g' .

$$k_g' = \frac{\sqrt{D_{CO_2} * k_3 * [amine]^2}}{H_{CO_2}} \quad 2.1$$

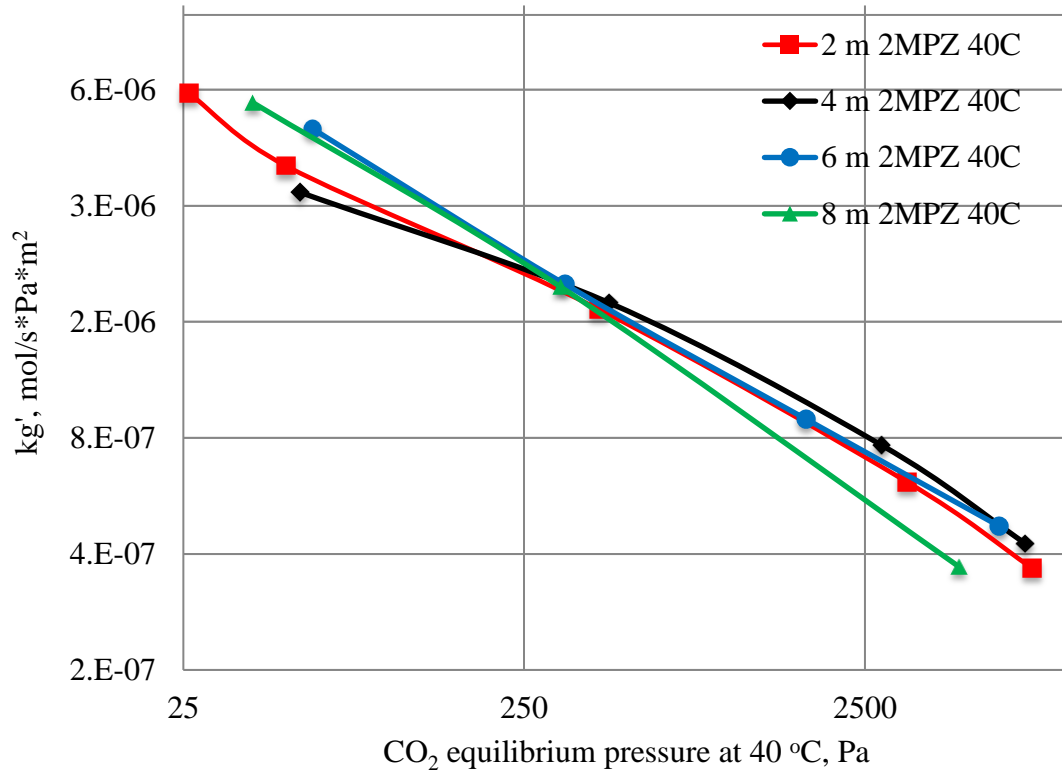


Figure 2.7: k_g' measured by the wetted wall column in 2 m, 4 m, 6 m, and 8 m 2MPZ at 40 °C

Figure 2.8 shows in HEP, similar to 2MPZ, at rich loading, k_g' decreases as concentration increases because viscosity depresses the absorption rate.

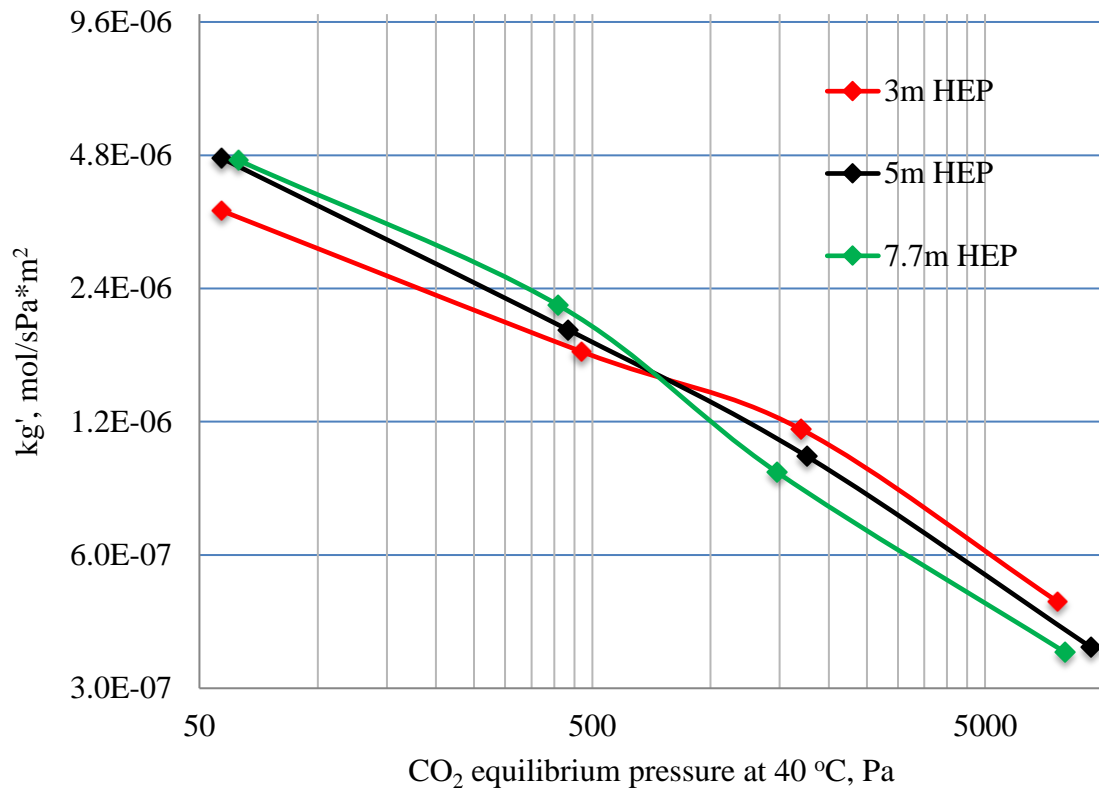


Figure 2.8: k_g' measured by the wetted wall column in 3, 5, and 7.7 m HEP at 40 °C

At 40 °C, the averaged liquid-film mass coefficient ($k_{g',avg}$) from P^* 0.5 to 5 kPa of 4 m 2MPZ is $8.3 \cdot 10^{-7}$ mol/s*Pa*m², higher than $7.1 \cdot 10^{-7}$ of 4 m/4 m 2MPZ/PZ blend, $5.9 \cdot 10^{-7}$ of 8 m 2MPZ, and is close to $8.5 \cdot 10^{-7}$ mol/s*Pa*m² of 8 m PZ. k_g' of 2.5/2.5 2MPZ/PZ is close to 4 m 2MPZ. To compare k_g' of these solvents on the same basis, k_g' is plotted against P^* at 40 °C in Figure 2.9. k_g' of 4 m 2MPZ and 2.5/2.5 2MPZ/PZ is greater than other concentrations, close to 8 m PZ, but is still smaller than 5 m PZ.

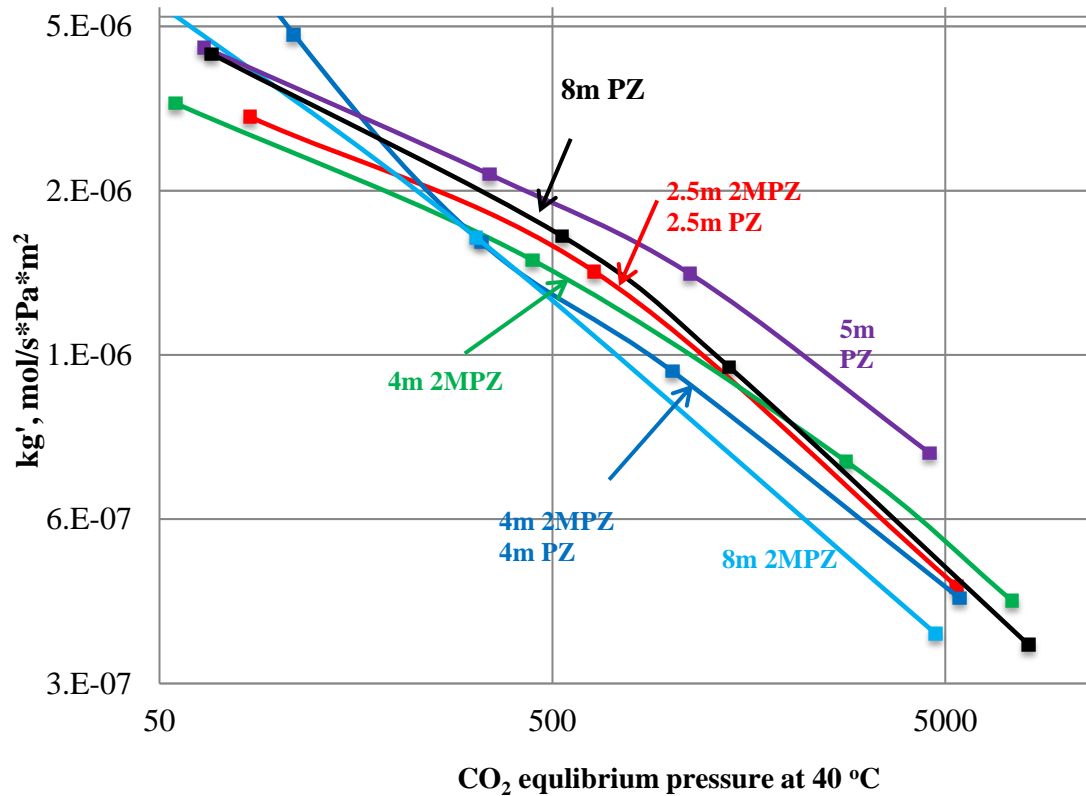


Figure 2.9: kg' in 4 m 2MPZ, 8 m 2MPZ, 5 m PZ, 8 m PZ, 2.5 m/2.5 m 2MPZ/PZ, and 4 m/4 m 2MPZ/PZ (Dugas, 2009; Chen, 2011).

2.5 EFFECT OF VISCOSITY

The solvent capacity is calculated using Equation 2.2, where the rich (α_{rich}) and lean (α_{lean}) loadings are 5 and 0.5 kPa $P^*_{CO_2}$ at 40 °C. As concentration increases, cyclic capacity increases. 2MPZ has higher cyclic capacity than PZ.

$$\Delta C = \frac{(\alpha_{rich} - \alpha_{lean}) * (mol\ alk)}{mass\ (amine + H_2O)} \quad 2.2$$

Cyclic capacity determines how much solvent needs to be circulated and is a direct indicator of heat exchanger duty and sensible heat requirement. Considering the

effect of viscosity on heat transfer coefficient in the cross heat exchanger, cyclic capacity is normalized by viscosity by Equation 2.3.

$$\Delta C_{\mu} = \frac{\Delta C}{\left(\mu_{\alpha mid} / \mu_{8mPZ}\right)^{0.175}} \quad 2.3$$

The heat transfer coefficient generally depends on solvent viscosity to about -0.35 power (Ayuh, 2003), which leads to -0.175 power on heat exchanger CAPEX and sensible heat requirement. Due to the rapidly increased viscosity, the normalized capacity in 2MPZ, PZ, 2MPZ/PZ from 5 m to 8 m does not increase as concentration increases. Although higher concentration has higher capacity, it does not necessarily result in a lower cost heat exchanger.

$k_g'_{avg}$ from $P^*_{CO_2}$ 0.5 to 5 kPa, CO_2 cyclic capacity, and normalized capacity in 2MPZ, PZ, and 2MPZ/PZ are calculated, listed in Table 2.9. Figure 2.10 plots these properties of 2MPZ versus concentration. When concentration goes up, viscosity and capacity increase, and normalized capacity and $k_g'_{avg}$ are maximized between 4 m and 6 m, and the values are comparable to results of 8 m PZ (Dugas, 2009) and 2.5/2.5 2MPZ/PZ.

Table 2.9: Capacity and $k_{g',avg}$ of 2MPZ and PZ at 40 °C

Conc. m	Amine	μ cP	Capacity mol CO ₂ /kg solvent	Normal. Capacity capacity/ $(\mu/\mu_{8mPZ})^{0.175}$	$k_{g',avg} * 10^7$ mol/s*Pa*m ²
2	2MPZ	2	0.38	0.5	7.3
4	2MPZ	3.8	0.68	0.83	8.3
6	2MPZ	7.5	0.75	0.81	7.9
8	2MPZ	16	0.84	0.82	5.9
2.5/2.5	2MPZ/PZ	5.1	0.76	0.88	8.0
5	PZ	4	0.63	0.73	11.3
8	PZ	12	0.79	0.79	8.5

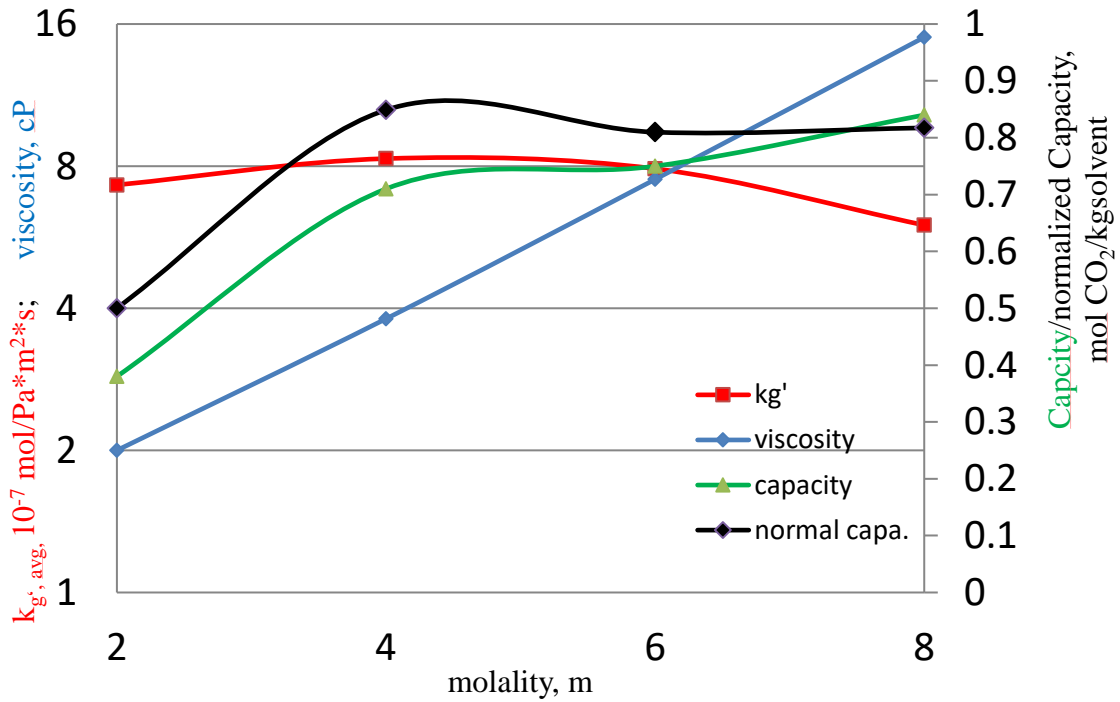


Figure 2.10: $k_{g'}$, viscosity, capacity, and normalized capacity of 2MPZ

2.6 CONCLUSION

2MPZ and PZ/2MPZ blend are competitive solvents, as they maintained the high absorption rate and remediate the solid solubility of PZ. 2MPZ has smaller k_g' than PZ, k_g' avg of 4 m 2MPZ and 2.5/2.5 m 2MPZ/PZ is similar to 8 m PZ, and 30% lower than 5 m PZ; However, the cyclic capacity is 15% higher than 5 m PZ. HEP has similar k_g' as 2MPZ, but the cyclic capacity is much lower.

2MPZ, PZ and PZ/2MPZ should be used at a total amine concentration of 5 m rather than 8 m, because the high solvent viscosity at high concentration depresses both CO₂ absorption rate and normalized capacity, and lower PZ concentration causes less precipitation.

Chapter 3: Rigorous Thermodynamic and Kinetic Modeling of 2MPZ and 2MPZ/PZ in Aspen Plus^{®2}

3.1 INTRODUCTION

Concentrated piperazine (PZ) and its derivative 2-methyl-piperazine (2MPZ), a moderately hindered secondary amine, are solvents of interest due to their multiple advantages over monoethanolamine (MEA), such as higher resistance to degradation, higher kinetic rates, and higher CO₂ cyclic capacity (Chen, 2011). PZ precipitation can be mitigated by lowering the PZ concentration or blending PZ with 2MPZ.

In Chapter 2, CO₂ cyclic capacity and absorption rate of 2 m, 4 m, and 6 m 2MPZ, and 2.5/2.5 m 2MPZ/PZ are measured by the wetted wall column. The results are compared to 8 m 2MPZ and 4/4 m 2MPZ/PZ data (Chen, 2011). For 2MPZ, the optimal concentration for lowest absorber cost (highest kg³) and lowest heat exchanger cost (highest normalized capacity) is around 5 m. 2MPZ/PZ was only measured by the WWC at 2.5/2.5 and 4/4 m. A rigorous thermal and kinetic model for 2MPZ and 2MPZ/PZ is desired for two reasons:

1. To predict the optimal concentration for 2MPZ/PZ;
2. To allow process simulation in Aspen Plus[®].

There are thermodynamic and kinetic models for both 2MPZ and 2MPZ/PZ (Chen, 2013; Sherman, 2013); however, these two models were built for 8 m amine, and cannot predict other concentrations accurately. Using the Aspen Plus[®] eNRTL framework, experiment results from Chapter 2, together with 8 m 2MPZ and 4/4 m 2MPZ/PZ data (Chen, 2011) are regressed to rebuild thermodynamic and kinetics models

²This Chapter is based on joint work with Brent Sherman, who contributed greatly to the modeling. Parts of this chapter have been published in the Energy Procedia: Yuan, Y., Sharman, B., Rochelle, G.T., (2016). Effects of viscosity on CO₂ absorption in aqueous piperazine/2methylpiperazine. Energy Procedia, Volume 114,2103-2120

of 2MPZ and 2MPZ/PZ for 2-8 m, 0.15-0.4 CO₂ loading, and 20–100 °C. With the model, CO₂ absorption rate kg', CO₂ cyclic capacity, and normalized capacity are compared from 2 m to 8 m.

3.2 MODELING METHOD

3.2.1 Thermodynamic Modeling

A thermodynamic model is the foundation of the mass transfer model. Together with a hydrodynamic model, these models comprise the basis of a process model. The electrolyte non-random two-liquid (e-NRTL) model in Aspen Plus® V8.8 was used to provide a rigorous, activity coefficient model. The vapor phase is modeled using Redlich-Kwong. Sequential regression methodology was employed. The method is identical to that used by Chen (2011), Sherman (2013), and Frailie (2014). The targeted accurate domain was $T = [20,160]$ °C, loading = [0.01, 0.5] mole CO₂/mole alk, and [Am] = [2, 8] m for 2MPZ, [1/1, 4/4] m for 2MPZ/PZ.

The methyl group attached to the ring of 2MPZ hinders one of the amino groups, which reduces the likelihood of linking CO₂ to the amino group to form hindered 2MPZ carbamate (2MPZCOO) and hindered H2MPZCOO zwitterion. The chemistry of the thermodynamic model was modified from that of Chen (2013) to improve the convergence. Proton and hydroxide ions were eliminated, and hindered 2MPZ carbamate and hindered H2MPZCOO zwitterion were not considered due to their insignificant concentrations. Parameters of the 2MPZ model were first updated, and then merged with PZ Independence model (Frailie, 2014) to build the 2MPZ/PZ model. The binary parameters for 2MPZ-H₂O were kept the same as the original 2MPZ model by Chen (2013). The regressed parameters in 2MPZ-H₂O-CO₂ were $\Delta_f G_i$ and $\Delta_f H_i$ for molecules, and $\Delta_f G_i^{\infty,aq}$ and $\Delta_f H_i^{\infty,aq}$ for ions, as well as some of the local contribution

terms of the excess Gibbs free energy function ($\tau_{i,j}/\tau_{j,i}$). This local contribution was partially calculated by Equation 3.1. α is the non-randomness parameter, and $\tau_{i,j}$ is the binary interaction parameter defined in Equation 3.2.

$$G = \exp(-\alpha\tau_{i,j}) \quad 3.1$$

$$\tau_{i,j} = C_{i,j} + \frac{D_{i,j}}{T} \quad 3.2$$

Table 3.1 summarizes all the significant species (molecules, cations, and anions) in the liquid phase. Using this table, it is possible to write out all e-NRTL parameters ($\tau_{i,j}$). Since they are asymmetric, molecule-cation/anion and cation/anion-molecule parameters differ ($\tau_{i,j} \neq \tau_{j,i}$). The default values are 10, -2 if the molecule is an amine and 8, -4 for other molecules, the same as for the PZ model (Frailie, 2014). For the 2MPZ/PZ thermodynamic model, two additional e-NRTL parameters that represent the interaction between PZ and 2MPZ species were regressed to fit 2MPZ/PZ VLE.

Table 3.1: Molecule and electrolyte components for e-NRTL parameters

i or j	j or i	
Molecule	Cation	Anion
Am		AmCOO-
HAmCOO	AmH+	AmCOO2--
CO ₂		HCO ₃ -
H ₂ O		CO ₃ --

Table 3.2 shows the CO₂ solubility data used for 2MPZ and 2MPZ/PZ thermodynamic regression. Nine parameters were regressed using 81 VLE data points, and seven viscosity parameters were used to fit 44 points by Equation 3.3. Two additional parameters were adjusted to make the activity coefficient of CO₂ in loaded

solution well behaved. As no activity coefficient of CO₂ (γ_{CO_2}) data were available for loaded solvent, the trends with loading and temperature were checked for reasonable behavior.

Table 3.2: Thermodynamic data for the 2MPZ system

Data Type	Points Regressed	Source	Notes
VLE, 8 m	20	Chen, 2013	WWC
High temp VLE, 8 m	7	Xu, 2011	Total pressure
VLE, 2 m, 4 m, 6 m	20	This work	WWC
VLE, 4 m/4 m	16	Chen, 2013	WWC
High temp VLE, 4 m/4 m	7	Xu, 2011	Total pressure
VLE, 2.5 m/2.5 m	11	This work	WWC
Total	81		

The viscosity was correlated by Equation 3.3.

$$\frac{\mu_{2MPZ}}{\mu_{H_2O}} = \exp \left\{ \begin{aligned} & [x_{2MPZ}(Ax_{2MPZ} + B)T + Cx_{2MPZ} + D] \\ & * [(Ex_{2MPZ} + FT + G)\alpha + 1] * \frac{1}{T^2} \end{aligned} \right\} \quad 3.3$$

Here x_i is mass fraction, μ_{H_2O} is the viscosity of water, α is loading in mol CO₂/mol alk, and A–G are adjustable parameters. Parameters were regressed in Excel[®] by minimization of the sum of relative errors (MSRE). The equation and regressed parameters were implemented as FORTRAN[®] subroutines.

3.2.2 Kinetic Modeling

The wetted wall column (WWC) experiment was simulated in Aspen Plus[®] by a packed column. The WWC interfacial area, diffusivity of amine-products, and gas-side resistance were implemented using custom FORTRAN[®] subroutines. At each temperature and loading, the WWC is operated at three desorption and three absorption

conditions. Only the strongest desorption and absorption fluxes were simulated as these have the least relative experimental error.

To account for the highly non-ideal nature of the solvent, the kinetics are modeled with activities as shown in Equation 3.4. k is the reaction constant and a_i is the activity of component i . k is computed using Equation 3.5.

$$r = k \prod_i a_i \quad 3.4$$

$$k = k_0 \exp \left[\left(\frac{-E_A}{R} \right) \left(\frac{1}{T} - \frac{1}{T_{ref}} \right) \right] \quad 3.5$$

Here k_0 is the reaction pre-exponential, E_A is the activation energy, R is the universal gas constant, and T_{ref} is set to 313.15 K. Table 3.3 lists the reactions in a 2MPZ/PZ system, and it has two types of reactions: kinetic and equilibrium. Equilibrium reactions are handled by the thermodynamic model calculating the excess Gibbs free energy. Kinetic reactions are a pair of forward and reverse reactions, where each reaction rate is calculated by Equation 3.4. The reaction pre-exponential k_0 is regressed for the forward reactions, while the reverse rate is backcalculated from the reaction equilibrium constant from the thermodynamic model. This ensures consistency with the thermodynamic model. The 2MPZ model only includes kinetic reactions 4–6, and the pre-exponential constants were regressed using sixty-four data points from 20 to 100 °C to fit the predicted flux to experimental flux. The 2MPZ/PZ model is constructed by combining the 2MPZ model with the PZ model (Frailie, 2014).

Table 3.3: Reaction set for 2MPZ/PZ.

Type	Stoichiometry	Reaction
kinetic	$\text{PZCOO}^- + \text{H}_2\text{O} + \text{CO}_2 \leftrightarrow \text{HPZCOO} + \text{HCO}_3^-$	1
kinetic	$2 \text{PZ} + \text{CO}_2 \leftrightarrow \text{PZH}^+ + \text{PZCOO}^-$	2
kinetic	$2 \text{PZCOO}^- + \text{CO}_2 \leftrightarrow \text{PZ}(\text{COO}^-)_2 + \text{HPZCOO}$	3
kinetic	$2\text{MPZCOO}^- + \text{H}_2\text{O} + \text{CO}_2 \leftrightarrow \text{H2MPZCOO} + \text{HCO}_3^-$	4
kinetic	$2 \text{2MPZ} + \text{CO}_2 \leftrightarrow 2\text{MPZH}^+ + 2\text{MPZCOO}^-$	5
kinetic	$2 \text{2MPZCOO}^- + \text{CO}_2 \leftrightarrow 2\text{MPZ}(\text{COO}^-)_2 + \text{H2MPZCOO}$	6
equilibrium	$2\text{MPZCOO}^- + 2\text{MPZH}^+ \leftrightarrow \text{H2MPZCOO} + 2\text{MPZ}$	7
equilibrium	$2\text{MPZ} + \text{HCO}_3^- \leftrightarrow 2\text{MPZH}^+ + \text{CO}_3^{2-}$	8
equilibrium	$2\text{MPZ} + \text{PZH}^+ \leftrightarrow 2\text{MPZH}^+ + \text{PZ}$	9
equilibrium	$\text{PZCOO}^- + \text{PZH}^+ \leftrightarrow \text{HPZCOO} + \text{PZ}$	10

The diffusivity of amine and products is assumed to be half the diffusion of free CO_2 , which is based on Sherman (2016).

$$D_{Am-Prod} = 0.5 * D_{CO2-soln} \quad 3.6$$

The diffusion of free CO_2 in solvent is shown in Equations 3.7 (Sherman, 2016).

$$D_{CO2-soln} = D_{CO2-water} \left(\frac{\mu_{water}}{\mu_{soln}} \right)^{0.8} \quad 3.7$$

$D_{CO2-water}$ (m^2/s) is the diffusivity of CO_2 in water defined in Equation 3.8 (Versteeg, 1988).

$$D_{CO2-water} = 2.35\text{E} - 06 * \exp\left(\frac{-2119}{T}\right) \quad 3.8$$

These kinetic reactions and diffusivities are calculated throughout the liquid boundary layer. The layer is discretized at thirty-two points. The experimental loading was adjusted to count the relative error of the absorption and desorption points. This has the effect of ensuring that at zero driving force, there is zero flux. This adjustment corrects for experimental errors as well any errors in the equilibrium model. Regression proceeds by changing the reaction pre-exponential to match the predict flux with the

experimental flux. The non-linear regression was done in MATLAB[®] using a response surface methodology (RSM) modified from Sherman (2016)

3.3 RESULTS

3.3.1 Viscosity

Viscosity of 4 m and 8 m 2MPZ at 20, 40, and 60 °C were measured and fitted, and the sum of relative errors was 0.25. Figure 3.1 shows the fit. The viscosity parameters are shown in Table 3.4.

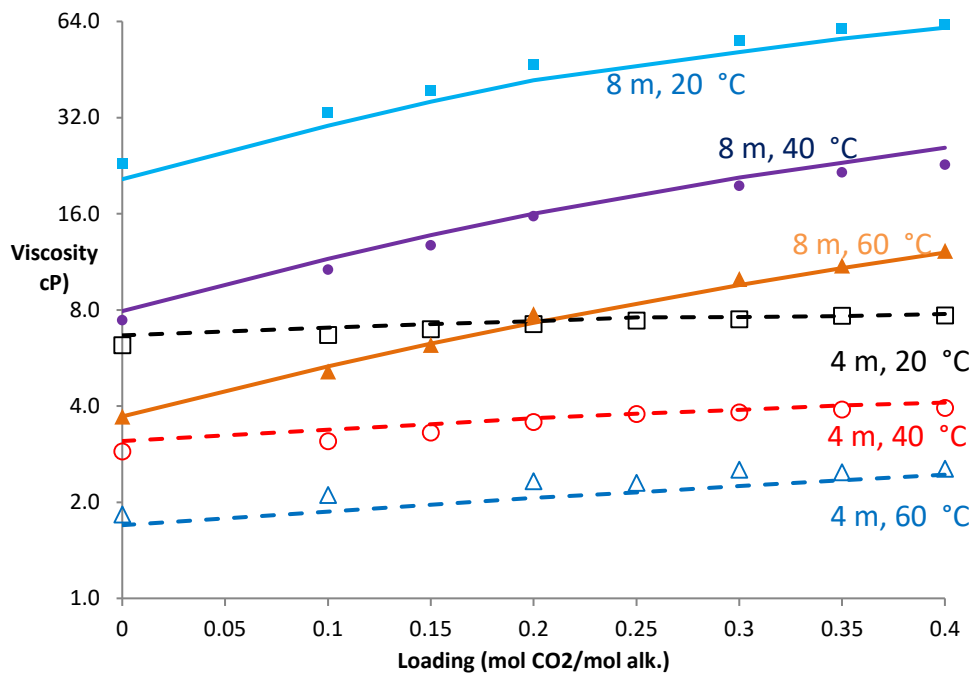


Figure 3.1: 4 m and 8 m 2MPZ viscosity. Solid Points: 8 m data; sold line: 8 m fitted; open points: 4 m data; dash line: 4 m fitted.

Table 3.4: Viscosity parameters for Equation 3.3.

Parameter	Value	Parameter	Value
a	387	e	7.34
b	-1836	f	1.23e-2
c	9.85	g	-5.07
d	1.07e6		

3.3.2 Thermodynamic Modeling Results

The parameters regressed to fit VLE are shown in Table 3.5. The standard deviations are insignificant compared to the values, which demonstrates a high confidence level in the regression results. The VLE fit in Figures 3.2 and 3.3 shows that the predicted and experimental data are matched. For 8 m 2MPZ, 40-100 °C data is from Chen (2013), and high temperature (120-160 °C) VLE data is from Xu (2011). An examination of correlations between these parameters shows that these parameters are not strongly correlated to each other. $\Delta_f G_i^{\infty,aq}$ and $\Delta_f H_i^{\infty,aq}$ of 2MPZCOO2-- were not regressed, because [2MPZCOO2--] is too low to produce meaningful regression results. $\Delta_f H_i^{\infty,aq}$ of 2MPZCOO2-- was obtained as an analogy of PZCOO2--, and $\Delta_f G_i^{\infty,aq}$ was manually adjusted to fit the NMR data measured by Chen (2013) shown in Figure 3.4. Since the concentration of dicarbamate is very small at lean loading, the uncertainty in the measured concentration is relatively high at lean loading.

Table 3.5: VLE parameters for 2MPZ with their standard deviation.

Parameter	Component i	Component j	J/kmol	Std. Dev.
$\Delta_f G_i^{\infty,aq}$	2MPZCOO-		-2.18E+08	5.11E+05
$\Delta_f G_i$	H2MPZCOO		-2.39E+08	1.97E+05
$\Delta_f G_i^{\infty,aq}$	2MPZCOO2--		-5.65E+08	n/a
$\Delta_f H_i^{\infty,aq}$	2MPZCOO-		-4.99E+08	1.62E+06
$\Delta_f H_i$	H2MPZCOO		-5.35E+08	1.86E+06
$\Delta_f H_i^{\infty,aq}$	2MPZCOO2--		-4.90E+08	n/a
$C_{i,j}$ ($\tau_{i,j} = C_{i,j} + \frac{D_{i,j}}{T}$)	(2MPZH+,2MPZCOO)	H2O	-3.87	0.09
	(2MPZH+,2MPZCOO)	2MPZ	-9.20	0.29
	(2MPZH+, HCO3-)	H2MPZCOO	-5.41	0.37

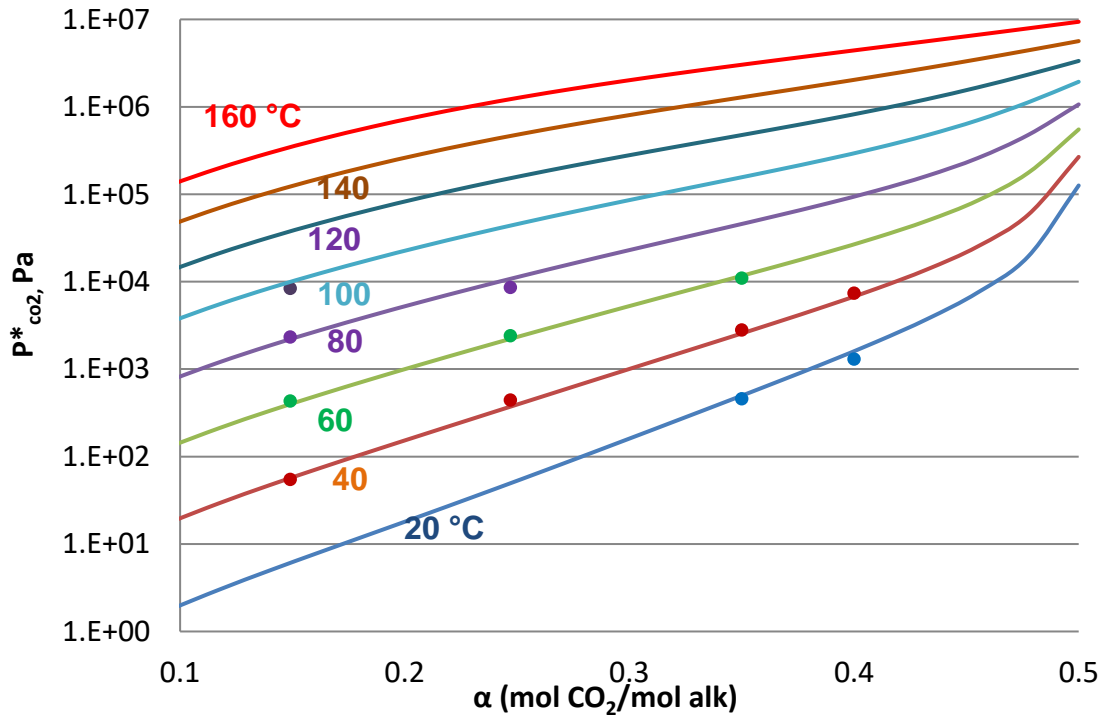


Figure 3.2: CO₂ solubility in 4 m 2MPZ. Lines: model prediction; Points: experimental results from WWC.

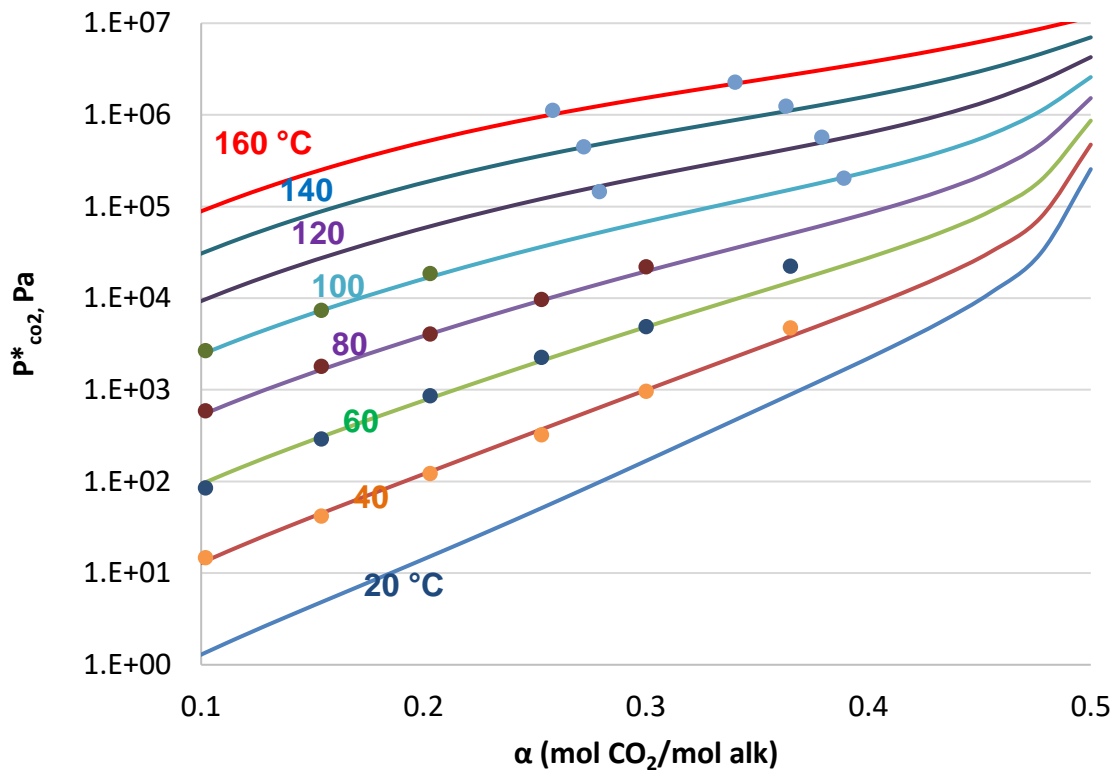


Figure 3.3: CO₂ solubility in 8 m 2MPZ. Lines: model prediction; Points: experimental data (Chen, 2013; Xu, 2011).

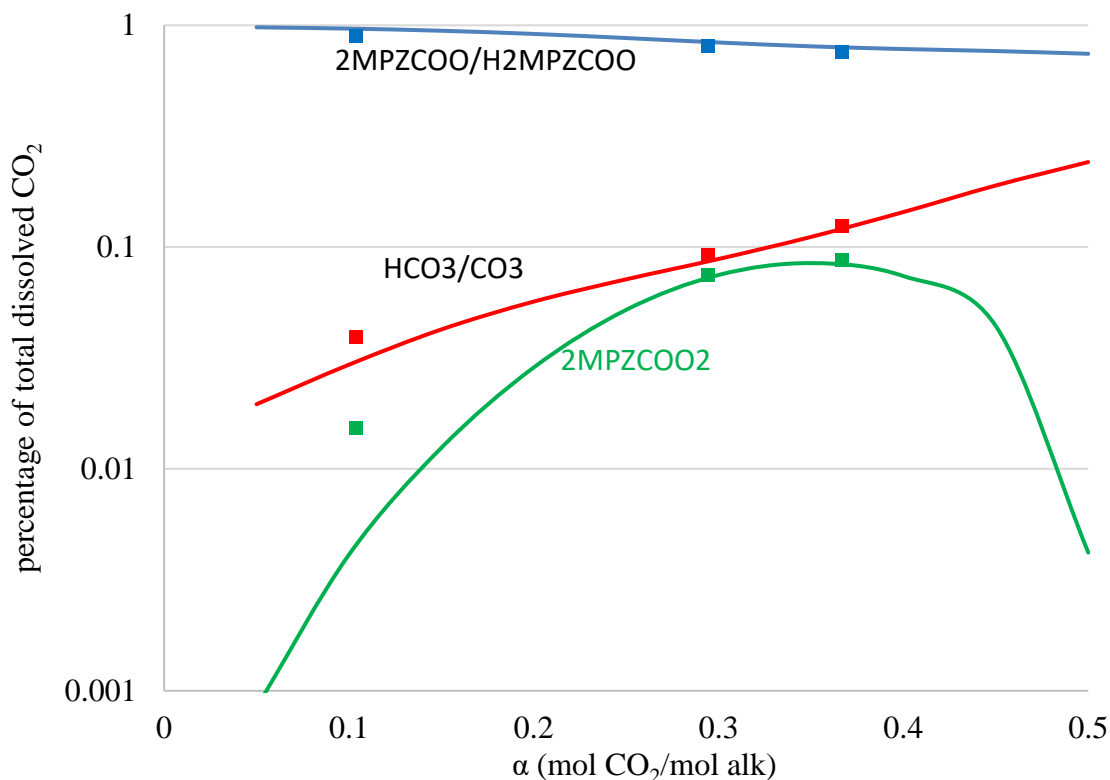


Figure 3.4: CO₂ distribution in loaded 8 m 2MPZ at 40 °C; Points: experimental data (Chen, 2013), lines: model prediction.

Figures 3.5 and 3.6 plot the fraction of all the species against CO₂ loading at 40 °C for 8 m 2MPZ and 4 m 2MPZ, respectively. At lean loading of 0 to 0.2 mol CO₂/mol alkalinity, the amount of 2MPZ decreases rapidly, while 2MPZH⁺ and 2MPZCOO⁻ increase at the approximately same rate. This indicates that 2MPZ is the dominant reacting species, which reacts with CO₂ and also acts as a base to catalyze the carbamate. As loading exceeds 0.2, the 2MPZCOO⁻ becomes another important base catalyzing the carbamate formation, hence a rapid rise of H₂MPZCOO is observed. 2MPZH⁺ also starts to react with CO₂ with the other available amino group, causing a drop in [2MPZCOO⁻] and [2MPZH⁺]. The amount of dicarbamate increases very slowly with

loading, peaks at 0.4 loading, and then drops again. Bicarbonate starts to form in the solution at a loading of 0.2 and increases rapidly after that. The ratio of bicarbonate to H₂MPZCOO and 2MPZCOO is higher in 4 m 2MPZ than in 8 m 2MPZ, which means more bicarbonate forms in 4 m 2MPZ. When bicarbonate forms, 1 mole CO₂/mol amino group is captured; while when carbamate forms, only 0.5 mole CO₂/mol amino group is captured. This explains why 4 m 2MPZ has the higher cyclic loading ($\alpha_{rich} - \alpha_{rich}$) than 8 m 2MPZ. The amount of each species present links the thermodynamic model to the kinetic model.

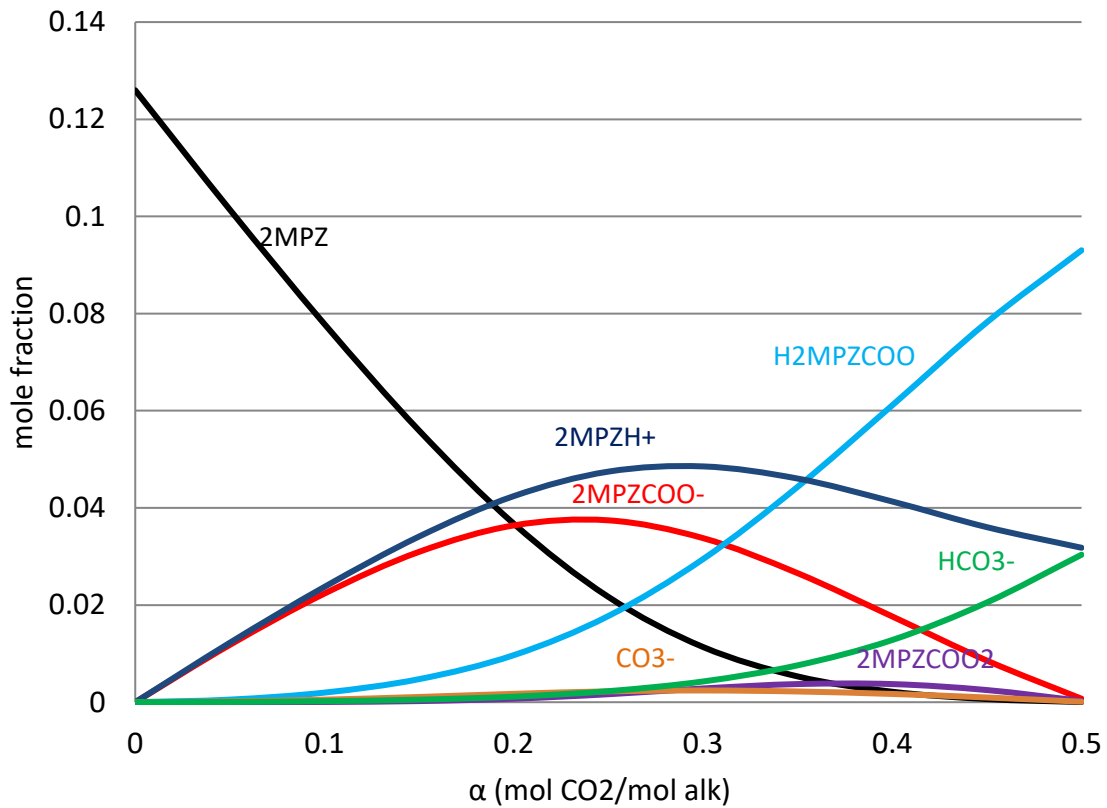


Figure 3.5: Predicted speciation of 8 m 2MPZ at 40 °C.

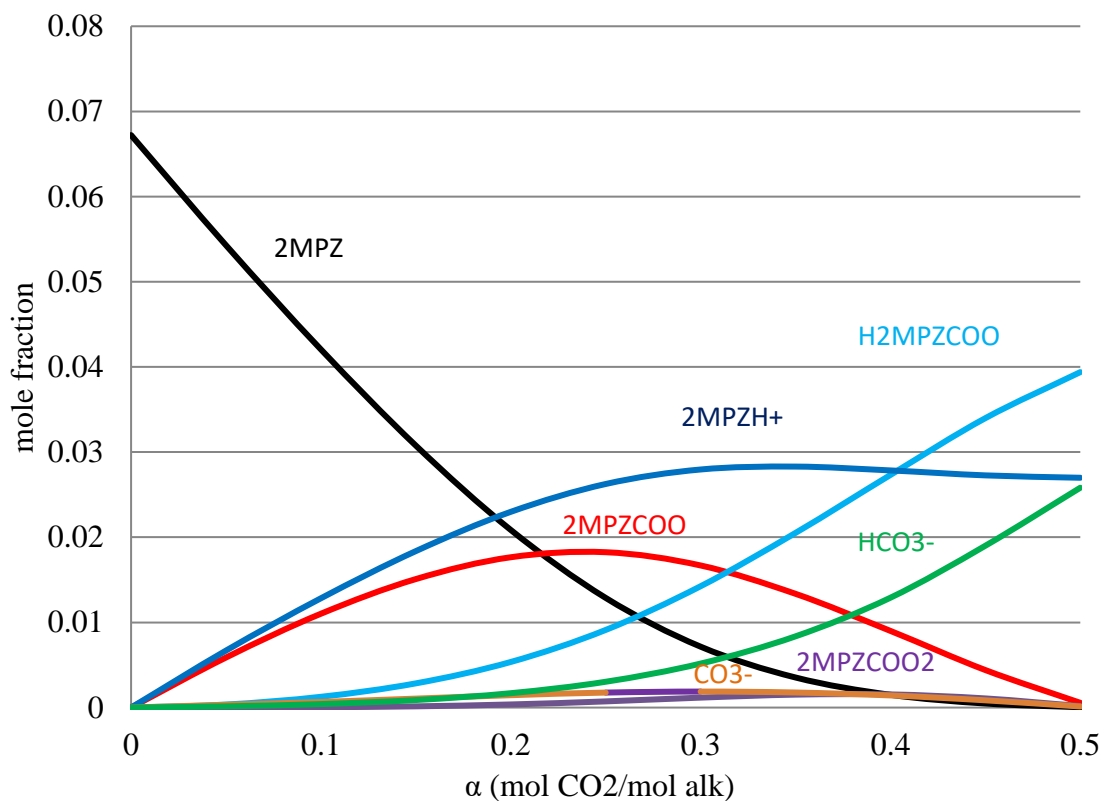


Figure 3.6: Predicted speciation of 4 m 2MPZ at 40 °C.

Based on this new 2MPZ model and the PZ model by Frailie (2014), 2 more parameters for eNRTL were regressed to get the best fit of CO₂ solubility data for 4/4 and 2.5/2.5 m 2MPZ/PZ, and results are summarized in Table 3.6. The standard deviation for each parameter is small compared to the final value. A comparison of VLE prediction by the model with experimental data is shown in Figures 3.7 and 3.8. The agreement between them is satisfactory.

Table 3.6: Additional parameters regressed for data of CO₂ solubility in 2MPZ/ PZ

Parameter	Component i	Component j	Value	Std dev.
A_{ij}	(2MPZH ⁺ ,PZCOO ²⁻)	H ₂ O	-5.14	0.29
	(2MPZH ⁺ ,HCO ₃ ⁻)	HPZCOO	-6.89	0.21

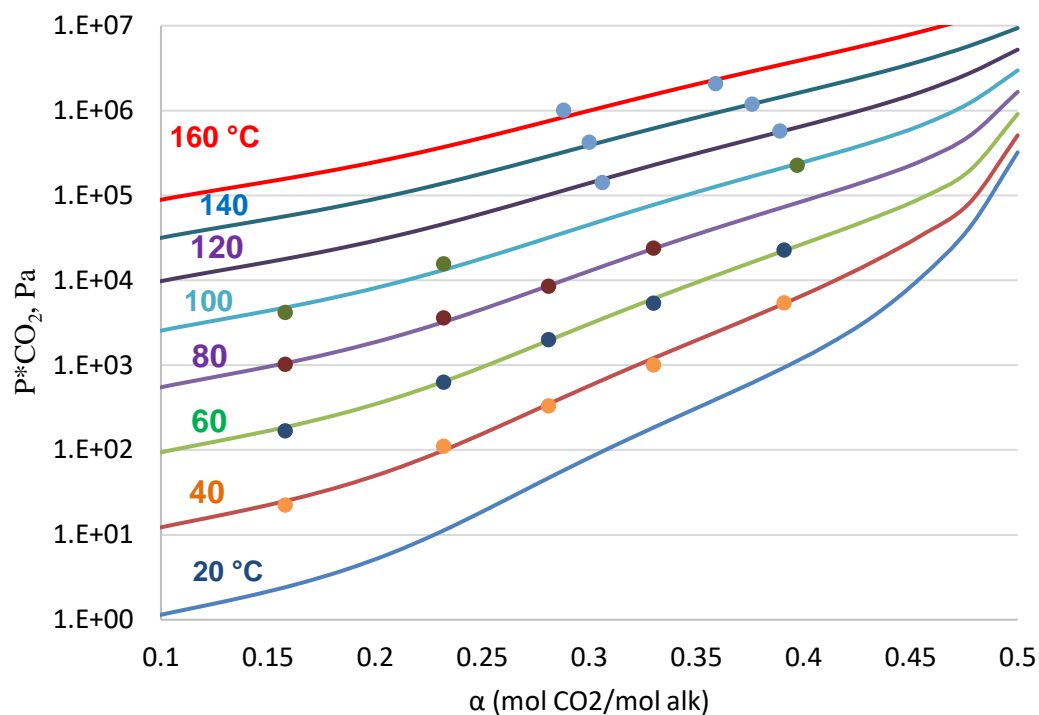


Figure 3.7: CO₂ solubility for 4 m 2MPZ/4 m PZ. Lines: model; Points: experimental data (Chen, 2013; Xu, 2011).

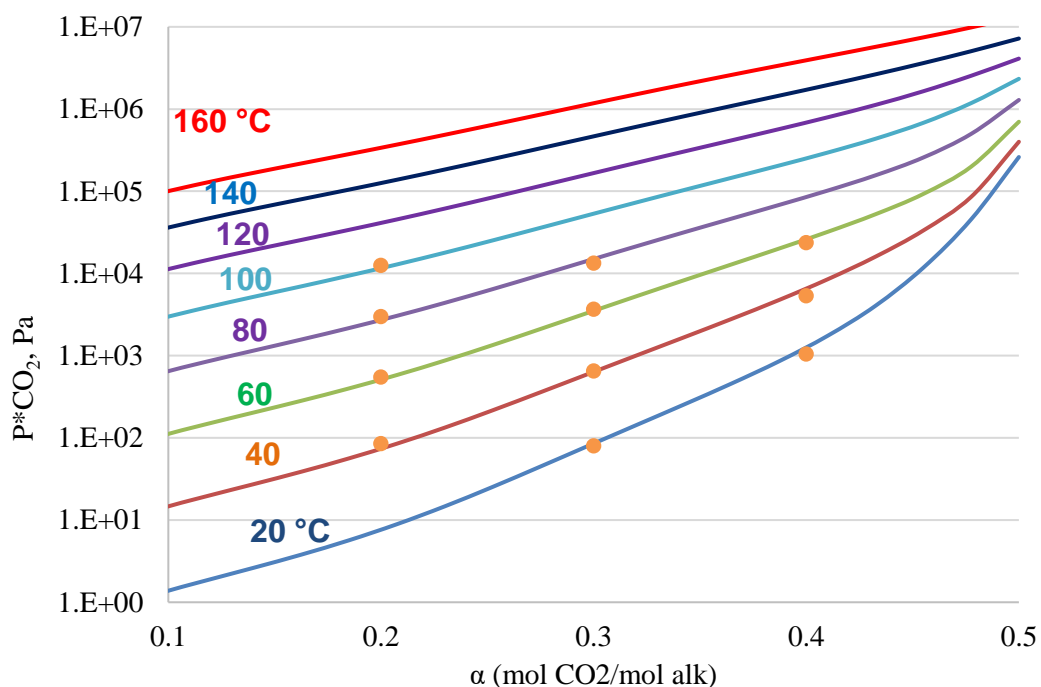


Figure 3.8: CO₂ solubility for 2.5 m 2MPZ/2.5 m PZ. Lines: model; Points: experimental data.

Speciation prediction from the model for 4/4 m 2MPZ/PZ at 40 °C is shown in Figure 3.9, and the speciation in 2.5/2.5 m 2MPZ/PZ is in Figure 3.10. At lean loading, CO₂ reacts with both PZ and 2MPZ to form carbamate. Since the pK_a of PZ is slightly higher than that of 2MPZ, [PZ] drops faster than [2MPZ], and more PZCOO⁻ and PZH⁺ are formed than 2MPZCOO⁻ and 2MPZH⁺. Both [2MPZ] and [PZ] drop quickly with loading and become depleted at around 0.4 loading. In the loading range of 0.2 to 0.4, [HPZCOO], [H₂MPZCOO], and [HCO₃⁻] increase rapidly while [PZCOO⁻] and [2MPZCOO⁻] drops quickly, which suggests that PZCOO⁻ and 2MPZCOO⁻ are the main species reacting with CO₂. [PZCOO₂²⁻] is maximized at 0.4 with a relatively small amount. [CO₃²⁻] and [2MPZCOO₂²⁻] are too low and hence omitted in the plot.

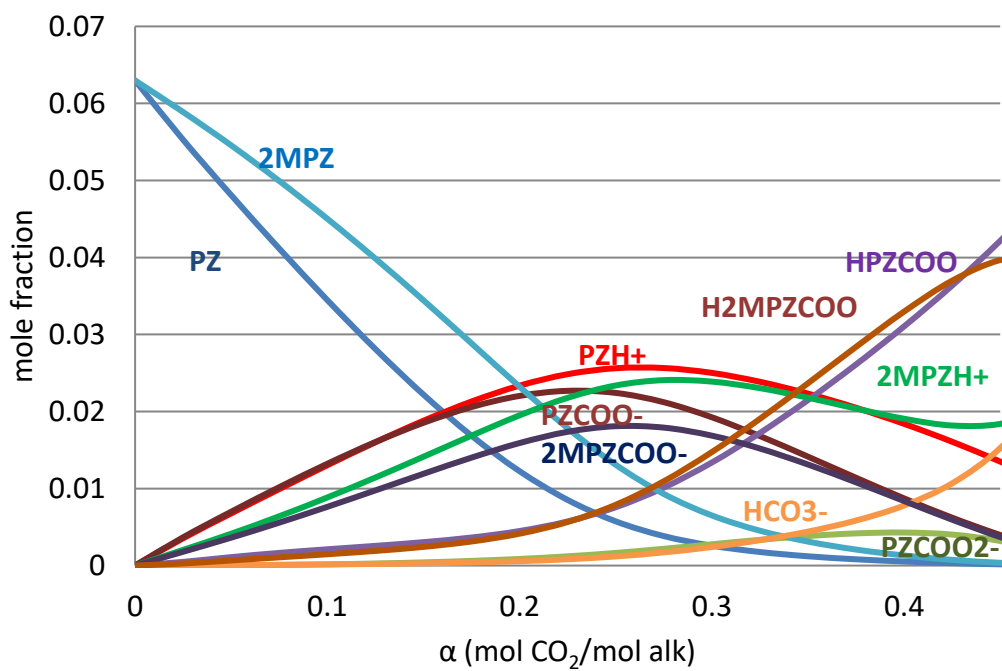


Figure 3.9: Speciation prediction for 4/4 m 2MPZ/PZ at 40 °C

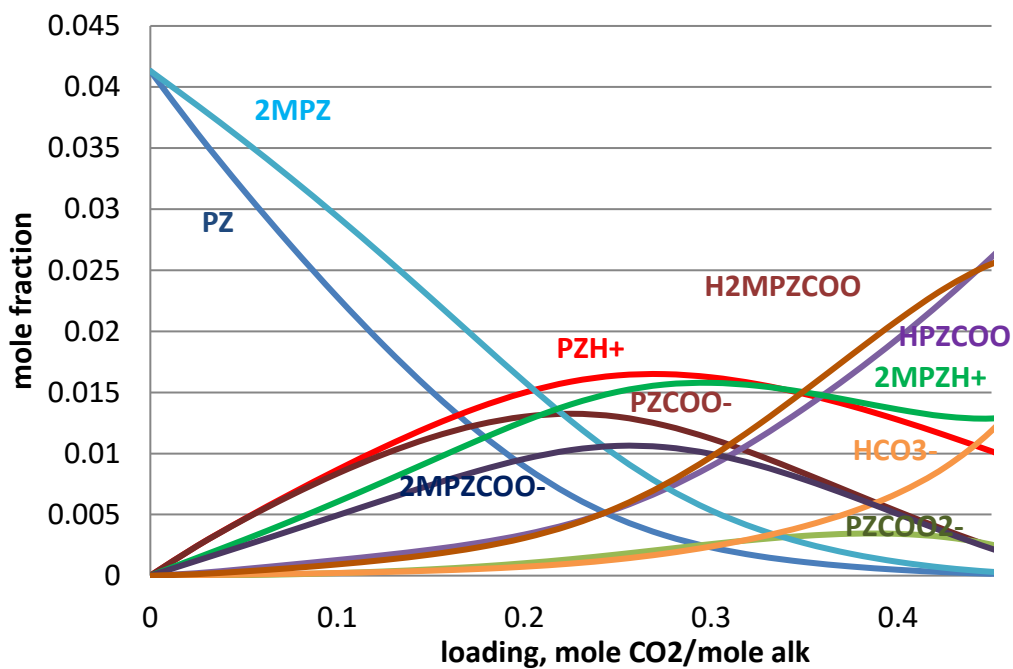


Figure 3.10: Speciation prediction for 2.5/2.5 m 2MPZ/PZ at 40 °C

3.3.3 Kinetic Modeling

A nonlinear regression method: Response Surface Methodology (RSM) adapted from Sherman (2016) is used to match predicted CO₂ flux with experimental flux. Table 3.7 lists the three regressed values for k_o and the standard deviations. The standard deviations are relatively small compared to the values. Activation energy (E_a) is left the same as the previous model by Chen (2013).

Based on the 2MPZ model, 2MPZ/PZ model is created by adding PZ reaction. Reaction parameters for PZ species are the same as Independence model by Frailie (2014). Table 3.8 shows all the reaction parameters.

Table 3.7: Regressed parameters for 2MPZ species

Stoichiometry		k_o (kmol/s-m ³)	
		fwd	Std. Dev.
2MPZCOO ⁻ + H ₂ O + CO ₂	↔ H2MPZCOO + HCO ₃ ⁻	2.71E+08	5.54E+07
2 2MPZ + CO ₂	↔ 2MPZH ⁺ + 2MPZCOO ⁻	2.34E+10	2.38E+09
2 2MPZCOO ⁻ + CO ₂	↔ 2MPZ(COO ⁻) ₂ + H2MPZCOO	2.79E+10	1.49E+10

Table 3.8: Reaction parameters for reactions.

Stoichiometry		k_o (kmol/s-m ³)		E_A (10 ⁴ J/mol)	
		Fwd	rev	fwd	rev
PZCOO ⁻ + H ₂ O + CO ₂	↔ HPZCOO + HCO ₃ ⁻	2.20E+04	9.74E+01	4.90	7.37
2 PZ + CO ₂	↔ PZH ⁺ + PZCOO ⁻	2.04E+10	4.27E+03	1.42	8.51
2 PZCOO ⁻ + CO ₂	↔ PZ(COO ⁻) ₂ + HPZCOO	2.76E+10	2.63E+05	1.42	8.93
2MPZCOO ⁻ + H ₂ O + CO ₂	↔ H2MPZCOO + HCO ₃ ⁻	2.71E+08	3.17E+05	5.80	10.7
2 2MPZ + CO ₂	↔ 2MPZH ⁺ + 2MPZCOO ⁻	2.34E+10	1.10E+05	2.20	9.55
2 2MPZCOO ⁻ + CO ₂	↔ 2MPZ(COO ⁻) ₂ + H2MPZCOO	2.79E+10	5.65E+06	2.20	13.3

The ratio of predicted flux over experimental flux is plotted against loading in Figures 3.11 and 3.12, showing no bias with increasing loading or concentration. The error is less than 15% for 2MPZ, and less than 25% for 2MPZ/PZ. Each point is a

WWC run containing both absorption and desorption cases. The temperature of the cases varies from 20 to 100 °C. No bias on temperature is found, suggesting good estimation on Ea.

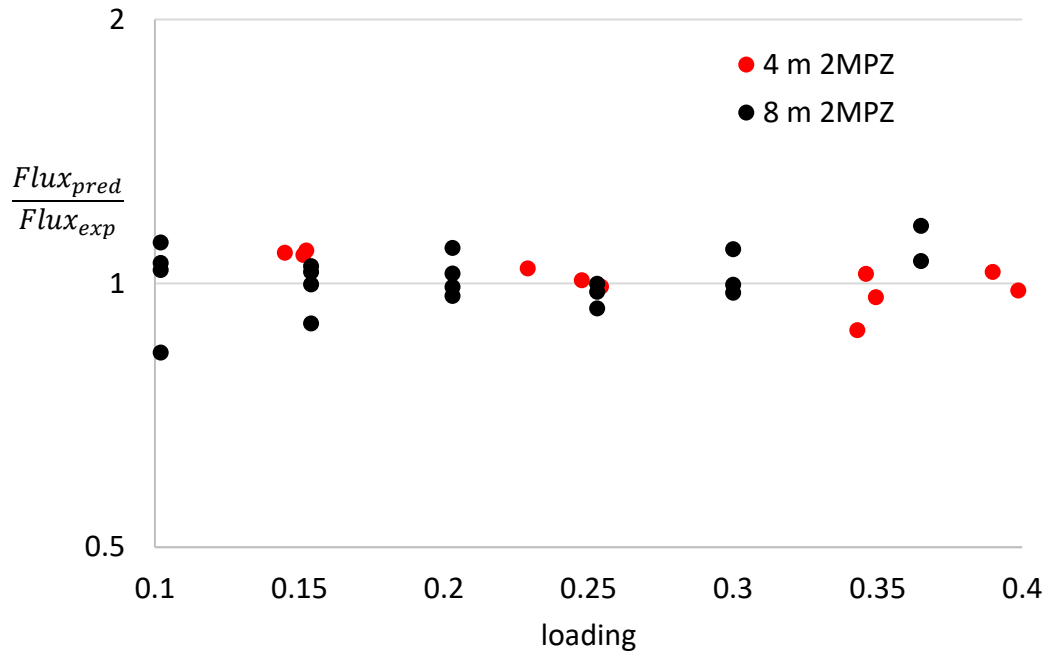


Figure 3.11: Flux Predictions ratioed to experimental data. Black for 8 m, red for 4 m 2MPZ

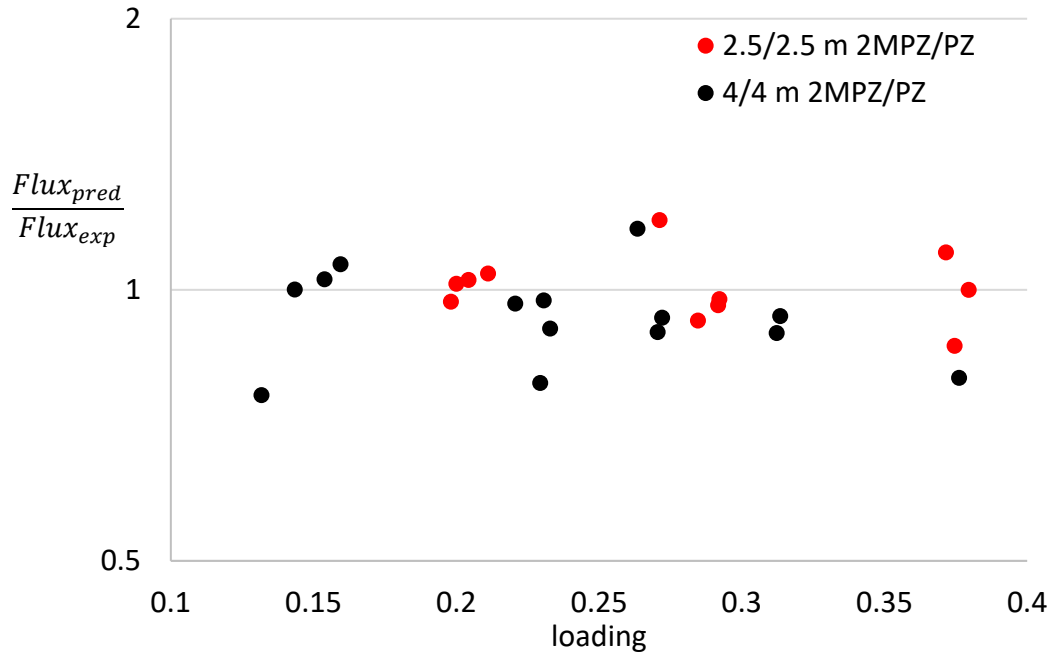


Figure 3.12: Flux Predictions ratioed to experimental data. Black for 4/4 m, red for 2.5/2.5 m 2MPZ/PZ

3.3.4 Effect of viscosity

The CO₂ partial pressure at 40 °C is set to be 50 Pa in lean solvent and 5000 Pa in rich solvent. The average CO₂ absorption rate, $k_g'_{avg}$, CO₂ capacity, and normalized capacity in 2MPZ, PZ, and 2MPZ/PZ are calculated using the thermodynamic and kinetics model, and the results are plotted against concentration in Figures 3.13, 3.14, and 3.15. As amine concentration increases, k_g' increases to the maximum at around 5 m, and then drops. By Pseudo First Order approximation (PFO), Equation 3.9, besides concentration, k_g' also depends on diffusivity. At higher concentration, the viscosity increases rapidly, which reduces the diffusivity of amine-product, hence lower k_g' . k_g' determines the absorber packing height, which dominates the absorber capital cost.

$$k_g' \approx \frac{\sqrt{D_{CO_2} k_2 [Am]_b}}{H_{CO_2}} \quad 3.9$$

The solvent capacity is calculated using Equation 3.10, where the rich (α_{rich}) and lean (α_{lean}) loadings correspond to $P_{CO_2^*}$ of 5 and 0.05 kPa at 40 °C. As concentration increases, capacity increases.

$$\Delta C = \frac{(\alpha_{rich} - \alpha_{lean}) * (mol\ alk)}{mass\ (amine + H_2O)} \quad 3.10$$

This capacity does not account for viscosity. Considering the effect of viscosity on the heat exchanger cost leads to normalized capacity as in Equation 3.11 (Du, 2016). The heat transfer coefficient generally depends on solvent viscosity to about -0.35 power (Ayub, 2003), which leads to -0.175 power in Equation 3.11. Here α_{mid} is the middle loading between the rich and lean loading at 40 °C. Due to the rapidly increased viscosity, the normalized capacity in 2MPZ, PZ, 2MPZ/PZ from 5 m to 8 m does not increase as concentration increases. Normalized capacity, rather than capacity determines heat exchanger capital cost and sensible heat required. Although increasing concentration increases capacity, it does not necessarily result in a lower solvent regeneration cost on the heat exchanger.

$$\Delta C_{\mu} = \frac{\Delta C}{\left(\mu_{\alpha_{mid}} / \mu_{8mPZ}\right)^{0.175}} \quad 3.11$$

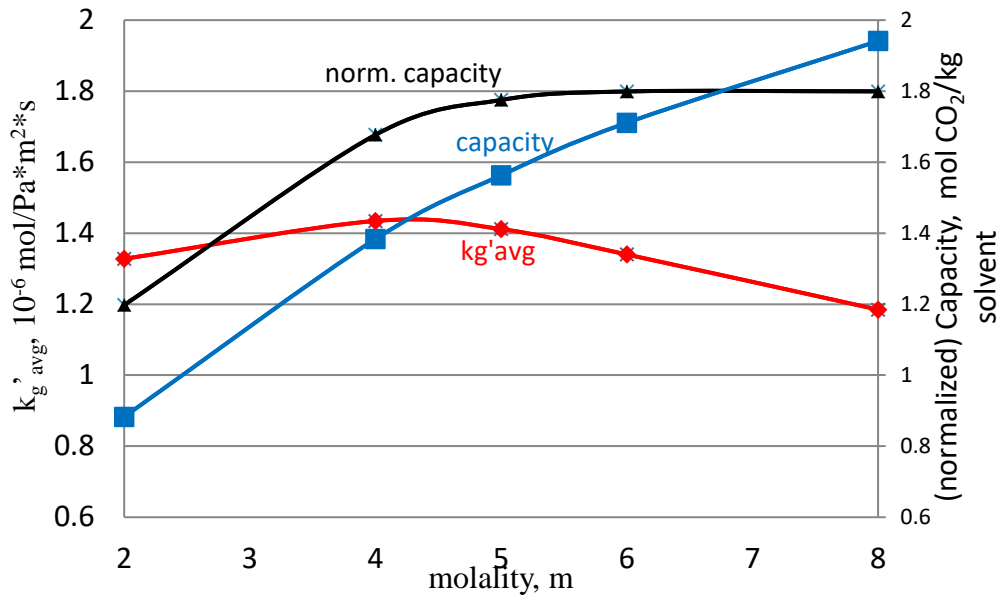


Figure 3.13: Predicted kg'_{avg} (left y-axis), ΔC , ΔC_u (right y-axis) in 2MPZ, operation condition 50-5000 Pa at 40°C

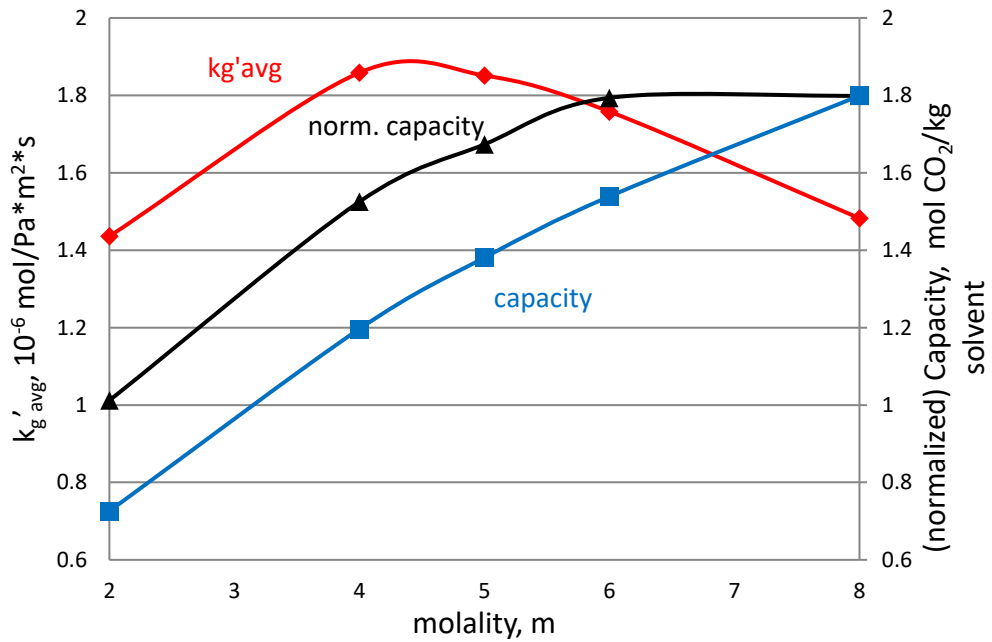


Figure 3.14: Predicted kg'_{avg} (left y-axis), ΔC , ΔC_u (right y-axis) in PZ, operation condition 50-5000Pa at 40°C

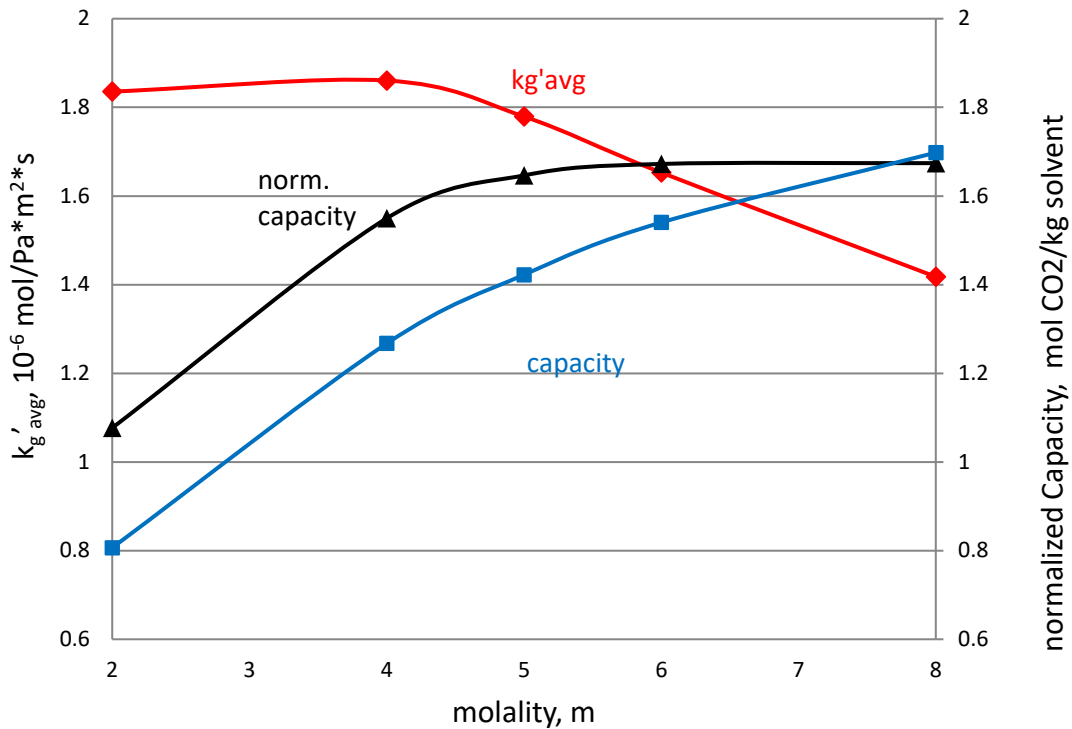


Figure 3.15: Predicted kg'_{avg} (left y-axis), ΔC , ΔCu (right y-axis) in 2MPZ/PZ, operation condition 50-5000Pa at 40°C

Figure 3.16 plots kg'_{avg} against normalized capacity for 2MPZ, PZ, and 2MPZ/PZ. PZ has high kg' and normalized capacity; 2MPZ has high normalized capacity, no solubility issues, but smaller kg' ; 2MPZ/PZ has high kg' but the normalized capacity is smaller. Higher kg'_{avg} reduces absorber cost, and higher normalized capacity lowers heat exchanger cost and sensible heat, so the solvent on the top right corner of the figure has lower cost for both the absorber and the heat exchanger. As a result, for 2MPZ, PZ, and 2MPZ/PZ, 5 m is better than 8 m. PZ is cheaper than 2MPZ; however, if solid precipitation issue of 5 m PZ is a concern, the 2.5/2.5 m blend or 5 m 2MPZ is a good alternative.

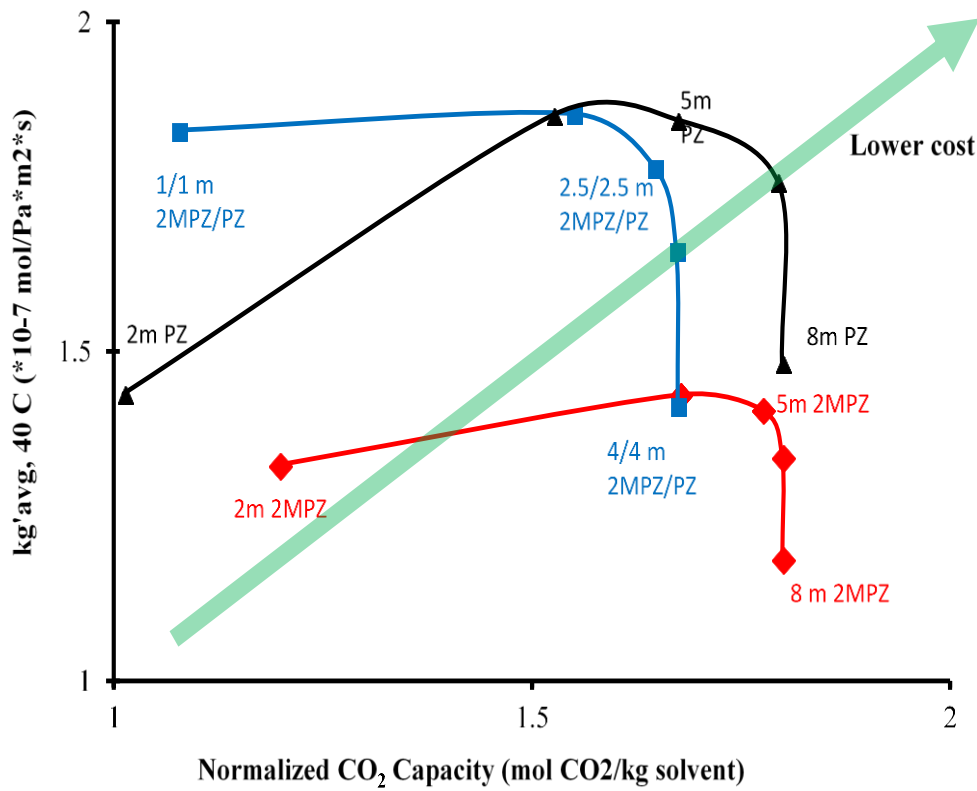


Figure 3.16: Comparing 2MPZ, PZ, 2MPZ/PZ kg'_{avg} and normalized capacity at 2, 4, 5, 6, and 8 m.

3.4 CONCLUSIONS

2MPZ and equimolar 2MPZ/PZ from 2 m to 8 m was modeled by regressing 9 parameters in Aspen Plus® using the e-NRTL thermodynamic framework. The thermodynamic model correctly predicts the CO₂ equilibrium partial pressure within 5% error from 2 m to 8 m, 0.01-0.5 CO₂ loading, and 20–160°C.

The 2MPZ kinetic model used three reactions and the 2MPZ/PZ kinetics model used six reactions to capture the rate behavior from 2 m to 8 m, 0.15-0.4 CO₂ loading, and 20–100°C. The model fits experiment data well.

2MPZ, PZ and PZ/2MPZ should be used at a total amine concentration of 5 m rather than 8 m, because the high solvent viscosity at high concentration depresses both CO₂ absorption rate and normalized capacity, and lower PZ concentration causes less precipitation.

2MPZ and PZ/2MPZ blend are competitive solvents, and this thermodynamic and kinetic model can be used for techno-economic assessments, and process modeling.

3.5 ACKNOWLEDGEMENTS

The viscosity data were collected by Rohan Small and Adil Danawala. Aspen Plus® proprietary software was provided by an academic license from AspenTech®, and Aspen Plus® are trademarks of Aspen Technology, Inc. All rights reserved.

NOMENCLATURE

Abbreviations

m	molality, mole/kg water
PZ	piperazine
2MPZ	2-methylpiperazine
MEA	monoethanolamine
eNRTL	electrolyte non-random two-liquid
WWC	wetted wall column
T	temperature
VLE	vapor-liquid equilibrium

symbols

D_{CO_2}	diffusivity of CO ₂ in solution
D_{AM}	diffusivity of amine and product in amine solution
μ	viscosity
$[Am]_b$	free amine concentration in bulk solution
H_{CO_2}	Henry's constant of CO ₂ in amine solution
T_{ref}	reference temperature
$\alpha_{rich/lean}$	loading, rich or lean
γ	activity coefficient
α	non-randomness parameter
G	Gibbs free energy
$\Delta_f G_i$	Ideal gas free energy of formation at 298.15K
$\Delta_f H_i$	Ideal gas enthalpy of formation at 298.15K
$\Delta_f G_i^{bo,aq}$	Aqueous phase free energy of formation at infinite dilution and 298.15K.
$\Delta_f H_i^{j\infty,aq}$	Aqueous phase heat of formation at infinite dilution and 298.15K
ΔC_{cyc}	CO ₂ cyclic capacity
ΔC_μ	CO ₂ cyclic capacity normalized to viscosity

Chapter 4: CO₂ Absorption Rate in Semi-Aqueous MEA³

4.1 INTRODUCTION

Amine scrubbing using aqueous ethanolamine was first patented in 1930 for the removal of acid gases (CO₂ and H₂S) from natural gas (Bottoms, 1930). It is the most mature technology for large-scale post-combustion carbon capture that can be quickly deployed (Rochelle, 2009). Increasing CO₂ absorption rate (k_g') reduces the absorber capital cost, which is the cost center of the capture plant, about 30% of the overall capital cost (CAPEX) as estimated by Frailie (2014). Greater k_g' reduces the amount of packing required for the same CO₂ removal.

Physical absorption is another CO₂ capture approach to absorb CO₂ under high pressure > 2MPa (Ban et al., 2014). Some widely used physical solvents are dimethylethers (Selexol[®]), methanol (Rectisol[®]), N-methyl-2-pyrrolidone (NMP), and 2-(2-Ethoxyethoxy) ethanol (CARBITOL[™]), which all have good CO₂ physical solubility (IEAGHG, 2008). Water-lean amines or semi-aqueous amines, consisting of amine, water, and physical solvent, are potentially attractive as they combine the advantages of chemical absorption and physical absorption. MEA in methanol-water (Usubharatana and Tontiwachwuthikul, 2009), MEA in glycerol-water (Shamiro et al., 2016), amines in N-functionalized imidazoles (Bara, 2013), N-methyldiethanolamine (MDEA) in methanol-water (Tamajon et al., 2016), and N-ethylmonoethanolamine (EMEA) in N,N-diethylethanolamine (DEEA) with/without water (Chen et al., 2015) are some recently studied semi-aqueous solvents. In addition, a commercial hybrid solvent developed by Shell containing MDEA, PZ, Sulfolane (as physical solvent), and water has been characterized by pilot plant testing (Nikolic et al., 2009). Heldebrant (2017) reviewed

³Parts of this chapter have been published in Chemical Engineering Science: Yuan, Y., Rochelle, G.T. (2018). CO₂ absorption rate in semi-aqueous monoethanolamine for CO₂ capture. Chemical Engineering Science, volume 182, 55-66

water-lean solvent and demonstrated that replacing water could increase k_g' , but most organic solvents are much more volatile than MEA and cannot be used in current amine scrubbing designs due to their high volatility.

Systematic study of the rate behavior in semi-aqueous amine has been done. The effect of viscosity, CO₂ physical solubility (Henry's constant), and amine activity on rate were explored.

NMP was selected as the primary organic physical solvent in this study due to the following reasons:

1. Good CO₂ physical solubility (IEA GHG, 2008).
2. Low viscosity and good miscibility with water (Tan et al., 2015), which reduces pumping costs. Also, low viscosity increases the heat transfer coefficient in the heat exchanger and reduces the exchanger size.
3. Relative low vapor pressure of 31.6 Pa at 20 °C (Aim, 1978), compared to 13 kPa of Methanol (Gibbard and Creek, 1974) and 133 Pa of DEEA (U.S. Department of Transportation, 1990) at 20 °C.
4. Good thermal stability. Its maximum operating temperature is high (200 °C) (Tan et al., 2015).

To prove that NMP is not the only physical solvent that could increase k_g' , absorption rate in MEA in 2-(2-Ethoxyethoxy) ethanol (CARBITOL™) and water was screened. Diglycolamine® (DGA®), another primary amine, similar to MEA was also tested with NMP.

The rate-increasing mechanism of semi-aqueous amines is interpreted by the pseudo-first-order (PFO) approximation in this chapter. Since the system is highly non-ideal, the kinetics should be activity-based rather than concentration-based. As the concentration of CO₂ on the interface increases due to higher physical solubility, more

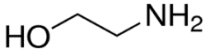
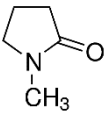
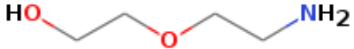
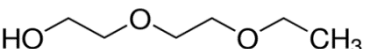
amine is reacted with CO₂. Also, the diffusivity of amine decreases due to higher viscosity. The net effect causes the depletion of amine and accumulation of products on the surface, which means the concentration of amine on the interface cannot be assumed to be equal to the concentration in the bulk liquid. As a result, the pseudo-first-order (PFO) approximation may not be accurate for semi-aqueous systems. Rigorous mass transfer modeling in MATLAB[®] was done in Chapter 6.

4.2 METHOD

4.2.1 Materials

The solvent was prepared by mixing chemicals gravimetrically. Initial chemical species are listed in Table 4.1. Molality (m) was used for the convenience of calculation. 7 m MEA in 3 NMP/1 water means 7 mole MEA is mixed with 750 g NMP and 250 g water, and MEA is exactly 30 wt %. To achieve each loading condition, CO₂ was added by bubbling gaseous CO₂ (99.99%, Praxair) into the solvent. The CO₂ loading was checked by total inorganic carbon (TIC) analysis, described previously in Freeman et al. (2010).

Table 4.1: Materials used for solvent preparation

	structure	purity	source
monoethanolamine (MEA)		99.5%	Sigma-Aldrich
N-Methyl-2-pyrrolidone (NMP)		99.0%	Sigma-Aldrich
Diglycolamine [®] (DGA [®])		99.0%	Sigma-Aldrich
2-(2-Ethoxyethoxy)ethanol (CARBITOL [™])		99.0%	Sigma-Aldrich
DDI water		100.0%	Millipore, Direct-Q
Carbon Dioxide		99.99%	Praxair

4.2.2 Viscosity

Viscosity was measured at 40 °C using a Physica MCR 300 cone-and-plate rheometer. The method was described in detail by Freeman et al. (2010). Details are in the Appendix.

4.2.3 CO₂ solubility and absorption rate by the wetted wall column (WWC)

k_g' and CO₂ solubility ($P_{CO_2}^*$) were measured simultaneously using the WWC. The method is identical to that used by Chen and Rochelle (2011), Li et al. (2013), and Du et al. (2016) and can approximate real packing hydrodynamics to allow direct scale-up. More details about the WWC is in Appendix.

As shown in Figure 4.1, the amine solvent counter-currently contacts N₂/CO₂ on the surface of a stainless rod with known surface area. The solvent rate (Q_{liquid}) was approximately 4 ml/s. The total gas flow rate (Q_{gas}) was 5 standard liters/minute. Liquid and gas were controlled at 40 °C using oil baths. The outlet CO₂ was measured

continuously by an infrared CO₂ analyzer (Horiba 2000 series). The inlet CO₂ was measured by bypassing the WWC chamber to the CO₂ analyzer.

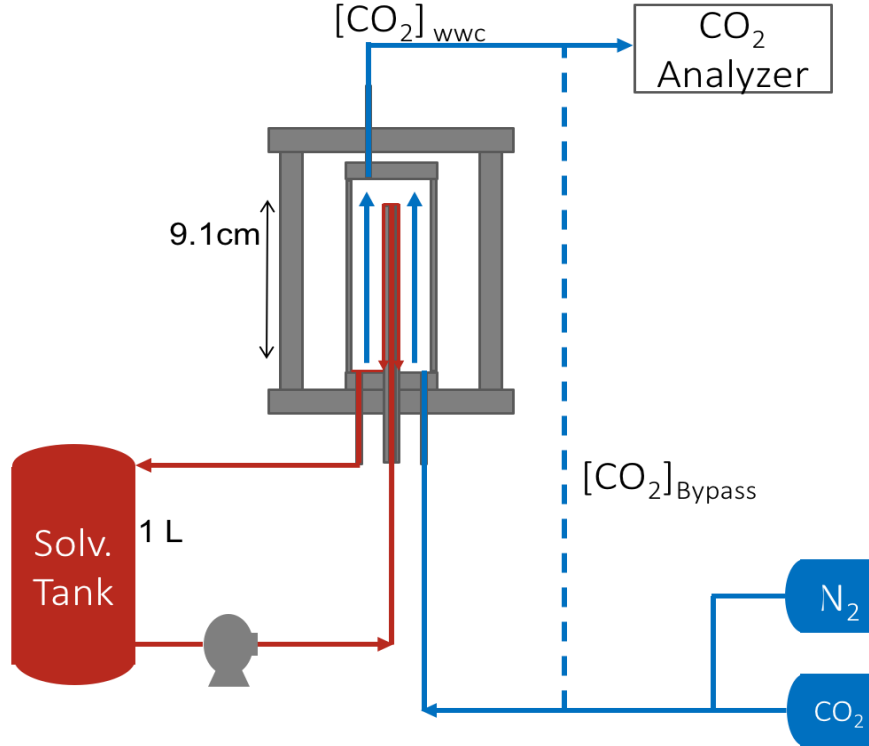


Figure 4.1: Diagram of the WWC

The CO₂ flux was obtained using Equation 4.1. V_M is the molar volume of an ideal gas at standard condition; A is the total gas-liquid contact area.

$$N_{CO_2} = \frac{(P_{CO_2,in} - P_{CO_2,out})}{P_{tot}} \cdot Q_{gas} \cdot \frac{1}{V_M \cdot A} \quad 4.1$$

Six measurements with variable inlet P_{CO_2} were made for each CO₂ loading, with three for absorption and three for desorption. The operating time of absorption/desorption was less than 3 min. The CO₂ flux was relatively small compared to the amount of solvent in the system and NMP volatility was relatively low. The liquid composition and total gas flow rate were assumed to be constant. Experiment error was

minimized by running absorption and desorption alternatively. The validation of the assumptions and discussion of experiment error are in Li (2015). Flux is plotted against the logarithmic mean of the driving force as in Figure 4.2. The slope of the line represents the overall mass transfer coefficient from bulk gas to bulk liquid (K_G), as described by Equations 4.2 and 4.3:

$$(P_{CO_2} - P_{CO_2}^*)_{LM} = \frac{(P_{CO_2,out} - P_{CO_2}^*) - (P_{CO_2,in} - P_{CO_2}^*)}{\ln\left(\frac{P_{CO_2,out} - P_{CO_2}^*}{P_{CO_2,in} - P_{CO_2}^*}\right)} \quad 4.2$$

$$N_{CO_2} = K_G (P_{CO_2} - P_{CO_2}^*)_{LM} \quad 4.3$$

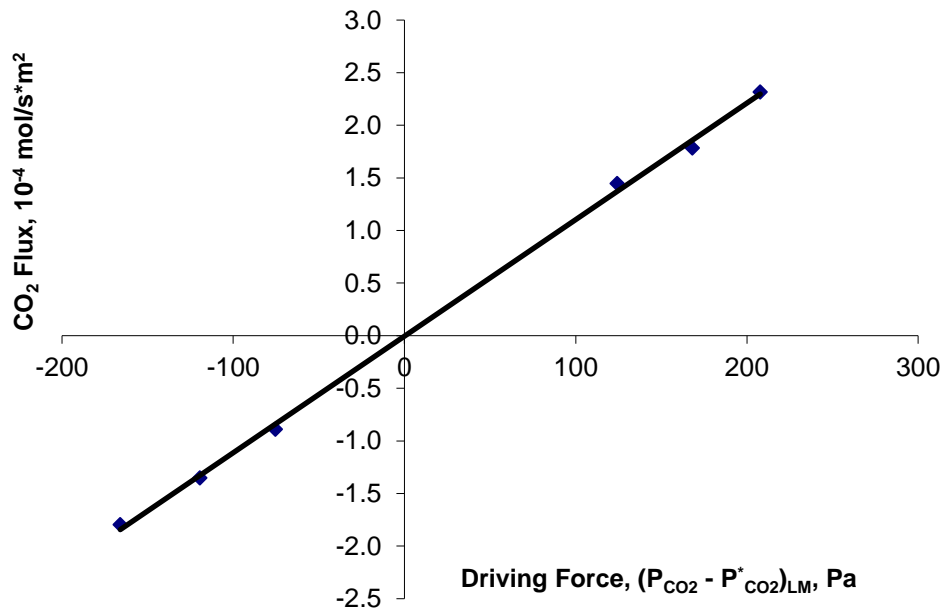


Figure 4.2: Plot of flux of CO₂ vs. driving force for 0.38 loaded 7 m MEA in 1 NMP/3 water in the WWC

A pre-determined correlation for gas film mass transfer coefficient (k_g) for this WWC (Bishnoi and Rochelle, 2000) was combined with the experimental results for K_G

to calculate the liquid film mass transfer coefficient (k_g') with a partial pressure driving force:

$$\frac{1}{k_g'} = \frac{1}{K_G} - \frac{1}{k_g} \quad 4.4$$

4.2.4 CO₂ physical solubility by N₂O analogy

CO₂ physical solubility was measured using the N₂O analogy in a total pressure apparatus. The method is similar to that used by Versteeg and Van Swaaij (1988).

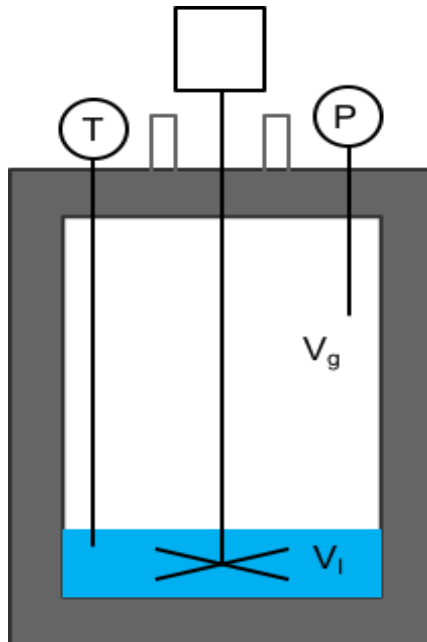


Figure 4.3: Diagram of the total pressure apparatus

The total pressure apparatus, as shown in Figure 4.3, uses a 500-mL stainless steel autoclave which acts as an equilibrium reactor. Mechanical agitation of both gas and liquid phases in the reactor is provided by a stainless-steel agitator powered by a magnetic air motor.

During an experiment, the reactor is initially flushed with N₂O and sealed, and then the pressure (P_i) is recorded. Approximately 100 mL of liquid solvent with CO₂ loading is injected by a syringe through a sealed septum. The reactor is assumed to be a closed system which contains the solvent sample and gaseous N₂O only. The pressure of the reactor is measured continuously as the liquid and gas reach equilibrium. Usually, the equilibrium pressure (P_{eq}) is reached in 3 minutes. $P_{CO_2}^*$ was subtracted from P_{eq} to get P_f . The partial pressure of MEA, NMP, and water is at less than 1% of P_{eq} , thus ignored.

The apparent Henry's law coefficient, $H_{CO_2 \text{ in solution}}$ ($\frac{P_{CO_2}}{[N_2O]}$, $\frac{Pa \cdot m^3}{mol}$) is calculated using Equations 4.5 and 4.6.

$$H_{CO_2 \text{ in solution}} = \frac{H_{CO_2 \text{ in water}}}{H_{N_2O \text{ in water}}} * H_{N_2O \text{ in solution}} \quad 4.5$$

$$H_{N_2O \text{ in solution}} = \gamma_{N_2O} * H_{N_2O} = \frac{RT P_f V_l}{P_i V_{total} - P_f (V_{total} - V_l)} \quad 4.6$$

Where

$\frac{H_{CO_2 \text{ in water}}}{H_{N_2O \text{ in water}}}$ is 0.73, 15-40 °C (Haimour and Sandall, 1984).

R is the gas constant;

T is the equilibrium temperature;

V_l is the volume of the liquid;

V_{total} is the total volume of apparatus, 500ml;

P_i is the initial pressure;

P_f is the P_{eq} minus $P_{CO_2}^*$.

γ_{N_2O} is the activity coefficient, reference is unity at infinite dilution in water;

$H_{CO_2 \text{ or } N_2O}$ is the Henry's constant of CO₂ or N₂O at infinite dilution in water

The method was checked by measuring H_{CO_2} in water three times, and the results show agreement with Versteeg and Van Swaalj (1988) within $\pm 5\%$.

4.2.5 Volatility/activity measurement using FTIR

The mole fraction of amine, NMP, and CO_2 in the gas phase above the solution was measured in a stirred reactor coupled with a hot gas FTIR analyzer (Fourier Transform Infrared Spectroscopy, Temet Gasmet Dx-4000) as shown in Figure 4.4. This was the same method and apparatus used by Nguyen (2013) and Du et al. (2016) to measure amine volatility. Given the mole fraction of MEA from the FTIR, P_{MEA} was obtained.

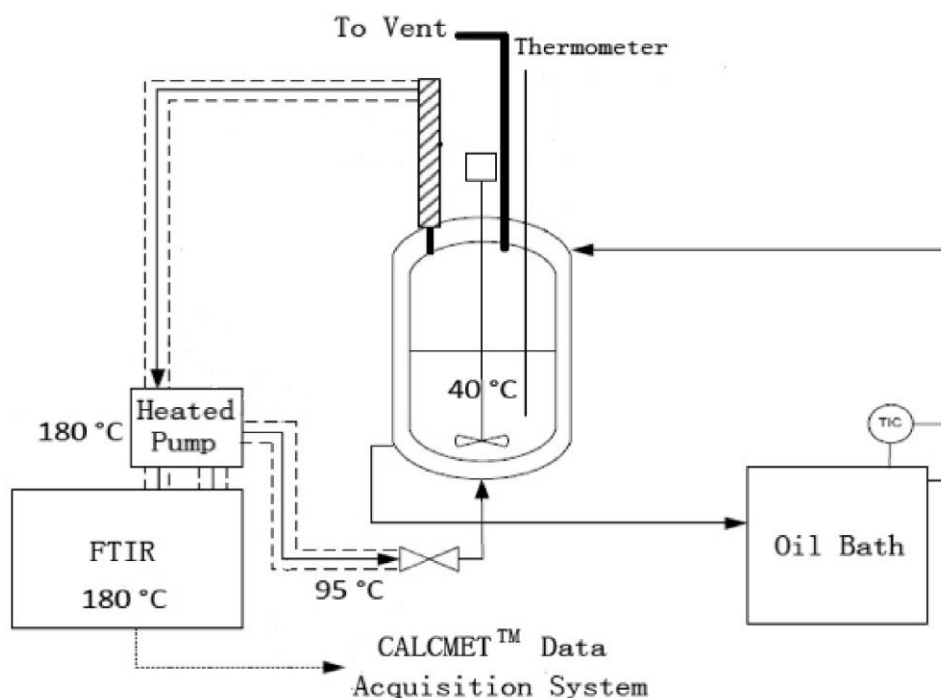


Figure 4.4: FTIR system for volatility measurement. Figure adapted from Nguyen (2013).

In this non-ideal CO_2 -MEA-water-NMP system, the activity of MEA is significantly different from that in water. As shown in Henry's law (Equation 4.7), the

amine partial pressure could be used to obtain amine activity. Since H_{MEA} is constant, P_{MEA} is a direct indicator of a_{MEA} . $a_{MEA,semi-aqueous}$ used in the mass transfer model in Chapter 5 were obtained by Equation 4.8.

$$P_{MEA} = H_{MEA}\gamma_{MEA}x_{MEA} = H_{MEA}a_{MEA} \quad 4.7$$

$$\frac{a_{MEA,semi-aqueous}}{a_{MEA,aq}} = \frac{P_{MEA,semi-aqueous}}{P_{MEA,aq}} \quad 4.8$$

where:

H_{MEA} is the Henry's constant of MEA at infinite dilution in water;

γ_{MEA} is the activity coefficient, unity at infinite dilution in water;

a_{MEA} is the activity of MEA.

4.2.6 Pseudo-first-order (PFO) assumption

In most practical absorber conditions, the pseudo-first-order (PFO) assumption can be applied to the kinetics of CO₂ and amine, which assumes amine concentration is constant over the boundary layer, and the equation that describes the reaction and diffusion of CO₂ and MEA can be simplified to one differential equation on CO₂.

$$D_{CO_2} \frac{d^2 c_{CO_2}}{dx^2} - k_3 * a_{MEA}^2 * \gamma_{CO_2} * (C_{CO_2} - C_{CO_2,eq}) = 0 \quad 4.9$$

Plugging in the boundary conditions, and assuming the reaction is much faster than pure physical absorption, flux can be obtained.

$$N_{CO_2} = \frac{\sqrt{D_{CO_2} k_3 * a_{MEA}^2}}{\gamma_{CO_2}^{0.5} H_{CO_2}} * (P_{CO_2}^{interface} - P_{CO_2}^*) \quad 4.10$$

The PFO rate expression assuming the rate is first order in CO₂ and second order in MEA is:

$$k_g' = \frac{\sqrt{D_{CO_2} k_3 a_{MEA}}}{\gamma_{CO_2}^{0.5} H_{CO_2}} \quad 4.11$$

The PFO k_g' expression shows that k_g' depends on k_3 , D_{CO_2} , γ_{MEA} , γ_{CO_2} to the order of 0.5, 0.5, 1, -0.5 respectively, and does not depend on D_{MEA} . This dependency is discussed later with the modeling results.

$$k_g' = \frac{\sqrt{D_{CO_2} k_3 a_{MEA}}}{\gamma_{CO_2}^{0.5} H_{CO_2}} \propto \frac{\sqrt{D_{CO_2} \gamma_{MEA}}}{\gamma_{CO_2}^{0.5}} \quad 4.12$$

where:

a_{MEA} is the activity of MEA;

D_{CO_2} is the diffusivity of CO₂ in the solution;

$D_{CO_2} \propto \mu^{-0.6 \sim 0.84}$ according to Dugas (2009);

γ_{CO_2} is the activity coefficient of CO₂ in the solution;

H_{CO_2} is the Henry's constant of CO₂ at infinite dilution in water.

4.3 RESULTS AND DISCUSSION

4.3.1. Absorption rate

The absorption rate (k_g') and CO₂ solubility ($P^*_{CO_2}$) of 7 m MEA in NMP/water with variable NMP to water mass ratios were measured at variable CO₂ loading across the lean and rich operating range at 40 °C. The CO₂ equilibrium pressure ($P^*_{CO_2}$) is plotted against loading in Figure 4.5. $P^*_{CO_2}$ increases with the addition of organic solvent

As explained by Du et al. (2016), NMP is less polar than water, and the addition of NMP increases the activity the ionic species that determine $P^*_{CO_2}$. A typical amine scrubbing process has a lean loading with $P^*_{CO_2}$ at 100–500 Pa, and a rich loading with

$P^*_{CO_2}$ at 5000 Pa. The increased $P^*_{CO_2}$ with addition of NMP allows lower operating lean and rich loading. As Figure 4.5 shows, the CO_2 solubility and the operating range shift to lower loading with the addition of NMP.

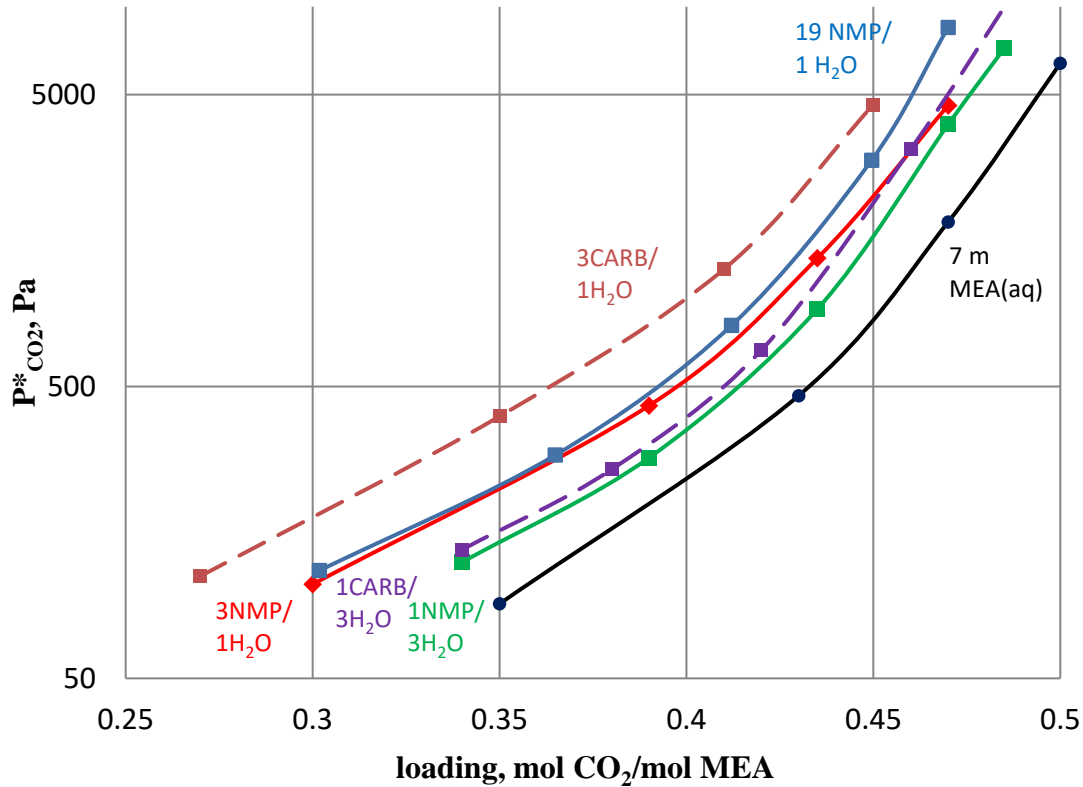


Figure 4.5: CO_2 solubility of 7 m MEA in NMP/water at 40 °C by WWC

The k_g' of 7 m MEA in water, 1 NMP/3 water, 3 NMP/1 water, and 19 NMP/1 water is plotted against loading at 40 °C in Figure 4.6, allowing direct comparison at the same loading. Figure 4.7 plots k_g' against $P^*_{CO_2}$ and compares 7 m semi-aqueous MEA to 5 m aqueous PZ (Rochelle et al., 2011) from 100 Pa to 5000 Pa. The k_g' increases with the addition of NMP. Table 4.2 provides estimates of $k_g'_{lean}$ at $P^*_{CO_2} = 100$ Pa and $k_g'_{rich}$ at $P^*_{CO_2} = 5000$ Pa. The k_g' of 7 m MEA in 3 NMP/1 water and 19 NMP/1 water is even higher than that in 5 m aqueous PZ at lean and moderate loading. The results of

adding CARBITOL™ are also plotted in Figures 4.5 and 4.7. Similar rate increase is observed after adding NMP.

When k_g' is very high ($> 5 * 10^{-6}$ mol/s*Pa*m²), the overall mass transfer coefficient (K_g) is limited mostly by the gas side mass transfer (k_g) rather than by k_g' . k_g is determined by a correlation by Bishnoi and Rochelle (2000), and the uncertainty in k_g may result in significant errors in k_g' when k_g' is very high. Figure 4.7 also shows the error bars for the three high k_g cases, constructed by varying k_g by $\pm 5\%$. In addition to lower lean loading, higher MEA activity and CO₂ physical solubility are two significant reasons for the increased k_g' .

Table 4.2: CO₂ absorption at lean and rich conditions in 7 m semi-aqueous MEA at 40 °C

Solvent mass ratio		Loading range (100–5000 Pa) mol CO ₂ /mol MEA	k_g' , lean	k_g' , rich
NMP	water		10^{-6} mol/s*Pa*m ²	10^{-7} mol/s*Pa*m ²
0	1	0.36–0.50	2.0	3.5
1	3	0.33–0.48	2.5	4.0
3	1	0.30–0.47	8.2	4.0
19	1	0.29–0.46	35	4.5

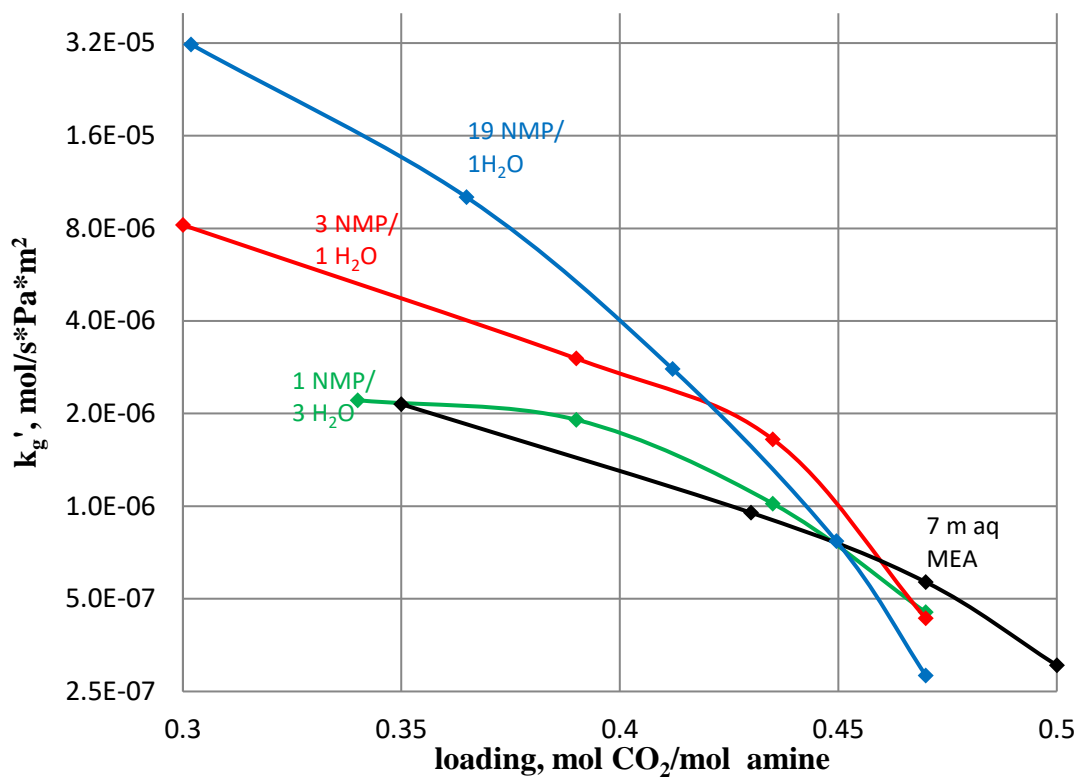


Figure 4.6: k'_g of 7 m MEA in NMP/H₂O at 40 °C by WWC

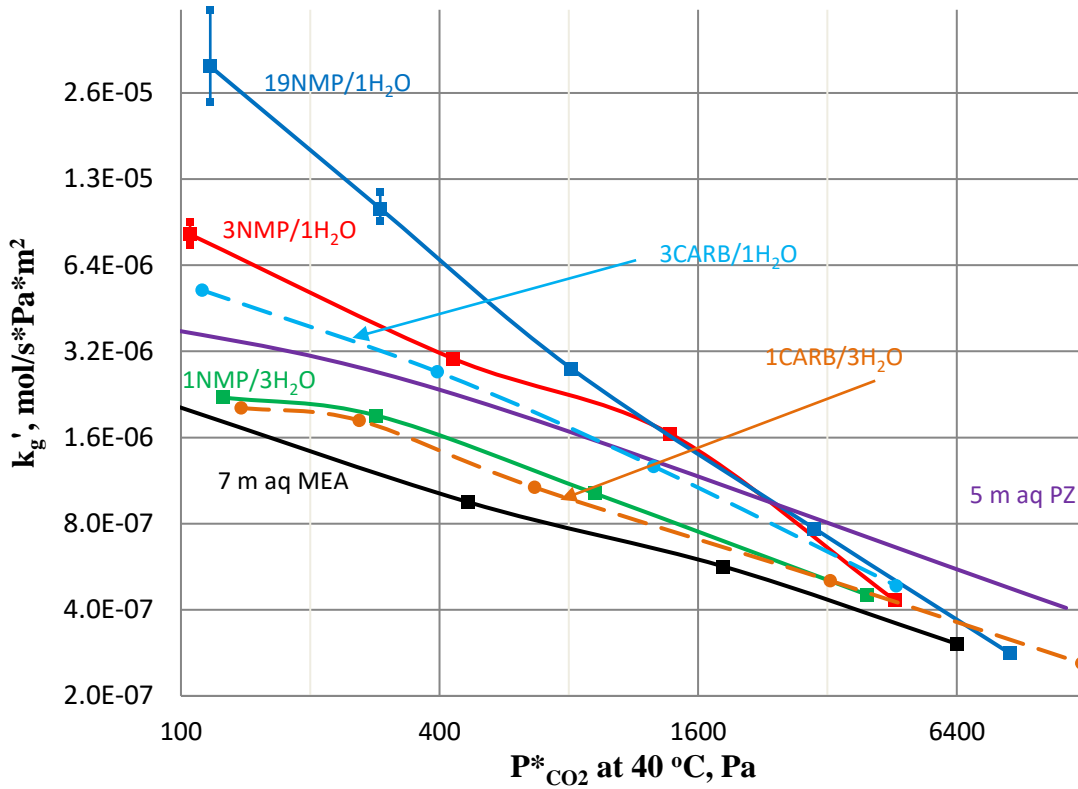


Figure 4.7: k_g' of 7 m MEA in NMP (Carbitol)/water and 5 m PZ (aq) (Dugas, 2009) at 40 °C

4.3.2. MEA activity

P_{MEA} was measured using a stirred reactor and FTIR at 40 °C (Figure 4.8). When the mass fraction of NMP increases, the activity of MEA (a_{MEA}) increases dramatically at lean loading. As loading increases, a_{MEA} decreases. At rich loading of around 0.45 mole CO_2 /mole MEA, adding NMP does not affect a_{MEA} . This is probably because of the change of polarity. With the addition of CO_2 , the solution becomes more ionic and polar, which solubilizes MEA. The increase of MEA activity at lean loading significantly contribute to the increase of kg'_{lean} after adding NMP.

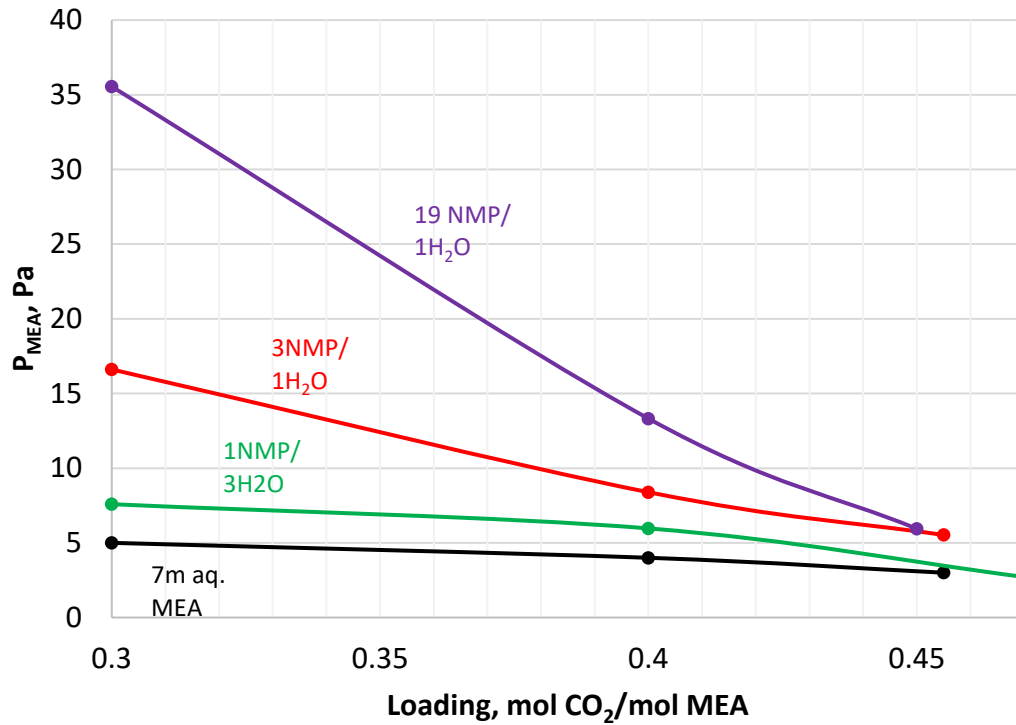


Figure 4.8: P_{MEA} above 7 m semi-aqueous MEA at 40 °C by the FTIR

4.3.3. Viscosity and physical solubility

Physical solubility of N_2O in 7 m MEA was measured at room temperature. γ_{CO_2} was calculated using $H_{CO_2} = 2631 \text{ Pa}\cdot\text{m}^3/\text{mol}$ at 20 °C (Versteeg and Van Swaaij (1988)) as reference state by Equation 4.13.

$$H_{CO_2\text{-solution}} = \gamma_{CO_2} H_{CO_2} \quad 4.13$$

CO_2 loading of 0.37 and 0.45 mole CO_2 /mole MEA was chosen to approximate the lean and rich loading for amine scrubbing. The results are listed together with viscosity in Table 4.3. With a higher NMP mass fraction, CO_2 physical solubility is higher. Lower γ_{CO_2} means higher physical solubility. At rich loading, the CO_2

physical solubility decreases compared to lean loading, especially in 19 NMP/1 water, because the polarity increases as loading goes up. The viscosity increases as NMP mass fraction increases, except for 19 NMP/1 water. The viscosity is not monotonic as NMP fraction increases because of the intermolecular force between NMP and water. This behavior of viscosity is similar to that in methanol-water (Mikhail and Kimel, 1961).

Table 4.3: Viscosity and γ_{CO_2} of 0.37 and 0.45 loaded 7 m semi-aqueous MEA

Solvent mass ratio		μ , 40 °C		γ_{CO_2}	
		0.37	0.45	0.37	0.45 loading
NMP	water	cP			
0	1	2.5	2.6	1.61	1.72
1	3	4.6	5	1.54	1.43
3	1	15.2	17.2	0.94	1.01
19	1	14.4	15.4	0.45	0.94

4.3.4. Net effect of amine activity, viscosity, and physical solubility on k_g' based on PFO

7 m aqueous MEA was used as the base case for the analysis, and important parameters measured in different semi-aqueous MEA solvents were compared to the basis. Since $P_{MEA} = H_{MEA} * \gamma_{MEA} * x_{MEA}$ and H_{MEA} is constant, the ratio of γ_{MEA} in each solution to γ_{MEA} in 7 m aqueous MEA is equal to the ratio of the corresponding P_{MEA} as Equation 4.13 shows. Due to the limitations of the apparatus, γ_{CO_2} was only measured at room temperature; however, the ratio of γ_{CO_2} in each solution to γ_{CO_2} in the base case at 40 °C can be approximated by the ratios at room temperature, assuming the ratios do not vary. The relative values of all the parameters are listed in Tables 4.4 and 4.5. In addition, the PFO predicted k_g' ratio by Equation 4.12 is included.

Table 4.4: Relative viscosity, H_{CO_2} , activity, and k_g' of 7 m semi-aqueous MEA at 0.37 mol CO₂/mol MEA.

Solvent mass ratio		μ , 40 °C	γ_{CO_2}	γ_{MEA}	k_g' , exp	k_g' , predict	k_g' , predict
NMP	water					$a_{MEA} * \mu^{-0.3} * \gamma_{CO_2}^{-0.5}$	$a_{MEA} * \mu^{-0.42} * \gamma_{CO_2}^{-0.5}$
0	1	1	1	1	1	1	1
1	3	1.84	0.95	1.60	1.2	1.3	1.3
3	1	6.08	0.58	2.67	2.1	2	1.6
19	1	5.76	0.28	4.44	5.2	5	4

As Table 4.4 shows, at lean loading, viscosity increases as NMP mass fraction increases, except for 19 NMP/1 water, which decreases slightly. Since $D_{CO_2} \propto \mu^{-0.72 \pm 0.12}$ (Dugas, 2009) and $k_g' \propto D_{CO_2}^{0.5}$, $k_g' \propto \mu^{-0.3 \sim 0.42}$, which means higher viscosity depresses the absorption rate. The predicted k_g' using both -0.3 and -0.42 viscosity dependence is listed in Table 4.5, and $k_g' \propto \mu^{-0.3}$ gives better prediction. The k_g' predicted by the PFO from Equation 4.12 roughly matches the experimental k_g' , which explains that adding NMP to 7 m aqueous MEA increases k_g' at 0.37 loading by increasing the activity of MEA and CO₂ physical solubility. The discrepancy may result from the PFO approximation, the uncertainty of dependence of D_{CO_2} on viscosity, and experimental error. Since our purpose is to explain why k_g' increases by adding NMP, rather than to quantitatively predict k_g' without directly measuring it, the discrepancy between $k_g'_{exp}$ and $k_g'_{predict}$ is acceptable.

Table 4.5 explains why k_g' does not increase at rich loading when NMP is added using PFO. Higher viscosity depresses the rate. The increase of CO₂ physical solubility should increase the rate, but at rich loading, the increase of CO₂ physical solubility is weaker than at lean loading. Also, at rich loading, the MEA activity does not increase as much as at lean loading when NMP increases as Figure 4.8 shows. The net effect of

viscosity, CO₂ physical solubility, and MEA activity results in almost no change in k_g' . Compared to lean loading (Table 4.4), which matches k_g' well, at rich loading, k_g' predict by $k_g' \propto \mu^{-0.3}$ overestimates k_g' at high NMP. At rich loading, the MEA concentration on the surface is lower than at lean loading. After adding NMP, which increases CO₂ concentration and consumes more MEA at the interface, the MEA concentration at the surface should be lower than that in the bulk. Hence the PFO approximation may not be accurate. Rigorous modeling of the kinetics without the PFO approximation is necessary. The set of the diffusion and reaction differential equations that describes the reaction and diffusion between CO₂ and MEA was solved by MATLAB® in the next chapter

Table 4.5: Relative viscosity, H_{CO_2} , activity, and k_g' of 7 m semi-aqueous MEA with 0.45 mol CO₂/mol MEA

Solvent mass ratio		$\mu, 40$ °C	γ_{CO_2}	γ_{MEA}	k_g', exp	$k_g', \text{predict}$	$k_g', \text{predict}$
NMP	water					$a_{MEA} * \mu^{-0.3} * \gamma_{CO_2}^{-0.5}$	$a_{MEA} * \mu^{-0.42} * \gamma_{CO_2}^{-0.5}$
0	1	1	1	1	1	1	1
1	3	1.92	0.83	1.09	1	1	0.9
3	1	6.62	0.59	1.72	1.2	1.3	1
95	5	5.92	0.54	1.72	1	1.4	1.1

4.3.5 Rate enhancement by 2-(2-Ethoxyethoxy) ethanol (CARBITOL™)

To further test this rate increase in semi-aqueous MEA, 2-(2-Ethoxyethoxy) ethanol (CARBITOL™) was added to 7 m MEA, and k_g' of 7 m MEA in 1 CARBITOL™/3 water and 3 CARBITOL™/1 water was measured by the WWC. CARBITOL™ increases the k_g' as expected.

Results of adding CARBITOL™ are plotted in Figures 4.5 and 4.7, and are compared to NMP. Although amine activity and physical solubility were not measured,

the k_g' and $P^*_{CO_2}$ results from the WWC suggest that CARBITOL™ is another solvent that would increase the k_g' of 7 m MEA, probably by the same mechanisms as NMP.

4.3.6 Rate behavior in DGA®-Water-NMP

DGA®, another primary amine, was also tested with NMP. 7 m Diglycolamine® (DGA®) in 3 NMP/1 water was measured in the WWC, which also showed enhanced absorption rate at lean and middle loading. This demonstrates that MEA is not the only amine that has this kind of rate behavior. P^* is plotted against loading in these hybrid solutions in Figure 4.9. k_g' is plotted against P^* at 40 °C in Figure 4.10. 7 m MEA was measured by Dugas (2009), and 10 m DGA® was measured by Chen (2011).

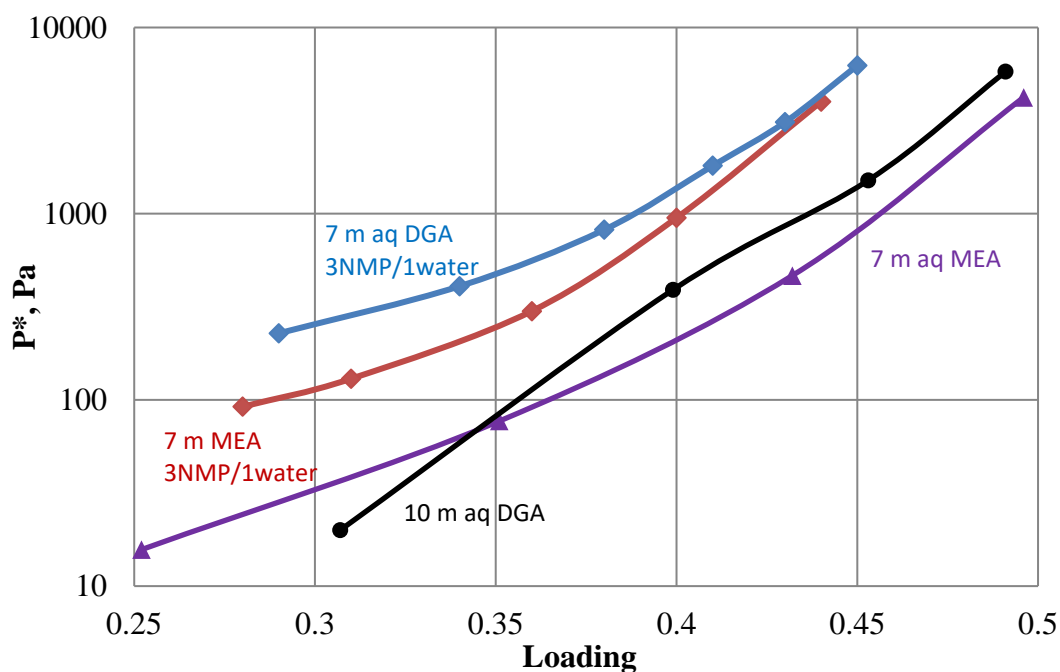


Figure 4.9: CO₂ solubility of MEA or DGA® in NMP/water at 40 °C by WWC

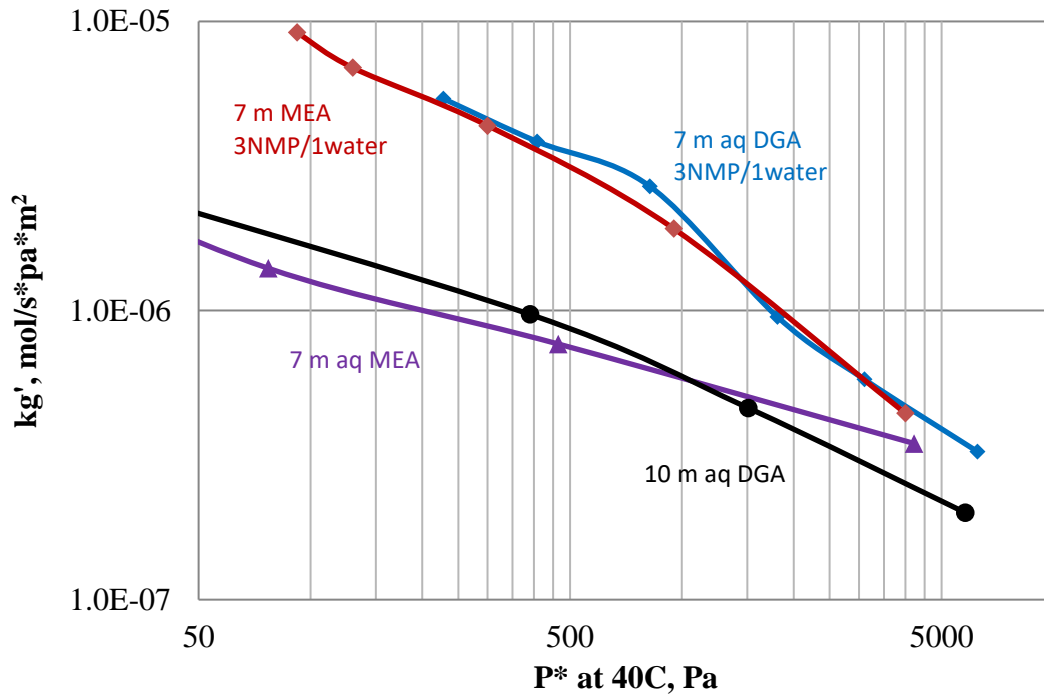


Figure 4.10: k_g' of MEA or DGA[®] in NMP/H₂O at 40 °C by WWC

4.3.7 Comparison of key properties to 5 m PZ

The liquid film mass transfer coefficient (k_g') measured in the WWC can be directly used in plant design using Equation 4.14 (Li et al., 2013). It is calculated as the ratio of CO₂ flux to the liquid film partial pressure driving force, and the average k_g' (k_g' avg) for an isothermal absorber at 40 °C and 90% CO₂ removal is calculated, assuming a linear concentration profile and equilibrium curve in the absorber.

$$\begin{aligned}
 k_{g' avg} &= \frac{Flux_{CO_2, LM}}{(P_{CO_2} - P_{CO_2}^*)_{LM}} \\
 &= \frac{(Flux_{CO_2, top} - Flux_{CO_2, bottom}) / \ln(Flux_{CO_2, top} / Flux_{CO_2, bottom})}{(P_{CO_2, top} - P_{CO_2, lean}^*) - (P_{CO_2, bottom} - P_{CO_2, rich}^*) / \ln\left(\frac{P_{CO_2, top} - P_{CO_2, lean}^*}{P_{CO_2, bottom} - P_{CO_2, rich}^*}\right)}
 \end{aligned}
 \tag{4.14}$$

For coal-fired flue gas treating, the P_{CO_2} in the bulk gas at the bottom and top of the absorber are 12 and 1.2 kPa. With a reasonable driving force, the rich and lean $P_{CO_2}^*$ are selected to be 5 and 0.1 kPa in this analysis. Experimental values at 40 °C are used to interpolate k_g' that corresponds to $P_{CO_2}^*$ at 5 and 0.1 kPa, which are then used to calculate the corresponding flux. $k_g'_{avg}$ of 7 m MEA in 3 water/1 NMP, 1 water/3 NMP, and 5 water/95 NMP is 1.1 times, 2 times, and 5 times that of 7 m aqueous MEA, respectively. The latter two are even higher than $k_g'_{avg}$ of 5 m PZ (Dugas, 2009), as listed in Table 4.6.

The CO_2 cyclic capacity (ΔC_{solv}) of solvent is defined by as Equation 4.15. α_{lean} and α_{rich} are the CO_2 loading at lean and rich conditions (mol CO_2 /mol amine) corresponding to $P_{CO_2}^*$ of 0.1 kPa and 5 kPa, respectively. $\Delta\alpha_{CO_2}$ is the difference between α_{lean} and α_{rich} .

$$\Delta C_{solv} = \Delta\alpha_{CO_2} \cdot \text{molality of alkalinity/kg (solvent)}$$

$$\Delta\alpha_{CO_2} = (\alpha_{rich} - \alpha_{lean}) \quad 4.15$$

Cross-exchanger optimization involves evaluating the trade-off between the capital cost of the exchanger and the value of sensible heat requirement. When the temperature driving force (ΔT_{LM}) increases, sensible heat required in the reboiler increases and heat exchanger Area/CAPEX decreases. ΔT_{LM} was optimized for lowest exchanger CAPEX and sensible heat requirement. At $\Delta T_{LM,opt}$, the overall cost of heat exchanger and sensible heat is proportional to viscosity to the power of 0.175 (Lin, 2016). The 0.175 power is based on the conclusion that the heat transfer coefficient generally depends on solvent viscosity to about -0.35 power (Ayub, 2003). $\Delta C\mu$ is the normalized CO_2 cyclic capacity of a solvent considering the effect of viscosity on the optimized heat exchanger cost and sensible heat (Li et al., 2013), as defined in Equation 4.16. μ_{mid} is

the viscosity of each solvent at mid-loading ($P_{CO_2}^* = 2.0$ kPa), with 5 m PZ used as the base.

$$\Delta C_\mu = \frac{\Delta C_{solv}}{(\mu_{mid}/\mu_{5\text{ m PZ}})^{0.175}} \quad 4.16$$

Table 4.7 compares some important properties of the related solvent at 40 °C (μ_{mid} , k_g' , ΔC_{solv} , ΔC_μ , and P_{org}). ΔC_{solv} increases as physical solvent increases, because lower α_{lean} increases $\Delta\alpha_{CO_2}$ as shown in Figure 4.5. This is because the addition of physical solvent salts out the CO₂-related species in the liquid phase (Du et al., 2016), and probably the salting-out effect is stronger at lean loading when the system is less ionic than at rich loading. However, the increased viscosity reduced the normalized capacity with the addition of physical solvent. ΔC_μ of 7 m MEA in water/physical solvent is slightly lower than that in water.

Table 4.6: μ_{mid} , k_g' , ΔC_{solv} , and ΔC_μ of 7 m semi-aqueous MEA and 5 m PZ (aq) (Dugas, 2009).

Solvent		μ_{mid}	ΔC_{solv}	ΔC_μ	k_g'	P_{org}
7 m MEA		cP	0.1-5 kPa, $\frac{\text{mol CO}_2}{\text{kg solvent}}$		mol/s*Pa*m ²	Pa
water		2.5	0.68	0.76	9.18E-07	
3 water	1 NMP	4.6	0.72	0.72	1.05E-06	17
1 water	3 NMP	16	0.85	0.69	1.96E-06	63
1 water	19 NMP	15	0.83	0.68	5.10E-06	102
3 water	1 CARBITOL™	5.4	0.7	0.69	1.05E-06	
1 water	3 CARBITOL™	19	0.94	0.73	1.66E-06	
7 m DGA						
1 water	3 NMP	20	0.93	0.71	1.96E-06	
5 m PZ		4.5	0.95	0.95	1.40E-06	

4.3.8 Considerations of volatility

The volatility of the physical solvent is a major drawback of the semi-aqueous amine. NMP and CARBITOL™ are less volatile than most organic solvents, with a vapor pressure of 132 Pa for NMP (Kneisl and Zondlo, 1987) and 69 Pa for CARBITOL™ (Gardner and Brewer, 1937) at 40 °C. P_{NMP} at 40 °C measured by FTIR in 7 m MEA in 3 water/1 NMP, 1 water/3 NMP, and 1 water/19 NMP is 17 Pa, 63 Pa, and 102 Pa, respectively. P_{CARBITOL} was not measured. Based on the vapor pressure, P_{CARBITOL} should be approximately 50% less than P_{NMP} ; however, the volatility of NMP or CARBITOL™ is still significantly higher than MEA, requiring a more rigorous water wash system or other capture technique. Less volatile physical solvents should be identified. Another possible solution is lowering the absorber temperature to less than 40 °C, which reduces the volatility of the organic components; however, maintaining the absorber to a lower temperature will result in higher intercooling cost, especially for the plants do not have very cold cooling water. Lowering absorber temperature could increase absorption rate (Heldebrant, 2017), which is interesting to study. Further study including thermodynamic, kinetics, process simulation and optimization needs to be done on this option. The presence of the physical solvent will also complicate reclaiming of the spent amine.

4.4 CONCLUSIONS

Semi-aqueous amines could have much faster absorption rate than aqueous amine. In the operating range of 100–5000 Pa CO_2 equilibrium partial pressure ($P_{\text{CO}_2}^*$), CO_2 absorption rate (kg'avg) of 7 m MEA in 3 water/1 NMP, 1 water/3 NMP, and 1 water/19 NMP is 1.1 times, 2 times, and 5 times that of 7 m aqueous MEA, respectively. kg' increases when replacing water by NMP because of reduced operating CO_2 loading (higher free MEA concentration), greater CO_2 physical solubility, and greater MEA

activity. The increase in kg' becomes less significant at richer loading as the increase in physical solubility and MEA activity is not as great. CARBITOL™, another physical solvent, shows similar effect on kg' as NMP. Besides MEA, DGA® , another primary amine, also showed that kg' could be increased by adding NMP.

The difference between rich and lean loading ($\Delta\alpha_{CO_2}$) increases with the addition of physical solvent, but the increased viscosity after adding physical solvent reduced the normalized capacity (ΔC_μ). The net effect makes ΔC_μ of the semi-aqueous MEA 10% less than that of aqueous MEA. Compared to 5 m PZ(aq), kg' avg between 100 and 5000 Pa $P_{CO_2}^*$ of 7 m MEA in 1 water/3 NMP and 1 water/19 NMP is 1.4 times and 3.6 times that of 5 m aqueous PZ; but the normalized capacity (ΔC_μ) is 20% less than that of 5 m PZ.

The volatility of NMP and CARBITOL™ is still too high, and water wash or other capture processing will be required to meet environmental regulations. Physical solvents with lower volatility or process with lower absorber temperature could be further explored.

Nomenclature

α	mol CO ₂ /mol amine	Loading
a_i	mol/m ³	Activity of a component
C_i	mol/m ³	Concentration of a component
D_{CO_2}	m ² /s	Diffusivity of CO ₂ in the solution
D_{MEA}	m ² /s	Diffusivity of MEA in the solution
H_{CO_2}	Pa*m ³ /mol	Henry's constant of CO ₂ at infinite dilution in water
H_{N_2O}	Pa*m ³ /mol	Henry's constant of N ₂ O at infinite dilution in water
H_{MEA}	Pa*m ³ /mol	Henry's constant MEA at infinite dilution in water
k_g'	mol/s*Pa*m ²	Liquid film mass transfer coefficient
K_G	mol/s*Pa*m ²	Overall mass transfer coefficient
k_g	mol/s*Pa*m ²	Gas film mass transfer coefficient
k_3	m ⁶ /s*mol ²	Third order rate constant between amine and CO ₂
K_{eq}		Equilibrium constant
m	mol/kg solvent	Molality, mole per kg of solvent (water + NMP/CARB)
$P_{CO_2}^*$	Pa	CO ₂ equilibrium partial pressure
$P_{CO_2,in/out}$	Pa	CO ₂ partial pressure going in/out of the WWC
P_i	Pa	The initial pressure of the total pressure apparatus
P_f	Pa	The final pressure of the total pressure apparatus
P_{MEA}	Pa	Partial pressure of MEA
V_M	L/mol	molar volume of an ideal gas
V_l	ml	Volume of the liquid
V_{total}	L	Volume of the total pressure apparatus
N_{CO_2}	mol/(s*m ²)	Flux of CO ₂ in the WWC
$Q_{liquid/gas}$	ml/s or l/s	Liquid/gas flow rate
t_c	s	Contacting time in the WWC
ρ	Kg/ m ³	Density
h	meter	Height of the annulus in the WWC
d	meter	Diameter of the annulus in the WWC
S_i		Sensitivity of k_g' to different parameters
γ_i		Activity coefficient of a component
μ	cP	Viscosity
ΔC_{solv}	mol CO ₂ /kg total solvent	CO ₂ cyclic capacity
ΔC_{μ}	mol CO ₂ /kg total solvent	CO ₂ cyclic capacity normalized by viscosity

Chapter 5: CO₂ Absorption rate in semi-aqueous PZ

5.1 INTRODUCTION

Chapter 4 demonstrates organic solvents such as N-methyl-2-pyrrolidone (NMP) and 2-(2-Ethoxyethoxy) ethanol (CARBITOL™) with high physical CO₂ solubility could improve the chemical absorption rate of MEA, especially at lean loading. Our group introduced Piperazine (PZ) as the new standard for CO₂ capture, which is superior to MEA (Rochelle et al., 2010). PZ has a high absorption rate, good stability, low viscosity, and high capacity, but a narrow solid solubility window may limit its application (Chen, 2010). The solid solubility issue could be addressed by two ways. One is partially replacing PZ with another amine, such as 2methylpiperazine (2MPZ), as shown in Chapter 2 & 3. Another approach is to replace water with a physical solvent to solubilize PZ. Semi-aqueous PZ consisting of PZ, water, and a physical solvent is potentially attractive as it may combine the advantages of fast absorption rate and good solid solubility. NMP solubilizes PZ at lean loading but causes precipitation at rich loading (0.35 mol CO₂/mol alkalinity). Shell Oil Company (Nikolic et al., 2009) has developed Sulfinol®-X, a commercial hybrid solvent containing MDEA, PZ, SUF, and water for high pressure natural gas sweetening. The solubility of 5 m PZ in 1 SUF/3 water, 1 SUF/1 water, 1 IMI/3 water, 1 IMI/1 water has been tested, and no precipitation was observed in the loading range of 0.15–0.45 mole CO₂/mole alkalinity at 20 to 60 °C. Absorption rate (k_g') and CO₂ solubility were measured at different CO₂ loadings across the lean and rich operating range in the wetted wall column.

5.2 METHOD

5.2.1 Materials

The solvent was prepared by mixing chemicals gravimetrically. Initial chemical species are listed in Table 5.1. Molality (m) was used for the convenience of calculation. 5 m PZ in 1 NMP/3 water means 5 mole PZ is mixed with 250 g NMP and 750 g water, and PZ is exactly 30 wt %. To achieve each loading condition, CO₂ was added by bubbling gaseous CO₂ (99.99%, Praxair) into the solvent.

Table 5.1: Materials used for solvent preparation

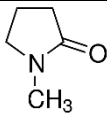
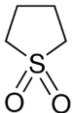
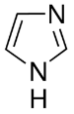
	structure	purity	source
Piperazine (PZ)		99.5%	Sigma-Aldrich
N-Methyl-2-pyrrolidone (NMP)		99.0%	Sigma-Aldrich
Triethylene glycol (TEG)		99.0%	Sigma-Aldrich
Sulfolane (SUF)		99.00%	Sigma-Aldrich
Imidazole (IMI)		99.0%	Sigma-Aldrich
DDI water		100.0%	Millipore, Direct-Q
Carbon Dioxide		99.99%	Praxair

Table 5.2: Chemical species in 5 m PZ in 1TEG/2water

	Molecular weight (g/mol)	Mass (g)	wt %
PZ	86.14	516.8	30.1%
TEG	150.2	400.0	23.3%
Water	18.02	800.0	46.6%

Table 5.3: Chemical species in 5 m PZ in 1physical solvent/3water

	Molecular weight (g/mol)	Mass (g)	wt %
PZ	86.14	516.8	30.1%
NMP/SUF/IMI	99.13/120.2/68.08	300.0	17.5%
Water	18.02	900.0	52.4%

Table 5.4: Chemical species in 5 m PZ in 1physical solvent/1water

	Molecular weight (g/mol)	Mass (g)	wt %
PZ	86.14	516.8	30.1%
water	18.02	600.0	35.0%
SUF/IMI	120.2/68.08	600.0	35.0%

5.2.2 CO₂ loading by TIC

The CO₂ loading was checked by total inorganic carbon (TIC) analysis, described previously in Freeman et al. (2010).

5.2.3 Viscosity

Viscosity was measured at 40 °C using a Physica MCR 300 cone-and-plate rheometer. The method was described in detail by Freeman et al. (2010). Details in Appendix A.

5.2.4 CO₂ solubility and absorption rate by the wetted wall column (WWC)

k_g and CO₂ solubility ($P_{CO_2}^*$) were measured simultaneously using the WWC. The method is identical to that used by Chen and Rochelle (2011), Li et al. (2013), and Du et al. (2016) and can approximate real packing hydrodynamics to allow direct scale-up. More details about the WWC are in Appendix A.

5.3 RESULTS AND DISCUSSION

5.3.1 PZ in NMP/water and PZ in TEG/water

5 m PZ in 1 NMP/3 water and 1 TEG/2 water was measured at 40 °C in the WWC. 5 m PZ in 1 NMP/3 water showed a 15% higher rate at lean and median loading.

k_g' is plotted against $P^*_{CO_2}$ at 40 °C in Figure 5.1 and compared to 5 m aqueous PZ. Both TEG and NMP have high CO_2 physical solubility, but TEG has a much higher viscosity (49 cP) than NMP (1.7cP). The high physical solubility should enhance k_g' , as CO_2 concentration in the interface increases, while high viscosity reduces the diffusivity of both CO_2 and amines, which limits k_g' . The net effect of high CO_2 physical solubility and high viscosity results in the k_g' of 5 m PZ in TEG/water being close to that of 5 m aqueous PZ at lean and median loading. NMP has similar CO_2 physical solubility and lower viscosity and therefore higher k_g' was obtained. However, at rich loading, 0.35 mol CO_2 /mole alkalinity, solid precipitation was observed in 1 NMP/3 water and 1 TEG/2 water at ambient temperature. After heating to 40 °C, 5 m PZ was dissolved in 1 NMP/3 water, and k_g' was measured in the WWC. k_g' of 5 m PZ in 1 NMP/3 water at rich loading is slightly smaller than 5 m PZ(aq).

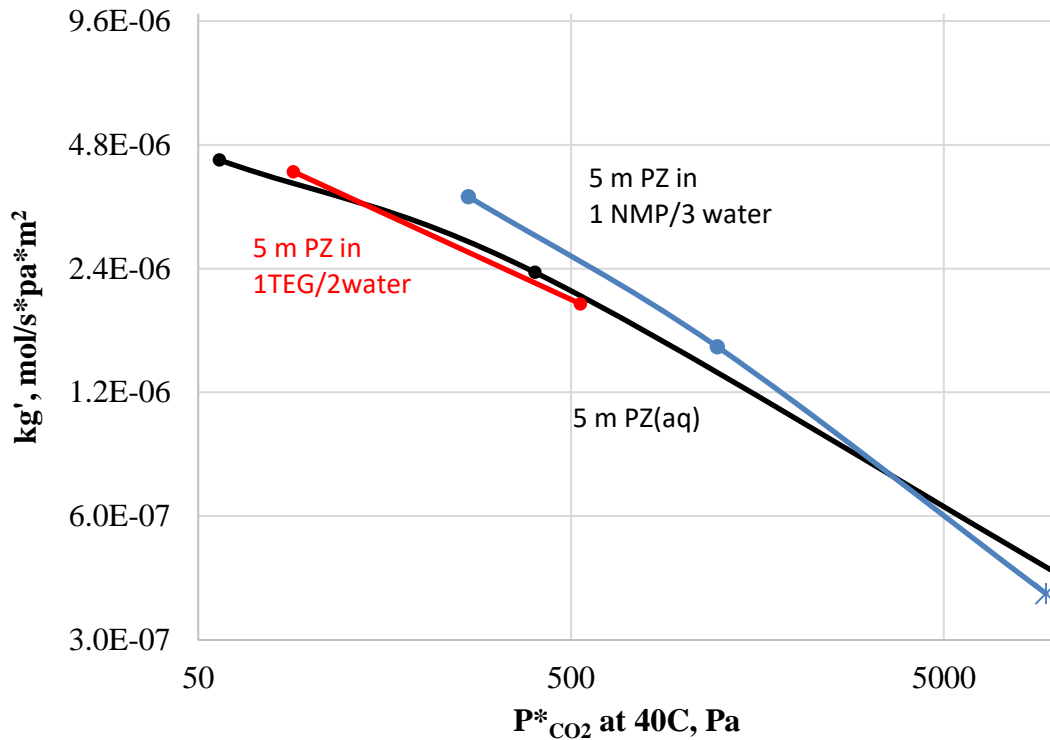


Figure 5.1: kg' of 5 m PZ in 1TEG/2water and 1NMP/3water at 40 °C by WWC

5.3.2 CO₂ solubility and absorption rate of PZ in SUF/water

The absorption rate (kg') and CO₂ solubility of 5 m PZ in 1 SUF/3 water and 1 SUF/water were measured at variable CO₂ loading across the lean and rich operating range at 20, 40, and 60 °C. The experimental data are presented in Appendix B.

The CO₂ equilibrium pressure ($P^*_{CO_2}$) is plotted against loading in Figures 5.2 and 5.3, together with previous results for 5 m PZ(aq). At 40 °C, $P^*_{CO_2}$ in 5 m PZ in 1 SUF/3 water increases, but the slope of the VLE curve is the same, which means the cyclic capacity is roughly the same. The increase of $P^*_{CO_2}$ is probably because the activity coefficient of the PZ carbamate is increased. As temperature increases, $P^*_{CO_2}$ increases at the same rate as in water alone, so the heat of CO₂ absorption is not affected by SUF.

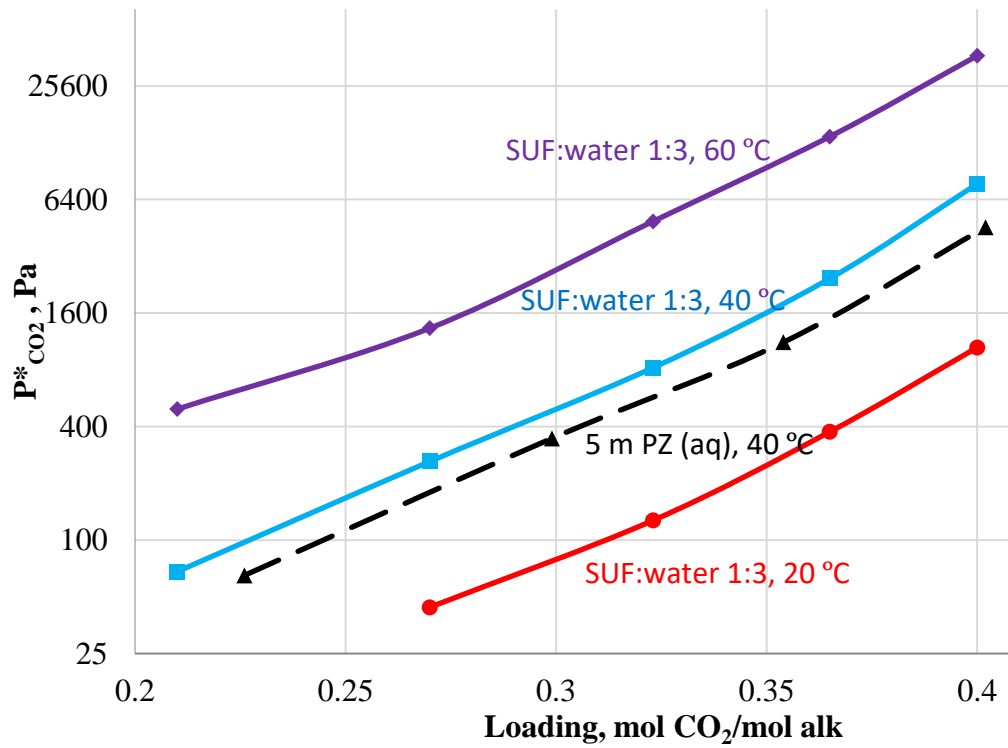


Figure 5.2: CO₂ solubility in 5 m PZ in 1 SUF/3 water

CO₂ equilibrium partial pressure ($P^*_{CO_2}$) in 5 m PZ in 1 SUF/1 water also increases compared to 5 m PZ(aq). As Figure 5.3 shows, at very lean loading, $P^*_{CO_2}$ in 1 SUF/1 water increases significantly. The smaller slope of the VLE curve suggests a higher the cyclic capacity of 5 m PZ in 1 SUF/1 water than 5 m PZ(aq).

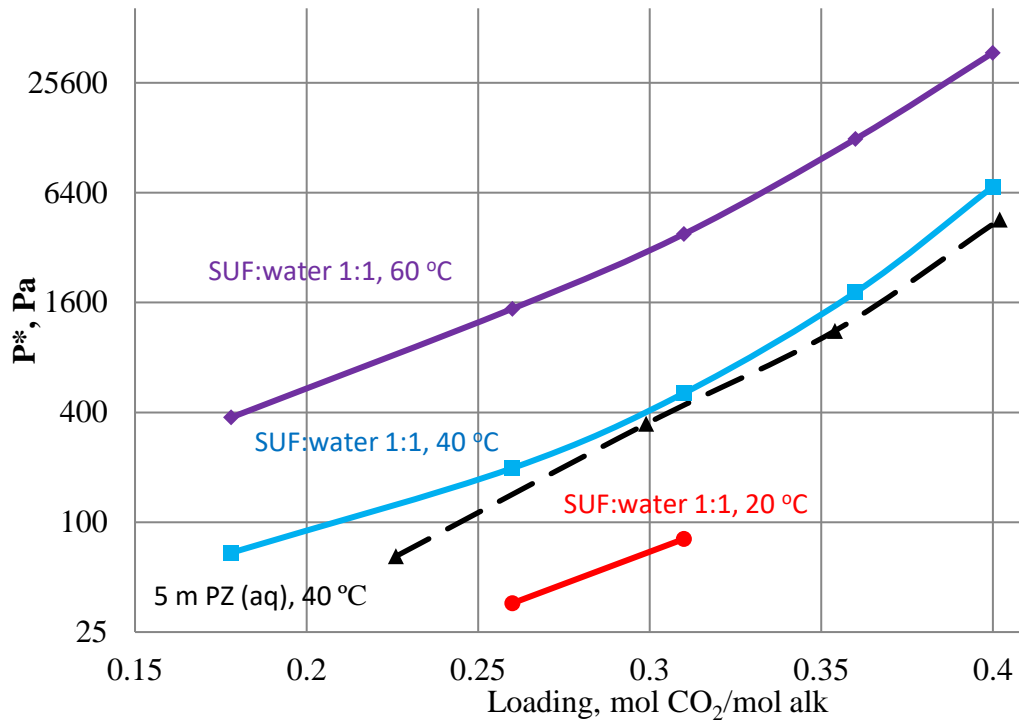


Figure 5.3: CO₂ solubility in 5 m PZ in 1 SUF/1 water

k_g' of 5 m PZ in 1 SUF/3 water is plotted against loading in Figure 5.4. At lean loading, adding SUF increases k_g' because of higher CO₂ physical solubility, but at rich loading, adding SUF decreases k_g' .

k_g' depends on temperature (20 °C > 40 °C > 60°C). As temperature increases, CO₂ physical solubility decreases, which should decrease k_g' , while diffusivity and reaction rate constant k increase, which should increase k_g' . The strong dependency of CO₂ physical solubility on temperature in semi-aqueous solvent results in lower k_g' at higher temperature. This temperature dependency is different from that of aqueous PZ which shows no obvious k_g' dependency on temperature.

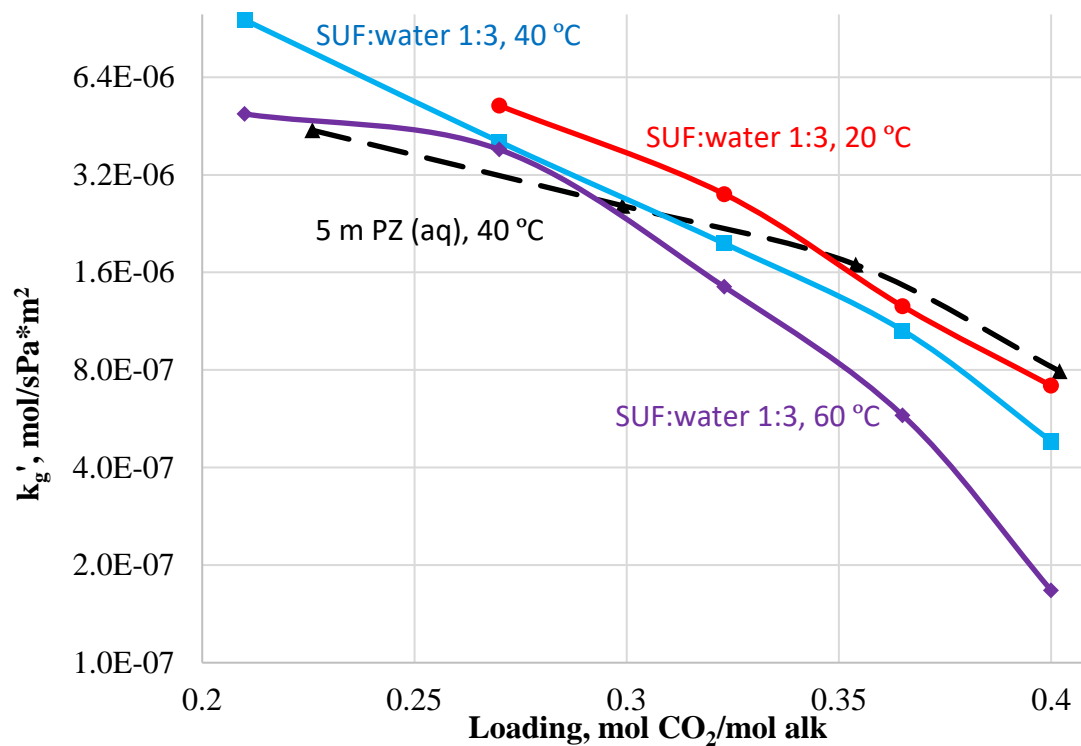


Figure 5.4: k_g' of 5 m PZ in 1 SUF/3 water at 20–60 °C in WWC

k_g' is also plotted against $P^*_{CO_2}$ at 40 °C in Figure 5.5. Because of the increased $P^*_{CO_2}$ at the same loading, at rich loading, k_g' of 5 m PZ in 1 SUF/3 water is comparable to that of 5 m PZ(aq) at the same $P^*_{CO_2}$.

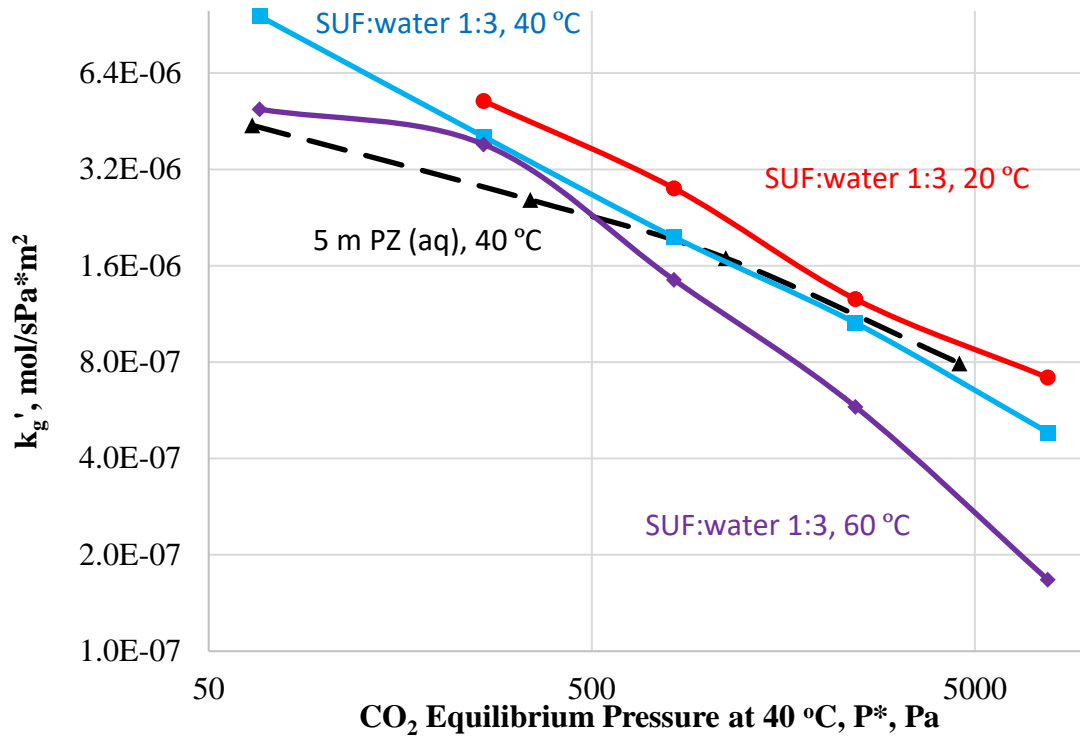


Figure 5.5: k_g' of 5 m PZ in 1 SUF/3 water at 20–60 °C in WWC

k_g' of 5 m PZ in 1 SUF/1 water is plotted against $P^*_{CO_2}$ at 40 °C in Figure 5.6. At lean loading, adding SUF increases k_g' because of higher CO₂ physical solubility, but at rich loading, adding SUF decreases k_g' , because of higher viscosity and lower diffusivity. The viscosity of 5 m PZ in 1 SUF/1 water is about 6 times that of 5 m PZ(aq), so the diffusivity of CO₂, PZ and PZ carbamate is significantly lower, which depresses k_g' .

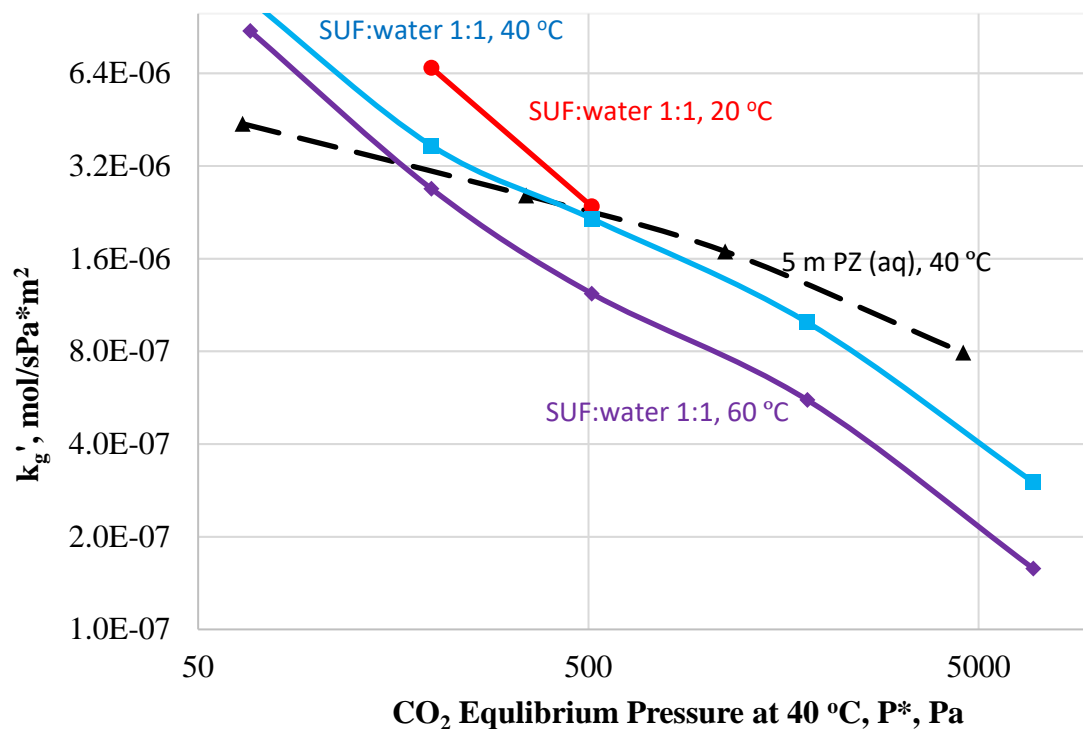


Figure 5.6: k_g' of 5 m PZ in 1 SUF/1 water at 20–60 °C in WWC

5.3.3 CO₂ solubility and absorption rate of 5 m PZ in IMI/water

The effect of adding imidazole (IMI) was also tested. IMI is a tertiary amine with a pKa of about 7 which is too low to act as a base in the system. IMI was treated as a physical solvent instead of amine in this study. Adding IMI to PZ(aq) showed similar effects on $P^*_{CO_2}$ and k_g' as adding SUF.

Figures 5.7 and 5.8 show adding IMI into 5 m PZ(aq) increases $P^*_{CO_2}$ slightly. Figures 5.9 and 5.10 show k_g' is greater at lean loading, but lower at rich loading compared to PZ(aq). The more SUF or IMI added, the faster the absorption rate is at lean loading. This rate behavior is similar to that of semi-aqueous MEA (Yuan and Rochelle, 2018). At lean loading, k_g' increases as activity of amine, concentration of free amine, and concentration of free CO₂ increase. At rich loading, k_g' decreases as

diffusivity of PZ and PZ carbamate significantly drops because the viscosity of PZ-IMI-water is about 5 times that of PZ(aq), which causes depletion of free PZ and accumulation of PZ carbamate near the gas-liquid interface.

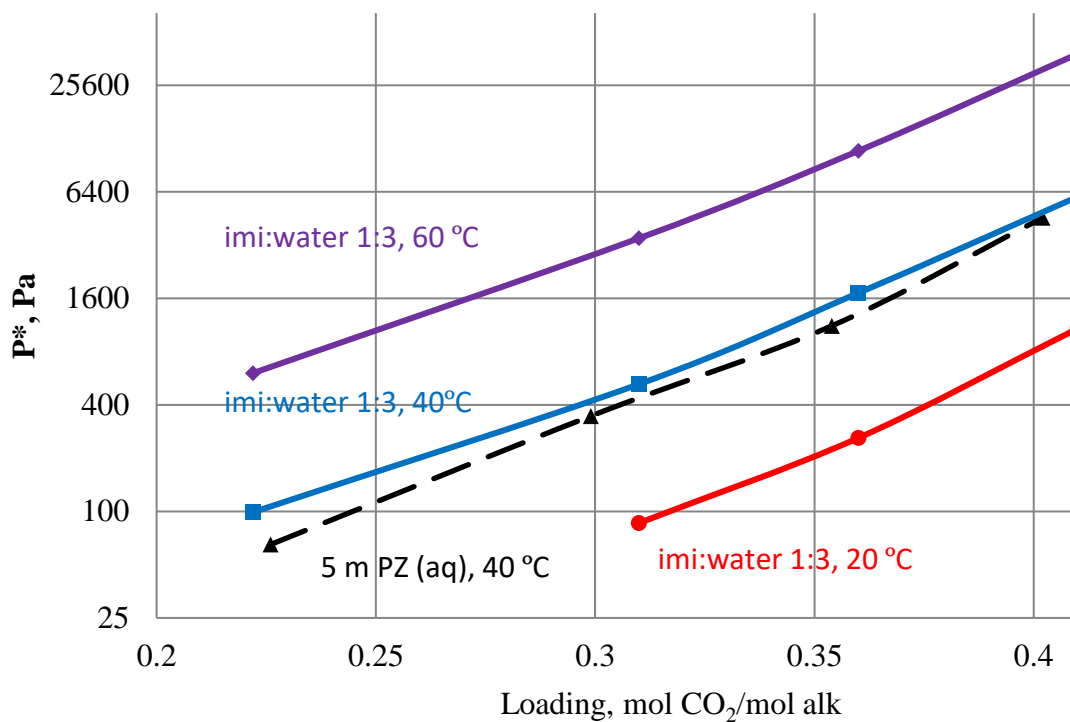


Figure 5.7: CO₂ solubility in 5 m PZ in 1 IMI/3 water

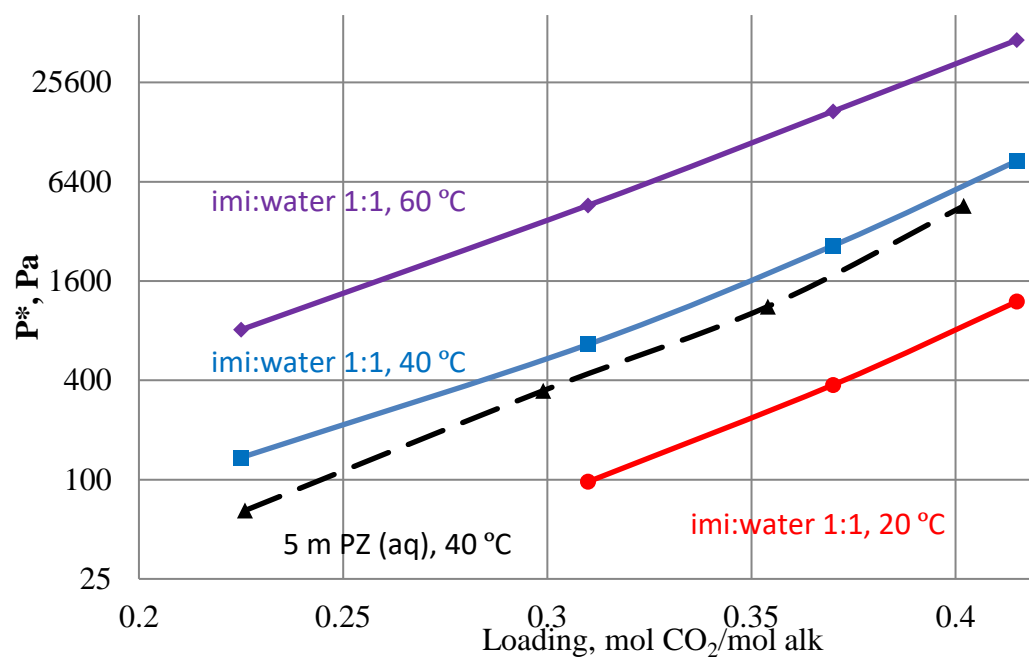


Figure 5.8: CO₂ solubility in 5 m PZ in 1 IMI/1 wat

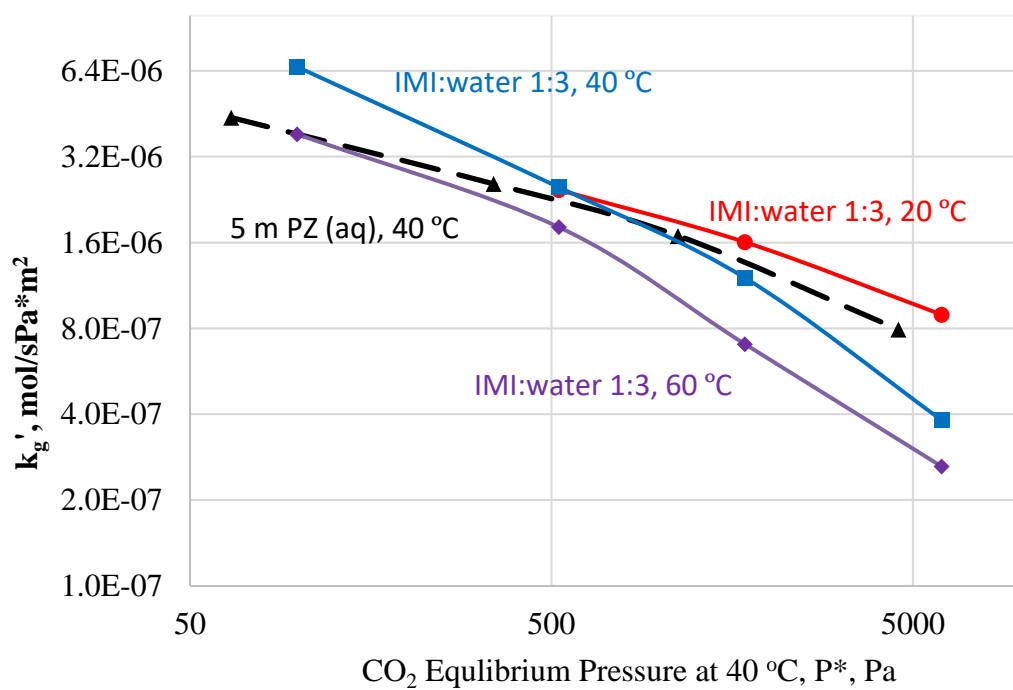


Figure 5.9: k_g' of 5 m PZ in 1 IMI/3 water at 20–60 °C in WWC

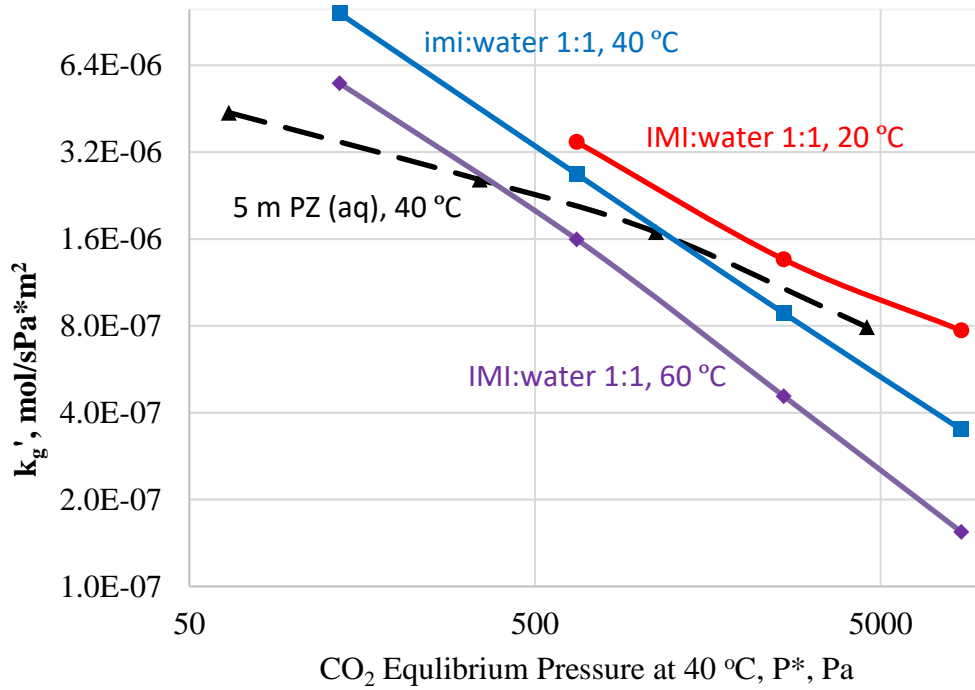


Figure 5.10: k_g' of 5 m PZ in 1 IMI/1 water at 20–60 °C in WWC

The absorber normally runs at 40 °C, so k_g' of all the studied solvents in this chapter is plotted against $P^*_{CO_2}$ at 40 °C in Figure 5.11. Compare to aqueous PZ, k_g' is greater at lean loading, but lower at rich loading. 5 m PZ in 1 IMI/ 1 water shows the highest rate at lean loading, which is a net effect of CO₂ physical solubility and viscosity.

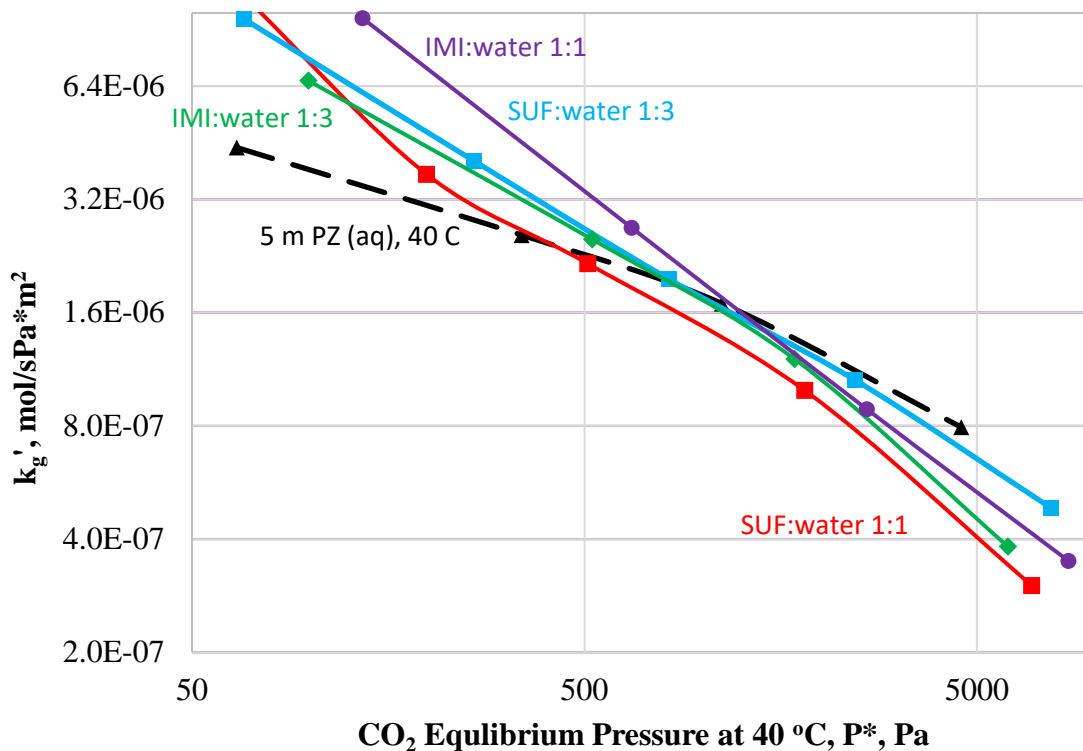


Figure 5.11: k_g' of 5 m semi-aqueous PZ at 40 °C in WWC

5.3.1 Viscosity of 5 m PZ in SUF/water and PZ in IMI/water

Viscosity of 5 m PZ in 1SUF/3water, 3SUF/1water, and 1IMI/1water was measured at different loadings at 20, 40, and 60 °C. The results are listed in Tables 5.5-5.7 and plotted in Figures 5.12-5.14. Viscosity was increased significantly after adding physical solvent. Also, the viscosity in semi-aqueous amine has a stronger dependency on loading than in aqueous amine. SUF is more viscous than IMI, so the viscosity in SUF/water is higher than in IMI/water. The average viscosity between lean and rich loading is 25 cP in 5 m PZ in 1SUF/1water, 9.5 cP in 5 m PZ in 1SUF/3water, and 15 cP in 5 m PZ in 1IMI/1water. The average viscosity of 5 m PZ is about 4 cP at 40 °C.

Table 5.5: Viscosity (cP) in 5 m PZ in 1SUF/1water

loading,	20 °C	40 °C	60 °C
0.4	74	34.3	21.5
0.36	59	27.9	18.5
0.31	48	22	13.6
0.26	42	20	10.7
0.178	36	14	7.7

Table 5.6: Viscosity (cP) in 5 m PZ in 1SUF/3water

loading,	20 °C	40 °C	60 °C
0.4	19.9	10.8	7.3
0.365	19.2	10.5	7.2
0.323	17.6	9.8	6.8
0.27	14.3	8.1	5.5
0.21	12.9	6.9	4.6

Table 5.7: Viscosity (cp) in 5 m PZ in 1IMI/1water

loading,	20 °C	40 °C	60 °C
0.415	46.5	21	12
0.37	41.9	19.2	10.8
0.31	33.9	16.2	9.2
0.225	26.6	12.8	7.8

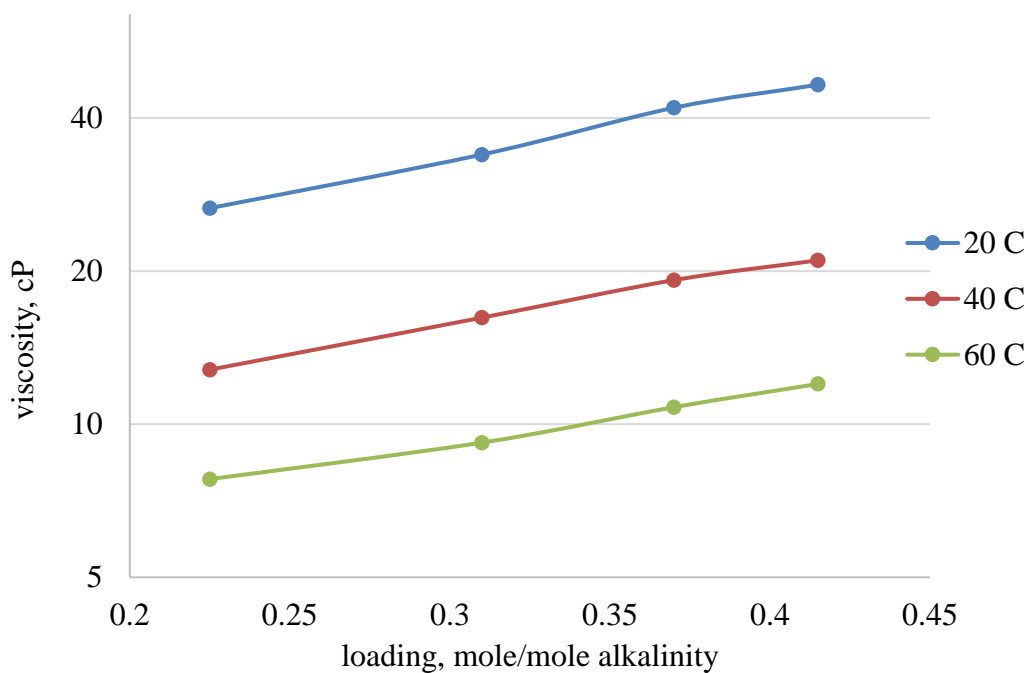


Figure 5.12: Viscosity of 5 m PZ in 1IMI/1water at 20–60 °C in WWC

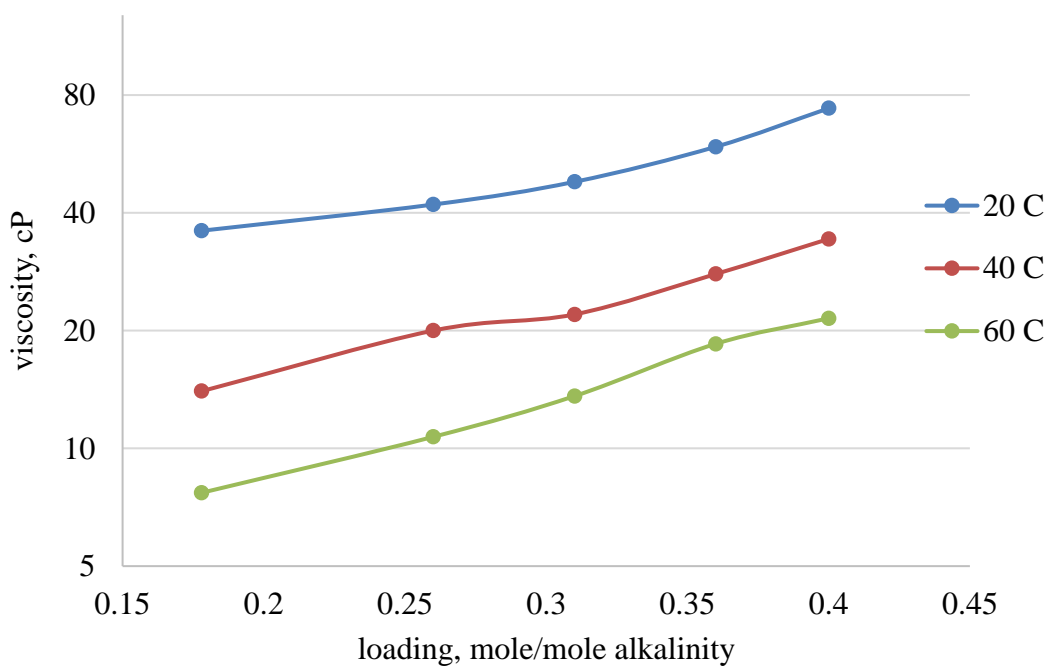


Figure 5.13: Viscosity of 5 m PZ in 1SUF/1water at 20–60 °C in WWC

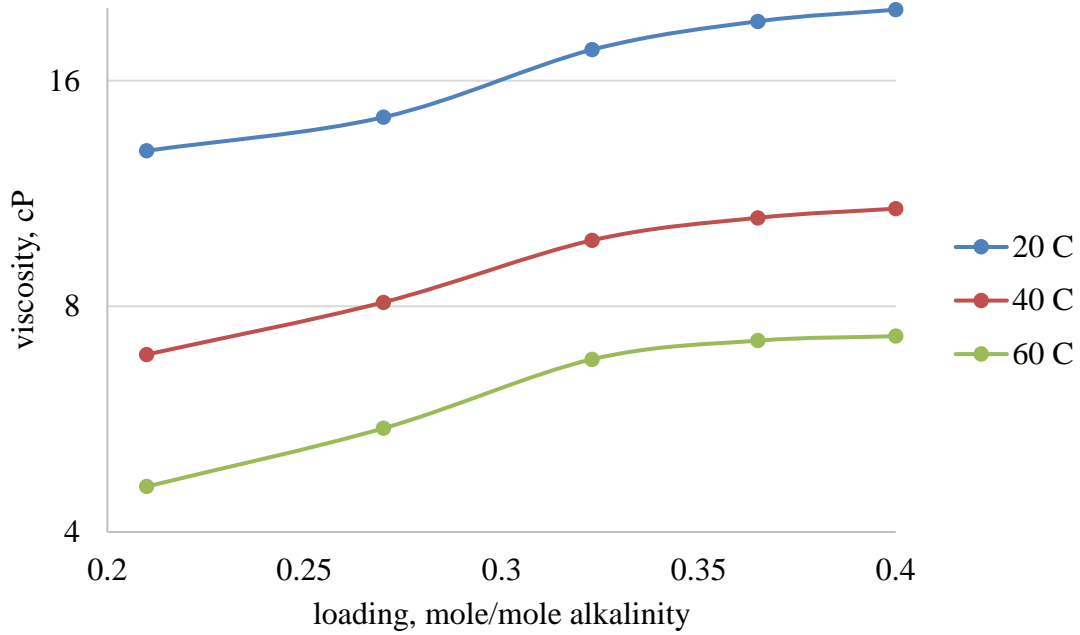


Figure 5.14: Viscosity of 5 m PZ in 1SUF/3water at 20–60 °C in WWC

5.3.1 Comparisons of semi-aqueous PZ solvents

The average k_g' ($k_g'_{avg}$) for an isothermal absorber at 40 °C and 90% CO₂ removal is calculated to compare the solvents. It is calculated as the ratio of CO₂ flux to the partial pressure driving force, assuming a linear concentration profile and equilibrium curve in the absorber. Experimental values at 40 °C are used to interpolate k_g' that corresponds to $P_{CO_2}^*$

$$\begin{aligned}
 k'_{g\ avg} &= \frac{Flux_{CO_2,LM}}{(P_{CO_2} - P_{CO_2}^*)_{LM}} \\
 &= \frac{(Flux_{CO_2,top} - Flux_{CO_2,bottom}) / \ln(Flux_{CO_2,top} / Flux_{CO_2,bottom})}{(P_{CO_2,top} - P_{CO_2,lean}^*) - (P_{CO_2,bottom} - P_{CO_2,rich}^*) / \ln\left(\frac{P_{CO_2,top} - P_{CO_2,lean}^*}{P_{CO_2,bottom} - P_{CO_2,rich}^*}\right)}
 \end{aligned}
 \tag{5.1}$$

For coal-fired flue gas treating, P_{CO_2} in the bulk gas at the bottom and top of the absorber are 12 and 1.2 kPa. The typical rich loading corresponds to $P_{CO_2}^*$ of 5 kPa, and

lean loading is around 0.1–0.5 kPa. For the operating range 0.5–5 kPa, kg'_{avg} in semi-aqueous 5 m PZ is about the same as 5 m PZ(aq); for the operating range 0.1–5 kPa, kg'_{avg} is about 15–35% higher than in 5 m PZ (aq) depending on the amount of IMI/SUF added. In CO₂ capture for a natural gas-fired power plant, P_{CO_2} in flue gas is 3.5 kPa instead of 12 kPa, and rich loading $P^*_{CO_2}$ is reduced to about 1.5 kPa from 5 kPa. For the operating range 0.1–1.5 kPa (natural gas conditions), kg'_{avg} in semi-aqueous 5 m PZ water is 20–50% higher than in 5 m PZ(aq). The results are listed in Table 5.8.

The CO₂ cyclic capacity (ΔC_{solv}) of solvent is defined by Equation 5.2. α_{lean} and α_{rich} are the CO₂ loading at lean and rich conditions (mol CO₂/mol amine). Adding SUF/IMI slightly increases the capacity due to a flatter VLE curve on the lean side.

$$\Delta C_{solv} = (\alpha_{rich} - \alpha_{lean}) \cdot \text{molality of alkalinity/kg solvent} \quad 5.2$$

Table 5.8: Cyclic capacity and kg'_{avg} of 5 m PZ

Mass ratio	Viscosity	Cyclic capacity			$kg'_{avg} \cdot 10^6$ at 40 °C			
		0.1–5kPa	0.5–5kPa	0.1–1.5kPa	0.1–5kPa	0.5–5kPa	0.1–1.5kPa	
	cP	mol CO ₂ /kg solvent			mol/s*Pa*m ²			
5 m PZ(aq)	4.2	0.95	0.6	0.78	1.41	1.13	2.09	
SUF	wat er							
1	3	10	1.06	0.56	0.82	1.74	1.28	2.37
1	1	24	1.21	0.56	0.98	1.99	0.94	3.05
IMI	wat er							
1	3	8.3	1.2	0.64	0.87	1.64	1.13	2.42
1	1	18	1.26	0.67	0.93	2.24	1.08	3.12

5.4 Conclusions

1. Solid precipitation in 5 m PZ(aq) can be solved by partially replacing water with physical solvent (SUF or IMI). No precipitation was observed in 5 m PZ in 1SUF/3 water, 1SUF/1 water 1 IMI/3 water, or 1 IMI/1 water in the loading range of 0.15–0.45 mole CO₂/mole alkalinity at 20–60 °C.
2. Adding SUF or IMI into aqueous PZ increases k_g' at lean and median loading but decreases k_g' at rich loading.
3. k_g' in semi-aqueous PZ increases as temperature decreases from 60 to 20 °C.
4. Compared to 5 m PZ(aq), $k_g'_{avg}$ in 5 m semi-aqueous PZ is about the same for 0.5–5kPa P*_{CO2}, 15–35% greater for 0.1–5 kPa P*_{CO2}, and 20–50% greater for 0.1–1.5kPa P*_{CO2} (natural gas conditions).
5. CO₂ cyclic capacity slightly increases after adding SUF/IMI; however, because of higher viscosity, the normalized capacity will be reduced. Normalized capacity of semi-aqueous PZ involving viscosity, thermal conductivity, and heat capacity will be covered in Chapter 7.

Chapter 6: Mass Transfer Modeling in Semi-aqueous Amines⁴

6.1 INTRODUCTION

Chapter 4 and Chapter 5 show that semi-aqueous amine composed of amine (MEA, PZ), water, and physical solvent have higher CO₂ absorption rate (kg') than aqueous amine at lean and median loading. However, as loading increases, kg' drops very fast in semi-aqueous amines. At lean loading, kg' in 7 m MEA in 19NMP/water could be as high as five times that of 7 m MEA(aq). At rich loading of P*_{CO2} around 5kPa, kg' in semi-aqueous MEA drop to close to MEA(aq); kg' of semi-aqueous PZ (PZ-SUF/IMI-water) is slightly lower than PZ(aq).

The rate behavior in semi-aqueous amines is not fully understood. Chapter 4 demonstrates that after adding physical solvent, kg' should increase because activity of amine and CO₂ physical solubility increase, should decrease because diffusivity of CO₂, amine, and amine products decreases. To get the overall effect on kg', the quantitative dependency of kg' on these parameters is required. Pseudo-first-order (PFO) approximation (details in Chapter 4) assumes the concentration of amine and amine products is constant across the interface, as a result kg' does not depend on diffusivity of amine and amine product, which is questionable in semi-aqueous amines. With the PFO rate expression (Equation 6.1), kg' is quantitatively linked to activity of amine, CO₂ physical solubility, and CO₂ diffusivity. However, as the CO₂ concentration on the interface increases and the amine diffusivity decreases due to higher viscosity, the amine at the interface will be lower than in the bulk liquid, and the amine product on the surface could be higher than in the bulk liquid. Hence the pseudo-first-order (PFO) approximation may not be accurate for semi-aqueous systems.

⁴Parts of this chapter have been published in Chemical Engineering Science: Yuan, Y., Rochelle, G.T. (2018). CO₂ absorption rate in semi-aqueous monoethanolamine for CO₂ capture. Chemical Engineering Science, volume 182, 55-66

$$k_g' = \frac{\sqrt{D_{CO_2} k_3^* a_{MEA}}}{\gamma_{CO_2}^{0.5} H_{CO_2}} \propto \frac{\sqrt{D_{CO_2}^* \gamma_{MEA}}}{\gamma_{CO_2}^{0.5}} \quad 6.1$$

Systematic study of the rate behavior in semi-aqueous amine was done by both experimental and modeling efforts. A mass transfer model was built in MATLAB® using the CO₂-MEA-NMP-water data collected in Chapter 4. The effect of rate constant, diffusivity of CO₂, MEA, and MEA product, CO₂ physical solubility (activity of CO₂), and activity of MEA on rate was explored.

6.2 MASS TRANSFER THEORY

The mass transfer between gaseous CO₂ in flue gas and liquid amine solvent involves four phenomena: molecular diffusion in the gas phase, physical solubility at the gas-liquid interface, molecular diffusion in the liquid phase, and chemical reactions in the liquid. The gas phase diffusion is relatively straightforward and can be easily accounted for by correlations (Bishnoi, 2000). However, the mass transfer process in the liquid with both diffusion and reversible chemical reactions is complicated. Understanding the reactive mass transfer of CO₂ in liquid amine is critical to interpret absorption rate as a function of solvent property parameters.

6.2.1 Mass transfer coefficients

The CO₂ mole flux (N_{CO_2}) represent the rate of mass transfer per unit area. As defined by Fick's law, the mole flux of CO₂ across the gas-liquid interface ($x=0$) can be written as Equation 6.2.

$$N_{CO_2} = -D_{CO_2} \left. \frac{\partial [CO_2]}{\partial x} \right|_{x=0} \quad 6.2$$

The mole flux can also be linked to the concentration/partial pressure driving force for mass transfer. In the case of CO₂ absorption from bulk gas to bulk liquid, CO₂ flux can be written for the driving force in the gas film, liquid film, or overall (Equation

6.3). The proportionality constant between mole flux and the corresponding driving force is the mass transfer coefficient: k_g, k_l, k'_g, K_G .

$$N_{CO_2} \left[\frac{mol}{s \cdot m^2} \right] = \begin{cases} k_g(P_{CO_2,bulk} - P_{CO_2,i}) \\ k_l(CO_{2,i} - CO_{2,bulk}) \\ k'_g(P_{CO_2,i} - P_{CO_2}^*) = \frac{k_l}{H_{CO_2}}(P_{CO_2,i} - P_{CO_2}^*) \\ K_G \cdot (P_{CO_2,bulk} - P_{CO_2}^*) \end{cases} \quad 6.3$$

The overall gas side mass transfer coefficient (K_G) corresponds to the concentration driving force between bulk gas and bulk liquid, where $P_{CO_2}^*$ is in equilibrium with $[CO_2]_{bulk}$. The gas film mass transfer coefficient (k_g) corresponds to the driving force across the gas film, and k_g is a function of relevant properties of the gas which can be calculated by correlation (Bishnoi, 2000). At the gas-liquid interface, the CO_2 in the gas and liquid are in equilibrium, and can be related using the Henry's constant. The liquid film mass transfer coefficient (k_l) corresponds to the CO_2 concentration gradient in the liquid phase. The parameter k'_g is also the liquid film mass transfer coefficient, which differs from k_l only in that it has partial pressure units. k'_g is referred to as the CO_2 absorption rate in this work, and its dependency on solvent parameters is studied.

The flux across each mass transfer film should be the same, and the mass transfer coefficients can be written in the series resistance form:

$$\frac{1}{K_G} = \frac{1}{k_g} + \frac{H_{CO_2}}{k_l} = \frac{1}{k_g} + \frac{1}{k'_g} \quad 6.4$$

6.2.2 Mass Transfer Without Reaction (Physical Absorption)

The case of physical mass transfer of CO_2 without chemical reaction is considered to evaluate the effect of molecular diffusion on the liquid film mass transfer coefficient

(k_1 or k_g'). The dependence of k_1 on the diffusion coefficient can be determined by solving the simplified continuity equation 6.5, which assumes mass transfer of CO_2 occurs only in the x direction via molecular diffusion.

$$D_{CO_2} \frac{\partial^2 [CO_2]}{\partial x^2} = \frac{\partial [CO_2]}{\partial t} \quad 6.5$$

Without any reactive species in the solution, the absorption rate of CO_2 for unit area (CO_2 flux, N_{CO_2}) depends on the physical solubility of CO_2 in the solution (Henry's constant, H_{CO_2}) and the liquid phase mass transfer coefficient (k_l^0):

$$N_{CO_2} = k_l^0 ([CO_2] - [CO_2]^*) = k_l^0 \left(\frac{P_{CO_2}}{H_{CO_2}} - [CO_2]^* \right) \quad 6.6$$

k_l^0 is a function of the liquid viscosity and CO_2 diffusivity in the liquid.

Several mass transfer models have been proposed to describe the physical process and solve the differential equation with its own specified boundary conditions. Although these theories are discussed in the scenario of physical absorption, they can also be applied to mass transfer with chemical reactions.

6.2.2.1 Film Theory

Film theory proposes a steady state model, which assumes the diffusion of CO_2 occurs within a boundary layer close to the interface (Whitman 1962). As Figure 6.1 shows a gas film and a liquid film exists right next to the interface. They are stagnant with thickness of δ_g and δ_l . Also, the bulk liquid is assumed to be well mixed, and the convection in the liquid bulk ultimately determines the film thickness. The effect of convection is neglected within the diffusion boundary. The governing equation and boundary conditions based on film theory is:

$$\frac{\partial^2 [CO_2]}{\partial x^2} = 0; \quad \begin{array}{l} @ x=0, [CO_2]=[CO_2]_i \\ @ x=\delta_l, [CO_2]=[CO_2]_{bulk} \end{array} \quad 6.7$$

The solution of Equation 6.7 gives a first order dependence of k_1 on D_{CO_2} :

$$N = k_l^0 (C_i^* - C_i) = \frac{D_i}{\delta_l} (C_i^* - C_i) \quad 6.8$$

$$k_l^0 = \frac{D_{CO_2}}{\delta} \quad 6.9$$

The CO₂ concentration profile in the gas and liquid film as proposed by the film theory is shown in Figure 6.1.

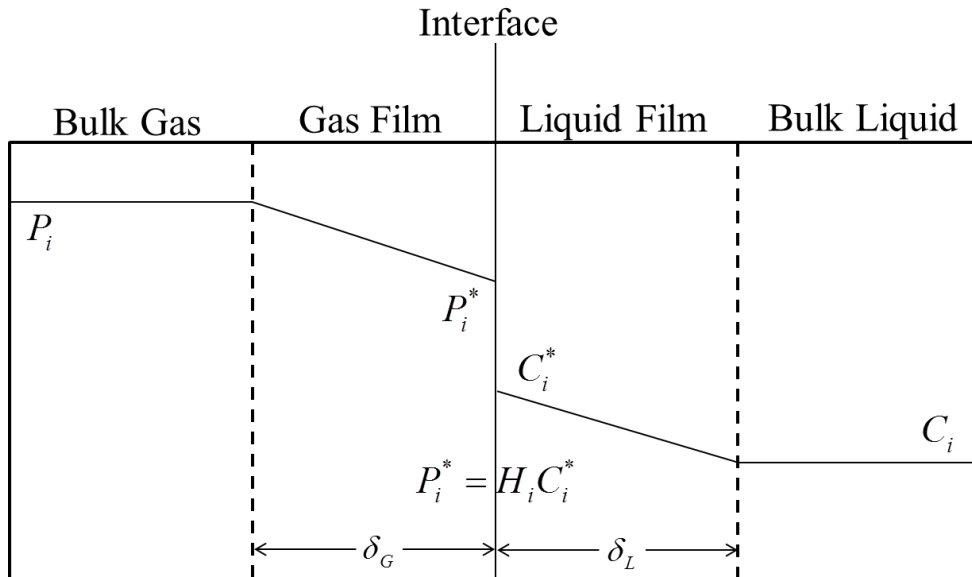


Figure 6.1: Steady state concentration profile of CO₂ absorption without chemical reaction in the liquid phase, using film theory (not drawn to scale).(Chen, 2011)

The film model is widely used to illustrate the diffusion of CO₂ in the liquid phase due to its simplicity. However, it is largely criticized as the first order dependence of k_l on D_{CO_2} has been shown to be incorrect when compared with experimental data (Danckwerts, 1970). Moreover, the discontinuity in the concentration profile at the diffusion boundary is highly unrealistic. To improve the discontinuity, the films are usually further divided into segments, and mass transfer equations are numerically solved for each segment. This strategy is implemented in the modeling software such as Aspen

Plus[®], but the first order dependence of k_1 on D_{CO_2} still exists. The purpose of this work is to find the dependence of k_1 on solvent parameters, so film theory cannot be used.

6.2.2.2 Penetration theory

The Penetration theory (Higbie 1935) argued that the film theory with its steady flow was not valid if the penetration period is of same magnitude to or longer than the contact time between gas and liquid. As a result, each element spends only a finite amount of time at the interface participating in the diffusion process. The times spent at the interface (τ) are assumed to be constant among all the liquid elements. The solution derived using this model shows a half order dependence of k_1 on D_{CO_2} :

$$k_l = \sqrt{\frac{4D_{CO_2}}{\tau\pi}} \quad 6.10$$

The Surface Renewal theory (Danckwerts 1951) improves on the Penetration Theory model by replacing the constant contacting time assumption. Instead, contacting time is described using probability distribution function to represent the range of time spend at the interface by each liquid element. The result also shows a half order dependence of k_1 on D_{CO_2} :

$$k_l = \sqrt{D_{CO_2}s} \quad 6.11$$

In Equation 6.11, the parameter s represents the fraction of renewal surface.

The Penetration theory and The Surface Renewal theory are unsteady state theories, which complicates the mathematics in applications. The square root dependence on D_{CO_2} agrees with experimental data (Danckwerts 1970). In addition, The Penetration theory and The Surface Renewal theory are more close to reality. In the WWC, liquid surface contacts with gas only inside the chamber by a short contacting time. The contacting time is less than 1 second, which is far away from steady state. In the packed column, the surface contact time (maybe a distribution of τ) also exists

between mixing points in the packing. As viscosity of the solvent increases, contacting time increases for each element and the surface renewal frequency decreases, which should decrease absorption rate. This viscosity dependency could be captured by the Penetration theory.

6.2.2.3 Eddy Diffusivity Theory

The eddy diffusivity theory (King, 1966) postulates that the eddy diffusivity for a liquid element near or at the gas-liquid interface can be described by a power law:

$$D_E = a\delta^n \quad 6.12$$

Where δ is the distance normal to the interface. At the interface where $\delta = 0$, the eddy diffusivity is zero and the mass transfer is completely dominated by molecular diffusion.

It is a steady state model which proposes the presence of eddy currents in the liquid film that affect the diffusion of CO₂ in the solvent. This microscopic convection effect is added to the continuity equation as Equation 6.13.

$$\frac{\partial}{\partial x}(D_{CO_2} + \varepsilon x) \frac{\partial [CO_2]}{\partial x} = 0 \quad 6.13$$

The parameter ε varies the size of the current as function of the depth into the liquid film, where the current is assumed to be smallest close to the interface and will increase as CO₂ moves into the liquid film (King 1966). The solution using this model shows the square root dependence of k_l on D_{CO_2} :

$$k_l = \frac{\sqrt{4D_{CO_2}\varepsilon}}{\pi} \quad 6.14$$

The Eddy Diffusivity model is attractive as it correctly predicts the half order dependence of k_l on D_{CO_2} . Also, it is still a steady state model, which simplifies solution of equations.

The dependence of k_l on D_{CO_2} predicted by the mass transfer models are summarized in Table 6.1.

Table 6.1: Summary of k_l dependence on diffusion coefficient by various physical mass transfer models

Theory	n: $k_l = f(D_{CO_2}^n)$	Model form
Film	1	Steady State
Penetration	0.5	Unsteady State
Surface Renewal	0.5	Unsteady State
Eddy Diffusivity	0.5	Steady State

6.2.3 Mass transfer with chemical reaction

For the reactive absorption of CO_2 by aqueous amines, the effects of both molecular diffusion and chemical reaction need to be accounted for. The general continuity equation for this reactive mass transfer problem is:

$$\frac{dc_i}{dt} = -Di \frac{d^2c_i}{dx^2} + V_i * R \quad 6.15$$

where:

C_i : concentration of each component (CO_2 , amine, amine products);

V_i : stoichiometric coefficient;

R : reaction rate;

6.2.3.1 Instantaneous Reactions

Instantaneous reaction is a limiting case when the reaction between CO_2 and some highly reactive solvents like MEA and PZ is extremely fast at high temperature. Reaction rates increase exponentially with temperature, and can be assumed to be instantaneous relative to diffusion rate. The instantaneous limit is also helpful in demonstrating the mass transfer behavior in the diffusion film for systems with moderate Hatta numbers (Danckwerts, 1970). At moderate Hatta numbers, a diffusion film exists where the chemical reactions are at equilibrium, which is similar to the case of

instantaneous reaction. In both cases, the overall mass transfer is entirely driven by the diffusion of reactants and products.

The reversible CO₂ reaction with amines can be simplified as Equation 6.16, with the corresponding equilibrium constant in Equation 6.17.

$$CO_2 + R \leftrightarrow P \quad 6.16$$

$$K = \frac{[P]_e}{[CO_2]_e[R]_e} = \frac{[P]_i}{[CO_2]_i[R]_i} = \frac{[P]_{bulk}}{[CO_2]_{bulk}[R]_{bulk}} \quad 6.17$$

At the gas-liquid interface, [CO₂]_i is not in equilibrium with P_{CO₂i}, but is in chemical equilibrium with the other species in the liquid due to instantaneous reaction.

Mathematically, the mass balance of this case can be simplified to

$$D_{CO_2} \frac{\partial^2 [CO_2]}{\partial x^2} + D_P \frac{\partial^2 [P]}{\partial x^2} = 0 \quad 6.18$$

With the boundary conditions of:

$$\begin{aligned} & @x=0, \\ & [P]=[P]_i; [CO_2]=[CO_2]_i; [R]=[R]_i \\ & @x=\delta, \\ & [P]=[P]_{bulk}; [CO_2]=[CO_2]_{bulk}; [R]=[R]_{bulk} \end{aligned} \quad 6.19$$

As shown by Danckwerts (1970), the flux expression derived from Equation 6.18 and 6.19 is:

$$N_{CO_2} = k_l^\circ \left[\left([CO_2]_i + \frac{D_P [P]_i}{D_{CO_2}} \right) - \left([CO_2]_{bulk} + \frac{D_P [P]_{bulk}}{D_{CO_2}} \right) \right] \quad 6.20$$

At moderate to high CO₂ loading, the concentration of free CO₂ is much lower than the reaction products, and Equation 6.20 can be simplified to:

$$N_{CO_2} = k_l^\circ \frac{D_P}{D_{CO_2}} ([P]_i - [P]_{bulk}) \quad 6.21$$

To convert the concentration driving force in Equation 6.21 into partial pressure driving force, the slope of the equilibrium can be used ($\frac{\Delta P_{CO_2}^*}{\Delta [CO_2]_T}$). $\Delta [CO_2]_T$ is the total

concentration of all the species that contains CO₂ (free CO₂, HCO₃⁻, and amine products with carboxylic acid group).

If k_l° expression from film theory is used, the flux expression can be further reduced to Equation 6.22. If a square root dependence of k_l° on D_{CO_2} is assumed, the flux expression is derived in Equation 6.24.

$$N_{CO_2} = k_{l-prod}^\circ \left(\frac{\Delta P_{CO_2}^*}{\Delta [CO_2]_T} \right) \cdot (P_{CO_2,i} - P_{CO_2}^*) \quad 6.22$$

$$N_{CO_2} = k_{l-prod}^\circ \left(\sqrt{\frac{D_p}{D_{CO_2}}} \right) \left(\frac{\Delta P_{CO_2}^*}{\Delta [CO_2]_T} \right) \cdot (P_{CO_2,i} - P_{CO_2}^*) \quad 6.23$$

$$k'_{g,INST} = k_{l-prod}^\circ \left(\sqrt{\frac{D_p}{D_{CO_2}}} \right) \left(\frac{\Delta P_{CO_2}^*}{\Delta [CO_2]_T} \right) \quad 6.24$$

This rate expression is based on steady state film theory. In the scenario of extremely low diffusivity (high viscosity), D_p approaches 0. Equation 6.24 gives a zero absorption rate. However, if CO₂ can still diffuse into the solution, a decent absorption rate should exist. This case can only be captured by unsteady state penetration theory.

6.2.3.2 Finite-Rate Reaction

Figure 6.2 is a representation of film analysis for CO₂ absorption by bulk liquid with fast chemical reaction. Reaction rate is not so fast to be instantaneous while still fast enough for most of the reaction to occur within a thin boundary layer near gas-liquid interface. This scenario represents most of CO₂ absorption by amine solvents. The CO₂ concentration at the interface is now related to reaction kinetics, molecular diffusion of CO₂, and the diffusion of reactants and products.

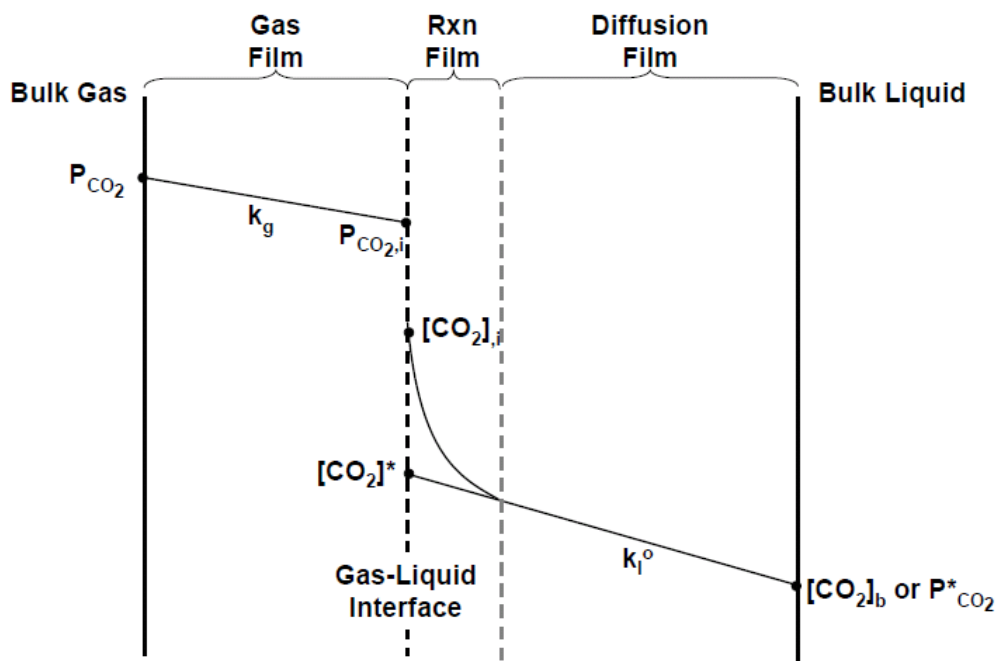


Figure 6.2: Mass transfer of CO₂ into bulk liquid with fast chemical reaction. (Cullinane 2005)

Certain simplifications reduce the complexity in solving the differential equation and lead to useful analytical expressions. If the amine concentration is effectively constant across the reactive boundary layer, then the pseudo-first order (PFO) reaction assumption applies. However, the assumption of constant amine concentration is not valid in semi-aqueous amines for the following two reasons:

1. Physical solubility of CO₂ increases $[CO_2]_i$ which decreases the concentration of amine at interface.
2. Higher viscosity of semi-aqueous amine reduces the diffusivity of both amine and amine products.

The net effect cause depletion of amine on the surface and accumulation of amine product. As a result, the analytical expressions by PFO cannot be used. Instead, the full

continuity equation was solved in MATLAB numerically, and then sensitivity analysis of absorption rate on property parameters was conducted.

6.2.4 CO₂ mass transfer in MEA-NMP-water

For semi-aqueous amine solvents, the CO₂ reaction rate is not instantaneous but is fast enough for most of the reaction to occur within a thin boundary layer (reaction film) near the gas-liquid interface. Penetration Theory was used to better capture the dependence of k_l or k_g' on D_{CO_2} . Mathematically, the reaction-diffusion problem in CO₂ absorption by amines can be described by the species continuity equations for each component (Equations 6.25) (Danckwerts, 1970). The solution to the coupled differential equations and associated boundary conditions yield concentration profiles and transfer rates for each component in the system. The concentration profiles in Figure 6.3 provide a general representation with film theory of absorption and reaction of CO₂ in amine solvents.

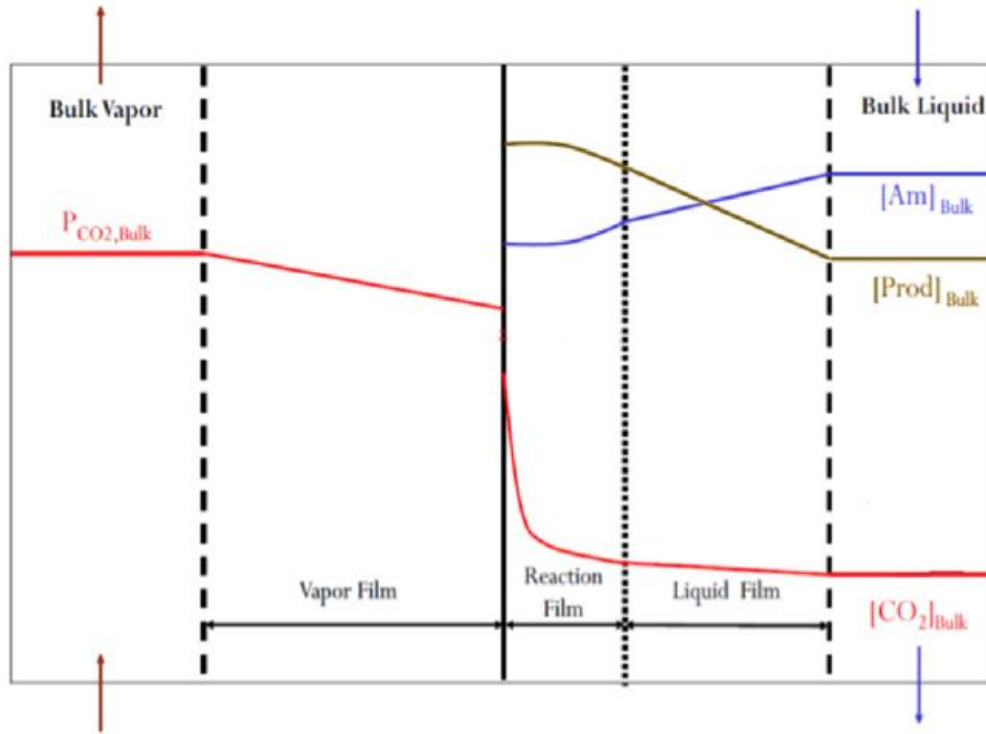


Figure 6.3: Concentration profiles (not to scale). The entire liquid film (liquid and reaction film) is discretized for numerical integration.

$$\frac{dc_i}{dt} = -Di \frac{d^2c_i}{dx^2} + V_i * R \quad 6.25$$

$$R = k_3 * a_{CO_2} * a_{MEA}^2 - \frac{k_3}{K_{eq}} a_{MEACOO} * a_{MEA}H \quad 6.26$$



$$K_{eq} = \frac{a_{CO_2} * a_{MEA}^2}{a_{MEACOO} * a_{MEA}H} \quad 6.28$$

$$a_i = \gamma_i * C_i \quad 6.29$$

$$D_{CO_2} = D_{CO_2,aq} \left(\frac{\mu}{\mu_{aq}}\right)^{-x} \quad 6.30$$

$$D_{MEA} = D_{MEA,aq} \left(\frac{\mu}{\mu_{aq}}\right)^{-0.6} \quad 6.31$$

where:

K_{eq} : equilibrium constant;

C_i : concentration of each component (CO_2 , MEA, MEACOO, MEAH);

a_i : activity of each component;

V_i : stoichiometric coefficient;

γ_i : activity coefficient;
 D_i : diffusion coefficient, m^2/s ;
 $D_{CO_2,aq} = 10^{-9}$, $D_{MEA,aq} = 3.5 * 10^{-10}$, at 40 °C (Dugas, 2009)
 μ : viscosity, cP, 40 °C;
 R : reaction rate;
 k_3 : third order reaction rate constant (first order for CO₂ and second order for MEA);

Two representative loadings are selected to study: 0.37 mol CO₂/mol MEA for lean loading and 0.45 for rich loading. At both loadings, Equation 6.27 is the dominant reaction between CO₂ and MEA because the concentration of HCO₃⁻ is always less than 5% of MEACOO⁻ at this condition (Plaza, 2011). Concentration and activity of MEACOO⁻ and MEAH⁺ were assumed to be equal based on the stoichiometry. Dugas (2009) and Li (2015) have show that in concentrated MEA, the reaction between MEA and CO₂ is second order in amine and first order in CO₂. Diffusivity of CO₂ and MEA in water at 40 °C was taken from Dugas (2009), and the diffusivity of MEA carbamate and protonated MEA in the solvent were assumed to be the same as D_{MEA} . The diffusivity is a function of viscosity according to Equations 6.30 and 6.31 (Versteeg and Van Swaalj, 1988). The dependence of D_{CO_2} on viscosity (x in Equation 6.30) was regressed, as well as the activity based third-order rate constant (k_3) to match predicted k_g' with experimental k_g' .

Equation 6.25 was solved from $t = 0$ to $t = \tau$ (the contact time of CO₂ and solvent in the WWC). τ was calculated by the liquid flow rate, the geometry of the wetted wall column, and the viscosity of the solvent.

$$\tau = \frac{2h}{3} \left(\frac{3\mu}{\rho g} \right)^{\frac{1}{3}} \left(\frac{\pi d}{Q_{liq}} \right)^{\frac{2}{3}} \quad 6.32$$

where:

h : height of the column;
 μ : viscosity;
 ρ : density;
 g : gravity constant;

d : diameter of the column;
 Q_{liq} : liquid flowrate.

The concentration of each component (mol/L) in the bulk liquid at a given CO₂ loading was from Plaza (2011). The interface and bulk CO₂ concentration was calculated by Henry's constant with measured CO₂ activity coefficient. Plaza (2011) also reported the activity of each component in aqueous MEA. Adding NMP changes the ionic strength of the system and varies the activity of each component, but the concentration of MEA and MEACOO is still constant. In semi-aqueous MEA, a_{MEA} was estimated by FTIR measurement (details in Chapter 4). Using K_{eq} , concentration and activity coefficient of CO₂ and MEA, and concentration of MEAC, γ_{MEACOO} were calculated in semi-aqueous MEA.

Table 6.2: Concentration and activity coefficient in aqueous MEA (Plaza, 2011)

	MEA	MEACOO
Lean loading		
0.37 mol CO ₂ /mol MEA		
Concentration, mol/L	1.31	1.82
Activity coefficient	0.65	0.3
Rich loading		
0.45 mol CO ₂ /mol MEA		
Concentration, mol/L	0.59	2.21
Activity coefficient	0.7	0.26

The equation set was solved using the MATLAB® PDE solver. With the concentration profile calculated by MATLAB®, CO₂ flux (N_{CO_2}) was obtained by Fick's Law in Equation 6.33. The absorption rate or liquid film mass transfer coefficient (kg') is the flux over the CO₂ partial pressure driving force (Equation 6.34). The average kg' over the contact time predicted by the model was compared to experimental data.

$$N_{CO_2} = -D_{CO_2} \frac{\partial[CO_2]}{\partial x} \Big|_{x=0} \quad 6.33$$

$$k'_g = \frac{N_{CO_2}}{(P_{CO_2}^{interface} - P_{CO_2}^*)_{lm}} \quad 6.34$$

6.2.5 Parameter Regression

The activity based third-order rate constant (k_3) and dependency of D_{CO_2} on viscosity (x in Equation 6.30) were regressed by matching the predicted liquid side mass transfer coefficient (k'_g) with experimental data at two different loadings and four different NMP concentrations (wt %). The fit of the model to the experimental data was quantified by calculating the average absolute relative deviation (AARD), as shown in Equation 6.35.

$$AARD = \frac{1}{n} * \frac{|k_{g,pred'} - k_{g,exp'}|}{k_{g,exp'}} \quad 6.35$$

The two parameters were regressed using response surface methodology (RSM), adapted from Sherman (2016). This method combines the speed of manual method with statistical rigor. RSM is a statistical science that deals with relationships between multiple (independent) variables and one (or more) response (dependent) variables (Myers et al., 2016). The method started with manually adjusting the two parameters to roughly fit k'_g , which established a basis. Next, each parameter was individually increased by 10% to get a $k'_{g,i+10\%}$. This determined the response surface by calculating the sensitivity S_i by Equation 6.36. The response surface took the form of Equation 6.37.

$$S_i = \frac{\ln \frac{k'_{g,i+10\%}}{k'_{g,basis}}}{\ln 1.1} \quad 6.36$$

$$\frac{k'_{g,pred}}{k'_{g,exp}} = \left(\frac{k'_{g,pred,basis}}{k'_{g,exp}} \right) * \left(\frac{k_3}{k_{3,basis}} \right)^{S_{k3}} * \left(\frac{x}{x_{basis}} \right)^{S_x} \quad 6.37$$

The nonlinear regression was done with the “*fitnlm*” command of MATLAB® using Equation 6.37 as the model equation. Once the parameters were regressed, AARD calculated by updated k_g' was checked.

6.3 RESULTS

6.3.1 Mass transfer modeling results

The third-order rate constant k_3 and the D_{CO_2} dependency on viscosity were regressed by matching the predicted liquid side mass transfer coefficient (k_g') with experimental data at two different loadings and four different NMP wt %. The fit of the model to the experimental data was quantified by calculating the average absolute relative deviation (AARD), as shown in Equation 6.35. Using the response surface methodology (RSM), k_3 is $149711 \frac{m^6}{mol^2*s}$ with a standard error of $9493 \frac{m^6}{mol^2*s}$, and the D_{CO_2} dependency on viscosity is 0.4 with a standard error of 0.09, resulting $D_{CO_2,2} = D_{CO_2,1} \left(\frac{\mu_2}{\mu_1}\right)^{-0.4}$. Figure 6.4 shows that the model fits experimental data, and AARD is 0.08. The small value indicates a good fit.

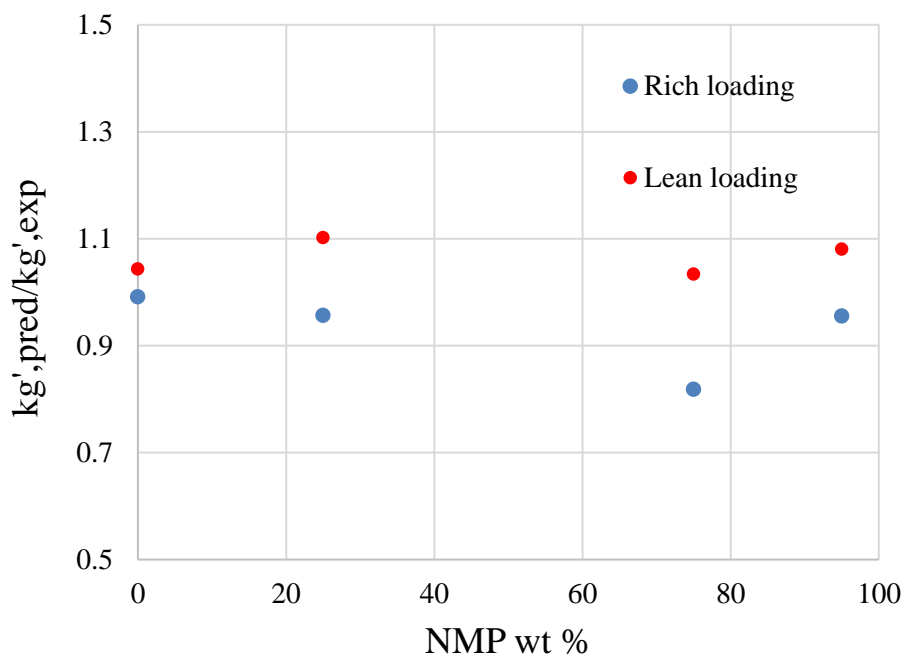


Figure 6.4: Fit of the mass transfer model, red points are 0.37 loading, blue points are 0.45 loading

The regressed dependence on viscosity (-0.4) is lower than the values regressed from aqueous amines by Dugas (2009) (-0.72 ± 0.12) and Versteeg and Van Swaaij (1988) (-0.8). The increase in viscosity from the addition of physical solvent does not reduce D_{CO_2} as much as previous correlations predict. In this study, viscosity varies by changing NMP wt %; while in Dugas and Versteeg, viscosity changes with amine type and concentration. In a semi-aqueous system, although the intermolecular force between NMP and MEA increases the viscosity, CO_2 can still diffuse through the space between molecular clusters. This behavior is also apparent in the fast rate observed in aminosilicones in TEG solvent (GAP-TEG) by Heldebrant (2017). The GAP-0 (the smallest GAP molecule) in TEG has a viscosity of 1300 cP at 40 °C, due to the formation of a hydrogen-bonding network between the carbamate and TEG solvent; however, k_g' is

still comparable or even higher than that in aqueous amines whose viscosity is lower than 10 cP. This is because CO₂ can diffuse through the hydrogen-bonding network easily. If D_{CO_2} depends as strongly on viscosity in this system as in aqueous amine, GAP-TEG could not have such a high k_g' .

6.3.2 Sensitivity analysis

With the model ready, the dependence of k_g' on solvent property parameters was obtained by sensitivity analysis. The sensitivity of k_g' to the various parameters was calculated by $\frac{\partial \ln k_g'}{\partial \ln parameter}$. The results from the model are compared to those found by PFO approximation. If PFO is valid, the sensitivity of k_g' to k_3 , D_{CO_2} , and γ_{CO_2} should be 0.5, 0.5, and -0.5; respectively.

Figures 6.5 and 6.6 show that without NMP, the sensitivity of k_g' to k_3 , D_{CO_2} , and γ_{CO_2} matches PFO prediction very well. The sensitivity of k_g' to γ_{MEA} is exactly double of the sensitivity to k_3 , which is determined by the form of the rate expression (Equation 6.26). This result supports the widely use of PFO assumption in aqueous amines.

$$k_g' \propto \frac{k_3^{0.5} D_{CO_2}^{0.5} \gamma_{MEA}}{\gamma_{CO_2}^{0.5}}, \text{ without NMP} \quad 6.38$$

As NMP (wt %) increases, the sensitivity deviates from PFO approximation, because adding NMP increases CO₂ at the interface, which will consume MEA at the surface faster than it can be diffused from the bulk. This depletion of MEA is much more obvious at rich loading than lean loading, because MEA is lower at rich loading and viscosity is higher at richer loading.

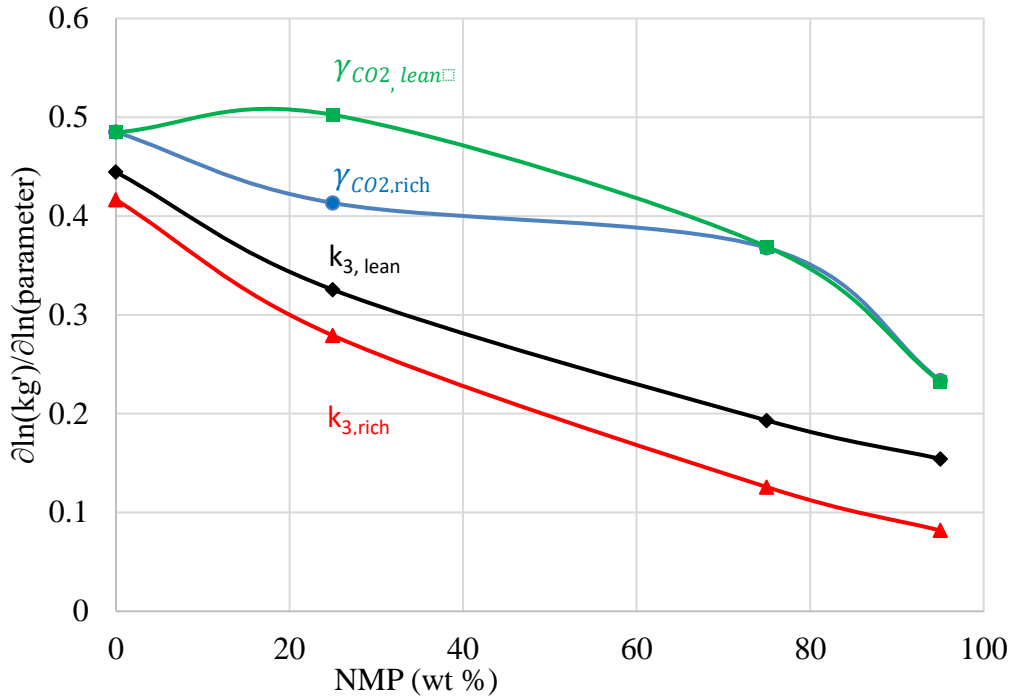


Figure 6.5: Sensitivity of k_g' to k_3 and CO_2 activity coefficient at lean/rich loading. The sensitivity to γ_{CO_2} is negative, absolute value is plotted.

Figure 6.6 also shows that D_{MEA} affects k_g' significantly after adding NMP, especially at rich loading. This is because when MEA depletes on the surface, the diffusion rate of MEA from bulk to surface start to dominant k_g' . The summation of sensitivity on D_{MEA} and D_{CO_2} is about 0.5. The sensitivity analysis shows that PFO approximation is not appropriate after adding NMP.

At rich loading, 0,45 mol CO_2 /mol MEA, for 7 m MEA in 19NMP/1water. k_g' depends on these properties by Equation 6.39.

$$k_g' \propto \frac{k_3^{0.08} D_{CO_2}^{0.16} D_{MEA}^{0.36} \gamma_{MEA}^{0.16}}{\gamma_{CO_2}^{0.5}} \quad 6.39$$

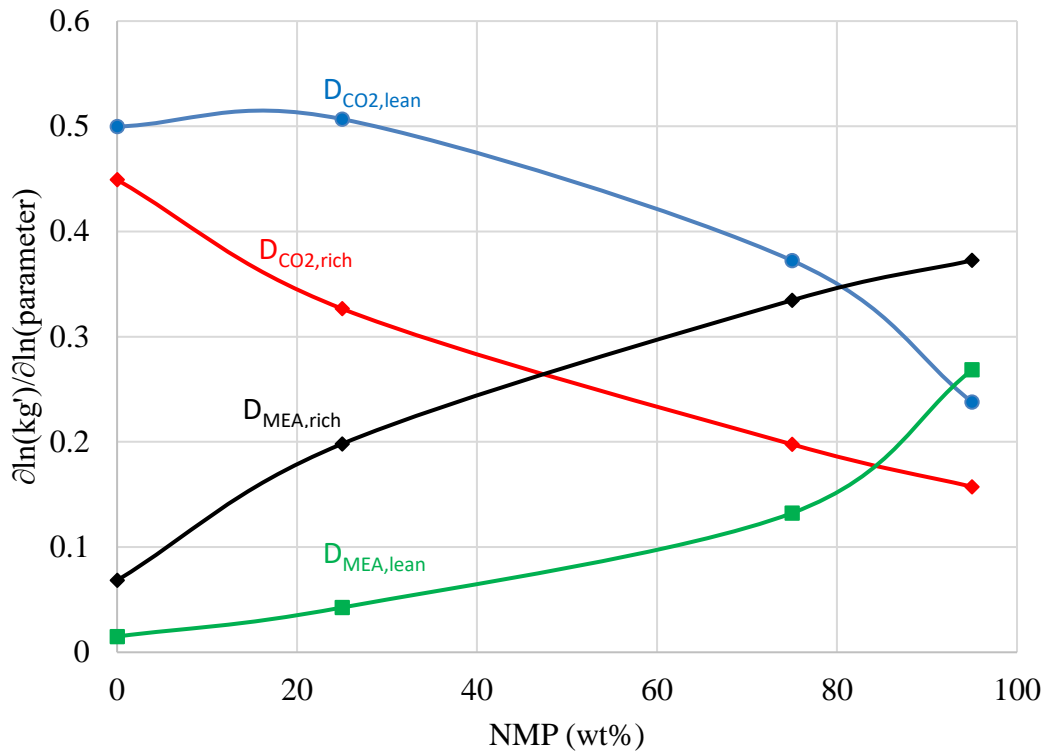


Figure 6.6: Sensitivity of k_g' to D_{CO_2} and D_{Am}

The concentration profile of MEA generated by the model for four representative cases are plotted below. Figure 6.7 shows that at lean loading without NMP, MEA concentration is almost constant near the surface, which allows PFO approximation. Figure 6.8 shows that with 95 wt % NMP, MEA concentration on the surface is 10% lower than in the bulk after contacting with CO_2 .

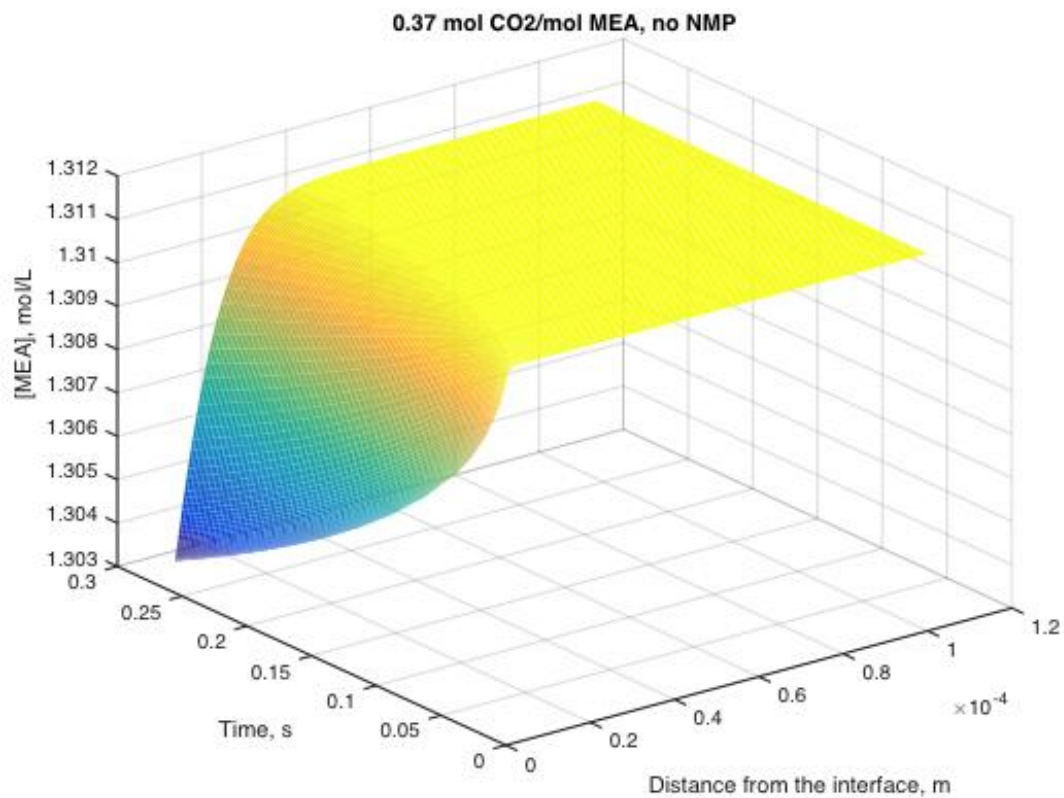


Figure 6.7: MEA concentration profile near the interface for 7 m MEA (aq). Lean loading: 0.37 mol CO₂/mol MEA.

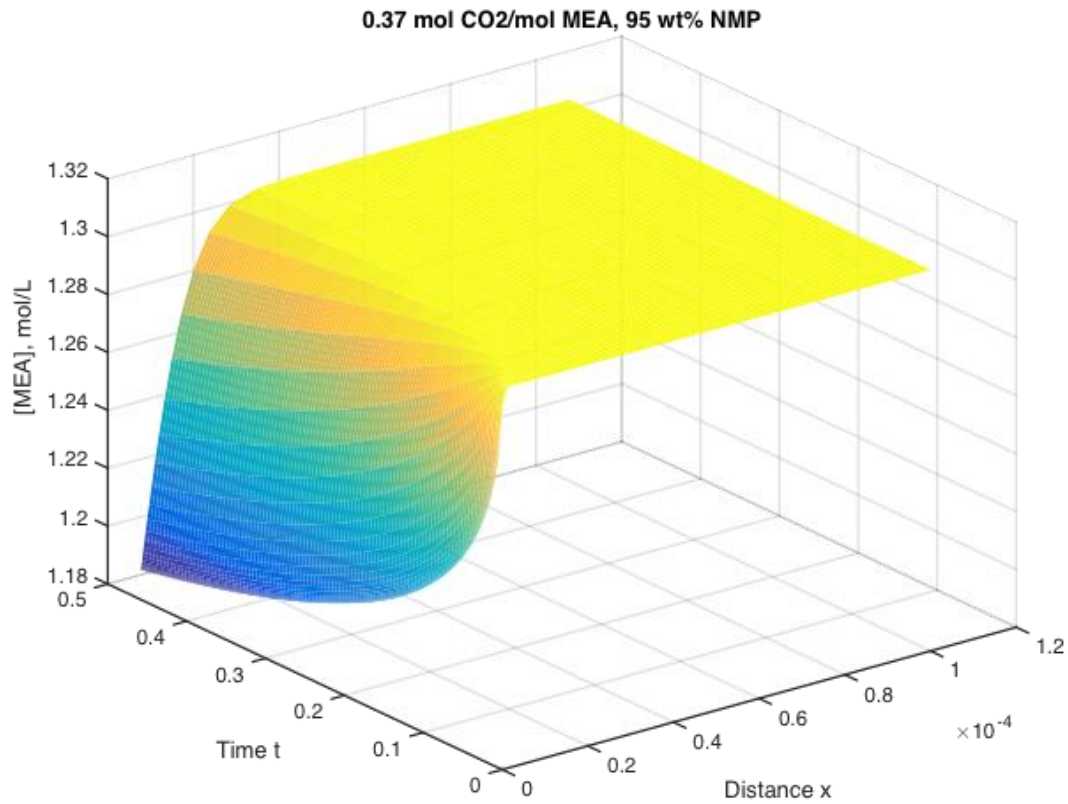


Figure 6.8: MEA concentration profile near the interface for 7 m MEA in 1 water/19 NMP. Lean loading: 0.37 mol CO₂/mol MEA.

Figure 6.9 shows that at rich loading without NMP, MEA concentration at the interface is only about 3% lower than in the bulk. Figure 6.10 shows that with 95 wt % NMP, MEA concentration on the surface is 30% lower than in the bulk after contacting with CO₂.

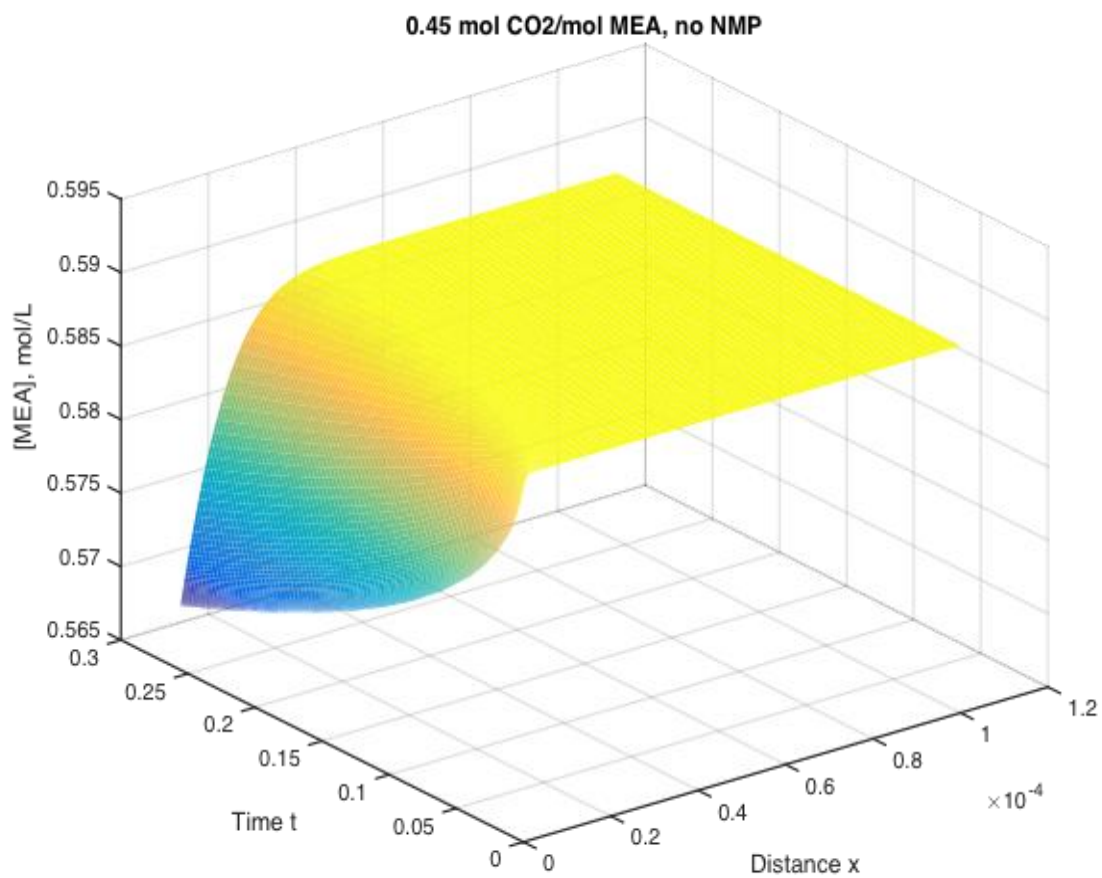


Figure 6.9: MEA concentration profile near the interface for 7 m MEA (aq).
loading: 0.45 mol CO₂/mol MEA.

Rich

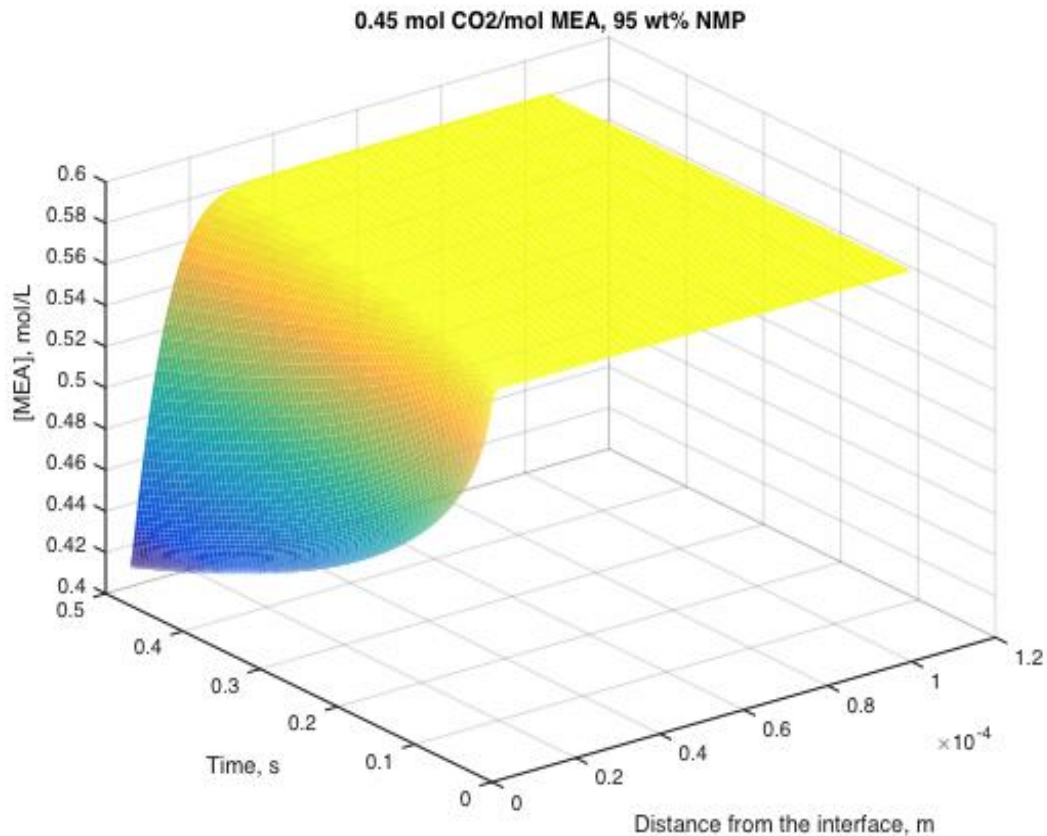


Figure 6.10: MEA concentration profile near the interface for 7 m MEA in 1 water/19 NMP. Rich loading: 0.45 mol CO₂/mol MEA.

6.4 CONCLUSIONS

Semi-aqueous amines could have much faster absorption rate than aqueous amine. At lean loading, 0.37 mol CO₂/mol MEA, CO₂ absorption rate (kg) of 7 m MEA in 3 water/1 NMP, 1 water/3 NMP, and 1 water/19 NMP is 1.1 times, 2 times, and 5 times that of 7 m aqueous MEA, respectively. The rate increase is because of greater CO₂ physical solubility and greater MEA activity.

However, at rich loading, 0.45 mol CO₂/mol MEA, adding NMP does not increase kg'. This is because the increase in physical solubility and MEA activity is not

as great as at lean loading. MEA is significantly depleted near the gas/liquid interface. The high viscosity decreases D_{CO_2} and D_{Am} , which limits k_g' .

The PFO approximation adequately represents the CO_2 mass transfer in aqueous MEA but is not applicable to semi-aqueous MEA. The mass transfer model of CO_2 diffusion and reaction with semi-aqueous MEA was built in MATLAB[®]. D_{CO_2} only depends on the viscosity to the power of -0.4 in semi-aqueous system, which is substantially lower than around -0.8 in aqueous amines. k_g' does depend on diffusivity of amine and amine product (D_{MEA}) with NMP present.

Chapter 7: Energy use estimation by lost work analysis

7.1 INTRODUCTION

Amine scrubbing technology using aqueous CO₂-reactive amine is the current state-of-the-art technology, but it is still not widely used due to high capital and energy cost. Progress has been made to reduce the energy use by new solvents and advanced process configurations. KS-1 developed by MHI (Iijima et al, 2011), DC103 by Shell Cansolv (Stephene, 2014), and piperazine (Rochelle et al, 2011) are some representative second-generation aqueous amines that can achieve reboiler duty of 2.1-2.4 GJ/ton CO₂ with advanced regeneration configurations. Another strategy to reduce the energy use of capture is to reduce the water concentration in the solvent (Heldebrant, 2017). Water lean solvents were proposed as “more advanced” solvents for CO₂ capture as they are claimed to reduce reboiler duty due to lower heat capacity (C_p) and reduced water evaporation and condensation. NASs by RTI (Lail et al., 2014) and CO₂BOLs (Mathias et al., 2013) are two representative water lean solvents. This chapter compares the energy use of water-lean solvents and second generation aqueous amines.

Piperazine (PZ), a representative second-generation solvent for amine-scrubbing has been heavily studied by the University of Texas. Frailie (2014) estimated the minimum total cost of amine scrubbing including annualized capital expenditure (CAPEX) and operational expenditure (OPEX) cost to be \$35/ton CO₂ using aqueous PZ with the advanced flash stripper (AFS). The OPEX and annualized CAPEX are roughly the same. Simulation in Aspen Plus by Lin (2014) shows that the cold bypass and warm bypass of the advanced flash stripper (AFS) recover most of the latent heat from the overhead vapor. Recent pilot plant campaigns with 5 m PZ using the AFS have achieved 2.1 GJ/tonne CO₂ reboiler duty (Chen et al., 2017; Rochelle et al., 2018).

RTI (Lail et al., 2014) has developed non-aqueous solvent (NASSs) with very low heat capacity (1.28-1.49 J/gK), and estimates the reboiler duty is reduced to 2 GJ/ton CO₂ due to lower Cp and no water evaporation. The CO₂ binding organic liquid (CO2BOL) is another novel water lean solvent that has claimed to further reduce energy use by polarity swing assisted regeneration (Mathias et al., 2013; Mathias et al., 2015; Zheng et al., 2016). Hexadecane (C16), is used as an anti-solvent that varies the polarity of the system, which helps release CO₂ in the stripping process (Mathias et al., 2013). It is only miscible with CO2BOL at high temperature (>100 °C), and it can easily phase separate from CO2BOL at low temperature (Mathias et al., 2013). The thermodynamics in these water lean solvent is intrinsically complicated, and it is unclear how rigorous different research teams handle the ever-changing physical and thermodynamic properties of their solvent when they estimate the energy use. For example, the capital cost and sensible heat cost of the heat exchanger depends on various solvent properties. Comparing sensible heat based on an arbitrary heat exchanger makes little sense.

A generic method that could estimate energy use of both aqueous and non-aqueous solvents on the same basis is desirable for fair comparison. Energy consumption of PZ has been estimated by rigorous simulation in Aspen Plus with the “Independence” model (Frailie, 2014) prepared for PZ using e-NTRL and rate-based mass transfer, which has been validated by pilot plant data (Chen et al, 2017). The energy use can also be determined by summing the minimum work of separation and irreversibility (lost work) of each unit. The two methods should give the same results, and the latter one allows the comparison of energy use without rigorous process simulation which could take years to develop and validate. For a water lean solvent, a rigorous thermodynamic and kinetics model might not be available, and it may not be

time-efficient to develop a rigorous model for all water lean solvents as they are more complicated than aqueous systems.

This thermodynamic method using lost work to estimate total energy use is validated with 5 m PZ. Then lost work for water lean solvents on major units is estimated based on solvent properties. By comparing the lost work on each unit, the total energy consumption using water lean solvent is compared to aqueous PZ.

The lost work analysis also gives the thermodynamic efficiency of the process. The thermodynamic efficiency (η_{th}) of the separation process is defined as the ratio of minimum work to actual work as shown in Equation 7.1. The actual work is the sum of the minimum work and the lost work (irreversibility). As a process reduces lost work, the thermodynamic efficiency will approach 100%. The thermodynamic efficiency of typical distillation is about 20% (Fitzmorris et al., 1980; Kim, 2012; Yoo et al., 1988). The thermodynamic efficiency of the process shows how much room is left for improvement.

$$\eta_{th} = \frac{W_{min}}{W_{act}} = \frac{W_{min}}{W_{min} + W_{lost}} \quad 7.1$$

7.2 METHODS

Energy use for various solvents can be estimated by adding minimum work of the process and the lost work on major units. This method allows energy use comparison without developing a rigorous thermodynamic model for each individual solvent.

7.2.1 Minimum work of amine scrubbing

The minimum work or reversible work of the process can be calculated by the difference of Gibbs free energy between inlet and outlet streams. The enthalpy (H) and entropy (S) of CO₂ were obtained from the NIST Web Book. Since Gibbs free energy is

a state function, this minimum work is not a function of the internal elements of the process. CO₂ in the flue gas is assumed to be 12 mol % at 1 bar, and the output CO₂ is pure at 150 bar.

$$W_{min} = \Delta G = \sum_{out}(H - T_o S) - \sum_{in}(H - T_o S) \quad 7.2$$

The isothermal minimum work at 40 °C for separating 90% of 12% CO₂ at 1 bar to pure CO₂ at 150 bar is 18.2 kJ/mol CO₂. This includes 7.3 kJ/mol CO₂ separation work (12% CO₂ to pure CO₂ at 1 bar) and 10.9 kJ/mol compression work (pure CO₂ from 1 bar to 150 bar). As the stripper pressure varies, the starting pressure of compression varies, and the minimum separation work and compression work changes. However, the total minimum work of 18.2 kJ/mol CO₂ stays constant.

7.2.2 Lost work

The lost work is defined as the maximum useful work of a stream (streams) that would be obtained during the process if the system were brought into equilibrium with the heat sink. The lost work is a result of irreversible operations. The sources of lost work can be mass transfer driving forces in the absorber; heat transfer driving forces in the heat exchanger(s), steam heater, and condenser; and mechanical inefficiency and intercooler driving force in compressor systems.

If the enthalpy and the entropy can be accurately obtained from simulations in Aspen Plus[®], the lost work of the entire process or each unit operation can be calculated by exergy balance using Equation 7.2. The sink temperature, T_{ref} is set to be 313.15 K (40 °C). T_H is the temperature of the heat source. For aqueous PZ, the heat source temperature is 155 °C, 5 K higher than the reboiler temperature. Q is the heat duty and W is the work input.

$$W_{lost} = \sum \left(1 - \frac{T_{ref}}{T_H}\right) Q + \sum W + \sum_{in}(H - T_o S) - \sum_{out}(H - T_o S) \quad 7.3$$

The minimum work, 18.2 kJ/mol CO₂, is determined only by inlet and outlet conditions, but the amount of lost work (W_{lost}) depends on how the process is operated. The lost work can be reduced by a more reversible process design that makes and leads to less actual work (Lin, 2014). If lost work could be reduced by using a water lean solvent, the energy use would be reduced. Without a rigorous thermodynamic and kinetic model that gives a good estimation of H and S in Equation 7.3, other ways to estimate lost work in each unit have been developed.

7.2.3 Lost work estimation

According to Lin (2016), the irreversibility in the absorber, main heat exchanger, reboiler, condenser, and compressor count for more than 90% of the lost work.

7.2.3.1 Lost work in the absorber

The lost work of the absorber is associated with the partial pressure driving force assuming an isothermal absorber. Figure 7.1 shows the flue gas inlet and outlet pressure (12kPa and 1.2kPa) and the equilibrium line of 5 m aqueous PZ for an isothermal absorber. The distance between the two lines is the driving force for absorption. Lost work of absorber could be calculated using Equation 7.3 if entropy and enthalpy of all inlet and outlet streams were available. If not, lost work can also be calculated by entropy or free energy balance. The change of entropy of the gas phase from 12 kPa to 1.2 kPa for CO₂ defines the minimum work requirement by Equation 7.4, where x is the mole fraction of CO₂ in the gas. The change of entropy for CO₂ in the liquid phase is given by integration of the equilibrium partial pressure by Equation 7.5. Combining the two gives the lost work in Equation 7.6, which looks like the driving force integration. Since the entropy balance is a state function, we can assume isothermal at the ends and what

happens in the middle does not matter. Loss of entropy with the cooling water can be neglected as its temperature is close to sink/reference temperature.

$$W_{min} = -RT\Delta S/(0.12 * 0.9) = -RT \Delta(x \ln x + (1 - x) \ln(1 - x))/0.108 \quad 7.4$$

$$W_{actual} = - \int_{bot}^{top} RT \ln\left(\frac{P_{CO_2}^*}{1 \text{ bar}}\right) dn_{CO_2} = RT \left(\frac{a}{2} * (n_{CO_2,lean} + n_{CO_2,rich}) + b\right) \quad 7.5$$

$$W_{lost} = W_{actual} - W_{min} = \int_{bot}^{top} RT \ln\left(\frac{P_{CO_2,gas}}{P_{CO_2}^*}\right) dn_{CO_2} \quad 7.6$$

To solve Equation 7.5, $\ln P_{CO_2}^*$ is assumed to be $\ln P_{CO_2}^* = a * n_{CO_2} + b$ (n_{CO_2} is CO₂ mol/kg in solvent). The assumption is based on the VLE curve in Figure 7.1. Assuming for this example that the $P_{CO_2}^*$ of the lean solvent is 0.1 kPa and that of the rich solvent is 5 kPa, the W_{lost} in absorber for 5 m PZ calculated by this method is 5.5 kJ/mol CO₂, close to the value calculated by Equation 7.3. The lean loading (0.25 mol CO₂/mol alkalinity in Figure 7.1) can vary as process design varies. A lower lean loading will increase driving force, but increase lost work. Since the inlet and outlet flue gas conditions of the absorber are fixed, the driving force varies with the equilibrium partial pressure ($P_{CO_2}^*$) of the solvent, which is determined by lean and rich loading. If the process runs at a lower lean loading, a larger P_{CO_2} driving force results in greater lost work in the absorber. As $P_{CO_2}^*$ of the solvent increases, the mass transfer driving force decreases, resulting in reduced lost work, and the absorber requires more packing area due to reduced mass transfer driving force. For the same amount of packing, a higher mass transfer rate allows a smaller driving force and reduced lost work.

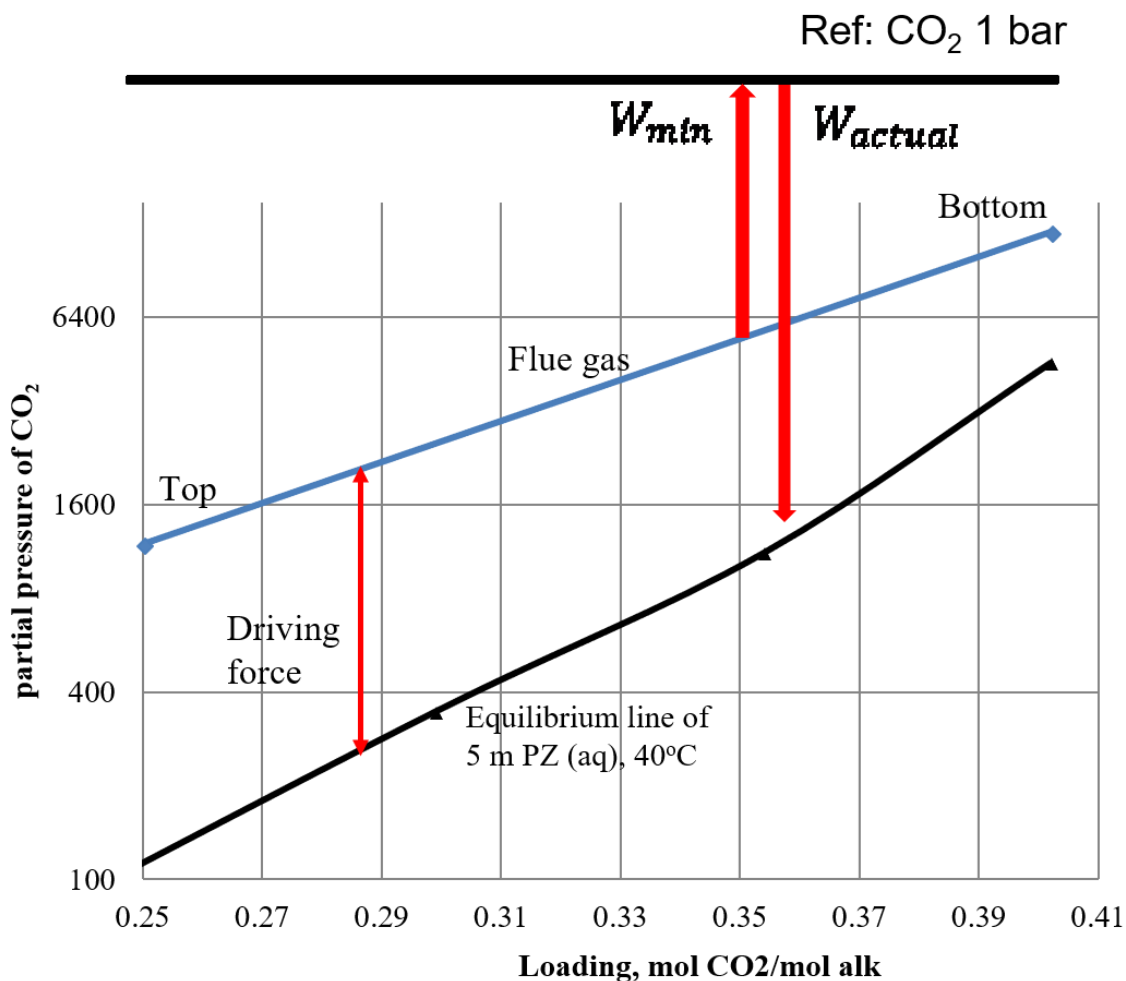


Figure 7.1: Partial pressure driving force and lost work in an isothermal absorber,

7.2.3.2 Lost work in reboiler

The lost work of the reboiler or steam heater for the advanced flash stripper is caused by the temperature difference between the steam and the solvent, as shown in Equation 7.7 using the Carnot energy cycle. In this example, a 5 K temperature driving force is used for the reboiler. Ideally, using steam with temperature as low as possible can minimize the lost work of the reboiler. However, an excessively small temperature approach should be avoided.

$$W_{\text{lost}} = Q_R * \frac{T_{\text{stm}} - T_{\text{reb}}}{T_{\text{stm}}} \quad 7.7$$

$$W_{\text{EQ}} = \eta Q_R * \frac{T_{\text{stm}} - 313K}{T_{\text{stm}}} \quad 7.8$$

The lost work in reboiler is different from the equivalent work of reboiler duty. The lost work counts for the energy lost due to heat transfer, while the equivalent work converts the total reboiler duty to electricity lost. Equation 7.8 shows the conversion factor to represent heat duty as equivalent work. When the steam is extracted from the power plant, steam at a higher temperature will cause more electricity loss. For example, using steam at 180 °C leads to an additional 15% electricity penalty compared to that at 155 °C with equivalent reboiler duty (Lin, 2016).

7.2.3.3 Lost work in the compressor

The lost work of compression is obtained from the difference between the actual work of polytropic compression and the isothermal minimum work of compression at 40 °C (Lin, 2016). The lost work of the compression system comes from the mechanical inefficiency of the compressors (86% polytropic efficiency is used) and non-isothermal operation resulting in temperature driving forces in the intercoolers.

7.2.3.4 Lost work in the main heat exchanger

In the amine scrubbing process, the lean/rich cross exchanger recovers the sensible heat from the hot lean solvent. The exchanger heat duty is large, about 3–5 times the reboiler duty (Lin, 2016). The log mean temperature driving force (ΔT_{LM}) determines the trade-off between the capital cost and energy cost of the cross exchanger. Equations 7.9 and 7.10 relate the sensible heat requirement (Q_{HX}) and exchanger Area to ΔT_{LM} . $\Delta T_{\text{approach}}$ can be approximated by ΔT_{LM} if $\dot{m}C_p$ of the cold and hot streams is equal. If ΔT_{LM} is bigger, the cross-exchanger size will be reduced, but Q_{HX} increases

because less sensible heat can be recovered. If ΔT_{LM} is smaller, larger cross exchanger area is required, but more sensible heat can be recovered.

$$Q_{HX} = \dot{m}C_p\Delta T_{approach} \quad 7.9$$

$$Area = \frac{\dot{m}C_p\Delta T_{crx}}{U_{LM}\Delta T_{LM}} \quad 7.10$$

The lost work (per mole CO₂ removed) in the heat exchanger can be calculated by Equation 7.11 based on the reversible Carnot energy cycle and assuming that the temperature driving force is constant across the exchanger.

$$W_{lost} = -\frac{\dot{m}C_p}{\dot{n}_{CO_2}} \int_{in}^{out} \frac{\Delta T_{LM}}{T_{lean}} dT = \frac{\dot{m}C_p}{\dot{n}_{CO_2}} \Delta T_{LM} \ln \frac{T_{in,lean}}{T_{out,lean}} \quad 7.11$$

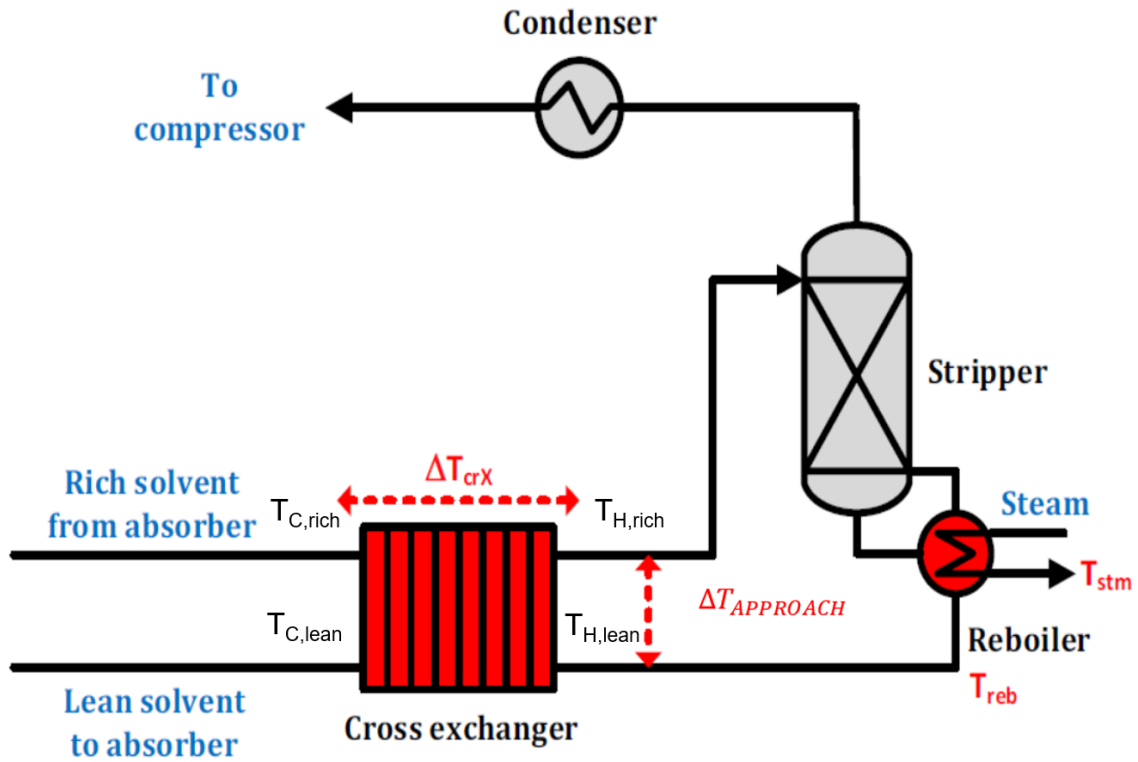


Figure 7.2: Optimization of cross exchanger LMTD (Lin, 2016)

ΔT_{LM} needs to be specified for energy analysis. Since ΔT_{LM} determines the trade-off between CAPEX and OPEX, it is critical to avoid low ΔT_{LM} that requires an

extremely large exchanger or high ΔT_{LM} that loses too much sensible heat. Lin (2014) identified a reasonable ΔT_{LM} to be 5 K for aqueous PZ, which might not be optimal for water lean solvents. As solvent properties vary, the optimal ΔT_{LM} that minimizes heat exchanger capital and energy cost needs to be identified.

7.2.3.5 Optimal ΔT_{LM} for main heat exchanger

The heat exchanger optimization is revised from previous work (Lin, 2016). In the amine scrubbing process, the lean/rich cross exchanger recovers the sensible heat from the hot lean solvent. The capital cost of the cross exchanger is one of the cost centers, roughly 20–30% of the overall capital cost (Lin, 2014). The plate-and-frame exchanger is selected over the tube-and-shell exchanger due to better performance and a smaller footprint. The LMTD (ΔT_{LM}) is optimized as it impacts the heat exchanger cost the most (Lin, 2016). The optimization includes the CAPEX of the cross exchanger and the reboiler sensible heat duty (OPEX). The optimization assumes:

1. The temperature change across the cross exchanger (ΔT_{crx}) and C_p are independent of ΔT_{LM} .
2. The sensible heat duty of the reboiler corresponds to $\Delta T_{approach}$ which is equal to ΔT_{LM} .

The reboiler duty is converted to the opportunity cost of the amount of steam consumed and is linked to the price of electricity (C_{POE}) by Equation 7.12.

Total cost (TC) including cross exchanger CAPEX and OPEX is shown in Equation 7.13. Where $C_{PEX,crx}$ is the exchanger cost per area including an annualizing factor, $C_{OPEX,reb}$ is the reboiler energy cost, and A is the area of the exchanger. At an optimum LMTD that minimizes total cost, the first derivative of Equation 7.13 is equal to zero to solve for $\Delta T_{LM,opt}$.

$$C_{OPEX,reb} = C_{POE}\eta_{tb} \frac{(T_{stm}-T_{sink})}{T_{stm}} Q_{reb} \quad 7.12$$

$$TC = C_{CPX,crx} A + C_{OPEX,reb} = C_{CPX,crx} \frac{\dot{m}C_p\Delta T_{crx}}{U_{LM}\Delta T_{LM}} + C_{COE}\eta_{tb} \frac{(T_{stm}-313K)}{T_{stm}} \dot{m}C_p\Delta T_{LM} \quad 7.13$$

$$\frac{\partial TC}{\partial \Delta T_{LM}} = C_{CPX,crx} \frac{\dot{m}C_p\Delta T_{crx}}{U_{LM}\Delta T_{LM}^2} + C_{COE}\eta_{tb} \frac{\dot{m}C_p(T_{stm}-T_{sink})}{T_{stm}} \quad 7.14$$

$$\Delta T_{LM,opt} = \sqrt{\frac{C_{CPX,crx}\Delta T_{crx}}{U_{LM}} \frac{T_{stm}}{C_{COE}\eta_{tb}(T_{stm}-313K)}} \quad 7.15$$

Putting $\Delta T_{LM,opt}$ back into Equation 7.13 gives Equation 7.16, which shows that CAPEX and OPEX are both proportional to $\dot{m}C_p\sqrt{\frac{\Delta T_{crx}}{U_{LM}}}$. The heat transfer coefficient (U_{LM}) depends on the hydrodynamics in the exchanger and solvent properties (Equation 7.18). U_{LM} has been heavily studied as listed in Table 7.1 (Lin, 2016). C_{Nu} , ρ , and D_e are constant and flow velocity (u) is assumed to be constant. Putting $n = 0.35$ and $m = 0.7$ (Lin, 2016) into Equation 7.18 shows that CAPEX, OPEX, and the total cost depend on solvent properties by Equation 7.19. The size of the heat exchanger and sensible heat lost increase as solvent flow rate, C_p , viscosity, and cross temperature increase. High thermal conductivity reduces the size of the heat exchanger and sensible heat lost. Changing from aqueous to water lean reduces C_p , but may not reduce or may even increase sensible heat lost due to much lower thermal conductivity and higher viscosity.

$$TC = C_{PEX,crx} \frac{\dot{m}C_p}{\sqrt{\frac{C_{PEX,crx}U_{LM}}{\Delta T_{crx}} \frac{T_{stm}}{C_{COE}\eta_{tb}(T_{stm}-T_{sink})}}} + C_{COE}\eta_{tb} \dot{m}C_p \sqrt{\frac{C_{PEX,crx}\Delta T_{crx}}{U_{LM}} \frac{T_{stm}-T_{sink}}{T_{stm}C_{COE}\eta_{tb}}} \quad 7.16$$

$$CAPEX, OPEX, TC \propto \dot{m} \propto \dot{m}C_p \sqrt{\frac{\Delta T_{crx}}{U_{LM}}} \quad 7.17$$

$$U_{LM} = \frac{k}{2D_e} Nu = C_{Nu} Re^m Pr^n = C_{Nu} \rho^m D_e^{m-1} k^{1-n} C_p^n u^n \mu^{n-m} \quad 7.18$$

$$CAPEX, OPEX, TC \propto \dot{m} k^{\frac{n-1}{2}} C_p^{1-\frac{n}{2}} \mu^{\frac{m-n}{2}} \Delta T_{crx}^{0.5} = \dot{m} * k^{-0.325} C_p^{0.825} \mu^{0.175} * \Delta T_{crx}^{0.5} \quad 7.19$$

$$\Delta T_{LM,opt} \propto \sqrt{\frac{\Delta T_{crx}}{U_{LM}}} \propto k^{\frac{n-1}{2}} C_p^{-\frac{n}{2}} \mu^{\frac{m-n}{2}} \Delta T_{crx}^{0.5} \quad 7.20$$

Table 7.1: Summary of empirical correlations of heat transfer for PHE (Lin, 2016)

Author/year	Fluid	Heat transfer
(Kumar, 1984)	Water	$Nu = 0.348 Re^{0.663} Pr^{0.33} \left(\frac{\mu}{\mu_w}\right)^{0.17} (\theta = 60)$
		$Nu = 0.108 Re^{0.703} Pr^{0.33} \left(\frac{\mu}{\mu_w}\right)^{0.17} (\theta = 30)$
(Heavner et al., 1993)	Water	$Nu = 0.308 Re^{0.667} Pr^{0.33} \left(\frac{\mu}{\mu_w}\right)^{0.17} (\theta_{avg} = 56.5)$
		$Nu = 0.118 Re^{0.720} Pr^{0.33} \left(\frac{\mu}{\mu_w}\right)^{0.17} (\theta_{avg} = 33.5)$
(Roetzel et al., 1994)	Water	$Nu = 0.371 Re^{0.703} Pr^{0.33}$
(Thonon et al., 1995)		$Nu = 0.2946 Re^{0.7} Pr^{0.33} (\theta = 60)$
		$Nu = 0.2267 Re^{0.631} Pr^{0.33} (\theta = 30)$
(Talík et al., 1995)	Propylene glycol/water	$Nu = 0.2 Re^{0.75} Pr^{0.4} (\theta = 60)$
(Manglik et al., 1995)	Water	$Nu = 0.105 Re^{0.755} Pr^{0.33} \left(\frac{\mu}{\mu_w}\right)^{0.14} (\theta = 45)$
(Muley et al., 1999)	Water	$Nu = C_1(\theta) C_2(\phi) Re^{a(\theta)} Pr^{0.33} \left(\frac{\mu}{\mu_w}\right)^{0.14}$
(Warnakulasuriya et al., 2008)	Salt solution	$Nu = 0.292 Re^{0.725} Pr^{0.35} \left(\frac{\mu}{\mu_w}\right)^{0.14} (\beta = 60)$
(Khan et al., 2010)	Water	$Nu = 0.1368 Re^{0.7424} Pr^{0.35} \left(\frac{\mu}{\mu_w}\right)^{0.14} \beta = 30$
		$Nu = 0.1449 Re^{0.8414} Pr^{0.35} \left(\frac{\mu}{\mu_w}\right)^{0.14} \beta = 60$

7.3 RESULTS

This work studies the energy use and lost work of three cases: 5 m PZ using AFS, 8 m PZ using simple stripper, and a generic water-lean solvent using simple stripper. The method is first validated in 5 m PZ using AFS. Total energy use calculated by the

summation of lost work and minimum work is compared with the total energy use in the reboiler and compression.

7.3.1 Method validation using 5 m aqueous PZ AFS

Energy use of 5 m aqueous PZ has been rigorously simulated (methods in Table 7.2) by Lin (2016) in Aspen Plus[®] using the Independence model developed by Frailie (2014).

Table 7.2: Summary of modeling methods used by Lin (2016).

Solvent	5 m PZ
Process modeling tool	Aspen Plus [®] v8.4
Thermodynamic model	Independence, e-NRTL
Stripper packing	5 m Mellapak 250X
Correction factor for packing interfacial area	1

Table 7.3: Summary of process specifications for 5 m PZ/AFS.

Reboiler T (°C)	150
Steam condensing T (°C)	155
CO ₂ rich loading (mol CO ₂ /mol alkalinity)	0.40
CO ₂ lean loading (mol CO ₂ /mol alkalinity)	0.26
Cross exchanger ΔT_{LM} (K)	5
Cold rich exchanger ΔT_{LM} (K)	20

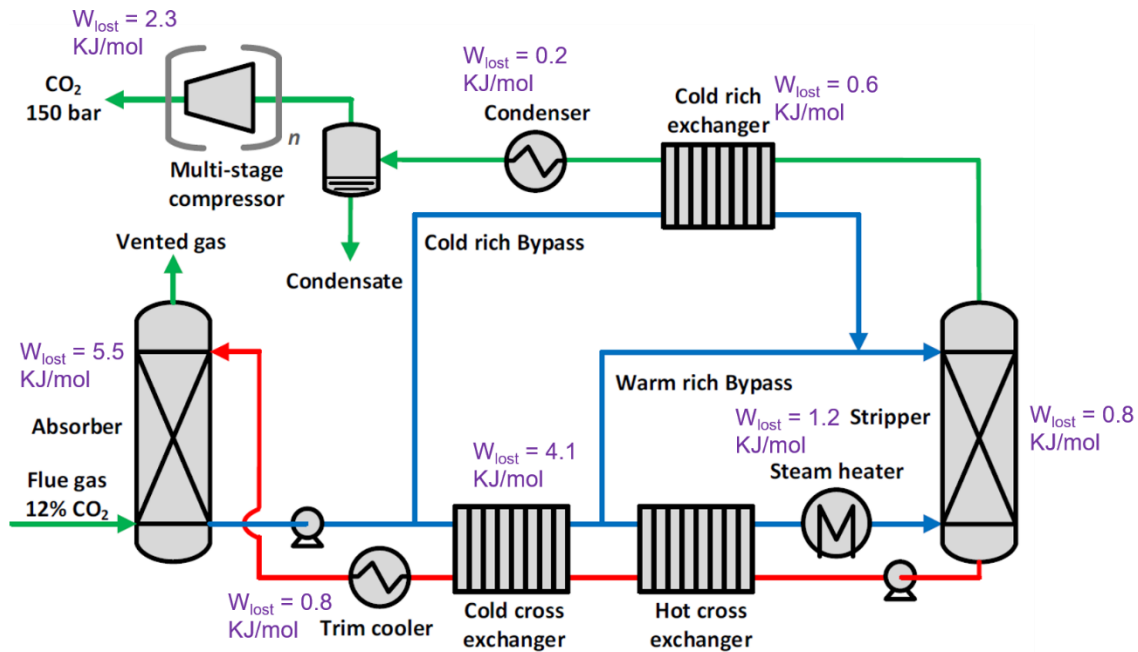


Figure 7.3: Process diagram of 5 m PZ using the advanced flash stripper.

The process flow is shown in Figure 7.3, with lost work labeled on each unit. The lost work at the absorber, cross exchanger, steam heater, and compressor is calculated using methods in section 7.2.3. The relatively small lost work at the trim cooler, cold rich exchanger, condenser, and stripper are calculated using Equation 7.3 with Aspen Plus simulation results. The summation of all the lost work and minimum work is 33.7 kJ/mol CO₂. The reboiler duty is 97.7 kJ/mol CO₂, which is equivalent to 26.4 kJ/mol CO₂ work using the Carnot energy cycle. The compression work is 8.11 kJ/mol CO₂. The reboiler equivalent work and compression work adds up to 34.5 KJ/mol, which is 0.8 kJ/mol CO₂ greater than the total work estimated by the sum of lost work and minimum work. Given the complexity of this system and some other minor lost work (such as mixing, flashing, etc.), this difference is acceptable.

7.3.2 lost work and energy use comparison.

The energy analysis of 8 m PZ with a simple stripper is based on an Aspen Plus simulation by Lin (2014). The same lost work analysis methodology is applied to the water-lean system to estimate the energy use. Some solvent properties (viscosity, thermal conductivity, heat capacity, and etc.) of CO2BOL/C16 are used to calculate lost work for the general water lean solvent case. The CO₂ binding organic liquid (CO2BOL) is a representative water lean solvent that could reduce energy use from the aqueous MEA benchmark (Mathias et al., 2013; Zheng et al., 2016). Hexadecane (C16), is used as an anti-solvent that varies the polarity of the system, which helps release CO₂ in the stripping process (Mathias et al., 2013). It is only miscible with CO2BOL at high temperature (>100 °C), and it can easily phase separate from CO2BOL at low temperature. Figure 7.4 shows the process diagram of CO2BOL/C16. This process includes all the major units of the simple stripper configuration and an extra coalescer that handles C16 separation. The lost work distribution for the three cases is listed in Table 7.4.

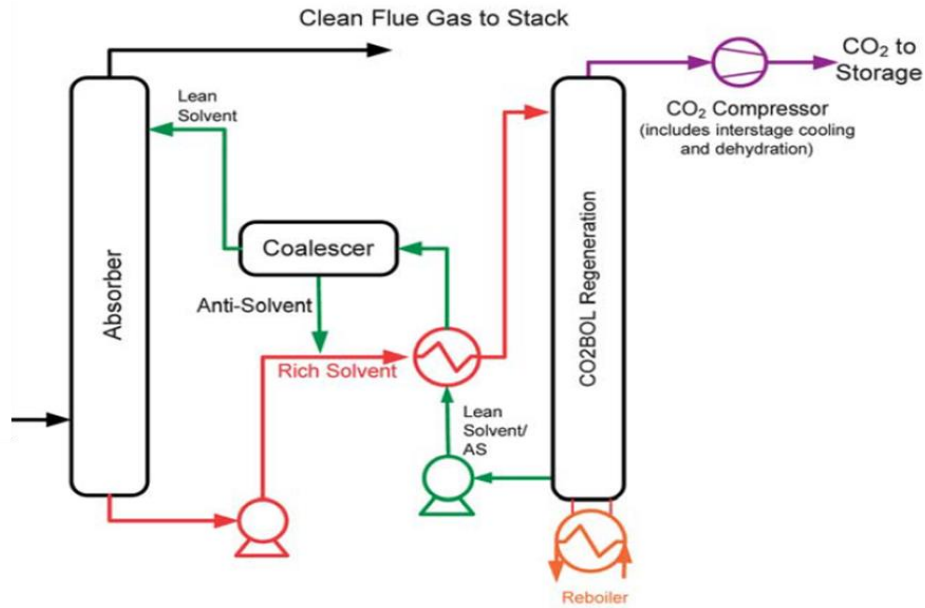


Figure 7.4: Process diagram of CO2BOL/C16. (Mathias et al., 2013)

Table 7.4: Summary of lost work analysis.

Stripper configuration	5 m PZ	8 m PZ	Water lean solvent
	AFS	Simple	Simple
	18.2 kJ/mol CO ₂ minimum work		
Absorber lost work ¹	5.5	5.5	5.5
Heat exchanger lost ²	4.1	4.2	4.5
compressor lost	2.3	2.3	2.5
Reboiler lost ³	1.2	1.7	1.2
condenser lost	0.8	5.8	0.8
Others (trim cooler and stripper)	1.6	1.6	1.6
Total (Lost work + minimum work)	33.7	39.3	34.3
Reboiler duty + compression work ⁴	34.5	39.5	
Compression work ⁵	8.1	8.3	12.8
Estimated reboiler work ⁶ (W _{EQ} , kJ/mol CO ₂)	25.6	31	20.9
Reboiler duty (Q _R , kJ/mol CO ₂) ⁷	95.3	115	97.1
Reboiler duty (Q _R , GJ/ton CO ₂)	2.16	2.6	2.21

Notes:

1. The lost work at absorber for all three cases are based on 0.1-5 kPa operating P*_{CO₂}, calculated by Equation 7.6.
2. By Equation 7.11 with optimal $\Delta T_{LM,opt}$.
3. By Equation 7.7.
4. Reboiler duty and compression work from Aspen process modeling, the values agree with summation of lost work and minimum work.
5. The stripper pressure for 5 m PZ, 8 m PZ, and water lean solvent is 7, 6.5, and 1.8 bar, respectively.

6. Estimated by subtracting compression work from estimated total work (Lost work + minimum work)
7. Convert equivalent work to actual steam reboiler duty by $W_{EQ} = Q_R * \frac{T_{stm} - 313K}{T_{stm}}$,

$$T_{stm} = 155 \text{ }^\circ\text{C for PZ, } 126 \text{ }^\circ\text{C for water lean.}$$

The lost work in the absorber is determined by the partial pressure driving force. A reasonable partial pressure driving that considers the tradeoff between lost work and absorber packing height needs to be specified. Assume the absorption rate of the water lean solvent is close to that in PZ(aq), for the same packing height, the operating partial pressure driving force for CO2BOL in the absorber is selected to be the same as PZ (0.1-5kPa). Same 5.5 kJ/mol CO₂ lost work was obtained for three cases.

The lost work in the heat exchanger is calculated using Equation 7.11. The optimal $\Delta T_{LM,opt}$ for 8 m PZ and water lean solvent that minimizes CAPEX and OPEX of the heat exchanger is ratioed to the 5 K $\Delta T_{LM,opt}$ for 5 m aqueous PZ by Equation 7.20. 5.8 K $\Delta T_{LM,opt}$ is calculated for 8 m PZ. A 7.2 K $\Delta T_{LM,opt}$ for water lean solvent is used based on CO2BOL properties (C_p , k , viscosity, and ΔT_{crx}) from Mathias et al. (2013) and Zheng et al. (2016). Although C_p of water lean solvent is smaller, the overall effect of C_p , k , viscosity, and ΔT_{crx} increases the sensible heat lost of heat exchanger.

Reboiler lost work is calculated using Equation 7.7 accounting for the temperature driving force. Compressor lost work is obtained by actual compression work minus the ideal isothermal compression work. The lost work in the condenser is 5.8 kJ/mole CO₂ for 8 m PZ with simple stripper due to the large heat lost of water evaporation from the stripper. This heat lost is be reduced to 0.8 kJ/mole CO₂ in 5 m PZ AFS because AFS recovers the heat from the water vapor by cold and warm bypass. Assuming water lean solvent can achieve the same heat lost reduction due to intrinsically less water, 0.8 kJ/mole CO₂ lost work is assigned as calculated for 5 m PZ AFS. Other minor lost work

(trim cooler and stripper) is assumed to be the same as the PZ process. The lost work in the mixing of CO₂BOL and C16 is ignored. The summation of lost work and minimum work is listed in Table 7.4 and reboiler duty is estimated for water lean solvent. The relative small energy use in pump, flue gas fan, DCC, etc. are not included. The energy use of these units adds up to about 3 kJ/mol CO₂.

The energy use of 5 m PZ AFS and 1CO₂BOL/2C16 is similar because both processes eliminate the heat lost in the water vapor (low lost work in the condenser). 5 m PZ AFS uses an Advanced Flash Stripper to recover the heat in the water vapor, while water lean solvent intrinsically contains little water (<5% wt %) and claims to accomplish the same result. Both processes could achieve a thermodynamic efficiency of about 50%.

7.3.3 Lost work analysis in the 1CO₂BOL/2C16 case.

Zheng et al. (2016) reported a reboiler duty and compression work for a specified design which has much lower lean and rich loading than the proposed general design for water lean solvent in previous section. Based on the Aspen simulation results, lost work on each unit is calculated. Process specifications are listed in Table 7.6. The lost work results are in Table 7.7.

Table 7.6: Summary of process specifications for 1CO2BOL/2C16. (Zheng et al., 2016)

	Current design
Reboiler T (°C)	121
Steam condensing T (°C)	126
P* _{CO2} , rich loading (kPa)	1.48
P* _{CO2} , lean loading (kPa)	0.0003
Cross exchanger ΔT_{LM} (K)	8.8
Hot lean T (°C)	108
Cold lean T (°C)	63

Table 7.7: lost work in 1CO2BOL/2C16 based on design in Table 7.6.

Energy	1CO2BOL/2C16
Stripper configuration	Simple
Minimum work	18.2 kJ/mol CO ₂
Absorber lost work ¹	14.6
Heat exchanger ²	4.6
compressor	2.5
reboiler	1.5
condenser	0.6
Others (trim cooler and striper)	1.6
Lost work + minimum work	43.6
Reboiler duty + compression work	31.7
Compression work	12.8
Estimated reboiler work ³ (W _{EQ} , kJ/mol CO ₂)	30.8
Reboiler duty ⁴ (Q _R , kJ/mol CO ₂)	142.9

Notes:

1. The lost work at absorber is based on 0.0003-1.48 kPa operating $P^*_{CO_2}$, calculated by Equation 7.6.
2. By Equation 7.11 with 8.8 K ΔT_{LM} .
3. Estimated by subtracting compression work from estimated total work (Lost work + minimum work)
4. Convert equivalent work to actual steam reboiler duty by $W_{EQ} = Q_R * \frac{T_{stm}-313K}{T_{stm}}$

ΔT_{LM} calculated from Zheng et al. (2016) is 8.8 K, close to the estimated optimal ΔT_{LM} of 7.2 K. The calculation assumes an isothermal absorber at 40 °C and no water transfer between the gas and liquid. The CO_2 partial pressure of the solvent at 40 °C (0.0003-1.48 kPa) is much lower than the normal operating range, which means the absorber operates more irreversibly. The large lost work (14.6 kJ/mol CO_2) comes from the large driving force in the absorber based on Equation 7.6. The operating absorber driving force is probably far from optimal. If 0.003-1.48 kPa is used for the calculation, lost work dramatically reduces to 11.5 kJ/mol CO_2 , which means the lean loading has not been optimized.

In a typical aqueous amine scrubbing process, stripping CO_2 from the solvent to achieve extremely low $P^*_{CO_2, lean}$ (0.0003 kPa) takes a lot of energy, which is why typical lean solvent still has a $P^*_{CO_2, lean}$ of 0.01-0.5 kPa. From the free energy balance, the larger lost work/driving force in the absorber is compensated by additional reboiler duty in the stripper. In this polarity-swing assisted regeneration, adding C16 increases $P^*_{CO_2}$ in the stripper to release CO_2 easily, that could reduce reboiler duty and temperature. After the heat exchanger, C16 is separated out at a lower temperature, and very low $P^*_{CO_2, lean}$ is achieved. This low $P^*_{CO_2, lean}$ provides large absorbing driving force in the absorber. The process seems very attractive, but there must be some energy input

missing. The use of C16 creates extra driving force (available work/ ΔG) in the lean solvent stream, without providing any additional energy or work, which is against the the second law of thermodynamics. The missed energy term could be the heat of mixing between C16 and CO2BOL as the entropy of the CO2BOL and C16 mixture stream may change significantly from two phases to one miscible phase.

7.4 NORMALIZED CAPACITY OF SEMI-AQUEOUS AMINES

For aqueous amines, Li (2013) and Lin (2016) introduced viscosity-normalized capacity (ΔC_μ) to include the heat exchanger cost in solvent cyclic capacity. ΔC_μ is defined in Equation 7.20, using 5 m PZ (aq) as the reference.

$$\Delta C_\mu = \frac{\Delta C_{solv}}{(\mu_{mid}/\mu_{5\text{ m PZ}})^{0.175}} \quad 7.20$$

In this chapter, rigorous heat exchanger optimization identified that the CAPEX and OPEX of heat exchanger both depend on solvent properties by Equation 7.21. Equation 7.20 only includes the effect of viscosity on heat exchanger cost because k and C_p generally do not change much in aqueous amines, where the water mass fraction is normally constant (70 wt %). However, k and C_p do change a lot after replacing water with a different physical solvent, and a more comprehensive normalized capacity is required.

$$TC \propto k^{-0.325} C_p^{0.825} \mu^{0.175} \quad 7.21$$

Higher viscosity and heat capacity increases total cost (TC), and higher thermal conductivity and cyclic capacity reduce TC. Based on the cost dependence on solvent properties, a new normalized capacity is defined by Equation 7.22, which allows the comparison of heat exchanger cost of different solvents directly. A greater value of $\Delta C_{k,Cp,\mu}$ means reduced heat exchanger capital cost and reduced sensible heat loss.

$$\Delta C_{k,C_p,\mu} = \frac{\Delta C_{solv}}{TC_factor} = \Delta C_{solv} \left(\frac{k}{k_{5mPZ}} \right)^{0.325} \left(\frac{C_p}{C_{p,5mPZ}} \right)^{-0.825} \left(\frac{\mu}{\mu_{5mPZ}} \right)^{-0.175} \quad 7.22$$

High cyclic capacity, high thermal conductivity, low heat capacity, and low viscosity are required for lower heat exchanger cost. Adding C16 into CO2BOL reduces the CO₂ carrying capacity. Table 7.8 summarized the normalized capacity of some representative solvents. Viscosity (μ) is measured except for CO2BOL, which is assumed to be 20 cP (Zheng et al., 2016).

k and C_p data for these semi-aqueous amines are not available in literature. Shokouhi et al. (2013) measured k and C_p of SUF-water mixture and showed that C_p of the mixture can be estimated by weighted average of each component. C_p of 5 m PZ (aq) was predicted to be $3.6 \frac{J}{K * g}$ by Frailie (2014). C_p of 5 m PZ in 1SUF/1water is estimated by Equation 7.23. C_p of semi-aqueous MEA is estimated using the same weighted average method. C_p of 30 wt% aqueous MEA is 3.4 J/gK by Weiland (1997). Heat capacity of CARB and NMP is obtained from NIST webbook.

$$C_{p,5mPZ-SUF-water} = C_{p,5mPZ-water} + \text{wt \% of SUF} * (C_{p,SUF} - C_{p,water}) \quad 7.23$$

Thermal conductivity (k) of PZ aqueous is not available. PZ is treated as SUF for approximation, and k of 65 wt % SUF/35 wt % water is used to approximate 5 m PZ in 1 SUF/1 water. Thermal conductivity of pure water, MEA, NMP, and CARB is obtained from NIST webbook to be 0.6, 0.2, 0.18, and 0.16 W/mK respectively. The values in the table are the mass weighted average. It is difficult to get a more accurate value of k ; however, since the dependency on k is only 0.325, a 20% error in k only results in about 6% error in the normalized capacity.

Table 7.8 Normalized capacity of some representative solvents. NMP=N-Methyl-2-pyrrolidone, CARB=2-(2-Ethoxyethoxy)ethanol, SUF=sulfolane.

	μ	k	C_p	ΔC_{cyc}^1	$\Delta C_{k, cp, \mu}$
	cP	W/mK	J/gK	$\frac{mol CO_2}{kg}$	
7 m MEA (1water/3NMP)	16	0.28	2.8	0.85	0.72
7 m MEA (1water/3CARB)	19	0.27	2.6	0.83	0.72
5 m PZ (aq)	4	0.41	3.6	0.95	0.95
5 m PZ (1SUF/1water)	20	0.27	2.8	1.21	0.98
1 CO2BOL, 1 C16	20	0.14	2.2	0.72	0.58
1 CO2BOL, 2 C16	20	0.14	2.4	0.59	0.44

Notes:

1. 0.1/5 kPa operating $P^*_{CO_2}$ except 0.0003/1.48 kPa operating $P^*_{CO_2}$ for CO2BOL

7.5 DISCUSSION ON ENERGY USE

It has been shown in section 7.3.2 that the optimal design for water lean solvent uses about the same amount of energy as 5 m PZ AFS. Water lean solvents can reduce the amount of water vapor exiting a simple stripper, which reduces the lost work in the condenser significantly from simple stripper. On the other hand, second generation amine processes use advanced stripper configurations that can accomplish the same effect with little additional capital cost. The piperazine system would use the Advanced Flash Stripper (Chen, 2017). MHI probably uses KS-1 with an interheated stripper in the demonstration at the Parrish power plant (Iijima, 2011). Shell Cansolv (Stephene, 2014) uses lean vapor compression in its ICCS Project at Boundary Dam. All three systems reduce water vapor from the stripper, and 2.1-2.4 GJ/ton CO₂ energy consumption has been demonstrated (Chen, 2017; Iijima, 2011, Stephene, 2014)

Papers on water lean solvents have claimed that the reduced heat capacity reduces the sensible heat loss of the cross exchanger because of lower heat duty being transferred. However, lower thermal conductivity and higher viscosity reduce the heat transfer coefficient. Rigorous heat exchanger optimization accounting for C_p , viscosity, and thermal conductivity (Table 7.9) results in no improvement of the normalized capacity with a number of water lean solvent compositions. As with all solvent development it is possible that a specific water lean solvent can be identified that has a greater normalized capacity, but there is no simple energy benefit moving from aqueous to water lean at the cost of more difficult solvent management (volatility, degradation, reclaiming), and many water solvents may have lower normalized capacity because of reduced thermal conductivity and greater viscosity.

7.6 CONCLUSIONS

- The energy use of CO₂ capture by amine scrubbing can be estimated by the sum of minimum work and lost work. Energy use will be reduced if a new process or solvent reduces lost work.
- The energy use of a typical water lean solvent with a simple stripper could be similar to that of 5 m aqueous PZ with advanced flash stripper.
- Water lean solvents can reduce the amount of water vapor exiting a simple stripper, which reduces the lost work in the condenser significantly from simple stripper. However; second generation amine processes use advanced stripper configurations that can accomplish the same effect with little additional capital cost.

- The energy use of CO2BOL/C16 and other water lean solvents will not be less than that of 5 m PZ AFS as lost work in the absorber and heat exchanger cannot be reduced.
- Comprehensive normalized capacity has been developed. An advanced solvent, whether water lean or not, with high normalized capacity will reduce the lost work in the heat exchanger.

$$\Delta C_{norm} = \Delta C_{solv} \left(\frac{\mu}{\mu_{5mPZ}} \right)^{-0.175} \left(\frac{k}{k_{5mPZ}} \right)^{0.325} \left(\frac{C_p}{C_{p,5mPZ}} \right)^{-0.825}$$

Chapter 8: Conclusions and Recommendations

8.1 CONCLUSIONS SUMMARY

8.1.1 Aqueous piperazine blend

- 2MPZ and PZ/2MPZ blend are competitive solvents, as they maintained the high absorption rate and remediate the solid solubility of PZ. kg'_{avg} of 4 m 2MPZ and 2.5/2.5 m 2MPZ/PZ is similar to 8 m PZ, and 30% lower than 5 m PZ; However, the cyclic capacity is 15% higher than 5 m PZ. HEP has similar kg' as 2MPZ, but the cyclic capacity is 20% lower than 5 m PZ.
- 2MPZ and equimolar 2MPZ/PZ from 2 m to 8 m was modeled in Aspen Plus® using the eNRTL thermodynamic framework. The thermodynamic model correctly predicts the CO₂ equilibrium partial pressure within 5% error from 2 m to 8 m, 0.01-0.5 CO₂ loading, and 20–160°C.
- The 2MPZ kinetic model used three reactions and the 2MPZ/PZ kinetics model used six reactions to capture the rate behavior from 2 m to 8 m, 0.15-0.4 CO₂ loading, and 20–100°C. The model fits experiment data well.
- 2MPZ and PZ/2MPZ thermodynamic and kinetic model can be used for techno-economic assessments, and process modeling.

8.1.2 Semi-aqueous MEA and PZ

8.1.2.1 Semi-aqueous MEA

- Semi-aqueous amines could have much faster absorption rate than aqueous amine at lean loading. At 100 Pa CO₂ equilibrium partial pressure ($P_{CO_2}^*$), CO₂ absorption rate (kg'_{avg}) of 7 m MEA in 3 water/1 NMP, 1 water/3 NMP, and 1 water/19 NMP is 1.1 times, 2 times, and 5 times that of 7 m aqueous MEA, respectively.

- At 5 kPa $P_{CO_2}^*$, CO_2 absorption rate (k_g' 'avg) of 7 m semi-aqueous MEA is similar to that of 7 m aqueous MEA.
- k_g' increases in semi-aqueous MEA because of reduced operating CO_2 loading (higher free MEA concentration at the same $P_{CO_2}^*$), greater CO_2 physical solubility, and greater MEA activity. The increase in k_g' becomes less significant at higher loading.
- At rich loading, 0.45 mol CO_2 /mol MEA, adding NMP does not increase k_g' . This is because the increase in physical solubility and MEA activity is not as great as at lean loading. MEA is significantly depleted near the gas/liquid interface due to low concentration and diffusivity.
- CARBITOL™, another physical solvent, shows similar effect on k_g' as NMP. Besides MEA, DGA® , another primary amine, also showed that k_g' could be increased by adding NMP.
- The difference between rich and lean loading ($\Delta\alpha_{CO_2}$) increases with the addition of physical solvent, but the overall effect of increase in viscosity and decrease in thermal conductivity and heat capacity reduced the normalized capacity, which increases the heat exchanger cost and sensible heat lost.
- Compared to 5 m PZ(aq), k_g' 'avg of 0.1-5 kPa $P_{CO_2}^*$ of 7 m MEA in 1 water/3 NMP and 1 water/19 NMP is 1.4 times and 3.6 times that of 5 m aqueous PZ; but the normalized capacity is 20% less than that of 5 m PZ.
- The PFO approximation adequately represents the CO_2 mass transfer in aqueous MEA but is not applicable to semi-aqueous MEA. The mass transfer model of CO_2 diffusion and reaction with semi-aqueous MEA was built in MATLAB®. D_{CO_2} only depends on the viscosity to the power of -0.4 in semi-aqueous system, which is

substantially lower than around -0.8 in aqueous amines. k_g' does depend on diffusivity of amine and amine product (D_{MEA}) with NMP present.

8.1.2.2 Semi-aqueous PZ

- Solid precipitation in 5 m PZ(aq) can be solved by partially replacing water with physical solvent (SUF or IMI). No precipitation was observed in 5 m PZ in 1SUF/3 water, 1SUF/1 water 1 IMI/3 water, or 1 IMI/1 water in the loading range of 0.15–0.45 mole CO₂/mole alkalinity at 20–60 °C.
- Adding SUF or IMI into aqueous PZ increases k_g' at lean and median loading but decreases k_g' at rich loading due to high viscosity.
- Compared to 5 m PZ(aq), $k_g'_{avg}$ in 5 m semi-aqueous PZ is about the same for 0.5–5kPa P*_{CO2}, 15–35% greater for 0.1–5 kPa P*_{CO2}, and 20–50% greater for 0.1–1.5kPa P*_{CO2} (natural gas conditions).
- k_g' in semi-aqueous PZ increases as temperature decreases from 60 to 20 °C.
- CO₂ cyclic capacity slightly increases after adding SUF/IMI; however, normalized capacity of semi-aqueous PZ involving viscosity, thermal conductivity, and heat capacity is lower, which increases the heat exchanger cost and sensible heat lost.

8.1.3 Lost work comparison

- The energy use of CO₂ capture by amine scrubbing can be estimated by the sum of minimum work and lost work. Energy use will be reduced if a new process or solvent reduces lost work.
- Water lean solvents can reduce the amount of water vapor exiting a simple stripper, which reduces the lost work in the condenser significantly from simple stripper. However; second generation amine processes use advanced stripper configurations that can accomplish the same effect with little additional capital cost.

- The energy use of CO2BOL/C16 and other representative water solvents will not be less than that of 5 m PZ AFS as lost work in the absorber and heat exchanger cannot be reduced.
- An advanced solvent that has a higher mass transfer coefficient that allows lower driving force could reduce the lost work in the absorber.
- Comprehensive normalized capacity has been developed. An advanced solvent with high normalized capacity can reduce the lost work in the heat exchanger no matter the solvent is water lean or not.

$$\Delta C_{norm} = \Delta C_{solv} \left(\frac{\mu}{\mu_{5mPZ}} \right)^{-0.175} \left(\frac{k}{k_{5mPZ}} \right)^{0.325} \left(\frac{C_p}{C_{p,5mPZ}} \right)^{-0.825}$$

8.2 RECOMMENDATIONS FOR FUTURE WORK

8.2.1 Aqueous piperazine blend

- 2MPZ and PZ/2MPZ are promising second generation solvents for CO₂ amine scrubbing cause of high absorption rate and high cyclic capacity.
- 2MPZ, PZ and PZ/2MPZ should be used at a total amine concentration of 5 m rather than 8 m, because the high solvent viscosity at high concentration depresses both CO₂ absorption rate and normalized capacity, and lower PZ concentration causes less precipitation.

8.2.2 Semi-aqueous MEA and PZ

- NMP or CARBITOL™ could be added into aqueous MEA to increase the absorption rate of CO₂.
- The volatility of NMP and CARBITOL™ is still too high, and water wash or other capture processing will be required to meet environmental regulations. Physical

solvents with lower volatility or process with lower absorber temperature could be further explored.

- Physical solvent (sulfolane or imidazole) could be added into 5 m PZ(aq) to reduce solid precipitation. No precipitation was observed in 5 m PZ in 1SUF/3 water, 1SUF/1 water 1 IMI/3 water, or 1 IMI/1 water in the loading range of 0.15–0.45 mole CO₂/mole alkalinity at 20–60 °C.
- Semi-aqueous amine with low viscosity and high CO₂ physical solubility could have high CO₂ absorption rate, which can be further explored.

8.2.3 Energy use

- Replacing water with low heat capacity physical solvent does not necessarily reduce heat exchanger cost. Comprehensive normalized capacity including the net effect of viscosity, heat capacity, thermal conductivity, and cyclic capacity can be used to compare the heat exchanger cost.
- An advanced solvent, no matter water lean or not, with high cyclic capacity, high thermal conductivity, low heat capacity, and low viscosity is desired to lower the heat exchanger cost
- An advanced solvent that has a higher mass transfer coefficient is desired. High mass transfer coefficient could reduce the required packing height for the same driving force (lower CAPEX), or reduce lost work by driving force for the same packing height (lower OPEX).

Appendix A: Experimental Methods

A.1 WETTED WALL COLUMN

CO₂ solubility and absorption rate of amine solutions were measured in the wetted wall column (WWC). It was originally built by Mshewa (Mshewa 1995) and further improved by other researchers (Pacheco 1998; Bishnoi 2000; Dang 2000; Cullinane 2005; Okoye 2005; Dugas 2009; Chen; 2011; Li 2013).

A.1.1 Design

The detailed view of the WWC is shown in Figure A.1. The stainless steel hollow column in the center is 9.1 cm in height and 1.26 cm in outer diameter (OD). The column is enclosed in a thick-walled glass tube whose inner diameter (ID) and OD is 1.83 cm and 2.54 cm respectively. The gap between the vertical surface of the column and the inner wall of the glass tube must be properly designed because the hydraulic diameter of the annulus affects the velocity of gas flow as well as the gas film mass transfer resistance. If the gap is too large, the gas film resistance is too high due to low gas flow rate, which makes the measurement of liquid mass transfer coefficient difficult; on the other hand, if the gap is too small, the liquid film on the surface will be disturbed by the fast gas flow.

The gas enters the small chamber through a small orifice on the Teflon annular collar at the bottom of the column. The collar keeps the gas from being mixed with the liquid. The gas exit on the top of the chamber at the opposite side to the entrance point to ensure uniform distribution. It is assumed that the composition of the gas is uniform horizontally but not vertically in experiments.

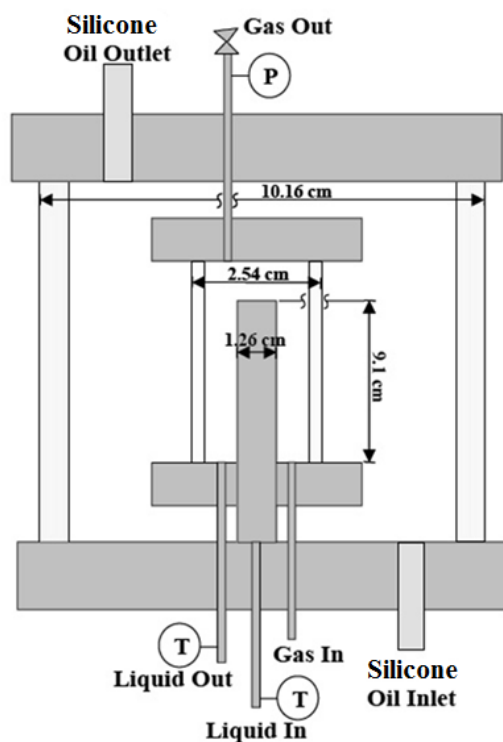


Figure A.1: Detailed view of the WWC.

As liquid flows through the middle of the column, the flow rate is carefully controlled so that the liquid will not overshoot from the top of the column but form a quasi-semi-sphere on the top and then flow down the column evenly. On the other hand, flow rate needs to be high enough to ensure a relatively high $k_{l,o}$. The column has to be clean and free of oil, or the surface of the column may not be wetted by the solution to form a continuous film. The liquid level is maintained at just slightly below the inner edge of the tilted annular surface of the collar. For an ideally formed liquid film, the total contact area between gas and liquid should be 38.52 cm^2 .

The whole smaller chamber is enclosed in the larger chamber which is filled and circulated with silicone oil to maintain the desired temperature. Temperature is measured by a probe located at the liquid exiting point.

A.1.2 Operating Procedure

A schematic diagram of the entire apparatus is shown in Figure A.2. The flow rate of nitrogen (N_2) and CO_2 is regulated by Brooks Mass Flow Controllers (Model #5850, Brooks Instrument, Hatfield, PA, USA). The total flow rate of the gas is controlled to be 5 standard liter (STL)/min. Variable CO_2 partial pressure in the gas mixture is achieved by altering the ratio of the two inlet gases. A 20 STL/min mass flow controller is used for N_2 while two mass flow controllers (2, 0.1 STL/min) are used for CO_2 to achieve high accuracy in flow control. If the desired CO_2 partial pressure is low, diluted CO_2 in N_2 (5000 ppm) instead of pure CO_2 is used. The gas mixture is first saturated with water at experimental temperature using a jacketed bubbling saturator (OD = 4 inches, ID = 3 inches, height =14 inches), and further heated by an oil bath before entering the WWC chamber from the bottom. The pressure in the WWC chamber is adjusted using a needle valve on the gas outlet, and is measured with a pressure gauge (Matheson, p/n 63-3112, 0 – 100 psig) with an accuracy of 0.2 psi.

The liquid in a 1-liter reservoir is circulated in the system at a rate of around 4 ml/s. The liquid volume flow rate is monitored using a rotameter. The liquid is heated by the oil bath and then pumped into the wetted wall inner column. It overflows from the top and then evenly distributes along the outer surface of the column, forming a laminar flow. The liquid is collected at the bottom and sent back to the reservoir.

Since the amount of the amine solvent is large and the typical contact time is relatively short, even the greatest CO_2 flux between the gas and the liquid will not significantly change the CO_2 loading of the solvent. The liquid composition remained essentially unchanged during an experimental run for each CO_2 loading and temperature. A 5-ml liquid sample is taken through the septum for each experiment run to confirm the liquid composition.

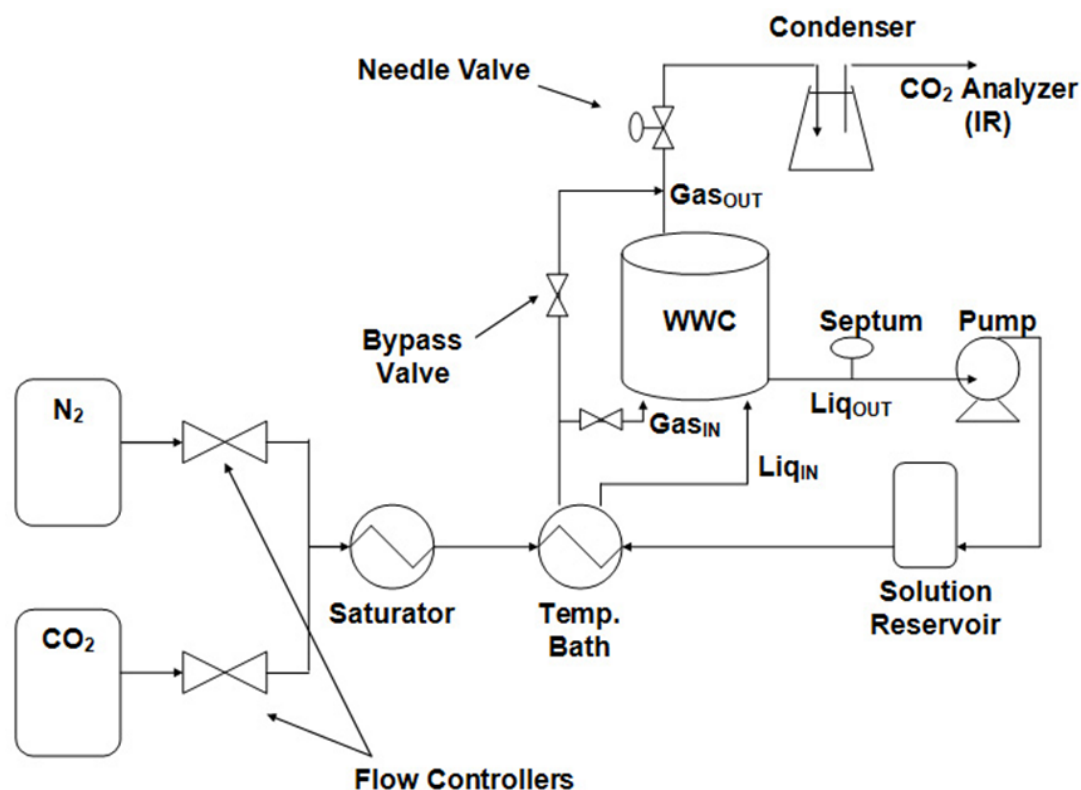


Figure A.2: Flow diagram of the entire WWC setup.

The gas leaving from the top is passed through a condenser (a 500 ml flask immersed in an ice-water bath) and a desiccation unit (a tube filled with CaSO_4) to remove water and amine vapor to protect the analyzer. For those highly volatile amines, the amine content in the solution is expected to slightly decrease over the course of experiments, especially at high temperature. What's more important is the amine, water, and CO_2 could react in the vapor phase between the column and the knock-out bottle, which means the WWC cannot measure the CO_2 absorption rate in the highly volatile amine. A portion of the dried outlet gas is sent to the CO_2 analyzers while the rest is vented. There are two Horiba VIA-510 infrared analyzers available for the range of 0-1 vol% and 0-20 vol% CO_2 respectively. The analyzers are connected to a computer equipped with a PicoLog Data Acquisition program.

The WWC is switched between two modes using the bypass valve: operation mode and bypass mode. In the operation mode, the gas is brought into contact with the liquid and the CO₂ concentration is measured after mass transfer; in the bypass mode, the inlet gas goes around the WWC, which directly measure the inlet CO₂ concentration is by the CO₂ analyzer. The length of time in the contact mode is always minimized to avoid unnecessary mass transfer between the gas and the liquid.

In a typical WWC experimental run, a solvent at certain CO₂ loading is prepared and loaded to the system. The equilibrium CO₂ partial pressure for the solution has to be estimated first by changing the CO₂ partial pressure in gas and locating the range of partial pressures where a transition from absorption and desorption occurs.

For each loading at each temperature, steady-state CO₂ fluxes and driving forces between gas and liquid for six CO₂ inlet concentrations are measured. Three of the CO₂ inlet concentrations induce absorption of CO₂ into solution and the other three correspond to desorption. The maximum CO₂ partial pressure used for absorption is approximately twice of the estimated equilibrium CO₂ partial pressure of the solvent. For each gas flow, the WWC is first bypassed to measure the inlet CO₂ concentration. Then the valve is switched to the operation mode. The CO₂ concentration after contacting in the WWC is measured to find out the CO₂ partial pressure at the top of the column.

The amine solvent for the WWC experiments starts with a lean loading. After the experiments at the loading are finished, the solvent is taken out and loaded with more CO₂ to reach a richer loading. The procedure is then repeated.

A.1.3 Data Analysis

The driving force between gas and liquid is defined as the logarithmic mean of the driving force at the top and the bottom of the column.

$$(P_{CO_2,g} - P_{CO_2}^*)_{LM} = \frac{(P_{CO_2,top} - P_{CO_2}^*) - (P_{CO_2,bottom} - P_{CO_2}^*)}{\ln\left(\frac{P_{CO_2,top} - P_{CO_2}^*}{P_{CO_2,bottom} - P_{CO_2}^*}\right)} \quad A.1$$

The CO₂ flux can also be calculated given the total pressure and flow rate as well as the difference of the CO₂ concentration (mol fraction) before and after the contact with liquid.

$$N_{CO_2} = \frac{1}{A} \frac{P_t V_t}{RT} ([CO_2]_{in} - [CO_2]_{out}) \quad A.2$$

A typical plot obtained from each run shown in Figure A.3 shows the correlation between flux and driving force. A straight line fits the six points. It is known that the flux has to be zero as the driving force is zero. The value of $P_{CO_2}^*$ that makes the line go through the origin should be the correct equilibrium CO₂ partial pressure for the solvent. The overall mass transfer coefficient (K_g) can also be obtained by extracting the slope of the line:

$$K_g = \frac{N_{CO_2}}{(P_{CO_2,g} - P_{CO_2}^*)_{LM}} \quad A.3$$

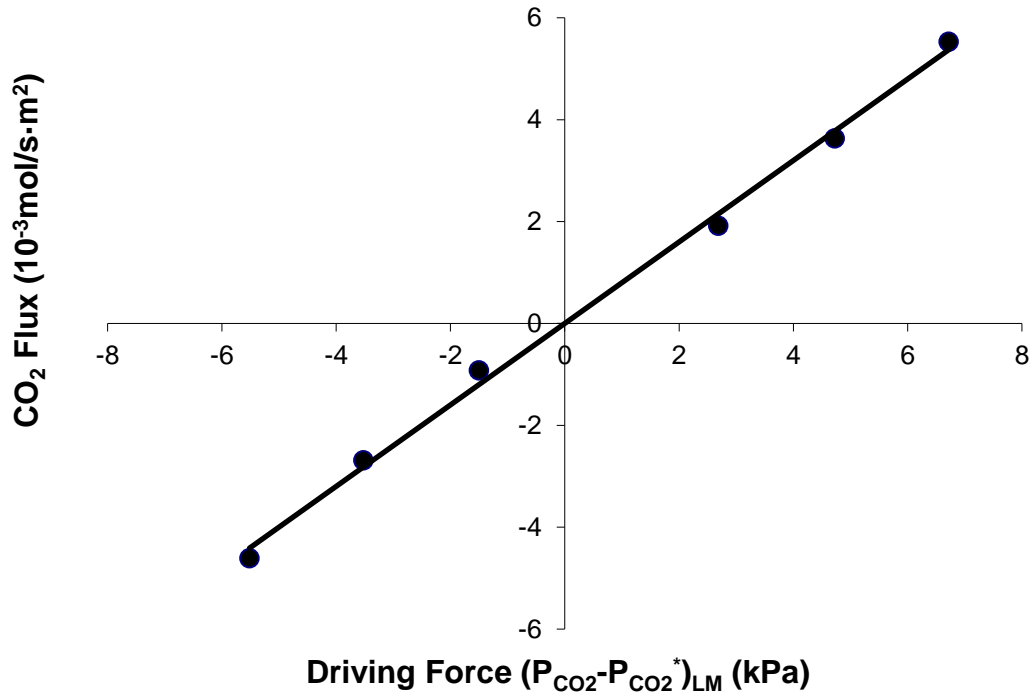


Figure A.3: Plot of flux of CO₂ vs. driving force obtained from a set of measurements for 4 m 2-methylpiperazine at 40 °C

A.1.4 Gas Film Mass Transfer Coefficient

To separate the contribution of the liquid film and the gas film to the total mass transfer resistance, the gas film mass transfer coefficient (k_g) needs to be determined beforehand.

A dimensionless analysis to correlate k_g in laminar flow was done by Hobler (Hobler 1966), who proposed the following expression.

$$Sh = A \cdot Re^B \cdot Sc^C \cdot \left(\frac{d}{h}\right)^D \quad \text{A.4}$$

Sh : Sherwood number

Re : Reynolds number

Sc : Schmidt number

d : the hydraulic diameter of the annulus (0.44 cm)

h : the height of the WWC (9.1 cm)

This form was adopted by Pacheco (Pacheco 1998) and Bishnoi (Bishnoi 2000) for the development of correlations for k_g . The general principle in measuring k_g is to use a dilute gas stream and a solvent that has a fast reaction rate with the gas. In this way, the mass transfer is mainly gas-film controlled. Although different solvents and gases were used to measure k_g in the WWC, the following expression was found to give a satisfactory fit to all the data.

$$Sh = 1.075 \left[\text{Re} Sc \left(\frac{d}{h} \right) \right]^{0.85} \quad \text{A.5}$$

The following equation allows the determination of k_g from Sh :

$$Sh = \frac{RTk_g l}{D_{CO_2}} \quad \text{A.6}$$

where l is the characteristic length, d is the diameter of the inner column.

k_g is, therefore, a strong function of the geometry of the WWC and gas flow rate. With k_g ready, the liquid mass transfer coefficient k'_g can be calculated from the following equation:

$$\frac{1}{k'_g} = \frac{1}{K_G} - \frac{1}{k_g} \quad \text{A.7}$$

A.2 ANALYTICAL METHODS

The analytical methods are used to determine the amine concentrations, CO₂ loadings, and viscosity for the samples.

A.2.1 Total Inorganic Carbon Analysis (TIC)

TIC Analysis realized quantification of CO₂ loading. A 20 – 50 X dilution was prepared for each CO₂-loaded concentrated amine solution. Then a small amount of the diluted sample was injected to a tube containing 30 wt% H₃PO₄. Due to the strong acid environment, CO₂-related species, including carbamate, carbonate and bicarbonate react to emit out CO₂. An N₂ stream carried the liberated CO₂ to a Horiba IR-2000 infrared analyzer. Each injection generated a signal peak, which was recorded by the Picolog Data Acquisition program. The peak area was obtained via integration. At the end of each analysis, a series of carbon standard (a mixture of K₂CO₃/KHCO₃ aqueous solution, 1000 ppm) the was injected to obtain a calibration curve which correlates CO₂ and peak area.

A.2.2 Acid Amine Titration

Titration can measure the concentration of amine in a liquid sample with 0.2 N H₂SO₄. An automatic Titrand series titrator with automatic equivalence point detection (Metrohm, Riverview, FL, USA) was used. Samples of known mass were diluted ~300 times with water and titrated. The pH value was monitored over time, and all the equivalence points were recorded. The point corresponding to total neutralization of amine was used to determine of amine concentration.

A.2.3 Viscosity Measurements

The viscosity was measured using a Physica MCR 300 cone and plate rheometer (Anton Paar GmbH, Graz, Austria). The cone shear rate was increased from 100 to 1000 s⁻¹ over a period of 100 second with 10 steps. The duration of each shear rate was 10 s, and the shear stress exerted on the solution was measured at the same time. The viscosities reported are the average values of the ten measurements.

Appendix B: Detailed WWC data

Table B.1: Detailed WWC data for 4 m 2MPZ

2MPZ	CO ₂ ldg	T	P*CO ₂	P	Gasdry	Gas	P _{CO₂} in dry	P _{CO₂} in wet	P _{CO₂} out dry	P _{CO₂} out wet	CO ₂ flux	K _G	kg	K _G /kg	kg'
m	mol/ mol alk	C	Pa	psig	std l/min	std l/min	Pa	Pa	Pa	Pa	mol/s cm ²	mol/s*Pa*cm ²	mol/s* Pa*cm ²		mol/s*Pa*cm ²
4	0.15	40	55	40	4.39	4.48	0.00	0.00	24.88	24.40	-5.56E-09	1.34E-10	2.57E-10	0.57	3.41E-10
							27.90	27.35	42.23	41.40	-3.22E-09	1.63E-10			
							85.59	83.91	72.01	70.60	3.15E-09	1.46E-10			
							113.1	110.9	87.47	85.76	6.03E-09	1.43E-10			
												1.46E-10			
4	0.15	60	431	40	4.52	4.77	0.00	0.00	213.8	202.5	-4.78E-08	1.50E-10	2.70E-10	0.55	3.34E-10
							130.1	123.2	281.6	266.8	-3.41E-08	1.49E-10			
							629.7	596.4	549.3	520.3	1.86E-08	1.51E-10			
							730.3	691.7	605.9	573.9	2.90E-08	1.48E-10			
												1.49E-10			
4	0.15	80	2340	60	4.37	4.81	0.00	0.00	1251.2	1136.1	-2.05E-07	1.20E-10	2.03E-10	0.60	3.07E-10
							895.9	813.5	1725	1566	-1.36E-07	1.22E-10			
							4387	3983	3476	3156	1.49E-07	1.26E-10			
							5406	4909	4032	3661	2.25E-07	1.20E-10			
												1.22E-10			
4	0.15	100	8400	60	4.38	5.45	0.00	0.00	6426	5161	-1.05E-06	1.94E-10	2.27E-10	0.85	1.29E-09
							5757	4624	8640	6940	-4.72E-07	1.94E-10			
							15488	12440	12450	10000	4.98E-07	1.89E-10			
							18680	15005	13634	10952	8.29E-07	1.94E-10			
												1.93E-10			

2MPZ	CO ₂ Idg	T	P* _{CO2}	P	Gas _{dry}	Gas	P _{CO2 in dry}	P _{CO2 in wet}	P _{CO2 out dry}	P _{CO2 out wet}	CO ₂ flux	K _G	kg	K _G /kg	kg'
m	mol/mol alk	C	Pa	psig	std l/min	std l/min	Pa	Pa	Pa	Pa	mol/s cm ²	mol/s*Pa*cm ²	mol/s*Pa*cm ²		mol/s*Pa*cm ²
2	0.13	40	50	20	5	5.16	15.07	14.60	29.42	28.51	-5.79E-09	2.08E-10	4.57E-10	0.47	4.07E-10
							98.54	95.50	79.41	76.96	7.72E-09	2.18E-10			
							77.26	74.87	66.97	64.90	4.15E-09	2.13E-10			
							25.59	24.80	36.36	35.23	-4.34E-09	2.23E-10			
												2.15E-10			
2	0.235	40	415	20	5	5.16	55.01	53.31	152.4	147.7	-3.93E-08	1.26E-10	4.57E-10	0.27	1.70E-10
							155.5	150.7	226.3	219.3	-2.86E-08	1.25E-10			
							253.1	245.2	297.3	288.1	-1.79E-08	1.21E-10			
							587.2	569.1	547.7	530.8	1.59E-08	1.19E-10			
							673.3	652.5	609.9	591.1	2.56E-08	1.25E-10			
							758.2	734.8	671.6	650.9	3.49E-08	1.27E-10			
					1.24E-10										
2	0.34	40	3350	40	5	5.1	433.60	425.11	978.4	959.3	-1.39E-07	5.27E-11	2.87E-10	0.18	6.12E-11
							908.7	890.9	1346.0	1319.7	-1.12E-07	5.00E-11			
							4253	4170	4106	4026	3.76E-08	5.05E-11			
							5863	5748	5437	5330	1.09E-07	5.00E-11			
							6953	6816	6334	6210	1.58E-07	5.02E-11			
							1416	1388	1759	1724	-8.78E-08	4.91E-11			
					5.04E-11										
2	0.37	40	7750	40	5	5.1	2081	2041	2771	2717	-1.77E-07	3.29E-11	2.87E-10	0.12	3.95E-11
							2730	2676	3299	3235	-1.46E-07	3.04E-11			
							5316	5212	5671	5560	-9.07E-08	3.85E-11			
							9388	9204	9162	8983	5.79E-08	4.32E-11			
							10896	10683	10557	10350	8.69E-08	3.14E-11			
							12480	12236	11952	11718	1.35E-07	3.20E-11			
					3.47E-11										

2MPZ	CO ₂ ldg	T	P*CO ₂	P	Gas _{dry}	Gas	P _{CO₂} in dry	P _{CO₂} in wet	P _{CO₂} out dry	P _{CO₂} out wet	CO ₂ flux	K _G	kg	K _G /kg	kg'
m	mol/mol alk	C	Pa	psig	std l/min	std l/min	Pa	Pa	Pa	Pa	mol/s cm ²	mol/s*Pa*cm ²	mol/s*Pa*cm ²		mol/s*Pa*cm ²
4	0.25	40	445	40	4.53	4.62	0.00	0.00	167.8	164.5	-3.75E-08	1.05E-10	2.62E-10	0.41	1.79E-10
							137.6	134.9	256.8	251.7	-2.68E-08	1.08E-10			
							736.0	721.6	633.0	620.7	2.39E-08	1.07E-10			
							969.4	950.4	792.5	777.0	4.16E-08	1.01E-10			
							855.9	839.1	707.7	693.8	3.46E-08	1.10E-10			
4	0.25	60	2420	40	4.36	4.61	0.00	0.00	916.2	867.8	-2.05E-07	1.05E-10	2.66E-10	0.40	1.80E-10
							625.9	592.8	1349.8	1278.4	-1.62E-07	1.11E-10			
							4649	4403	3891	3685	1.69E-07	1.06E-10			
							8325	7885	6214	5885	4.72E-07	1.08E-10			
4	0.25	80	2340	60	5	5.507	0.00	0.00	3465	3146	-6.50E-07	9.41E-11	2.28E-10	0.42	1.66E-10
							5134	4661	6776	6153	-3.08E-07	9.83E-11			
							13634	12380	12090	10977	2.90E-07	9.57E-11			
							16672	15138	13995	12707	5.02E-07	9.60E-11			
4	0.35	20	460	40	5	5.03	0.00	0.00	87.47	86.93	-2.24E-08	5.40E-11	2.82E-10	0.18	6.26E-11
							231.5	230.1	269.6	267.9	-9.75E-09	4.63E-11			
							1084	1078	969	963	2.95E-08	5.29E-11			
							1289	1281	1139	1132	3.85E-08	5.18E-11			

2MPZ	CO ₂ ldg	T	P*CO ₂	P	Gas _{dry}	Gas	P _{CO2 in dry}	P _{CO2 in wet}	P _{CO2 out dry}	P _{CO2 out wet}	CO ₂ flux	KG	kg	KG/kg	kg'
m	mol/mol alk	C	Pa	psig	std l/min	std l/min	Pa	Pa	Pa	Pa	mol/s cm ²	mol/s*Pa*cm ²	mol/s*Pa*cm ²		mol/s*Pa*cm ²
4	0.35	40	2800	40	5	5.1	0.00	0.00	580.6	569.3	-1.49E-07	5.94E-11	2.87E-10	0.21	7.65E-11
							1131	1109	1486	1456	-9.07E-08	6.01E-11			
							4879	4783	4445	4358	1.11E-07	6.30E-11			
							8461	8295	7322	7179	2.92E-07	5.93E-11			
4	0.35	60	11000	60	5	5.28	0.00	0.00	2473	2343	-6.33E-07	6.47E-11	2.98E-10	0.19	7.11E-11
							6157	5832	7168	6789	-2.59E-07	5.54E-11			
							21559	20419	19636	18598	4.92E-07	5.81E-11			
							17525	16598	16431	15563	2.80E-07	5.53E-11			
							9381	8885	9758	9242	-9.65E-08	5.00E-11			
							3197	3028	4856	4600	-4.25E-07	5.93E-11			
							23180	21955	20918	19812	5.79E-07	5.88E-11			
						5.74E-11									
4	0.4	20	1300	40	5	5.03	0.00	0.00	174.9	173.9	-4.48E-08	3.70E-11	2.82E-10	0.12	4.01E-11
							689.2	685.0	762.0	757.3	-1.86E-08	3.22E-11			
							2473	2457	2318	2304	3.96E-08	3.67E-11			
							3268	3248	3023	3004	6.27E-08	3.44E-11			
4	0.4	40	7400	40	5	5.1	0.00	0.00	1037	1017	-2.65E-07	3.86E-11	2.87E-10	0.13	4.25E-11
							3921	3844	4351	4266	-1.10E-07	3.29E-11			
							11273	11053	10746	10535	1.35E-07	3.99E-11			
							15308	15008	14290	14010	2.61E-07	3.67E-11			

Table B.2: Detailed WWC data for 2 m 2MPZ

2MPZ	CO ₂ ldg	T	P*CO ₂	P	Gas _{dry}	Gas	P _{CO₂ in dry}	P _{CO₂ in wet}	P _{CO₂ out dry}	P _{CO₂ out wet}	CO ₂ flux	K _G	kg	K _G /kg	kg'
m	mol/mol alk	C	Pa	psig	std l/min	std l/min	Pa	Pa	Pa	Pa	mol/s cm ²	mol/s*Pa*cm ²	mol/s*Pa*cm ²		mol/s*Pa*cm ²
2	0.13	40	50	20	5	5.16	15.07	14.60	29.42	28.51	-5.79E-09	2.08E-10	4.57E-10	0.47	4.07E-10
							98.54	95.50	79.41	76.96	7.72E-09	2.18E-10			
							77.26	74.87	66.97	64.90	4.15E-09	2.13E-10			
							25.59	24.80	36.36	35.23	-4.34E-09	2.23E-10			
2	0.235	40	415	20	5	5.16	55.01	53.31	152.4	147.7	-3.93E-08	1.26E-10	4.57E-10	0.27	1.70E-10
							155.5	150.7	226.3	219.3	-2.86E-08	1.25E-10			
							253.1	245.2	297.3	288.1	-1.79E-08	1.21E-10			
							587.2	569.1	547.7	530.8	1.59E-08	1.19E-10			
							673.3	652.5	609.9	591.1	2.56E-08	1.25E-10			
							758.2	734.8	671.6	650.9	3.49E-08	1.27E-10			
						1.24E-10									
2	0.34	40	3350	40	5	5.1	433.60	425.11	978.4	959.3	-1.39E-07	5.27E-11	2.87E-10	0.18	6.12E-11
							908.7	890.9	1346.0	1319.7	-1.12E-07	5.00E-11			
							4253	4170	4106	4026	3.76E-08	5.05E-11			
							5863	5748	5437	5330	1.09E-07	5.00E-11			
							6953	6816	6334	6210	1.58E-07	5.02E-11			
							1416	1388	1759	1724	-8.78E-08	4.91E-11			
						5.04E-11									
2	0.37	40	7750	40	5	5.1	2081	2041	2771	2717	-1.77E-07	3.29E-11	2.87E-10	0.12	3.95E-11
							2730	2676	3299	3235	-1.46E-07	3.04E-11			
							5316	5212	5671	5560	-9.07E-08	3.85E-11			
							9388	9204	9162	8983	5.79E-08	4.32E-11			
							10896	10683	10557	10350	8.69E-08	3.14E-11			
							12480	12236	11952	11718	1.35E-07	3.20E-11			
						3.47E-11									

Table B.3: Detailed WWC data for 6 m 2MPZ

2MPZ	CO ₂ ldg	T	P*CO ₂	P	Gas _{dry}	Gas	P _{CO2 in dry}	P _{CO2 in wet}	P _{CO2 out dry}	P _{CO2 out wet}	CO ₂ flux	KG	kg	KG/kg	kg'
m	mol/mol alk	C	Pa	psig	std l/min	std l/min	Pa	Pa	Pa	Pa	mol/s cm ²	mol/s*Pa*cm ²	mol/s*Pa*cm ²		mol/s*Pa*cm ²
6	0.15	40	60	20	5	5.16	18.90	18.31	38.99	37.78	-8.11E-09	2.62E-10	4.57E-10	0.52	4.90E-10
							27.51	26.66	42.57	41.26	-6.08E-09	2.40E-10			
							108.11	104.77	87.54	84.84	8.30E-09	2.45E-10			
							87.54	84.84	76.54	74.18	4.44E-09	2.34E-10			
							122.7	118.9	96.63	93.65	1.05E-08	2.33E-10			
							38.51	37.32	47.60	46.13	-3.67E-09	2.05E-10			
											2.37E-10				
6	0.25	40	330	20	5	5.16	55.01	53.31	140.6	136.3	-3.46E-08	1.48E-10	4.57E-10	0.29	1.88E-10
							152.6	147.9	202.1	195.9	-2.00E-08	1.27E-10			
							257.1	249.2	275.5	267.0	-7.43E-09	1.04E-10			
							488.4	473.3	444.9	431.2	1.76E-08	1.45E-10			
							567.8	550.3	504.7	489.1	2.55E-08	1.36E-10			
							620.2	601.1	540.6	523.9	3.21E-08	1.40E-10			
											1.33E-10				
6	0.34	40	1680	40	5	5.1	751.1	736.4	984.1	964.8	-5.97E-08	7.24E-11	2.87E-10	0.24	9.09E-11
							1414	1386	1470	1442	-1.45E-08	5.46E-11			
							2307	2262	2153	2111	3.96E-08	7.87E-11			
							2734	2680	2496	2447	6.08E-08	6.92E-11			
							3167	3105	2854	2798	8.01E-08	6.33E-11			
							1142	1120	1286	1261	-3.70E-08	7.61E-11			
											6.91E-11				
6	0.38	40	6150	40	5	5.1	2138	2096	2775	2721	-1.63E-07	4.37E-11	2.87E-10	0.14	4.86E-11
							3194	3131	3650	3578	-1.17E-07	4.19E-11			
							8031	7874	7729	7578	7.72E-08	4.92E-11			
							11010	10794	10369	10166	1.64E-07	3.80E-11			
							9388	9204	8974	8798	1.06E-07	3.73E-11			
							4355	4270	4623	4532	-6.85E-08	3.93E-11			
											4.15E-11				

Table B.4: Detailed WWC data for 2.5/2.5 m 2MPZ/PZ

	CO ₂ ldg	T	P* _{CO2}	P	Gas _{dry}	Gas	P _{CO2 in dry}	P _{CO2 in wet}	P _{CO2 out dry}	P _{CO2 out wet}	CO ₂ flux	K _G	kg	K _G /kg	kg'
m	mol/mol alk	C	Pa	psig	std l/min	std l/min	Pa	Pa	Pa	Pa	mol/s cm ²	mol/s*Pa*cm ²	mol/s*Pa*cm ²		mol/s*Pa*cm ²
2.5/2.5	0.2	40	85	40	5	5.1	0.00	0.00	41.10	40.29	-1.05E-08	1.68E-10	2.87E-10	0.53	3.28E-10
							45.62	44.73	61.83	60.62	-4.15E-09	1.31E-10			
							136.5	133.8	114.6	112.4	5.60E-09	1.51E-10			
							172.7	169.3	133.1	130.5	1.01E-08	1.61E-10			
							30.92	30.31	55.80	54.71	-6.37E-09	1.54E-10			
2.5/2.5	0.2	60	550	40	5	5.28	0.00	0.00	291.5	276.0	-7.46E-08	1.88E-10	2.98E-10	0.60	4.43E-10
							228.5	216.4	380.1	360.0	-3.88E-08	1.52E-10			
							1061	1005	819.3	776.0	6.19E-08	1.89E-10			
							2101	1990	1354	1282	1.91E-07	1.83E-10			
2.5/2.5	0.2	80	3000	60	5	5.51	0.00	0.00	1673	1519	-3.14E-07	1.46E-10	2.28E-10	0.61	3.63E-10
							880.5	799.5	2075	1884	-2.24E-07	1.40E-10			
							4845	4399	4083	3707	1.43E-07	1.41E-10			
							6477	5881	4969	4512	2.83E-07	1.33E-10			
2.5/2.5	0.2	100	12500	60	5	6.22	0.00	0.00	6719	5397	-1.26E-06	1.32E-10	2.54E-10	0.51	2.64E-10
							6307	5066	9963	8003	-6.85E-07	1.17E-10			
							17120	13751	16451	13214	1.25E-07	1.31E-10			
							22218	17846	18768	15075	6.47E-07	1.71E-10			
							27058	21733	22784	18301	8.01E-07	1.09E-10			
							24277	19500	20828	16729	6.47E-07	1.18E-10			

	CO ₂ ldg	T	P* _{CO2}	P	Gas _{dry}	Gas	P _{CO2 in dry}	P _{CO2 in wet}	P _{CO2 out dry}	P _{CO2 out wet}	CO ₂ flux	K _G	kg	K _G /kg	kg'
m	mol/ mol alk	C	Pa	psig	std l/min	std l/min	Pa	Pa	Pa	Pa	mol/s cm ²	mol/s*Pa*cm ²	mol/s* Pa*cm ²		mol/s*Pa*cm ²
2.5/2.5	0.3	20	67	40	5	5.03	0.00	0.00	19.23	19.11	-4.92E-09	8.65E-11	2.82E-10	0.34	1.42E-10
							31.29	31.10	43.36	43.09	-3.09E-09	1.05E-10			
							19.61	19.48	34.69	34.47	-3.86E-09	9.76E-11			
							152.7	151.8	126.7	125.9	6.66E-09	9.38E-11			
							121.8	121.0	104.8	104.2	4.34E-09	9.64E-11			
							107.8	107.2	96.15	95.55	2.99E-09	8.79E-11			
												9.45E-11			
2.5/2.5	0.3	40	640	40	5	5.1	0.00	0.00	218.7	214.4	-5.60E-08	1.07E-10	2.87E-10	0.37	1.70E-10
							203.6	199.6	354.4	347.5	-3.86E-08	1.07E-10			
							306.5	300.5	422.3	414.0	-2.96E-08	1.06E-10			
							1256	1231	1052	1031	5.21E-08	1.08E-10			
							1441	1413	1176	1153	6.80E-08	1.07E-10			
							1889	1852	1473	1444	1.06E-07	1.07E-10			
												1.07E-10			
2.5/2.5	0.3	60	3670	40	5	5.28	30.16	28.57	1271	1203	-3.18E-07	1.05E-10	2.98E-10	0.37	1.73E-10
							897.4	849.9	1885.2	1785.5	-2.53E-07	1.09E-10			
							1312	1243	2209	2093	-2.30E-07	1.17E-10			
							5825	5517	5211	4935	1.57E-07	1.02E-10			
							5275	4996	4807	4553	1.20E-07	1.10E-10			
							7993	7571	6587	6239	3.60E-07	1.13E-10			
												1.09E-10			
2.5/2.5	0.3	80	13400	60	5	5.51	41.19	37.40	5406	4909	-1.01E-06	9.36E-11	2.28E-10	0.39	1.44E-10
							6035	5479	9062	8228	-5.68E-07	8.80E-11			
							7368	6690	9768	8869	-4.50E-07	8.11E-11			
							28886	26228	23840	21646	9.46E-07	9.12E-11			
							22141	20104	19566	17766	4.83E-07	8.85E-11			
							26826	24358	22655	20571	7.82E-07	8.76E-11			

Table B.5: Detailed WWC data for 3 m HEP

HEP	CO ₂ ldg	T	P* _{CO2}	P	Gas% _{dry}	Gas	P _{CO2 in dry}	P _{CO2 in wet}	P _{CO2 out dry}	P _{CO2 out wet}	CO ₂ flux	K _c	kg	K _c /kg	kg'	
m	mol/mol alk	C	Pa	psig	std l/min	std l/min	Pa	Pa	Pa	Pa	mol/s cm ²	mol/s*Pa*cm ²	mol/s*Pa*cm ²		mol/s*Pa*cm ²	
3	0.07	40	57	20	5	5.16	6.5	6.3	27.3	26.4	-8.40E-09	2.11E-10	4.57E-10	0.44	3.60E-10	
							20.6	19.9	34.2	33.1	-5.50E-09	1.84E-10				
							37.3	36.2	45.4	44.0	-3.28E-09	1.98E-10				
							74.4	72.1	68.2	66.1	2.51E-09	2.12E-10				
							95.0	92.0	80.8	78.3	5.70E-09	2.06E-10				
							113.6	110.1	92.8	89.9	8.40E-09	1.99E-10				
3	0.15	40	470	20	5	5.16	193	187	275	266	-3.31E-08	1.37E-10	4.57E-10	0.27	1.73E-10	
							303	294	351	341	-1.94E-08	1.28E-10				
							353	342	385	373	-1.31E-08	1.18E-10				
							731	709	665	644	2.68E-08	1.31E-10				
							852	825	763	739	3.60E-08	1.16E-10				
							581	563	557	540	9.65E-09	1.19E-10				
3	0.2	40	1700	40	5	5.1	777	761	1033	1013	-6.56E-08	8.14E-11	2.87E-10	0.29	1.15E-10	
							965	946	1176	1153	-5.41E-08	8.39E-11				
							1276	1251	1399	1371	-3.14E-08	8.14E-11				
							2613	2562	2372	2325	6.18E-08	8.38E-11				
							2111	2070	2006	1967	2.70E-08	8.57E-11				
							2372	2325	2206	2163	4.25E-08	7.87E-11				
3	0.25	40	7650	40	3	3.06	2481	2432	3597	3527	-1.71E-07	3.69E-11	1.86E-10	0.20	4.70E-11	
							3665	3593	4528	4440	-1.33E-07	3.67E-11				
							5957	5841	6372	6247	-6.37E-08	3.99E-11				
							9841	9648	9426	9241	6.37E-08	3.57E-11				
							11349	11127	10595	10387	1.16E-07	3.75E-11				
							12405	12162	11387	11164	1.56E-07	3.92E-11				

Table B.6: Detailed WWC data for 5 m HEP

HEP	CO ₂ Idg	T	P* _{CO2}	P	Gas _{dry}	Gas	P _{CO2 in dry}	P _{CO2 in wet}	P _{CO2 out dry}	P _{CO2 out wet}	CO ₂ flux	K _G	kg	K _G /kg	kg'
m	mol/mol alk	C	Pa	psig	std l/min	std l/min	Pa	Pa	Pa	Pa	mol/s cm ²	mol/s*Pa*cm ²	mol/s*Pa*cm ²		mol/s*Pa*cm ²
5	0.07	40	57	20	5	5.16	15.1	14.6	33.5	32.5	-7.43E-09	2.28E-10	4.57E-10	0.51	4.72E-10
							37.1	35.9	46.6	45.2	-3.86E-09	2.42E-10			
							51.4	49.8	54.8	53.1	-1.35E-09	2.51E-10			
							86.3	83.7	75.3	73.0	4.44E-09	2.12E-10			
							108	105	86.1	83.4	8.98E-09	2.48E-10			
							128	124	98.8	95.7	1.18E-08	2.28E-10			
												2.32E-10			
5	0.15	40	435	20	5	5.16	161	156	243	235	-3.31E-08	1.40E-10	4.57E-10	0.30	1.93E-10
							107	103	200	194	-3.76E-08	1.32E-10			
							257	249	311	301	-2.16E-08	1.36E-10			
							497	482	483	468	5.79E-09	1.46E-10			
							599	581	559	542	1.61E-08	1.29E-10			
							734	711	653	633	3.26E-08	1.39E-10			
												1.36E-10			
5	0.2	40	1760	40	5	5.1	2307	2262	2183	2140	3.19E-08	7.27E-11	2.87E-10	0.26	1.00E-10
							797	782	1055	1035	-6.60E-08	7.81E-11			
							896	878	1124	1102	-5.83E-08	7.63E-11			
							1075	1054	1246	1221	-4.36E-08	7.06E-11			
							2010	1970	1968	1930	1.06E-08	5.61E-11			
							2764	2710	2526	2477	6.08E-08	7.35E-11			
												7.43E-11			
5	0.25	40	9300	40	3	3.06	1895	1858	3284	3220	-2.13E-07	3.17E-11	1.86E-10	0.17	3.71E-11
							3039	2979	4249	4166	-1.86E-07	3.26E-11			
							5806	5693	6545	6417	-1.14E-07	3.51E-11			
							16401	16080	14968	14675	2.20E-07	3.64E-11			
							14591	14306	13724	13456	1.33E-07	2.92E-11			
							12706	12457	12178	11940	8.11E-08	2.80E-11			
					3.09E-11										

Table B.7: Detailed WWC data for 7.7 m HEP

HEP	CO ₂ Idg	T	P*CO ₂	P	Gas _{dry}	Gas	PCO ₂ in dry	PCO ₂ in wet	PCO ₂ out dry	PCO ₂ out wet	CO ₂ flux	K _c	kg	K _c /kg	kg'
m	mol/mol alk	C	Pa	psig	std l/min	std l/min	Pa	Pa	Pa	Pa	mol/s cm ²	mol/s*Pa*cm ²	mol/s*Pa*cm ²		mol/s*Pa*cm ²
7.7	0.07	40	63	20	5	5.16	9.6	9.3	34.4	33.4	-1.00E-08	2.48E-10	4.57E-10	0.51	4.67E-10
							25.4	24.6	42.6	41.3	-6.95E-09	2.37E-10			
							45.2	43.8	52.9	51.2	-3.09E-09	2.04E-10			
							89.5	86.7	78.9	76.5	4.25E-09	2.34E-10			
							111	108	92.1	89.2	7.72E-09	2.23E-10			
							134	130	105.5	102.2	1.16E-08	2.23E-10			
												2.31E-10			
7.7	0.15	40	410	40	5	5.1	180	176	276	270	-2.45E-08	1.34E-10	2.87E-10	0.46	2.44E-10
							330	323	362	355	-8.21E-09	1.18E-10			
							106	104	234	230	-3.27E-08	1.38E-10			
							721	706	606	594	2.94E-08	1.25E-10			
							513	503	470	461	1.09E-08	1.56E-10			
							622	610	543	532	2.03E-08	1.28E-10			
												1.32E-10			
7.7	0.2	40	1475	40	5	5.1	770	754	944	926	-4.47E-08	7.08E-11	2.87E-10	0.24	9.23E-11
							973	954	1097	1076	-3.19E-08	6.96E-11			
							1180	1157	1254	1229	-1.88E-08	6.71E-11			
							1682	1649	1636	1604	1.16E-08	7.70E-11			
							2356	2310	2157	2114	5.12E-08	6.98E-11			
							2013	1974	1897	1859	2.99E-08	6.81E-11			
												6.99E-11			
7.7	0.25	40	8000	40	3	3.06	1625	1593	2764	2710	-1.75E-07	3.00E-11	1.86E-10	0.16	3.62E-11
							4807	4713	5411	5305	-9.27E-08	3.11E-11			
							3473	3405	4298	4214	-1.27E-07	3.04E-11			
							13536	13271	12593	12347	1.45E-07	3.02E-11			
							11839	11607	11198	10979	9.85E-08	3.00E-11			
							10218	10018	9841	9648	5.79E-08	3.17E-11			
												3.03E-11			

Table B.8: Detailed WWC data for 7 m MEA in 19 NMP/1 water

MEA	CO ₂ Idg	T	P*CO ₂	P	Gas _{dry}	Gas	P _{CO2 in dry}	P _{CO2 in wet}	P _{CO2 out dry}	P _{CO2 out wet}	CO ₂ flux	K _G	kg	K _G /kg	kg'
m	mol/mol alk	C	Pa	psig	std l/min	std l/min	Pa	Pa	Pa	Pa	mol/s cm ²	mol/s*Pa*cm ²	mol/s* Pa*cm ²		mol/s*Pa* cm ²
7 m	0.302	40	117	20	5	5.16	55.3	54.2	94.5	92.6	-1.60E-08	3.94E-10	4.57E-10	0.87	3.17E-09
							86.1	84.4	107.2	105.1	-8.59E-09	4.18E-10			
95 NMP							157.6	154.5	132.5	129.9	1.03E-08	4.44E-10			
5 water							208.6	204.5	154.0	151.0	2.23E-08	3.93E-10			
												4.00E-10			
7 m	0.365	20	291	20	5	5.16	83.5	81.8	196.1	192.3	-4.60E-08	3.13E-10	4.57E-10	0.69	1.01E-09
							206.9	202.8	256.4	251.4	-2.02E-08	3.33E-10			
95 NMP							446.1	437.3	367.6	360.4	3.20E-08	3.11E-10			
5 water							546.5	535.8	413.8	405.7	5.42E-08	3.16E-10			
												3.15E-10			
7 m	0.412	40	810	40	5	5.1	212.7	208.5	473.2	463.9	-6.67E-08	1.44E-10	2.87E-10	0.49	2.79E-10
							411.0	402.9	580.6	569.3	-4.34E-08	1.37E-10			
95 NMP							1410.1	1382.5	1165.1	1142.2	6.27E-08	1.42E-10			
5 water							1971.9	1933.3	1493.1	1463.8	1.23E-07	1.41E-10			
												1.42E-10			
7 m	0.45	40	2980	40	5	5.1	2504	2455	2624	2573	-3.09E-08	6.66E-11	2.87E-10	0.21	7.70E-11
							1894	1857	2145	2103	-6.44E-08	6.47E-11			
							3687	3615	3563	3493	3.19E-08	5.57E-11			
95 NMP							4898	4802	4581	4491	8.11E-08	4.88E-11			
5 water							4445	4358	4189	4107	6.56E-08	5.26E-11			
							1455	1427	1835	1799	-9.72E-08	7.16E-11			
												6.07E-11			
7 m	0.465	40	8500	40	3	3.06	4004	3926	4822	4728	-1.26E-07	3.02E-11	1.86E-10	0.13	2.82E-11
							4988	4891	5542	5434	-8.51E-08	2.56E-11			
							14026	13751	13347	13086	1.04E-07	2.12E-11			
95 NMP							10557	10350	10293	10092	4.05E-08	2.36E-11			
5 water							12932	12679	12480	12236	6.95E-08	1.76E-11			
							6900	6765	7183	7042	-4.34E-08	2.73E-11			
												2.45E-11			

Table B.9: Detailed WWC data for 7 m MEA in 3NMP/1 water

MEA	CO ₂ Idg	T	P* _{CO2}	P	Gas _{dry}	Gas	P _{CO2 in dry}	P _{CO2 in wet}	P _{CO2 out dry}	P _{CO2 out wet}	CO ₂ flux	K _G	kg	K _G /kg	kg'
m	mol/mol alk	C	Pa	psig	std l/min	std l/min	Pa	Pa	Pa	Pa	mol/s cm ²	mol/s*Pa*cm ²	mol/s* Pa*cm ²		mol/s*Pa*cm ²
7 m	0.3	40	105	20	5	5.07	106.0	104.6	225.8	222.8	-4.84E-08	1.85E-10	4.50E-10	0.40	3.02E-10
							301.6	297.6	346.8	342.2	-1.82E-08	1.68E-10			
3 NMP							574.0	566.4	526.2	519.2	1.93E-08	1.74E-10			
1 water							777.3	767.0	655.4	646.7	4.92E-08	1.81E-10			
												1.81E-10			
7 m	0.39	40	430	20	5	5.07	3.35	3.28	67.0	65.7	-2.60E-08	2.82E-10	4.57E-10	0.60	6.92E-10
							59.8	58.6	94.2	92.4	-1.41E-08	2.67E-10			
3 NMP							254.7	249.7	192.5	188.8	2.54E-08	2.96E-10			
1 water							576.4	565.1	362.4	355.3	8.74E-08	2.74E-10			
												2.75E-10			
7 m	435	40	1375	40	5	5.04	682.1	676.3	913.9	906.3	-5.94E-08	1.03E-10	2.85E-10	0.37	1.65E-10
							871.7	864.4	1037.6	1028.9	-4.25E-08	1.00E-10			
							965.2	957.1	1112.3	1102.9	-3.76E-08	1.11E-10			
3 NMP							1519	1507	1474	1462	1.16E-08	1.08E-10			
1 water							1706	1692	1590	1577	2.96E-08	1.16E-10			
							1998	1982	1798	1783	5.12E-08	1.02E-10			
												1.04E-10			
7 m	0.47	40	4590	40	3	3.03	3054	3028	3390	3361	-5.16E-08	3.71E-11	1.84E-10	0.19	4.32E-11
							3510	3481	3721	3690	-3.24E-08	3.24E-11			
3 NMP							5942	5892	5678	5630	4.05E-08	3.48E-11			
1 water							5486	5440	5320	5275	2.55E-08	3.33E-11			
							5033	4991	4951	4909	1.27E-08	3.55E-11			
							4057	4023	4170	4135	-1.74E-08	3.41E-11			
												3.50E-11			

Table B.10: Detailed WWC data for 7 m MEA in 1NMP/3 water

MEA	CO ₂ ldg	T	P* _{CO2}	P	Gas _{dry}	Gas	P _{CO2 in dry}	P _{CO2 in wet}	P _{CO2 out dry}	P _{CO2 out wet}	CO ₂ flux	K _G	kg	K _G /kg	kg'
m	mol/mol alk	C	Pa	psig	std l/min	std l/min	Pa	Pa	Pa	Pa	mol/s cm ²	mol/s*Pa*cm ²	mol/s*Pa*cm ²		mol/s*Pa*cm ²
7 m	0.38	40	230	40	5	5.1	5.28	5.18	187.0	183.4	-1.94E-08	1.05E-10	2.87E-10	0.37	1.70E-10
							297.9	292.0	398.2	390.4	-9.65E-09	1.09E-10			
1 NMP							1033.8	1013.6	961.5	942.6	1.25E-08	1.08E-10			
3 water							1314.0	1288.3	1150.0	1127.5	3.09E-08	1.08E-10			
												1.07E-10			
7 m	0.42	40	690	40	5	5.1	0.00	0.00	213.8	202.5	-4.65E-08	7.87E-11	2.87E-10	0.27	1.06E-10
							130.1	123.2	281.6	266.8	-2.57E-08	7.41E-11			
1 NMP							629.7	596.4	549.3	520.3	1.85E-08	6.47E-11			
3 water							730.3	691.7	605.9	573.9	4.20E-08	8.18E-11			
												7.76E-11			
7 m	0.46	40	10000	40	5	5.1	5.28	5.18	867.2	850.2	-2.21E-07	2.31E-11	2.87E-10	0.06	1.98E-11
							6436	6310	6681	6550	-6.27E-08	1.76E-11			
1 NMP							12367	12125	12254	12014	2.90E-08	1.40E-11			
3 water							16288	15969	15911	15600	9.65E-08	1.67E-11			
							20096	19703	19568	19185	1.35E-07	1.43E-11			
												1.85E-11			

Table B.11: Detailed WWC data for 7 m DGA in NMP/water

DGA	CO ₂ ldg	T	P* _{CO2}	P	Gas _{dry}	Gas	P _{CO2 in dry}	P _{CO2 in wet}	P _{CO2 out dry}	P _{CO2 out wet}	CO ₂ flux	K _G	kg	K _G /kg	kg'
m	mol/mol alk	C	Pa	psig	std l/min	std l/min	Pa	Pa	Pa	Pa	mol/s cm ²	mol/s*Pa*c m ²	mol/s* Pa*cm ²		mol/s*Pa*c m ²
7 m	0.29	40	228	20	5	5.16	3.35	3.28	110.0	107.9	-4.36E-08	2.61E-10	4.57E-10	0.54	5.40E-10
							130.4	127.8	169.6	166.3	-1.60E-08	2.02E-10			
3 NMP							362.4	355.3	308.5	302.5	2.20E-08	2.23E-10			
1 water							468.8	459.6	361.2	354.1	4.39E-08	2.53E-10			
												2.48E-10			
7 m	0.34	40	408	20	5	5.16	3.35	3.28	167.4	164.1	-6.70E-08	2.11E-10	4.57E-10	0.46	3.84E-10
							253.5	248.6	315.7	309.5	-2.54E-08	2.01E-10			
3 NMP							887.4	870.0	700.8	687.1	7.62E-08	2.10E-10			
1 water							1315.5	1289.7	961.5	942.7	1.45E-07	2.08E-10			
												2.09E-10			
7 m	0.38	40	820	40	5	5.1	205.9	201.8	473.2	463.9	-6.84E-08	1.44E-10	2.87E-10	0.48	2.69E-10
							426.1	417.7	592.0	580.4	-4.25E-08	1.35E-10			
3 NMP							1591.1	1560.0	1281.2	1256.1	7.94E-08	1.38E-10			
1 water							2051.1	2010.9	1553.4	1523.0	1.27E-07	1.38E-10			
												1.39E-10			
7 m	0.41	40	1810	40	5	5.1	716.37	702.35	991.6	972.2	-7.05E-08	7.29E-11	2.87E-10	0.25	9.50E-11
							1064	1043	1260	1235	-5.02E-08	7.54E-11			
3 NMP							3216	3153	2865	2809	8.98E-08	7.72E-11			
1 water							4004	3926	3473	3405	1.36E-07	7.39E-11			
							5279	5175	4479	4392	2.05E-07	6.92E-11			
						7.14E-11									
7 m	0.43	40	3100	40	5	5.1	1270.6	1245.7	1651.4	1619.1	-9.75E-08	5.87E-11	2.87E-10	0.17	5.78E-11
							2062	2022	2225	2181	-4.15E-08	4.17E-11			
3 NMP							5618	5508	5279	5175	8.69E-08	3.88E-11			
1 water							7239	7097	6734	6602	1.29E-07	3.45E-11			
							4815	4721	4577	4488	6.08E-08	4.05E-11			
						4.81E-11									
7 m	0.45	40	6250	40	3	3.06	3778	3704	4215	4133	-6.72E-08	2.89E-11	1.86E-10	0.15	3.25E-11
3 NMP							5429	5323	5569	5460	-2.14E-08	2.50E-11			
							8483	8317	8106	7948	5.79E-08	3.09E-11			
1 water							10708	10498	10029	9833	1.04E-07	2.67E-11			
												2.77E-11			

Table B.12: Detailed WWC data for 5 m PZ in NMP/water and TEG/water

PZ	CO ₂ ldg	T	P* _{CO2}	P	Gas _{dry}	Gas	P _{CO2 in dry}	P _{CO2 in wet}	P _{CO2 out dry}	P _{CO2 out wet}	CO ₂ flux	K _G	kg	K _G /kg	kg ⁱ
m	mol/mol alk	C	Pa	psig	std l/min	std l/min	Pa	Pa	Pa	Pa	mol/s cm ²	mol/s*Pa*cm ²	mol/s*Pa*cm ²		mol/s*Pa*cm ²
5 m	0.2	40	90	20	5	5.16	2.39	2.34	38.99	38.22	-1.49E-08	2.19E-10	4.57E-10	0.49	4.33E-10
in							49.03	48.07	67.21	65.89	-7.42E-09	2.31E-10			
1 TEG							196.6	192.8	153.08	150.08	1.78E-08	2.24E-10			
2 water							497.3	487.5	333.18	326.66	6.70E-08	2.16E-10			
												2.22E-10			
5 m	0.3	40	570	20	5	5.16	0.00	0.00	157.9	153.0	-6.37E-08	1.42E-10	4.57E-10	0.30	1.93E-10
in							192.3	186.4	291.8	282.8	-4.02E-08	1.37E-10			
1 TEG							369.1	357.7	414.0	401.2	-1.81E-08	1.21E-10			
2 water							906.5	878.5	801.3	776.5	4.25E-08	1.44E-10			
							1332.2	1291.1	1114.6	1080.2	8.78E-08	1.35E-10			
						1.36E-10									
5 m	0.25	40	265	20	5	5.16	0.00	0.00	109.3	105.9	-4.41E-08	2.13E-10	4.57E-10	0.44	3.66E-10
in							238.0	230.6	251	243	-5.31E-09	1.93E-10			
1 NMP							462	447	383	371	3.19E-08	2.26E-10			
3 water							698	677	539	522	6.44E-08	1.96E-10			
							897	869	658	637	9.65E-08	2.02E-10			
	48	46	130	126	-3.34E-08	1.90E-10									
											2.03E-10				
5 m	0.3	40	1235	20	5	5.16	0.00	0.00	311	302	-1.26E-07	1.17E-10	4.57E-10	0.25	1.53E-10
in							459	445	653	633	-7.82E-08	1.13E-10			
1 NMP							2523	2446	2229	2160	1.19E-07	1.12E-10			
3 water							3023	2930	2593	2513	1.74E-07	1.18E-10			
												1.15E-10			
5 m	0.35	40	9400	60	4.38	5.45	0.00	0.00	1406	1379	-3.60E-07	4.14E-11	2.87E-10	0.12	4.05E-11
in							3209	3146	4129	4048	-2.36E-07	4.06E-11			
1 NMP							7217	7075	7533	7386	-8.11E-08	3.73E-11			
3 water							11760	11530	11458	11234	7.72E-08	3.92E-11			
							17189	16853	16360	16039	2.12E-07	3.02E-11			
	19338	18960	18471	18110	2.22E-07	2.44E-11									
											3.55E-11				

Table B.13: Detailed WWC data for 5 m PZ in 1 SUF/3 water

PZ	CO ₂ deg	T	P* CO ₂	P	Gas dry	Gas	P _{CO₂in} dry	P _{CO₂in} wet	P _{CO₂but} dry	P _{CO₂but} wet	CO ₂ flux	K _G	kg	K _G /kg	kg'
in	mol/molalk	C	Pa	psig	stdl/min	stdl/min	Pa	Pa	Pa	Pa	mol/s*Pa^2	mol/s*Pa*c m^2	mol/s*Pa*c Pa*cm^2		mol/s*Pa*c m^2
5	0.21	40	68	20	5	5.16	0	0	37	35	-1.48E-08	3.07E-10	4.57E-10	0.68	9.62E-10
							20	19	46	45	-1.07E-08	3.12E-10			
							52	51	61	59	-3.57E-09	2.81E-10			
							121	117	93	90	1.14E-08	3.37E-10			
							92	89	81	79	4.15E-09	2.72E-10			
							132	128	100	97	1.29E-08	3.04E-10			
5	0.21	60	495	20	5	5.45	447	410	489	448	-1.69E-08	2.64E-10	4.83E-10	0.51	4.93E-10
							65	59	271	249	-8.35E-08	2.52E-10			
							201	184	344	316	-5.79E-08	2.42E-10			
							287	263	397	364	-4.44E-08	2.51E-10			
							776	711	673	617	4.15E-08	2.52E-10			
							1133	1038	885	811	1.00E-07	2.38E-10			
5	0.27	20	44	20	5	5.05	12	12	26	25	-5.50E-09	2.22E-10	4.46E-10	0.54	5.23E-10
							23	23	35	34	-4.63E-09	3.17E-10			
							32	32	37	36	-1.83E-09	1.91E-10			
							108	107	80	79	1.13E-08	2.38E-10			
							80	79	64	63	6.47E-09	2.47E-10			
							64	63	55	54	3.48E-09	2.43E-10			
5	0.27	40	261	20	5	5.16	124	121	183	177	-2.37E-08	2.16E-10	4.57E-10	0.47	4.05E-10
							182	176	212	205	-1.21E-08	1.74E-10			
							71	69	154	149	-3.32E-08	2.24E-10			
							477	462	393	381	3.38E-08	2.15E-10			
							378	366	335	325	1.74E-08	2.10E-10			
							317	307	297	288	7.92E-09	2.23E-10			

PZ	CO ₂ d _g	T	P* CO ₂	P	Gas dry	Gas	CO ₂ in _{dry}	CO ₂ in _{wet}	CO ₂ out _{dry}	CO ₂ out _{wet}	CO ₂ flux	K _G	kg	K _G /kg	kg'
in	mol/mol _{alk}	C	Pa	psig	std _l /min	std _l /min	Pa	Pa	Pa	Pa	mol/s _{cm} ²	mol/s*Pa*cm ²	mol/s*Pa*cm ²		mol/s*Pa*cm ²
5	0.27	60	1330	20	5	5.45	108	107	114	113	-2.70E-09	1.60E-10	4.83E-10	0.44	3.83E-10
							87	86	102	101	-5.79E-09	1.76E-10			
							199	197	174	172	9.85E-09	1.74E-10			
							163	161	151	149	4.73E-09	1.70E-10			
							70	69	90	89	-7.92E-09	1.68E-10			
							178	177	161	159	7.05E-09	1.74E-10			
5	0.323	20	127	20	5	5.05	233	214	722	662	-1.97E-07	2.26E-10	4.46E-10	0.38	2.79E-10
							513	470	899	824	-1.56E-07	2.34E-10			
							1488	1364	1461	1340	1.06E-08	5.53E-10			
							2181	2000	1930	1769	1.01E-07	1.86E-10			
							1837	1684	1722	1579	4.63E-08	1.55E-10			
							785	719	1072	982	-1.16E-07	2.48E-10			
						1.72E-10									
5	0.323	40	820	20	5	5.16	371	359	502	487	-5.31E-08	1.35E-10	4.57E-10	0.30	1.96E-10
							243	235	420	407	-7.14E-08	1.45E-10			
							773	749	798	773	-1.01E-08	1.74E-10			
							1301	1261	1177	1140	5.02E-08	1.33E-10			
							957	927	928	899	1.16E-08	1.25E-10			
							1122	1087	1048	1015	2.99E-08	1.30E-10			
						1.37E-10									
5	0.323	60	4900	20	5	5.45	1222	1120	2148	1969	-3.74E-07	1.12E-10	4.83E-10	0.23	1.44E-10
							2073	1900	2840	2604	-3.10E-07	1.18E-10			
							3338	3060	3772	3458	-1.75E-07	1.07E-10			
							10273	9417	9199	8432	4.34E-07	1.08E-10			
							8738	8010	7993	7327	3.01E-07	1.09E-10			
							6874	6302	6502	5960	1.50E-07	1.23E-10			
						1.11E-10									

PZ	CO ₂ fldg	T	P* co2	P	Gas dry	Gas	CO ₂ intdry	CO ₂ intwet	CO ₂ butdry	CO ₂ butwet	CO ₂ flux	K _G	kg	K _G /kg	kg'
in	mol/mol alk	C	Pa	psig	stdl/min	stdl/min	Pa	Pa	Pa	Pa	mol/s/cm ²	mol/s*Pa*cm ²	mol/s*Pa*cm ²		mol/s*Pa*cm ²
5	0.365	20	375	40	5	5.05	227	226	271	270	-1.13E-08	8.97E-11	2.82E-10	0.31	1.26E-10
							177	176	234	232	-1.45E-08	8.56E-11			
							701	697	608	604	2.38E-08	8.73E-11			
							558	555	507	504	1.30E-08	8.52E-11			
							607	604	542	539	1.67E-08	8.59E-11			
							271	270	303	301	-8.01E-09	9.03E-11			
											8.70E-11				
5	0.365	40	2440	40	5	5.1	1305	1279	1628	1596	-8.28E-08	8.33E-11	2.87E-10	0.27	1.06E-10
							2108	2066	2187	2144	-2.03E-08	6.08E-11			
							3310	3246	3107	3046	5.21E-08	7.44E-11			
							3725	3652	3420	3353	7.82E-08	7.41E-11			
							1629	1597	1854	1818	-5.77E-08	7.94E-11			
							2835	2780	2745	2691	2.32E-08	7.90E-11			
											7.74E-11				
5	0.365	60	13800	40	5	5.28	16298	15436	15986	15141	7.96E-08	5.37E-11	2.98E-10	0.16	5.80E-11
							6261	5930	7719	7311	-3.73E-07	5.22E-11			
							10940	10362	11528	10919	-1.50E-07	4.77E-11			
							19408	18382	18613	17629	2.04E-07	4.85E-11			
							21620	20477	20549	19462	2.74E-07	4.46E-11			
							9420	8922	10249	9707	-2.12E-07	4.75E-11			
											4.86E-11				

PZ	CO ₂ d _g	T	P* CO ₂	P	Gas dry	Gas	P _{CO₂in_{dry}}	CO ₂ in _{wet}	CO ₂ in _{dry}	CO ₂ in _{wet}	CO ₂ flux	K _G	kg	K _G /kg	kg'
in	mol/mol _{alk}	C	Pa	psig	std _l /min	std _l /min	Pa	Pa	Pa	Pa	mol/s _l m ²	mol/s*Pa*cm ²	mol/s*Pa*cm ²		mol/s*Pa*cm ²
5	0.4	20	1050	40	3	3.02	426	423	607	603	-2.78E-08	5.23E-11	1.83E-10	0.28	7.16E-11
							657	653	757	752	-1.53E-08	4.45E-11			
							1467	1458	1348	1340	1.82E-08	5.29E-11			
							1320	1311	1244	1237	1.16E-08	5.22E-11			
							1685	1675	1508	1499	2.72E-08	5.12E-11			
							792	787	879	873	-1.33E-08	6.13E-11			
												5.15E-11			
5	0.4	40	7750	40	3	3.06	4377	4291	5137	5037	-1.17E-07	3.80E-11	1.86E-10	0.21	4.83E-11
							8860	8686	8642	8473	3.34E-08	4.05E-11			
							10595	10387	10007	9811	9.03E-08	3.86E-11			
							5756	5643	6205	6084	-6.90E-08	3.68E-11			
							6302	6179	6634	6504	-5.10E-08	3.64E-11			
							10042	9845	9558	9371	7.43E-08	4.02E-11			
												3.83E-11			
5	0.4	60	37050	60	3	3.12	42222	40587	41797	40179	4.78E-08	1.44E-11	1.40E-10	0.11	1.67E-11
							31838	30605	32546	31286	-7.96E-08	1.31E-11			
							23342	22438	25230	24253	-2.12E-07	1.55E-11			
							53927	51839	52133	50115	2.02E-07	1.45E-11			
							47130	45306	46139	44353	1.11E-07	1.44E-11			
							28251	27157	29572	28427	-1.49E-07	1.61E-11			
												1.49E-11			

Table B.14: Detailed WWC data for 5 m PZ in 1 SUF/1 water

PZ	CO ₂ l/dg	T	P* _{CO2}	P	Gas _{dry}	Gas	P _{CO2 in dry}	P _{CO2 in wet}	P _{CO2 out dry}	P _{CO2 out wet}	CO ₂ flux	K _G	kg	K _G /kg	kg'
m	mol/mol alk	C	Pa	psig	std l/min	std l/min	Pa	Pa	Pa	Pa	mol/s cm ²	mol/s*Pa*cm ²	mol/s*Pa*cm ²		mol/s*Pa*cm ²
5	0.178	40	68	20	5	5.16	13	12	50	48	-1.50E-08	4.31E-10	4.57E-10	0.93	6.38E-09
							31	30	56	55	-1.04E-08	4.41E-10			
							47	45	61	59	-5.79E-09	3.92E-10			
							100	97	80	78	7.92E-09	4.53E-10			
							117	114	87	84	1.23E-08	4.28E-10			
							90	87	79	76	4.44E-09	3.45E-10			
5	0.178	60	375	20	5	5.45	98	89	263	241	-6.68E-08	3.34E-10	4.83E-10	0.65	8.78E-10
							283	259	341	312	-2.34E-08	2.70E-10			
							236	217	325	298	-3.59E-08	3.19E-10			
							928	851	666	611	1.06E-07	3.09E-10			
							706	647	561	514	5.85E-08	2.95E-10			
							560	513	482	442	3.14E-08	3.20E-10			
5	0.26	20	36	20	5	5.05	10	10	23	23	-5.21E-09	2.79E-10	4.46E-10	0.60	6.67E-10
							22	21	27	27	-2.32E-09	2.00E-10			
							69	69	54	54	6.08E-09	2.49E-10			
							61	60	50	50	4.25E-09	2.30E-10			
							85	85	61	60	9.94E-09	2.85E-10			
							108	107	73	72	1.40E-08	2.72E-10			
5	0.26	40	81	20	5	5.16	110	107	147	143	-1.50E-08	2.08E-10	4.57E-10	0.45	3.73E-10
							154	150	171	166	-6.76E-09	1.70E-10			
							71	68	124	121	-2.17E-08	2.14E-10			
							288	279	257	249	1.25E-08	1.93E-10			
							373	362	307	298	2.65E-08	2.06E-10			
							332	322	283	274	2.01E-08	2.05E-10			

PZ	CO ₂ ldg	T	P* _{CO2}	P	Gas _{dry}	Gas	P _{CO2 in dry}	P _{CO2 in wet}	P _{CO2 out dry}	P _{CO2 out wet}	CO ₂ flux	K _c	kg	K _c /kg	kg'
m	mol/mol alk	C	Pa	psig	std l/min	std l/min	Pa	Pa	Pa	Pa	mol/s cm ²	mol/s*Pa*cm ²	mol/s*Pa*cm ²		mol/s*Pa*cm ²
5	0.26	60	1480	20	5	5.45	465	426	825	756	-1.45E-07	1.65E-10	4.83E-10	0.36	2.70E-10
							646	592	983	901	-1.36E-07	1.88E-10			
							1167	1070	1323	1212	-6.27E-08	1.88E-10			
							3312	3036	2775	2543	2.17E-07	1.68E-10			
							2282	2092	2045	1875	9.56E-08	1.93E-10			
							3022	2770	2564	2350	1.85E-07	1.73E-10			
												1.73E-10			
5	0.31	20	81	20	5	5.05	208	206	169	167	1.58E-08	1.52E-10	4.46E-10	0.35	2.36E-10
							164	162	138	137	1.02E-08	1.51E-10			
							46	46	59	58	-4.92E-09	1.72E-10			
							11	11	35	34	-9.65E-09	1.67E-10			
							149	148	127	126	8.78E-09	1.60E-10			
							53	53	60	59	-2.61E-09	1.05E-10			
												1.55E-10			
5	0.31	40	510	20	5	5.16	203	197	304	294	-4.04E-08	1.55E-10	4.57E-10	0.32	2.16E-10
							294	285	362	351	-2.77E-08	1.46E-10			
							1165	1129	977	947	7.58E-08	1.45E-10			
							980	950	850	824	5.25E-08	1.41E-10			
							867	840	763	739	4.19E-08	1.51E-10			
							722	700	670	649	2.12E-08	1.30E-10			
												1.47E-10			
5	0.31	60	3800	20	5	5.45	1512	1386	2021	1853	-2.06E-07	9.46E-11	4.83E-10	0.20	1.23E-10
							1858	1704	2282	2092	-1.71E-07	9.01E-11			
							9067	8311	8080	7407	3.98E-07	9.85E-11			
							7138	6543	6524	5980	2.48E-07	1.01E-10			
							3143	2881	3428	3142	-1.15E-07	1.47E-10			
							10536	9658	9264	8492	5.13E-07	9.77E-11			
												9.82E-11			

PZ	CO ₂ ldg	T	P* _{CO2}	P	Gas _{dry}	Gas	P _{CO2 in dry}	P _{CO2 in wet}	P _{CO2 out dry}	P _{CO2 out wet}	CO ₂ flux	K _G	kg	K _G /kg	kg'	
m	mol/mol alk	C	Pa	psig	std l/min	std l/min	Pa	Pa	Pa	Pa	mol/s cm ²	mol/s*Pa*cm ²	mol/s*Pa*cm ²		mol/s*Pa*cm ²	
5	0.36	40	1820	40	5	5.1	1176	1153	1346	1320	-4.34E-08	7.50E-11	2.87E-10	0.26	9.93E-11	
							3307	3242	2964	2906	8.79E-08	7.05E-11				
							1746	1712	1765	1730	-4.83E-09	4.88E-11				
							799	784	1071	1050	-6.95E-08	7.75E-11				
							2541	2491	2364	2318	4.54E-08	7.82E-11				
							2960	2902	2688	2636	6.95E-08	7.38E-11				
5	0.36	60	12600	40	5	5.28	6371	6035	7502	7105	-2.89E-07	4.81E-11	2.98E-10	0.16	5.56E-11	
							9593	9085	10180	9642	-1.50E-07	4.66E-11				
							8003	7580	8867	8398	-2.21E-07	4.81E-11				
							17127	16222	16470	15600	1.68E-07	5.09E-11				
							18648	17662	17853	16909	2.04E-07	4.35E-11				
							21689	20543	20376	19299	3.36E-07	4.60E-11				
5	0.4	40	6900	40	3	3.06	3530	3461	4135	4054	-9.29E-08	2.97E-11	1.86E-10	0.14	3.01E-11	
							4851	4756	5155	5054	-4.67E-08	2.35E-11				
							2504	2455	3152	3090	-9.96E-08	2.42E-11				
							11597	11370	10906	10692	1.06E-07	2.58E-11				
							8922	8747	8583	8415	5.20E-08	3.10E-11				
							12772	12522	11908	11675	1.33E-07	2.56E-11				
5	0.4	60	13800	60	3	3.12	22964	22075	24522	23573	-1.75E-07	1.20E-11	1.40E-10	0.10	1.58E-11	
							19566	18809	22020	21168	-2.76E-07	1.59E-11				
							28251	27157	29572	28427	-1.49E-07	1.55E-11				
							46753	44943	45856	44081	1.01E-07	1.42E-11				
							51944	49934	50481	48527	1.65E-07	1.39E-11				
							55248	53110	53455	51386	2.02E-07	1.36E-11				

Table B.15: Detailed WWC data for 5 m PZ in 1 IMI/1 water

PZ	CO ₂ l/dg	T	P* _{CO2}	P	Gas _{dry}	Gas	P _{CO2 in dry}	P _{CO2 in wet}	P _{CO2 out dry}	P _{CO2 out wet}	CO ₂ flux	K _G	kg	K _G /kg	kg'
m	mol/mol alk	C	Pa	psig	std l/min	std l/min	Pa	Pa	Pa	Pa	mol/s cm ²	mol/s*Pa*c m ²	mol/s* Pa*cm ²		mol/s*Pa*c m ²
5	0.225	40	136	20	5	5.16	37	36	92	89	-2.21E-08	3.16E-10	4.57E-10	0.68	9.69E-10
							68	66	106	103	-1.53E-08	3.10E-10			
							87	84	114	110	-1.10E-08	2.95E-10			
							196	190	166	160	1.23E-08	3.30E-10			
							213	207	176	170	1.52E-08	3.02E-10			
							170	165	155	150	5.99E-09	2.91E-10			
5	0.225	60	830	20	5	5.45	470	431	667	612	-7.96E-08	2.66E-10	4.83E-10	0.53	5.55E-10
							204	187	512	470	-1.24E-07	2.55E-10			
							334	306	593	544	-1.05E-07	2.66E-10			
							1289	1182	1117	1024	6.95E-08	2.62E-10			
							1536	1408	1258	1153	1.12E-07	2.56E-10			
							1155	1059	1050	963	4.25E-08	2.41E-10			
5	0.31	20	97	20	5	5.05	201	199	161	160	1.59E-08	1.97E-10	4.46E-10	0.44	3.47E-10
							30	30	56	56	-1.06E-08	1.99E-10			
							49	48	67	66	-7.34E-09	1.87E-10			
							65	64	78	77	-5.31E-09	2.04E-10			
							172	171	144	143	1.13E-08	1.92E-10			
							151	149	131	130	7.92E-09	1.90E-10			
5	0.31	40	660	20	5	5.16	201	195	364	352	-6.55E-08	1.72E-10	4.57E-10	0.37	2.69E-10
							308	299	431	418	-4.96E-08	1.67E-10			
							422	409	508	493	-3.49E-08	1.69E-10			
							1055	1022	931	902	5.00E-08	1.68E-10			
							1122	1087	973	943	5.99E-08	1.71E-10			
							945	916	859	832	3.48E-08	1.65E-10			

PZ	CO ₂ ldg	T	P* _{CO2}	P	Gas _{dry}	Gas	P _{CO2 in dry}	P _{CO2 in wet}	P _{CO2 out dry}	P _{CO2 out wet}	CO ₂ flux	K _c	kg	K _c /kg	kg'
m	mol/mol alk	C	Pa	psig	std l/min	std l/min	Pa	Pa	Pa	Pa	mol/s cm ²	mol/s*Pa*c m ²	mol/s* Pa*cm ²		mol/s*Pa*c m ²
5	0.31	60	4600	20	5	5.45	8914	8171	7971	7307	3.81E-07	1.22E-10	4.83E-10	0.25	1.60E-10
							2500	2292	3114	2855	-2.48E-07	1.23E-10			
							2926	2682	3421	3136	-2.00E-07	1.19E-10			
							3798	3482	4079	3739	-1.13E-07	1.15E-10			
							7949	7286	7269	6663	2.74E-07	1.16E-10			
							7160	6563	6655	6101	2.04E-07	1.18E-10			
											1.20E-10				
5	0.37	20	375	40	5	5.03	169	168	232	230	-1.61E-08	9.27E-11	2.82E-10	0.33	1.36E-10
							204	202	257	256	-1.37E-08	9.49E-11			
							245	243	284	283	-1.01E-08	9.13E-11			
							508	505	469	467	9.94E-09	9.07E-11			
							569	565	510	507	1.51E-08	9.47E-11			
							633	629	559	555	1.90E-08	8.84E-11			
											9.18E-11				
5	0.37	40	2620	40	5	5.1	1201	1177	1531	1501	-8.45E-08	6.63E-11	2.87E-10	0.24	8.86E-11
							1417	1389	1689	1656	-6.97E-08	6.38E-11			
							1584	1553	1844	1808	-6.66E-08	7.13E-11			
							1801	1766	2013	1974	-5.43E-08	7.28E-11			
							3612	3541	3393	3327	5.60E-08	6.92E-11			
							3363	3297	3201	3138	4.15E-08	6.98E-11			
											6.77E-11				
5	0.37	60	17100	40	5	5.28	9385	8889	10629	10067	-3.19E-07	4.19E-11	2.98E-10	0.13	4.57E-11
							13947	13210	14466	13701	-1.33E-07	3.65E-11			
							10837	10264	11770	11148	-2.39E-07	3.74E-11			
							25871	24504	24800	23489	2.74E-07	3.99E-11			
							22242	21066	21689	20543	1.42E-07	3.83E-11			
							24350	23063	23486	22245	2.21E-07	3.99E-11			
											3.96E-11				

PZ	CO ₂ ldg	T	P* _{CO2}	P	Gas _{dry}	Gas	P _{CO2 in dry}	P _{CO2 in wet}	P _{CO2 out dry}	P _{CO2 out wet}	CO ₂ flux	K _c	kg	K _c /kg	kg'
m	mol/mol alk	C	Pa	psig	std l/min	std l/min	Pa	Pa	Pa	Pa	mol/s cm ²	mol/s*Pa*c m ²	mol/s* Pa*cm ²		mol/s*Pa*c m ²
5	0.415	20	1200	60	3	3.01	357	356	672	669	-3.54E-08	5.24E-11	1.33E-10	0.37	7.72E-11
							523	520	751	747	-2.57E-08	4.59E-11			
							676	672	843	840	-1.89E-08	4.30E-11			
							1455	1448	1370	1363	9.56E-09	4.71E-11			
							1931	1922	1673	1666	2.90E-08	4.95E-11			
							1681	1674	1511	1504	1.91E-08	4.99E-11			
												4.89E-11			
5	0.415	40	8550	60	3	3.04	4599	4533	5496	5417	-1.01E-07	2.84E-11	1.36E-10	0.21	3.50E-11
							3731	3677	4831	4761	-1.24E-07	2.87E-11			
							6369	6278	6884	6785	-5.79E-08	2.88E-11			
							12533	12354	11722	11554	9.13E-08	2.70E-11			
							11070	10912	10542	10391	5.95E-08	2.84E-11			
							13855	13656	12769	12586	1.22E-07	2.68E-11			
												2.78E-11			
5	0.415	60	46200	60	3	3.12	28770	27656	30799	29607	-2.28E-07	1.30E-11	1.40E-10	0.10	1.55E-11
							19660	18899	23059	22166	-3.82E-07	1.49E-11			
							33726	32420	35094	33736	-1.54E-07	1.17E-11			
							66529	63954	64358	61866	2.44E-07	1.46E-11			
							71579	68808	68936	66267	2.97E-07	1.40E-11			
							63036	60596	61479	59099	1.75E-07	1.29E-11			
												1.39E-11			

Table B.16: Detailed WWC data for 5 m PZ in 1 IMI/3 water

PZ	CO ₂ l/dg	T	P* _{CO2}	P	Gas _{dry}	Gas	P _{CO2 in dry}	P _{CO2 in wet}	P _{CO2 out dry}	P _{CO2 out wet}	CO ₂ flux	K _G	kg	K _G /kg	kg'
m	mol/mol alk	C	Pa	psig	std l/min	std l/min	Pa	Pa	Pa	Pa	mol/s cm ²	mol/s*Pa*cm ²	mol/s* Pa*cm ²		mol/s*Pa*cm ²
5	0.222	40	99	20	5	5.16	33	32	68	66	-1.40E-08	2.90E-10	4.57E-10	0.59	6.61E-10
							55	54	77	75	-8.98E-09	2.68E-10			
							70	67	83	81	-5.50E-09	2.26E-10			
							158	153	132	127	1.07E-08	2.68E-10			
							137	133	120	117	6.66E-09	2.69E-10			
							180	174	143	139	1.48E-08	2.66E-10			
5	0.222	60	605	20	5	5.45	227	208	390	357	-6.59E-08	2.08E-10	4.83E-10	0.44	3.84E-10
							329	302	456	418	-5.10E-08	2.12E-10			
							430	394	519	476	-3.60E-08	2.16E-10			
							895	820	808	741	3.48E-08	2.01E-10			
							1064	976	916	840	5.99E-08	2.01E-10			
							1174	1077	965	885	8.45E-08	2.30E-10			
5	0.31	20	86	20	5	5.05	33	32	50	50	-7.14E-09	1.61E-10	4.46E-10	0.35	2.45E-10
							44	44	58	57	-5.60E-09	1.59E-10			
							53	52	63	63	-4.15E-09	1.47E-10			
							130	129	116	115	5.79E-09	1.63E-10			
							150	148	129	128	8.30E-09	1.61E-10			
							169	167	143	142	1.05E-08	1.55E-10			
5	0.31	40	524	20	5	5.16	195	189	312	302	-4.69E-08	1.71E-10	4.57E-10	0.35	2.50E-10
							280	272	362	350	-3.28E-08	1.56E-10			
							324	314	390	378	-2.69E-08	1.53E-10			
							799	774	719	697	3.21E-08	1.53E-10			
							729	707	667	647	2.49E-08	1.65E-10			
							872	845	764	741	4.34E-08	1.64E-10			

PZ	CO ₂ l/dg	T	P* _{CO2}	P	Gas _{dry}	Gas	P _{CO2 in dry}	P _{CO2 in wet}	P _{CO2 out dry}	P _{CO2 out wet}	CO ₂ flux	K _c	kg	K _c /kg	kg'
m	mol/mol alk	C	Pa	psig	std l/min	std l/min	Pa	Pa	Pa	Pa	mol/s cm ²	mol/s*Pa*cm ²	mol/s* Pa*cm ²		mol/s*Pa*cm ²
5	0.31	60	3500	20	5	5.45	1259	1155	1922	1761	-2.67E-07	1.32E-10	4.83E-10	0.27	1.81E-10
							1667	1528	2229	2043	-2.27E-07	1.33E-10			
							2286	2095	2669	2447	-1.55E-07	1.27E-10			
							5954	5458	5384	4935	2.30E-07	1.37E-10			
							5406	4955	4989	4573	1.68E-07	1.34E-10			
							6414	5880	5756	5277	2.65E-07	1.29E-10			
											1.32E-10				
5	0.36	20	260	40	5	5.05	163	162	195	194	-8.30E-09	1.03E-10	2.82E-10	0.36	1.61E-10
							116	115	163	162	-1.20E-08	9.99E-11			
							80	79	140	139	-1.54E-08	1.04E-10			
							425	423	372	369	1.37E-08	1.02E-10			
							515	512	430	427	2.19E-08	1.06E-10			
							458	455	397	394	1.56E-08	9.61E-11			
											1.02E-10				
5	0.36	40	1715	40	5	5.1	892	874	1131	1109	-6.13E-08	8.55E-11	2.87E-10	0.30	1.20E-10
							1168	1145	1329	1303	-4.12E-08	8.47E-11			
							1337	1310	1453	1425	-2.98E-08	8.66E-11			
							2549	2499	2326	2281	5.70E-08	8.51E-11			
							2903	2846	2583	2532	8.21E-08	8.50E-11			
							2345	2299	2187	2144	4.05E-08	8.07E-11			
											8.48E-11				
5	0.36	60	10900	40	5	5.28	9212	8725	9593	9085	-9.73E-08	4.89E-11	2.98E-10	0.19	7.05E-11
							7709	7301	8400	7956	-1.77E-07	5.43E-11			
							5341	5059	6596	6247	-3.21E-07	6.15E-11			
							16989	16091	15917	15076	2.74E-07	5.88E-11			
							18440	17466	17162	16254	3.27E-07	5.51E-11			
							15364	14552	14673	13897	1.77E-07	5.34E-11			
											5.70E-11				

PZ	CO ₂ ldg	T	P* _{CO2}	P	Ga _{dry}	Gas	P _{CO2 in dry}	P _{CO2 in wet}	P _{CO2 out dry}	P _{CO2 out wet}	CO ₂ flux	K _c	kg	K _c /kg	kg'
m	mol/mol alk	C	Pa	psig	std l/min	std l/min	Pa	Pa	Pa	Pa	mol/s cm ²	mol/s*Pa*cm ²	mol/s* Pa*cm ²		mol/s*Pa*cm ²
5	0.4	20	1080	60	3	3.01	327	325	636	633	-3.48E-08	5.92E-11	1.33E-10	0.40	8.97E-11
							491	489	714	711	-2.51E-08	5.32E-11			
							594	591	759	756	-1.86E-08	4.64E-11			
							1363	1357	1267	1261	1.08E-08	4.77E-11			
							1511	1504	1345	1339	1.87E-08	5.59E-11			
							1660	1652	1447	1441	2.39E-08	5.21E-11			
												5.36E-11			
5	0.4	40	6000	60	3	3.04	1596	1573	2677	2639	-1.22E-07	3.14E-11	1.36E-10	0.22	3.82E-11
							1962	1934	2925	2883	-1.08E-07	3.03E-11			
							2677	2639	3445	3395	-8.63E-08	2.91E-11			
							10916	10759	9835	9694	1.22E-07	2.89E-11			
							3403	3355	3985	3928	-6.55E-08	2.79E-11			
							8650	8526	8032	7917	6.95E-08	3.15E-11			
												2.98E-11			
5	0.4	60	38500	60	3	3.12	13855	13319	18480	17765	-5.20E-07	2.27E-11	1.40E-10	0.16	2.62E-11
							16923	16268	20935	20124	-4.51E-07	2.23E-11			
							22587	21712	25419	24435	-3.19E-07	2.07E-11			
							47508	45669	46186	44398	1.49E-07	2.28E-11			
							52841	50796	50529	48573	2.60E-07	2.33E-11			
							57325	55106	54493	52384	3.19E-07	2.10E-11			
												2.21E-11			

References

- Aim, K. 1978. Measurement of Vapor-Liquid Equilibrium in Systems with Components of Very Different Volatility by the Total Pressure Static Method. *Fluid Phase Equilib.* (2) 119-142
- Ayub, Z.H., 2003. Plate heat exchanger literature survey and new heat transfer and pressure drop correlations for refrigerant evaporators. *Heat. Transf. Eng.* 24, 3–16.
- Ban, Z.H., Keong, L.K., Shariff, A.M., 2014. Physical Absorption of CO₂ Capture: A Review. *Advanced Materials Research* (Vol. 917, pp. 134-143). Trans Tech Publications.
- Bara, JE., 2013. N-Functionalized imidazole-containing systems and method of use. U.S. Patent 8506914 B2.
- Bishnoi, S., 2000. Carbon dioxide absorption and solution equilibrium in piperazine activated methyldiethanolamine. Ph.D. Dissertation. the University of Texas at Austin. Austin, TX.
- Bottoms, R.R., 1930. Separating acid gases, U.S. Patent 1783901. Washington, DC: U.S. Patent and Trademark Office.
- Browning, G.J. and Weiland, R.H., 1994. Physical solubility of carbon dioxide in aqueous alkanolamines via nitrous oxide analogy. *Journal of Chemical and Engineering Data*, 39(4), pp.817-822.
- Buchele, M., 2014 November 12 Climate Deal Puts Spotlight on Carbon Capture Technology. NPR State Impact. Retrieved from <http://stateimpact.npr.org/texas/2014/11/12/climate-deal-puts-spotlight-on-carbon-capture-technology/>
- Chen, S., Chen, S., Fei, X., Zhang, Y., Qin, L., 2015. Solubility and Characterization of CO₂ in 40 mass % N-Ethylmonoethanolamine Solutions: Explorations for an Efficient Nonaqueous Solution. *Ind. Eng. Chem. Res.* 54, 7212
- Chen, X. 2011. Carbon Dioxide Thermodynamics , Kinetics , and Mass Transfer in Aqueous Piperazine Derivatives and Other Amines. Department of Chemical Engineering, University of Texas at Austin. Ph.D. Dissertation.
- Chen, X., and Rochelle, G.T. 2011. Aqueous piperazine derivatives for CO₂ capture: Accurate screening by a wetted wall column. *Chemical Engineering Research and Design*, 89 (9): 1693-1710.

- Chen, X. and Rochelle, G.T., 2013. Modeling of CO₂ absorption kinetics in aqueous 2-methylpiperazine. *Industrial & Engineering Chemistry Research*, 52(11), pp.4239-4248.
- Chen, X., Cloosmann, F., Rochelle, G.T. 2011. Accurate screening of amines by the wetted wall column. *Energy Procedia*, 4: 101-108.
- Cloosmann, F. 2011. Oxidation and thermal degradation of methyldiethanolamine/piperazine in CO₂ capture. Department of Chemical Engineering, University of Texas at Austin. Ph.D. Dissertation.
- Cullinane, J. T. 2005. Thermodynamics and Kinetics of Aqueous Piperazine with Potassium Carbonate for Carbon Dioxide Absorption. Department of Chemical Engineering, The University of Texas at Austin. Ph.D. Dissertation.
- Danckwerts, P. V. 1951. Significance of Liquid-film Coefficients in Gas Absorption. *Industrial & Engineering Chemistry*, 43(6): 1460–1467.
- Danckwerts, P. V. 1970. *Gas Liquid Reactions*. New York: McGraw-Hill Book Co.
- Danckwerts, P. V. 1979. The reaction of CO₂ with ethanolamines. *Chemical Engineering Science*, 34(4): 443–446.
- Dlugokencky, E., Tans P., NOAA/ESRL (www.esrl.noaa.gov/gmd/ccgg/trends/) Retrieved on Oct 31, 2016
- Du, Y., Yuan, Y., Rochelle, G.T., 2016. Capacity and absorption rate of tertiary and hindered amines blended with piperazine for CO₂ capture. *Chemical Engineering Science*, 155, 397-404.
- Dugas, R., 2009. Absorption, desorption and mass transfer of carbon dioxide into monoethanolamine and piperazine. Ph. D. Dissertation. the University of Texas at Austin. Austin.
- EIA 2014. *International Energy Statistics*. Retrieved December 15, 2014, from <http://www.eia.gov/countries/data.cfm>
- EPA, 2016. *Sources of Greenhouse Gas Emissions*. Washington, DC, USA, U.S. Environmental Protection Agency.
- Fitzmorris, R. E., & Mah, R. S. H. 1980. Improving distillation column design using thermodynamic availability analysis. *AIChE Journal*, 26(2), 265–273.

- Frailie, P.T., 2014. Modeling of Carbon Dioxide Absorption / Stripping by Aqueous Methyl-diethanolamine / Piperazine. Ph.D. Dissertation, The University of Texas at Austin.
- Freeman, S. 2011. Thermal Degradation and Oxidation of Aqueous Piperazine for Carbon Dioxide Capture. Department of Chemical Engineering, The University of Texas at Austin. Ph. D. Dissertation.
- Freeman, S. A., Dugas, R., Van Wagener, D. H., Nguyen, T., and Rochelle, G. T. 2010. Carbon dioxide capture with concentrated, aqueous piperazine. *International Journal of Greenhouse Gas Control*, 4(2): 119-124.
- Gardner, G.S., Brewer, J.E., 1937. Vapor Pressure of Commercial High-Boiling Organic Solvents. *Industrial & Engineering Chemistry*, 29(2), 179-181.
- Gibbard H.F., Creek J.L., 1974. Vapor pressure of Methanol from 288.15 to 337.65 K. *J.Chem.Eng.Data* (19) 308-310
- Haimour, N., Sandall, O.C., 1984. Absorption of carbon dioxide into aqueous methyl-diethanolamine. *Chemical Engineering Science*, 39(12), 1791-1796.
- Heavner, R. L., Kumar, H., & Wanniarachchi, A. S. 1993. Performance of an Industrial Heat Exchanger: Effect of Chevron Angle. *AIChE Symposium Series*, 89, 262–267.
- Heldebrant, D.J., Koech, P.K., Glezakou, V.A., Rousseau, R., Malhotra, D. and Cantu, D.C., 2017a. Water-Lean Solvents for Post-Combustion CO₂ Capture: Fundamentals, Uncertainties, Opportunities, and Outlook. *Chemical Reviews*.
- Heldebrant, D.J., Koech, P.K., Rousseau, R., Glezakou, V.A., Cantu, D., Malhotra, D., Zheng, F., Whyatt, G., Freeman, C.J. and Bearden, M.D., 2017b. Are Water-Lean Solvent Systems Viable for Post-Combustion CO₂ Capture?. *Energy Procedia*, 114, pp.756-763.
- IEA Greenhouse Gas R&D Programme (IEA GHG), CO₂ Capture in Cement Industry, Page 3-9 2008/3, July 2008.
- Iijima, M., Nagayasu, T., Kamijyo, T., and Nakatani, S., 2011. MHI's energy efficient flue gas CO₂ capture technology and large scale CCS demonstration test at coal-fired power plants in USA. *Mitsubishi Heavy Industries Technical Review*, 48(1), p.26.
- IPCC 2014. "Organization: History." Retrieved December 20, 2014, from http://www.ipcc.ch/organization/organization_history.shtml

- Khan, T. S., Khan, M. S., Chyu, M.-C., & Ayub, Z. H. 2010. Experimental investigation of single phase convective heat transfer coefficient in a corrugated plate heat exchanger for multiple plate configurations. *Applied Thermal Engineering*, 30, 1058–1065.
- Kim, Y. H. 2012. Energy saving and thermodynamic efficiency of a double-effect distillation column using internal heat integration. *Korean Journal of Chemical Engineering*, 29(12), 1680–1687.
- Kneisl, P., Zondlo, J.W., 1987. Vapor pressure, liquid density, and the latent heat of vaporization as functions of temperature for four dipolar aprotic solvents. *Journal Of Chemical And Engineering Data*, 32(1), 11-13.
- Kumar, H. 1984. The Plate Heat Exchanger: Construction and Design. In *Institute of Chemical Engineering Symposium Series* (pp. 1275–1288).
- Lail, M., Tanthana, J. and Coleman, L., 2014. Non-aqueous solvent (NAS) CO₂ capture process. *Energy Procedia*, 63, pp.580-594.
- Li, L., 2015. Carbon Dioxide Solubility and Mass Transfer in Aqueous Amines for Carbon Capture (Ph.D. Dissertation). The University of Texas at Austin.
- Lin, Y., 2016. Modeling Advanced Flash Stripper for Carbon Dioxide Capture Using Aqueous Amines. Ph.D. Dissertation, The University of Texas at Austin.
- Manglik, R. M., & Muley, A. 1995. Thermal–hydraulic behavior of a mixed chevron single-pass plate-and-frame heat exchanger. In *Proceedings of the 30th National Heat Transfer Conference, ASME-Heat Transfer Division* (Vol. 314, pp. 89–96).
- Mathias, P.M., Afshar, K., Zheng, F., Bearden, M.D., Freeman, C.J., Andrea, T., Koech, P.K., Kutnyakov, I., Zwoster, A., Smith, A.R. and Jessop, P.G., 2013. Improving the regeneration of CO₂-binding organic liquids with a polarity change. *Energy & Environmental Science*, 6(7), pp.2233-2242.
- Mikhail, S.Z., Kimel, W.R., 1961. Densities and Viscosities of Methanol-Water Mixtures. *Journal of Chemical and Engineering Data*, 6(4), 533-537.
- Muley, A., & Manglik, R. 1999. Experimental study of turbulent flow heat transfer and pressure drop in plate heat exchanger with chevron plates. *Journal of Heat Transfer*, 121, 110–117.
- Nguyen, B. T. N. 2013. Amine Volatility in CO₂ Capture. Department of Chemical Engineering, University of Texas at Austin. Ph.D. Dissertation.

- Nguyen, T., Hilliard, M., and Rochelle, G. T. 2010. Amine volatility in CO₂ capture. *International Journal of Greenhouse Gas Control*, 4(5): 707-715.
- Nikolic, D., Wijntje, R., Patil Hanamant Rao, P., Van Der Zwet, G., 2009. Sulfinol-X: Second-generation Solvent for Contaminated Gas Treating. In *International Petroleum Technology Conference*. International Petroleum Technology Conference.
- Paul, S., and Thomsen, K. 2012. Kinetics of Absorption of Carbon Dioxide into Aqueous Potassium Salt of Proline. *International Journal of Greenhouse Gas Control*, 8: 169–179.
- Plaza, J.M., 2011. Modeling of Carbon Dioxide Absorption Using Aqueous Monoethanolamine, Piperazine and Promoted Potassium Carbonate. (Ph.D. Dissertation) The University of Texas at Austin.
- Rochelle, G. T. 2009. Amine Scrubbing for CO₂ Capture. *Science*. 325: 1652-1654.
- Rochelle, G., Chen, E., Freeman, S., Van Wagener, D., Xu, Q., and Voice, A. 2011. Aqueous piperazine as the new standard for CO₂ capture technology. *Chemical Engineering Journal*, 171(3): 725–733.
- Roetzel, W., Das, S., & Luo, X. 1994. Measurement of the heat transfer coefficient in plate heat exchangers using a temperature oscillation technique. *International Journal of Heat and Mass Transfer*, 37, 325–331.
- Shamiri, A., Shafeeyan, M.S., Tee, H.C., Leo, C.Y., Aroua, M.K., Aghamohammadi, N., 2016. Absorption of CO₂ into aqueous mixtures of glycerol and monoethanolamine. *Journal of Natural Gas Science and Engineering*, 35, 605-613.
- Sherman B, 2016. Thermodynamic and Mass Transfer Modeling of Aqueous Hindered Amines for Carbon Dioxide Capture. Ph.D. Dissertation, The Unverisity of Texas at Austin.
- Sherman, B., Chen, X., Nguyen, T., Xu, Q., Rafique, H., Freeman, S. A., Voice, A. K., and Rochelle, G. T. 2013. Carbon capture with 4 m piperazine/4 m 2-methylpiperazine. *Energy Procedia*, 37: 436-447.
- Shokouhi, M., Jalili, A.H., Mohammadian, A.H., Hosseini-Jenab, M. and Nouri, S.S., 2013. Heat capacity, thermal conductivity and thermal diffusivity of aqueous sulfolane solutions. *Thermochimica acta*, 560, pp.63-70.

- Stéphenne, K. 2014. Start-up of world's first commercial post-combustion coal fired ccs project: Contribution of shell cansolv to saskpower boundary dam iccs project. *Energy Procedia*, 63, 6106–6110.
- Talik, A. C., Fletcher, L. S., Anand, N. K., & Swanson, L. W. 1995. Heat Transfer and Pressure Drop Characteristics of a Plate Heat Exchanger. *Proceedings of the ASME/JSME Thermal Engineering Conference*, 4, 321–329.
- Tamajon, FJ., Álvarez E., Cerdeira F., Gómez-Díaz, D., 2016. CO₂ absorption into N-methyldiethanolamine aqueous-organic solvents. *Chemical Engineering Journal*.
- Tan, L.S., Shariff, A.M., Lau, K.K. and Bustam, M.A., 2015. Impact of high pressure on high concentration carbon dioxide capture from natural gas by monoethanolamine/N-methyl-2-pyrrolidone solvent in absorption packed column. *International Journal of Greenhouse Gas Control*, 34, pp.25-30.
- Thonon, B., Vidil, R., & Marvillet, C. 1995. Recent research and developments in plate heat exchangers. *Journal of Enhanced Heat Transfer*, 2, 149–155.
- U.S. Department of Transportation, U.S. Coast Guard, 1990. *Chemical Data Guide for Bulk Shipment by Water*. Washington, DC.
- Usubharatana, P., Tontiwachwuthikul, P., 2009. Enhancement factor and kinetics of CO₂ capture by MEA-methanol hybrid solvents. *Energy Procedia*, 1(1), 95-102.
- Versteeg, GF., Swaaij WPM Van., 1988. Solubility and Diffusivity of Acid Gases (CO₂, N₂O) in Aqueous Alkanolamine Solutions. *J Chem Eng Data* 1988;33:29–34.
- Warnakulasuriya, F. S. K., & Worek, W. M. 2008. Heat transfer and pressure drop properties of high viscous solutions in plate heat exchangers. *International Journal of Heat and Mass Transfer*, 51, 52–67.
- Weiland, R. H., Dingman, J. C., Cronin, D. B., & Browning, G. J. 1997. Density and viscosity of some partially carbonated aqueous alkanolamine solutions and their blends. *Journal of Chemical & Engineering Data*, 43(3): 378-382.
- Xu, Q. 2011. *Thermodynamics of CO₂ Loaded Aqueous Amines*. Department of Chemical Engineering, The University of Texas at Austin. Ph.D. Dissertation.
- Yoo, K. P., Lee, K. S., Lee, W. H., & Park, H. S. 1988. Diagnosis of thermodynamic efficiency in heat integrated distillation. *Korean Journal of Chemical Engineering*, 5(2), 123–130.

Zheng, F., Heldebrant, D.J., Mathias, P.M., Koech, P., Bhakta, M., Freeman, C.J., Bearden, M.D. and Zwoster, A., 2016. Bench-scale testing and process performance projections of CO₂ capture by CO₂-binding organic liquids (CO₂BOLs) with and without polarity-swing-assisted regeneration. *Energy & Fuels*, 30(2), pp.1192-1203.